UNIVERSITY OF SOUTHAMPTON

FACULTY OF MEDICINE

Clinical and Experimental Sciences and

National Centre for Advanced Tribology at Southampton

Micro computed tomography to diagnose and quantify biofilms in central venous catheters

by

Wilmari Lianne Niehaus

A thesis submitted in partial fulfillment for the degree of Doctor of Philosophy

April 2015

UNIVERSITY OF SOUTHAMPTON

ABSTRACT

FACULTY OF MEDICINE
Clinical and Experimental Sciences and
National Centre for Advanced Tribology at Southampton

Doctor of Philosophy

MICRO COMPUTED TOMOGRAPHY TO DIAGNOSE AND QUANTIFY BIOFILMS IN CENTRAL VENOUS CATHETERS

by Wilmari Lianne Niehaus

Central venous catheters (CVCs) are used to provide medium to long-term vascular access for chemotherapy, nutrition and dialysis. Bacterial and fungal infections and thrombus occlusion of CVCs are major complications. CVC related bloodstream infections (CRBSI) are usually diagnosed by concordant culture of blood and catheter tip. However, recent studies suggest that culture often fails to detect biofilm bacteria. The present work reported in this thesis describes the steps towards developing a direct non-invasive, non-destructive reliable *in vivo* biofilm detection method within central venous catheters.

Microbial culture, confocal laser scanning microscopy (CLSM) and scanning electron microscopy (SEM) were used to detect biofilms grown on catheters *in vitro* and also on *ex vivo* clinical catheters. X-ray micro computed tomography (x-ray μCT) techniques were developed in order to detect biofilms inside catheters non-destructively. Various contrast agents were compared using energy dispersive x-ray analysis (EDS) to test which stains gave the strongest x-ray signal and were retained best within the biofilms. Catheter material and biofilm were segmented using a semi-automated MATLAB script and quantified using VG Studio MAX and Avizo Fire software packages.

Method comparisons on clinical catheter samples revealed poor concordance for biofilm detection between culture and microscopy, 39% for CLSM and 43.3% for SEM for adult samples. There was better concordance for adult samples between CLSM and SEM, 63.6% but the number of samples compared were smaller between CLSM and SEM compared to microscopy and culture. In contrast, paediatric sample method comparisons showed that there was better concordance between culture and SEM (65%) followed by culture and CLSM (53%) compared to SEM and CLSM (42%). But for both adult and paediatric CVC samples SEM had the highest biofilm positive samples, 90% and 70% respectively. Biofilms within CVCs were heterogeneous, SEM showed that adult samples had more biofilm formation at the tip and the paediatric samples at the subcutaneous ends

However CLSM was not conducive to detect biofilms on catheters due to issues with sectioning the catheter to look inside, material auto-fluorescence and sample curvature. SEM required extensive sample preparation including sectioning and critical point drying,

which caused biomaterial loss. EDS revealed that 10 nm gold and silver nitrate was best suited of the stains tested as a contrast agent for x-ray μCT . X-ray μCT could detect and quantify biofilms in an *in vitro* catheter-flow model and *ex vivo* clinical catheters. Volume measurements were determined and aggregate distributions were investigated. X-ray μCT results were corroborated with SEM, which indicated evidence of polymicrobial biofilms.

X-ray μCT has good potential to study biofilms in 3D in CVCs non-destructively. Research into biofilm mapping could allow for whole catheter imaging without sample sectioning. Future work will assess biofilm specific contrast agents for potential clinical use. If safe clinical stains could be developed catheter related biofilm infections could be confirmed or excluded without removal.

Contents

List of Figures xi

List of Tables xv

Nomenclature xvii

Declaration of Authorship xix

Acknowledgements xxi

1 Introduction 1

2 Catheter related infection and the role biofilms play 3
2.1 Central venous catheters . . . 3
2.1.1 Peripherally inserted central catheters . . . 4
2.1.2 Tunnelled central venous catheters . . . 4
2.1.3 Implanted ports . . . 5
2.1.4 CVC materials . . . 6
2.2 Catheters as route of infection (CRI) . . . 6
2.2.1 Sources of catheter related infection . . . 7
2.2.2 Organisms that cause CRIs . . . 8
2.2.2.1 *Staphylococcus epidermidis* . . . 9
2.2.2.2 *Staphylococcus aureus* . . . 10
2.2.2.3 *Enterococcus faecalis* . . . 10
2.2.2.4 *Klebsiella pneumoniae* . . . 10
2.2.2.5 *Pseudomonas aeruginosa* . . . 10
2.2.2.6 *Candida albicans* . . . 11
2.2.3 Clinical diagnosis of CRIs . . . 11
2.2.3.1 Catheter-related bloodstream infection . . . 11
2.2.4 Management of catheter-related infections . . . 12
2.3 The biofilm problem . . . 12
2.3.1 Why biofilms form . . . 13
2.3.2 The mechanics of biofilm formation . . . 14
2.3.2.1 Loose attachment . . . 14
2.3.2.2 Robust adhesion . . . 14
2.3.2.3 Microcolony formation and maturation . . . 14
2.3.2.4 Dispersal . . . 15
2.3.3 Factors that may influence biofilm formation . . . 16

2.3.3.1 *In vitro* **biofilm formation and possible influence on clinical catheter use** . . . 16
2.3.3.2 Clinical factors influencing biofilm formation . . . 17
2.4 Clinical culture diagnostic methods . . . 18
2.4.1 The roll plate method . . . 19
2.4.2 Flushing the inside of catheters . . . 19
2.4.3 Culture after sonication . . . 19
2.5 Research detection methods . . . 19
2.5.1 Confocal laser scanning microscopy . . . 19
2.5.2 Scanning electron microscopy . . . 20
2.6 Radiography . . . 22
2.6.1 X-rays . . . 22
2.6.2 X-ray production for imaging . . . 24
2.6.3 The interaction of x-rays with matter . . . 24
2.6.4 Radiography on CVCs . . . 26
2.7 Aims and objectives . . . 27

3 Microbial culture to detect biofilms 29
3.1 Introduction . . . 29
3.1.1 Roll plate . . . 29
3.1.2 Quantitative sonication or flushing . . . 30
3.2 Experimental approach . . . 31
3.3 Materials and methods . . . 32
3.3.1 Clinical audit . . . 32
3.3.2 Clinical pilot study . . . 32
3.3.2.1 Adult specimen removal and collection . . . 32
3.3.2.2 Paediatric specimen removal and collection . . . 33
3.3.2.3 Clinical specimen transport and storage . . . 33
3.3.2.4 General clinical sample processing for all CVC types . . . 33
(a) Cuffed CVC . . . 34
(b) Tunnelled line subcutaneous section . . . 34
(c) Implanted port . . . 34
3.3.3 *In vitro* **inoculum preparation** . . . 36
3.3.4 Growing *in vitro* **biofilms** . . . 36
3.3.4.1 Static *in vitro* **CVC biofilm model** . . . 37
3.3.4.2 *In vitro* **CVC-flow biofilm model** . . . 37
3.3.5 Sonication for biofilm removal from CVCs . . . 38
3.3.6 Bacteria concentration determination . . . 39
3.3.7 Clinical culture by sonication . . . 40
3.3.7.1 Culture positive . . . 41
3.3.7.2 Gram stain . . . 42
3.3.8 Statistics . . . 42
3.4 Results . . . 42
3.4.1 Clinical audit . . . 42
3.4.1.1 Adult audit . . . 42
3.4.1.2 Paediatric audit . . . 42
3.4.2 Clinical pilot CVC information . . . 44

3.4.3 Clinical culture by sonication . . . 46
3.5 Discussion . . . 54

4 Confocal laser scanning microscopy to detect biofilms 57
4.1 Introduction . . . 57
4.2 Experimental approach . . . 58
4.3 Materials and methods . . . 58
4.3.1 Catheter material autofluorescence . . . 58
4.3.2 Sample preparation prior to sectioning . . . 59
4.3.3 Sectioning . . . 59
4.3.4 Sample staining . . . 60
4.3.5 Effect of stain order . . . 60
4.3.6 Microscopy . . . 60
4.3.7 Image analysis . . . 62
4.3.8 CLSM biofilm positive . . . 62
4.3.9 Statistics . . . 62
4.4 Results . . . 63
4.4.1 CVC material autofluorescence . . . 63
4.4.2 Effect of autofluorescence on stain fluorescence . . . 66
4.4.3 Biofilm detection in clinical CVCs . . . 67
4.4.4 Sample sectioning and heterogeneity . . . 68
4.4.5 Data and statistics . . . 71
4.5 Discussion . . . 73

5 Scanning electron microscopy for biofilm detection 75
5.1 Introduction . . . 75
5.2 Materials and methods . . . 76
5.2.1 Sample preparation . . . 76
5.2.2 Sectioning . . . 76
5.2.3 Ethanol dehydration series . . . 76
5.2.4 Critical point drying, stubbing and coating . . . 76
5.2.5 Microscopy . . . 77
5.2.6 Image analysis . . . 77
5.2.7 Clinical biofilm positive . . . 79
5.2.8 Statistics . . . 79
5.3 Results . . . 80
5.3.1 SEM on static *in vitro* **model samples** . . . 80
5.3.2 SEM on *in vitro* **CVC-flow biofilm model** . . . 80
5.3.3 Sample sectioning and heterogeneity of clinical samples . . . 83
5.3.4 Data and statistics . . . 84
5.4 Discussion . . . 86

6 Contrast stain for x-ray μCT 89
6.1 Introduction . . . 89
6.1.1 Attenuation coefficient of the sample . . . 89
6.1.2 Heavy metal stain selection . . . 91
6.2 Experimental approach . . . 93

6.3 Materials and methods . . . 94
6.3.1 Biofilm growth on glass slides . . . 94
6.3.2 Stain preparation . . . 94
6.3.2.1 Traditional stains . . . 94
6.3.2.2 Safer stains . . . 95
6.3.3 Sample staining . . . 95
6.3.4 Washing, ethanol dehydration and critical point drying . . . 95
6.3.5 EDS on single stains . . . 96
6.3.5.1 EDS on traditional single stains . . . 96
6.3.5.2 EDS on safer single stains . . . 96
6.3.6 EDS on dual stains . . . 96
6.3.7 Sonication culture of glass slides . . . 96
6.3.8 Statistics . . . 97
6.4 Results . . . 97
6.4.1 EDS on single stains . . . 97
6.4.1.1 EDS on traditional single stains . . . 97
6.4.1.2 EDS on safer single stains . . . 102
6.4.2 EDS on dual stains . . . 105
6.5 Discussion . . . 111

7 X-ray μCT for CVC-biofilm detection 113
7.1 X-ray computed tomography theory . . . 113
7.2 X-ray μ computed tomography . . . 113
7.2.1 X-ray μCT on small animals and invertebrates . . . 114
7.2.2 X-ray μCT on biofilms . . . 114
7.3 Experimental approach . . . 115
7.4 Materials and methods . . . 116
7.4.1 Sample preparation . . . 116
7.4.1.1 Dual contrast enhancing stain . . . 116
7.4.1.2 X-ray μCT sample holder . . . 116
7.4.1.3 Sample set up and scanner settings . . . 117
7.4.2 Image analysis . . . 118
7.4.2.1 CVC roughness for automated segmentation . . . 118
7.4.2.2 Semi-automated segmentation . . . 118
7.4.3 X-ray μCT biofilm sensitivity . . . 121
7.4.4 X-ray μCT on clinical samples . . . 122
7.4.5 Statistics . . . 122
7.5 Results . . . 123
7.5.1 Image analysis . . . 123
7.5.1.1 CVC roughness for automated segmentation . . . 123
7.5.1.2 Semi-automated segmentation . . . 124
7.5.2 X-ray μCT biofilm sensitivity . . . 125
7.5.2.1 Sample heterogeneity . . . 128
7.5.3 X-ray μCT on clinical samples . . . 131
7.5.3.1 Comparing culture, CLSM, SEM and μCT . . . 135
7.6 Discussion . . . 138
7.6.1 Image segmentation and analysis . . . 138

7.6.2 X-ray μCT biofilm sensitivity 139
7.6.3 X-ray μCT on clinical samples 142

8 Conclusions and prospects **145**

A Comparing biofilm detection methods **149**
A.1 Method comparison for adult samples 149
A.2 Method comparison for paediatric camples 152

B Optical profilometry **155**

C Micro computed tomography **157**
C.1 Applying the contrast stains 157
C.2 X-ray μCT segmentation pre MATLAB script 159
C.2.1 Digital volume sectioning and thresholding 159
C.2.2 Digital noise removal and quantification 159
C.3 MATLAB script for x-ray μCT segmentation 162
C.4 μCT of CVC-flow biofilm model samples 164

References **167**

List of Figures

2.1 PICC placement in a patient . . . 4
2.2 Tunnelled CVC placement . . . 5
2.3 Implanted port placement . . . 5
2.4 Infected totally implanted central venous access device . . . 7
2.5 Sources of catheter-related infection . . . 7
2.6 Biofilm formation . . . 15
2.7 Schematic of how a confocal laser scanning microscope works . . . 20
2.8 Schematic of how a scanning electron microscope works . . . 21
2.9 Characteristic radiation production . . . 23
2.10 Production of Bremsstrahlung radiation . . . 23
2.11 X-ray production for imaging . . . 24
2.12 The probability of coherent scattering, photoelectric effect, and Compton scattering interactions in water . . . 25

3.1 Sample processing for biofilm culture and microscopy detection . . . 31
3.2 A typical PICC removed from patients during the study . . . 34
3.3 Clinical pilot specimen processing flow diagram . . . 35
3.4 Steps to produce the inoculum. . . . 36
3.5 Static biofilm-CVC model . . . 37
3.6 Catheter-flow biofilm model with flow in the lumen only . . . 38
3.7 Preparation for sonication bacterial recovery from *in vitro* static CVC-biofilm model grown samples . . . 39
3.8 Sonication time for *S. epidermidis* biofilm removal from CVCs . . . 40
3.9 Blood agar plate with *S. epidermidis* bacterial colonies 12 hours after plate incubation . . . 41
3.10 Pictures of C16 and P6 Mannitol salt agar . . . 41
3.11 Plots comparing CFUs recovered from adult clinical samples . . . 48
3.12 P32 enhanced culture by sonication blood agar plate. . . . 48
3.13 Plots comparing CFUs recovered from paediatric clinical samples . . . 50
3.14 C6 *P. aeruginosa* on TSA and PIA agar plates 12 hours post culture . . . 51
3.15 C17 blood agar with colonies at 12 and 96 hours post culture . . . 51
3.16 Child 17 yellow colonies are Gram positive rod imaged with light microscope 52
3.17 C7 tip and subcutaneous growth rates . . . 52
3.18 Clinical culture results for paediatric and adult CVCs . . . 53

4.1 Sample processing for biofilm culture . . . 58
4.2 CLSM and SEM micrographs of static CVC-biofilm model grown and control samples to illustrate the different section methods. . . . 61

4.3 Representative illustration of the transverse confocal microscopy view of a CVC section . . . 62
4.4 Comparison of the mean emission fluorescence intensities (410 to 550 nm) of different CVC brands using the 405 nm laser line. . . . 63
4.5 Comparison of the mean emission fluorescence intensities (580 to 780 nm) of different CVC brands using the 561 nm laser line. . . . 64
4.6 Comparisons between the mean autofluorescence intensity produced by different CVC types. . . . 65
4.7 Comparison of the mean emission fluorescence intensities (650 to 780 nm) of different CVC brands using the 633 nm laser line. . . . 66
4.8 Plot of mean fluorescence intensity of CVC-autofluorescence and deposit stained with SYPRO Tangerine and SYTO 9 from clinical fouled CVCs . . 67
4.9 Transverse confocal laser scanning micrographs of subcutaneous sections from C5 and C22 showing biofilms attached to the inner lumen of a section of CVC. . . . 68
4.10 Confocal laser scanning micrographs of rod and cocci shaped bacterial cells on CVC sections. . . . 69
4.11 CLSM micrographs of tip and subcutaneous PICC regions removed from patient 29. . . . 70
4.12 Percentage positive clinical CLSM for paediatric and adult CVCs . . . 71

5.1 Micrographs showing the limited use of transverse sectioning for SEM samples 77
5.2 Scorecard for SEM analysis of bio-deposition in CVCs . . . 78
5.3 SEM micrographs of static *S. epidermidis* CVC-biofilm model samples. . . 81
5.4 Scanning electron micrographs of CVC sections grown in the CVC-vein model. . . . 82
5.5 Scanning electron micrographs of subcutaneous CVC sections from C5 . . 83
5.6 Plot for SEM percentage positive sections of adult and paediatric clinical samples . . . 84

6.1 Linear attenuation coefficient plots of gold, silver, tungsten and silicon . . . 91
6.2 EDS sample preparation . . . 94
6.3 A scanning electron micrograph of mercuric chloride crystals on 24 hour *S. epidermidis* biofilm grown on a glass coupon. . . . 98
6.4 EDS percentage of metal detected in single metal stains . . . 99
6.5 Micrographs of biofilms grown on glass slides analysed with EDS . . . 101
6.6 High magnification electron micrograph of a biofilm positive glass slide stained with nano gold used for EDS showing the presence of biofilm. . . . 102
6.7 Micrograph of biofilm grown on a glass slide and analysed with EDS . . . 103
6.8 Spectrum produced after energy dispersive x-ray analysis on single metal stains. . . . 104
6.9 Plot comparing element weight percentage metal composition in biofilm samples using EDS . . . 105
6.10 High magnification micrograph of a biofilm positive glass slide used for dual stain EDS showing the presence of bacteria. . . . 106
6.11 (i) Micrographs of biofilms that were grown on a glass slides, stained with two metal stains and analysed with EDS . . . 107

6.11 (ii) Micrographs of biofilms that were grown on a glass slides, stained with two metal stains and analysed with EDS . . . 108
6.12 Spectrum produced after energy dispersive x-ray analysis on samples stained with 10 *nm* gold and silver nitrate. . . . 109
6.13 EDS mean elemental weight percentage composition of metal detected in the sample . . . 110

7.1 Sample set-up in Nikon Metrology HMX scanner . . . 117
7.2 Calculating the centre point during MATLAB segmentation . . . 119
7.3 Calculating the average and standard deviation of the inner CVC radius during MATLAB segmentation . . . 119
7.4 Creating the mask during MATLAB segmentation . . . 119
7.5 Removing the outer biofilms from the MATLAB mask . . . 120
7.6 The segmented data from the MATLAB segmentation script before a 2 pixel median filter is applied. . . . 120
7.7 The final biofilm segmented from the CVC using the MATLAB segmentation script . . . 120
7.8 Two dimensional cross section slices from a 5 day old *S. epidermidis* biofilm in a CVC stained with nano gold and silver nitrate to illustrate the output steps from the MATLAB segmentation script . . . 121
7.9 Optical profilometry micrograph showing the roughness of a Lifecath CVC. 123
7.10 Manual and semi-automated MATLAB biofilm-CVC segmentation of x-ray μCT scanned CVC-flow biofilm model samples and corresponding scanning electron micrographs. . . . 124
7.11 Scanning electron micrograph of a static *S. epidermidis* CVC-biofilm grown for 2 hours. . . . 125
7.12 (i) X-ray μCT reconstructed and analysed tomographs and SEM micrographs of scanned samples . . . 125
7.12 (ii) X-ray μCT reconstructed and analysed tomographs and SEM micrographs of scanned samples. . . . 126
7.13 Plot comparing culture, CFUs/cm and x-ray μCT , sum volume in $\mu m^3/cm$ of CVC over time. . . . 127
7.14 Scanning electron micrograph of a biofilm negative control showing debris . 127
7.15 Correlation plot comparing biofilm detection using culture and x-ray μCT . 128
7.16 Scanning electron micrographs and x-ray μCT tomographs showing varying biofilm distribution and aggregate size on the same age biofilm samples within CVC sections. . . . 129
7.17 Volume distribution plot of biofilm aggregates at different time intervals. . 130
7.18 Percentage volume occlusion of the CVC at time intervals. . . . 131
7.19 μCT scanned and SEM micrographs of 12 hour *S. epidermidis* static CVC-biofilm model. . . . 132
7.20 Subcutaneous section from C13 tomograph stained with Osmium Tetroxide and Uranyl Acetate for one hour . . . 132
7.21 μCT tomographs and corroborating SEM micrographs of C5. . . . 133
7.22 μCT tomographs and corroborating SEM micrographs of C7. . . . 134
7.23 Plot showing biofilm volume distribution of C5 and C7. . . . 135
7.25 EDS analysis and micrographs of gold and silver nitrate biofilm negative control . . . 140

7.26 Volume of biofilm versus the volume of a few single cells added together . 142
7.27 Reconstructed tomographs of clinical CVC sections staked on top of each other showing variable x-ray attenuation coefficients 143
7.28 Segmentation editor from P32 and micro-computed tomograph from P29 subcutaneous CVC section showing the radiopaque 'substances 144
7.29 The process to analyse a μ-CT scanned CVC section using Avizo Fire software 144

A.1 Comparing methods used for detecting biofilms in adult CVC samples . . . 150
A.2 Comparing methods used for detecting biofilms in paediatric CVC samples . 152

B.1 Surface optical profilometry analysis of silicone and polyurethane PICCs to determine surface roughness 156

C.1 CT analysis using Avizo fire 161
C.3 Representative high magnification electron micrograph of a biofilm from the CVC-flow biofilm model sample. 164
C.4 Plot comparing the biofilm volume distribution of the x-ray μCT scanned CVC-flow model samples. 165
C.5 Bar chart showing percentage occlusion of CVC-flow model biofilms scanned with x-ray μCT 165
C.6 X-ray μCT tomographs and scanning electron micrographs of CVC-flow biofilm model samples 166

List of Tables

2.1 Organisms that most commonly cause catheter related infections 9

3.1 Adult oncology PICC audit data showing type of CVC, indication for insertion and removal and what the line was used for 43
3.2 Paediatric oncology CVC audit data indicating CVC type, CVC removal and infection rates 44
3.3 Adult patient CVC data showing removal date, clinical area, CVC type and clinical indication for removal 45
3.4 Paediatric patient oncology information, date removed, CVC type and clinical indication for removal 46
3.5 Colony forming units per ml per cm of CVC recovered from tip, middle and subcutaneous regions from adult patients 47
3.6 Colony forming units per ml per cm of CVC recovered from tip, middle and subcutaneous regions removed from paediatric oncology CVCs 49

4.1 Confocal laser scanning microscopy results for CVCs removed from adult patients 72
4.2 Confocal laser scanning microscopy results for paediatric oncology patients 72

5.1 Human blood, bacterial and fungal cell types and approximate sizes 79
5.2 Scanning electron microscopy scores and evidence for the presence biofilm for CVCs removed adult patients. 85
5.3 Scanning electron microscopy results of scores and evidence of biofilms on CVCs removed from paediatric oncology patients 85

6.1 Metal stain candidates 90
6.2 Metal stains analysed using EDS for potential x-ray contrast agents 93
6.3 Heavy metal stains used to enhance contrast for EDAX and x-ray μCT scans between CVC material, biofilm and liquid phase 97

A.1 Combined method results for adult patients for biofilm detection comparing culture, CLSM and SEM 151
A.2 Combined method results for paediatric oncology patients for biofilm detection comparing culture, CLSM and SEM 153

Nomenclature

% (w/v)	Weight/volume percent concentration
AGR	Accessory gene regulator
Bap	Biofilm associated protein
BSI	Bloodstream infection
C. albicans	*Candida albicans*
CABSI	Catheter associated bloodstream infection
CAT	Computed axial tomography
CC	Catheter colonisation
CDC	Centres for Disease Control and Prevention
CFU	Colony forming units
CLSM	Confocal laser scanning microscopy
cm	Centimetre
CPD	Critical point drying
CRBSI	Catheter related bloodstream infection
CRI	Catheter related infection
ct	Cycle threshold
CVC	Central venous catheter
E	Energy
E. faecalis	*Enterococcus faecalis*
eDNA	Extracellular deoxyribonucleic acid
EDS	Energy dispersive x-ray analysis
EDTA	Ethylenediaminetetraacetic acid
EPS	Extracellular polymeric matrix
ESI	Exit site infection
eV	Electron volt
h	Planck's constant = 6.63×10^{-34}J/s
HAI	Hospital acquired infection
HPA	Health Protection Agency
I	Radiation intensity
ICU	Intensive care unit
IDSA	Infectious Diseases Society of America

IJV	Internal jugular vein
J/s	Joules per second
K. pneumoniae	*Klebsiella pneumoniae*
keV	Kiloelectron volt
kVp	Peak kilovoltage
m	Mass
m*l*	Millilitre
MSCRAMM's	Microbial-surface components recognising adhesive matrix molecules
NI	Nosocomial infection
nm	Nanometres
NTCVC	Non tunnelled central venous catheter
PBS	Phosphate buffered saline
PCR	Polymerase chain reaction
PIA	Polysaccharide intercellular adhesin
PICC	Peripherally inserted central catheter
PIPES	Piperazine-N,N-bis 2-ethanesulfonic acid buffer
PNAG	Poly-N-acetylglucosamine
RIP	Regulatory inhibitory peptides
S. aureus	*Staphylococcus aureus*
S. epidermidis	*Staphylococcus epidermidis*
SCV	Subclavian vein
SEM	Scanning electron microscopy
SOP	Standard operating procedure
TCVC	Tunnelled central venous catheter
TSB	Tryptic soy broth
VRE	Vancomycin resistant enterococci
Z	Atomic number
Ze	Nucleus charge
μCT	Micro computed tomography
μl	micro-litre
μm	Micrometers

Declaration of Authorship

I, Wilmari Lianne Niehaus, declare that the thesis entitled *Micro computed tomography to diagnose and quantify biofilms in central venous catheters* and the work presented in the thesis are both my own, and have been generated by me as the result of my own original research. I confirm that:

- this work was done wholly or mainly while in candidature for a research degree at this University;
- where any part of this thesis has previously been submitted for a degree or any other qualification at this University or any other institution, this has been clearly stated;
- where I have consulted the published work of others, this is always clearly attributed;
- where I have quoted from the work of others, the source is always given. With the exception of such quotations, this thesis is entirely my own work;
- I have acknowledged all main sources of help;
- where the thesis is based on work done by myself jointly with others, I have made clear exactly what was done by others and what I have contributed myself;
- parts of this work have been published as:

Signed:.....

Date:.....

Acknowledgements

I would like to thank my supervisors Prof. Paul Stoodley and Prof. Saul Faust for all their help and support. I would also like to thank Dr. Stuart Clark for guidance and the use of his lab during clinical sample collection.

A huge thank you to Dr. Dave Johnston whom not only trained me to use the confocal and scanning electron microscopes but was always there when I needed to talk. cHe helped above and beyond when time was tight, even over weekends. Also, a special mention to Dr. Lizzie Angus, along with Dave and the staff from the Biomedical Imaging Unit whom helped with SEM sample preparation.

A special thank you to Dr. Libby Calton for helping me collect clinical samples, keeping an eye on me whilst processing the samples and staying around after hours. Sue Berger for a shoulder to cry on and for always ensuring our purchase orders go through without a hitch.

My lab and office colleagues for their advice and support through the good, bad and stressful times!

I would like to thank Dr. Gareth Jones for tolerating me during stressful periods and always giving the best writing advice. I would like to thank my parents, Andre and Wilma Niehaus and my family for all of their support and encouragement throughout my studies.

Chapter 1

Introduction

Hospital acquired or nosocomial infections (HAIs) cost the British National Health Service up to £ 1 billion per year (Emori and Gaynes, 1993). At any one time between 8.2 and 9% of patients within the NHS have a HAI (National Audit Office, 2000b; National Audit Office, 2004; Health Protection Agency, 2006). Over 80% of HAIs fall under one of 4 types of infection; (1) urinary tract, (2) surgery-site, (3) bloodstream infection (usually associated with an intravascular device), and (4) pneumonia (usually ventilator associated). Of the four, bloodstream and pneumonia infections are less prevalent with each accounting for just under a half of the most common type of infection (urinary tract). However, both pneumonia and bloodstream infections carry a higher mortality rate, and the cost of treatment is greatest for bloodstream infections (Burke, 2003).

According to the World Health Organisation the most common cause of hospital acquired bloodstream infections are attributed to intravenous catheters (World Health Organization, 2012). Specifically, central venous catheters (CVCs, described in detail in Section 2.1) pose the greatest risk of developing an infection by an intravascular device, accounting for between 3 and 5% of device-related infections (Maki, 1994). Putting catheter related infections (CRIs, Section 2.2) into context, 200,000 CVCs are inserted by the NHS annually and the catheter related bloodstream infection (CRBSI) rate is 3% or 6000 (*Surveillance of Central Venous Catheter Related Infection Protocol, National Health Service*, 2011; Hockenhull et al., 2008). The estimated cost of treating a bloodstream infection is £ 6,209 per patient (National Audit Office, 2000a; Hockenhull et al., 2008). Therefore, the total cost to the NHS in dealing with a CRBSI can be estimated at £ 37.2 million per year. The associated mortality rate is reported as being between 10 and 25% (600 to 1500 hundred patients) (Hockenhull et al., 2008).

Prevention, treatment and diagnosis of CVC related infections are difficult. Most CVCs are partially exposed to the external environment, while prolonged dwelling times and frequent handling all increase the risk of infection. Biofilms have been shown to form within 24 hours after CVC insertion, which may lead to infection (Donlan, 2001; Fux et al., 2003;

Gotz, 2002; Raad, 1998). Biofilms are composed of bacteria that bind to a surface and to each other and produces an extracellular matrix making the biofilm more tolerant to antibiotics (Section 2.3). Therefore, treating biofilms on catheter surfaces can be a problem and may lead to device removal. Furthermore, other indwelling medical devices may also become infected through seeding caused by biofilms on CVCs shedding bacteria into the bloodstream (Mack, 2007). Alternate construction of materials and management methods have been proposed yielding limited success; however a major challenge is the reliable diagnosis of an infected catheter.

Suspected CRI diagnosis is typically confirmed by the roll plate culture method, which is performed on the first 4 cm (starting from the tip) of a removed catheter by rolling across an agar plate followed by incubation and colony counts 12 hours later (Curtis, 2009; Mermel et al., 2009). In some cases culture can produce a negative result but on closer inspection of the sample (e.g. with scanning electron microscopy) biofilms can be found (Raad et al., 1993). There are alternate approaches to detecting biofilms that are routinely used in research that are less susceptible to these issues.

The two most commonly used imaging techniques for biofilm detection in research are confocal laser scanning microscopy (CLSM, Chapter 4) and scanning electron microscopy (SEM, Chapter 5). Out of CLSM and SEM, it is more commonplace to find SEM being used to image biofilms in catheters (Dobbins et al., 1999; Franson et al., 1984; Hachem et al., 2009). But one reason these techniques are not common is that most clinical microbiology diagnostic services do not have CLSM and SEM microscopes. Also, both microscopes requires highly specialised training.

Currently however SEM, CLSM and culture techniques suffer one of the same drawbacks, that being the necessity of catheter removal from the patient for a complete diagnosis. Ideally biofilm detection would be performed on a catheter *in vivo* not only to reduce the impact of removal on the patient, but also to allow an additional proactive approach to infection treatment. *In vivo* detection would require a technique that (1) allows for the catheter to be imaged while indwelling, (2) provides sufficient resolution to detect biofilms, (3) is non-destructive, (4) is quick, and (5) is safe.

Radiography, which is well established in clinical practice, may be a potential candidate for *in vivo* biofilm imaging, particularly if a computed tomography approach is adopted. However, an established method for radiographic imaging infectious biofilms currently does not exist and therefore development is required. Chapter 7 describes work towards establishing methods for x-ray tomography on biofilms in catheters.

Chapter 2

Catheter related infection and the role biofilms play

Central venous catheters (CVCs) can be broadly divided into four categories, tunnelled and non-tunnelled, peripherally or centrally inserted. The catheter type used will depend on the treatment involved and length of time required (Section 2.1). CRIs are one of the major complications associated with the use of CVCs (Section 2.2). Recently, bacterial biofilms have been implicated in CRIs (Section 2.3). Currently culture (Section 2.4) is the only diagnostic method and there are no bloodstream biofilm markers, thus treatment of a suspected catheter related infection cannot be directly confirmed without catheter removal. Imaging techniques (Section 2.5) have been suggested but because microscopy is based on morphology specific diagnosis is not possible. Therefore, radiography theory is explored (Section 2.6) for the potential to diagnose CRIs without the need for catheter removal.

2.1 Central venous catheters

CVCs are implantable medical devices that are essential in the treatment of hospital patients. Applications for CVCs include intravenous fluids, drug delivery, daily blood samples, haemodialysis, blood monitoring or total parenteral nutrition in critically ill patients (Mermel et al., 2001; Hagle, 2007; Kristinsson et al., 1989; Donlan, 2008; Polderman and Girbes, 2002). The three commonly used long-term CVC types and the materials they are made from are summarised in the Sections that follow.

2.1.1 Peripherally inserted central catheters

Peripherally inserted central catheters (PICCs) are mostly used for medium to long-term venous access and can be inserted at the bedside in adult patients. PICCs are used in patients who require infusions of solutions with extreme pH, or more commonly intravenous venous medication for a week to several months, and for blood sampling. Walshe et al. (2002) found that PICCs used in cancer patients resulted in an infection related complication rate of 7.4%. PICCs are inserted in a large vein, for example at or above the antecubital fossa through the skin into an upper extremity vein (non-tunnelled) such as the cephalic or basilic vein (Fig.2.1) and are threaded into the superior vena cava above the right atrium. PICCs tend to have a small gauge, (Hagle, 2007; Raad et al., 2007) but if larger lumen sizes are required tunnelled CVCs should be considered instead.

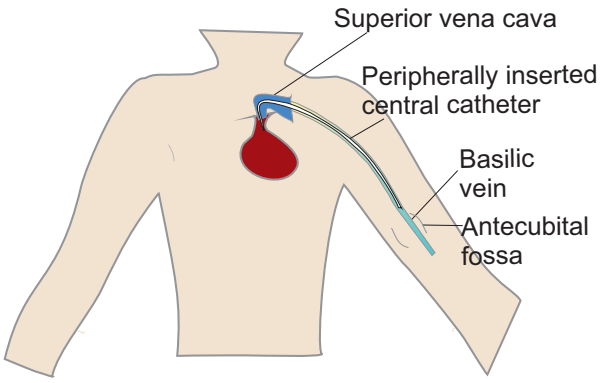

Figure 2.1: PICC placement in a patient. The PICC is inserted at or above the antecubital fossa and threaded towards the heart through the superior vena cava.

2.1.2 Tunnelled central venous catheters

In contrast to PICCs, tunnelled CVCs (TCVCs) are inserted surgically into the central vascular structures and then pulled under the skin through the subcutaneous tissue (tunnelled) for a short distance before exiting the skin (Fig.2.2). Typically, TCVCs also have a cuff where the catheter is tunnelled to anchor the catheter (Hagle, 2007; Raad et al., 2007). TCVCs include Hickman and Broviac catheters which are used for long-term infusions such as total parenteral nutrition (TPN), chemotherapy, hydration or chronic medication and blood infusion or retrieval. TCVCs can be single, double or triple lumen CVCs and varies in lumen size and length. Similar to PICCs TCVCs have a small section of the catheter non-dwelling hanging outside of the patient. If treatment for the patient is long term and intermittent but the clinician prefers none of the catheter to be non-dwelling an implanted port should be used instead.

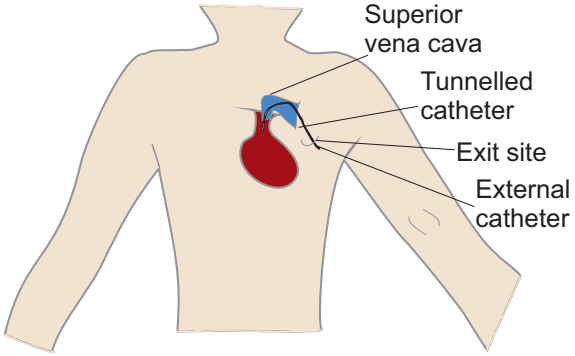

Figure 2.2: Tunnelled CVC placement. Tunnelled CVCs are surgically implanted and tunnelled under skin for a short distance before entering the superior vena cava.

2.1.3 Implanted ports

Implanted ports are devices with hollow cores, or ports, implanted under the skin either as a subclavian port in the chest wall or peripheral port in the antecubital fossa and are attached to the catheters (Fig. 2.3). Ports allow access through the skin for intermittent or continuous infusions of fluids or medications (Hagle, 2007; Raad et al., 2007). Ports are used in patients who require intermittent or cyclic treatment when daily access is not needed. Implanted ports are commonly used for chemotherapy and vein-compromised patients requiring long-term treatment.

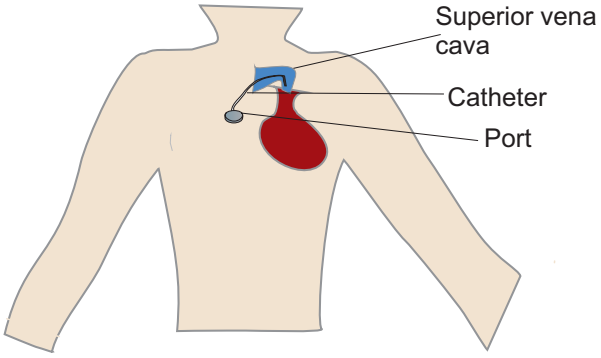

Figure 2.3: Implanted port placement. Ports are surgically implanted under the skin either in the chest wall or near the antecubital fossa and are attached to a catheter which is tunnelled to the superior vena cava.

Therefore, the type of longterm CVC used depends on the patient's medical condition and the treatment for which the CVC is required. The different catheter types can also vary regarding the material used for construction.

2.1.4 CVC materials

The ideal CVC material would inhibit thrombus and biofilm formation, would be easy to insert and be comfortable for the patient (Hagle, 2007). Catheters have been composed of polyvinyl-chloride/Teflon in the past, but the material was discontinued owing to lack of flexibility and resulting vein wall damage (Hagle, 2007). Elastomer hydrogel catheters combine hydrogel and polyurethane to obtain the lowest coefficient of surface friction, allowing for less formation of thrombosis and decreased mechanical tissue trauma. The hydrogel allows the catheter to soften, whereas the polyurethane provides strength and prevents absorption of the infusate into the catheter (Hagle, 2007).

Current clinical CVCs may be composed of polyurethane or silicone materials (Raad et al., 2007). Polyurethane is firm which allows for easy insertion, it softens after insertion, and is bio-compatible which means tissues do not reject the material and is less likely to cause thrombosis due to vein intima irritation than earlier materials. Polyurethane permits thinner walls due to the material strength which allows for larger inner diameters when compared to the same sized silicone catheters. Silicon is more flexible which makes insertion more difficult but the material is more bio-compatible compared to polyurethane (Hagle, 2007).

Both materials are commonly used for all CVC types and depend on the manufacturer. The material the CVC is made from is usually based on the preference of the trained personnel inserting the device. Irrespective of the material the CVC is constructed of, one of the most common risks associated with CVC use is CRIs with all materials susceptible to biofilm formation (Bakker et al., 2004; Gottenbos et al., 2002).

2.2 Catheters as route of infection (CRI)

Inevitably there are risks associated with the use of CVCs, with overall catheter related complications occurring at a rate of between 5 to 22 % (Merrer et al., 2001). Complications can be associated with catheter insertion, indwelling and removal.

Infection is the primary complication of indwelling CVCs (e.g. Fig. 2.4). Infection occurs in 5.3 per 1000 catheter days and the mortality rate can be as high as 35% (Kuminsky, 2007; Mermel et al., 2001; McGee and Gould, 2003). To determine the appropriate route of treatment, the infection has to be clinically diagnosed (Section 2.2.3) and the organism(s) (Section 2.2.2) involved have to be established.

Figure 2.4: Infected totally implanted central venous access device or port (from Inan et al. (2008)). With approximate scale bar = 75 mm as calculated from average clavicle length.

2.2.1 Sources of catheter related infection

The pathogenesis of CVC infection is often related to (1) extraluminal colonisation of the catheter, which originates from the skin and, less commonly, from haematogenous seeding from the catheter tip, or (2) intraluminal colonisation of the hub and lumen of the CVC (Mermel et al., 2001; O'Grady et al., 2011)(Fig.2.5). For tunnelled CVCs or implantable devices (Section 2.1.2 and 2.1.3), contamination of the catheter hub and intraluminal infection is the most common route of infection (Mermel, 2011; Raad and Bodey, 1992; Donlan, 2008).

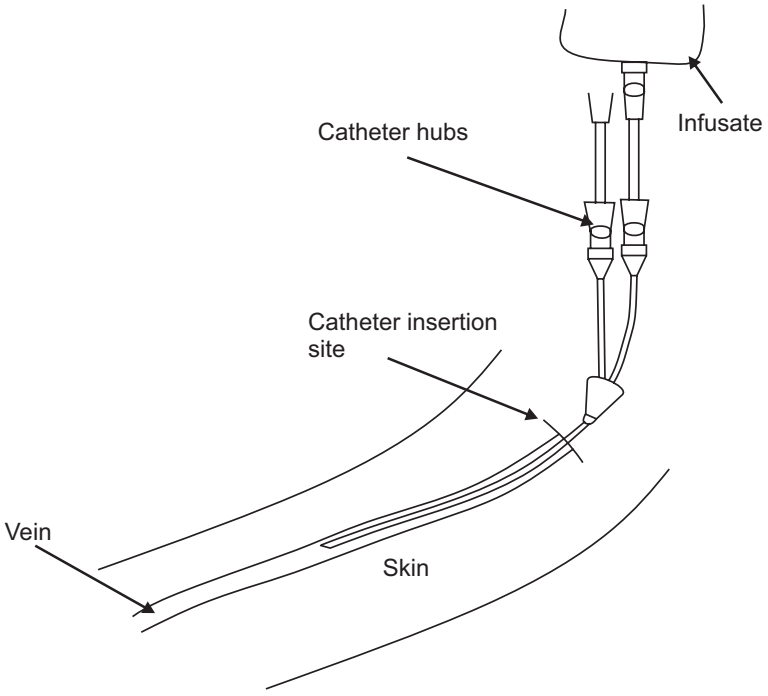

Figure 2.5: Sources of catheter-related infection.

A post mortem study by Broekhuizen et al. (2008) suggested an alternative source of infection, peri-catheter tissue. Peri-catheter tissue samples were highly culture positive (more than 10^4 CFUs) whereas the complimentary catheter segments were culture negative or yielded only low numbers of bacteria. The authors therefore established that the tissue surrounding biomedical devices may also form a habitat for bacteria, in addition to the device itself. Culture negativity, however, does not necessarily mean that there were no bacteria present. Indeed, it has been established that biofilms are not always culturable, even though they may be present (Donlan and Costerton, 2002). The absence of bacteria cultured from the catheter surfaces may also be explained by the presence of residual antibiotics in the catheter, thus inhibiting growth. In addition, Zaat et al. (2008) from the same research group suggested that the introduction of a biomaterial into mice that were already infected with *Staphylococcus epidermidis* (*S. epidermidis*) caused dysregulation of the immune system which resulted in *S. epidermidis* residing in macrophages surrounding the biomaterial. Thus, if bacteria were already present under the skin or whether inserting a catheter caused bacteria to survive in the tissue surrounding the catheter is unknown.

Bacteria within deeper layers of the skin have also been suggested as a potential source of CRIs (Costerton et al., 2004). The bacteria within deeper layers of the skin may not be reached by topical antimicrobial preparations before catheter or device insertion and may be a source of infection. Bacteria present within deeper layers of the skin could also explain why Broekhuizen et al. (2008) found bacteria in peri-catheter tissue.

2.2.2 Organisms that cause CRIs

An intensive care CVC-associated bloodstream infection (BSI) surveillance study by Woeltje et al. (2008) found that the most common organism isolated from blood samples were coagulase-negative staphylococci (45%), *Corynebacterium* species (6%), *Candida albicans* (*C. albicans* 5%), *Staphylococcus aureus* (*S. aureus* 5%), *Enterococcus faecalis* (*E. faecalis* 5%), *Enterococcus faecium* (5%) and *Klebsiella pneumoniae* (*K. pneumoniae* 3%) (Woeltje et al., 2008).

In addition, a 31 month retrospective cohort study on PICC BSIs was performed on Barnes-Jewish Hospital patients. BSIs were identified in 163 PICCs (3.13 BSIs per 1000 catheter days). Gram-positive bacteria accounted for 76% of isolates (out of 205). Of which, *S. epidermidis* accounted for 22% of isolates, *S. aureus* for 2% and methicillin resistant *S. aureus* for 7%, *Enterococcus* sp., vancomycin susceptible 17% and resistant 12%. Gram-negative bacteria included, *K. pneumoniae* were isolated in 4% (Table 2.1) followed by *Eschericia coli* (Ajenjo et al., 2011).

Although the proportions of the organisms varied between studies, the organisms most commonly isolated were similar. Thus, catheter-associated bloodstream infections (CABSIs) were most frequently caused by coagulase negative staphylococci, *S. aureus* , *E. faecalis* ,

C. albicans , *Pseudomonas aeruginosa* (*P. aeruginosa*) and *K. pneumoniae* (Table 2.1) (Mermel et al., 2001; Donlan, 2001). However, it should be noted that both of these studies were retrospective and only blood samples were cultured (not the CVC). The studies used catheter-associated bloodstream infection rather than catheter related bloodstream infection (CRBSI). Often CRBSI and CABSI are used interchangeably which may lead to confusion, oversimplification and misinterpretation. The term CRBSI should be used when a thorough clinical and laboratory investigation identifies the catheter as the source of infection (O'Grady et al., 2011). In contrast, CABSI is when a patient had a central line for 48 hours before developing a primary BSI that is not related to an infection at another site (O'Grady et al., 2011). Therefore, often CABSI often overestimate the incidence of CRBSIs. Each of the organisms that most commonly cause CABSIs are briefly discussed below.

Table 2.1: Organisms that most commonly cause catheter related infections. Data summarised from Donlan (2001); Weinstein (2007); Sawyer and Leon (2010); Lorente et al. (2006).

Organism	% reported
Staphylococcus epidermidis	22-43.5
Staphylococcus aureus	2-17
Enterococcus faecalis	5-17
Candida albicans	5.7-10
Pseudomonas aeruginosa	3.8-10
Klebsiella pneumoniae	2-4

2.2.2.1 *Staphylococcus epidermidis*

S. epidermidis is a commensurate member of the microbiota that lives on human skin. *S. epidermidis* is a Gram-positive organism formerly considered non-pathogenic has now been clinically acknowledged as an important opportunistic pathogen due to the ability to cause HAIs (Mack, 2007; Gotz, 2002; Otto, 2009). *S. epidermidis* is able to cause infection when the skin barrier is broken, such as during a surgical procedure for device or catheter insertion. *S. epidermidis* is equipped to handle extreme conditions that are encountered on the human skin such as high osmotic pressure. *S. epidermidis* is not well cleared from the innate and adaptive immune system (Otto, 2009). Lack of clearance of these infections may be because *S. epidermidis* is normally a colonising rather than pathogenic organism. When *S. epidermidis* becomes pathogenic the organism can cause bacteraemia, prosthetic device, wound, endophthalmitis and urinary tract infections in catheterised patients (Mack, 2007).

2.2.2.2 *Staphylococcus aureus*

S. aureus has been reported to colonise 27% of human hosts (from nose swabs) (Mack, 2007; Wertheim et al., 2005). *S. aureus* is a Gram-positive organism that exist as cocci clusters usually with a gold pigmentation on blood agar. Microbial-surface components recognising adhesive matrix molecules (MSCRAMMs) are surface proteins that play a role in allowing *S. aureus* to colonise host tissue as well as to polymer surfaces coated with host plasma proteins (Lowy, 1998; Hall-Stoodley et al., 2004). *S. aureus* can attach strongly to host derived proteins such as fibronectin, fibrinogen and laminin. *S. aureus* is a dangerous and adaptable pathogen that causes both hospital- and community acquired infections. The increasing number of multi-drug resistant strains has made treatment of *S. aureus* infections difficult (Lowy, 1998).

2.2.2.3 *Enterococcus faecalis*

The Gram-positive bacterium *E. faecalis* is found in soil, water, plants and can colonise the gastrointestinal and genital tracts of humans. *E. faecalis* is also associated with hospital acquired infections. Patients may have vancomycin resistant enterococci (VRE) in their stool, which can spread to their skin and immediate environment. The spread of *E. faecalis* may cause concern in intensive care units (ICU) where patients are immune suppressed or debilitated (Lin and Hayden, 2010).

2.2.2.4 *Klebsiella pneumoniae*

K. pneumoniae is a Gram-negative rod-shaped facultative anaerobe found in mammals and the natural environment and can cause nosocomial infections. Strains that produce extended-spectrum β-lactamases are a public health concern due to antibiotic resistance (Piednoir et al., 2011)

2.2.2.5 *Pseudomonas aeruginosa*

The aerobic, opportunistic pathogen *P. aeruginosa* is a Gram-negative, rod shaped, mono-flagellated bacterium that is found in soil, water, humans, animals, plants, sewage and hospitals. *P. aeruginosa* plays a major role in infections with people suffering from cystic fibrosis. Reduced mucociliary clearance leads to increased mucus in the lungs which leads to inflammation, bacterial infection and pulmonary hypertension among other effects (Davis, 2006). Biofilm infections in other regions of the body can also cause seeding to the catheter exacerbating the immune-compromised host.

2.2.2.6 *Candida albicans*

C. albicans is part of the normal human microbiota. The fungus can reach the blood stream when normal barriers have been broken down. *C. albicans* cause 10% of European nosocomial infections (Smith and Kauffman, 2010). Baena-Monroy et al. (2005) has isolated *S. aureus* and *C. albicans* from device-related oral biofilms which was later grown as model biofilms (Schlecht et al., 2012). *C. albicans* and *S. aureus* can form multi-species biofilms which may benefit *C. albicans* as it may protect the fungus from anti-fungal action (Wargo and Hogan, 2006). *C. albicans* and *S. aureus* mixed biofilm has yet to be shown in non-oral device related infection.

Therefore, the different microorganisms may cause bloodstream infections by forming biofilms on catheter surfaces and continuous shedding of bacteria into the bloodstream.

2.2.3 Clinical diagnosis of CRIs

Local and systemic, suspected and confirmed infections can all be classed under CRIs (Turcotte et al., 2006). The United States Centres for Disease Control and Prevention (CDC) divided CRI into the following categories: (1) exit site infection (ESI), (2) catheter colonisation (CC), and (3) catheter-related bloodstream infection (CRBSI) (Pearson, 1996).

2.2.3.1 Catheter-related bloodstream infection

The most serious CRI, bacteraemia, or bloodstream infection (the presence of bacteria in the blood) is accompanied by symptoms of systemic infection and hypotension in the absence of hypovolaemia or a cardiac event (Raad et al., 2007; Mermel et al., 2001). *S. aureus* and *C. albicans* are the most common organisms to cause CRBSIs.

Bacteraemia may be caused by biofilms that are adhered to the catheter which are continuously shedding bacteria into the bloodstream on a persistent basis which may also cause seeding to other indwelling medical devices (Mack, 2007).

Due to inconsistent definitions of CRBSIs, the Infectious Diseases Society of America (IDSA) has suggested that if a patient presents with symptoms of bacteraemia and a positive peripheral vein culture with no other source of infection one of the following microbiological methods is required to confirm clinical diagnosis of CRBSI (Mermel et al., 2001):

1. positive semi-quantitative (roll plate) or quantitative (vortex or sonication) culture of the catheter or
2. if the catheter is not removed simultaneous quantitative blood cultures drawn through the CVC and peripheral vein with a ratio of 5:1 (CVC versus peripheral) or
3. differential time to positivity for CVC versus peripheral blood cultures (e.g. radiometric methods)

But the problem with methods 2 and 3 is that there are currently no bloodstream markers to detect biofilms. The diagnosis of CRBSI does however remain biased. Diagnostic bias is due to institutions either not culturing the catheter after removal or still using the roll plate method regardless of dwell time, variable CFU cut-off points for a positive catheter and required length of catheter for culture.

2.2.4 Management of catheter-related infections

When there is diagnosis of a suspected CRBSI, in most cases for non-tunnelled catheters it should be removed (O'Grady et al., 2011). If there is doubt or the patient is in good health, or CVC access needs to be protected, systemic antimicrobial therapy can be given as well as an antibiotic lock therapy to try to and treat the infecting bacteria in place (Mermel et al., 2001; Fernandez-Hidalgo et al., 2006; Krishnasami et al., 2002). If the catheter is a tunnelled CVC or port, the decision to remove is dependant on the severity of the patient's condition, the pathogen involved (isolated from blood cultures) and the presence of complications (Mermel et al., 2001). If the tunnelled CVC or port is not removed and the pathogen has been identified suitable systemic antimicrobial therapy should given and antibiotic lock therapy evaluated (Mermel et al., 2001).

2.3 The biofilm problem

Biofilms play a major role in CRIs. Biofilms are formed by groups of sessile bacterial cells of either mono- or multi-species by attaching to a surface. The bacteria attach to a biotic or abiotic surface or to each other. The attached biofilm produces an anionic extracellular polymeric matrix/substance (EPS) which is composed of different components and accounts for over 90% of the dry mass of the biofilm (Flemming and Wingender, 2010). Extracellular DNA (eDNA) which is found in the EPS of biofilms have been found to play a key role in the structure of biofilms (Parsek and Singh, 2003; Boles and Horswill, 2011). Bacteria within biofilms have altered growth rates compared to planktonic counterparts. The bacteria within biofilms transcribe genes that planktonic cells do not which results in an altered phenotype. As a result of protection by the EPS, dense population and altered gene expression by bacteria within biofilms the bacteria can be up to 1000 times more

tolerant to antibiotics (Section 2.3.1)(Donlan and Costerton, 2002; Hall-Stoodley et al., 2004; Costerton et al., 1999; Donlan, 2002; Mah and O'Toole, 2001).

Biofilms provide a protective environment to the residential bacteria (Section 2.3.1). Due to the increased tolerance to antimicrobials biofilm formation within CVCs are critical to prevent, diagnose and treat biofilm CRIs (Section 2.3.2).

2.3.1 Why biofilms form

The biofilm mode of growth is thought to benefit the resident bacteria because the biofilm provides protection from the external environment through cooperative behaviour such as quorum sensing and DNA exchange (Costerton and Lewandowski, 1995). Quorum sensing is the regulation of gene expression as a result of an increase in cell density. Bacteria produce quorum signalling molecules to communicate or sense the population density. When the quorum molecules reach a threshold concentration, a signal transduction system is activated which leads to target gene activation. Quorum sensing enables bacteria to adapt to the environment (Otto, 2004). DNA on the other hand can be passed between bacteria from different species and between different organisms such as bacteria to fungi. The source of DNA can be from cell lysis, plasmids, spontaneous DNA release or even from eDNA. The DNA can be absorbed and incorporated by natural genetic transformation by bacteria in the vicinity (Lorenz and Wackernagelo, 1994).

Cells within an *in vitro* grown multi-species biofilm may arrange themselves that they can survive the heterogeneous environment within the biofilm. de Beer et al. (1994) found that oxygen concentrations within the biofilm differ. Therefore, in a multi-species biofilm aerobic bacteria will be found in the oxygen rich areas and anaerobes will be located where oxygen concentrations are poor (de Beer et al., 1994; Watnick and Kolter, 2000). The cell arrangement within an *in vitro* biofilm indicates that oxygen availability may be important when considering where biofilms form along the catheter. The origin of the bacteria within the biofilm should also be taken into account. The location the bacteria came from may also influence where in the CVC the biofilm is more likely to form.

Under the Donlan and Costerton definition of a biofilm, biofilm clumps (or daughter cells) that have detached from the primary biofilm and enter body fluids such as the bloodstream can also be classed as biofilm cells if they exhibit the same resistance characteristics (Donlan and Costerton, 2002). The fragments are important as *in vitro* studies have shown that these clusters of cells may still be as tolerant to antibiotics as the parent biofilm (Fux et al., 2005). Thus, it has been hypothesised that the clusters may spread the infection, for example to pace makers or heart valves and may be less susceptible to systemic antibiotics.

2.3.2 The mechanics of biofilm formation

Biofilm formation varies depending on the organisms involved, the surface on which the biofilm is growing and the environment in which it forms. Hall-Stoodley et al. (2004) describe 5 steps for *P. aeruginosa* biofilm formation: (1) loose attachment, (2) robust adhesion, (3) cell aggregation into microcolonies, (4) growth and maturation, and (5) dispersal.

2.3.2.1 Loose attachment

Using an adapted biofilm formation scheme from Hall-Stoodley et al. (2004) as a framework of understanding, the first step is for the bacterial cell(s) to locate and attach to a surface (Fig.2.6) (Hall-Stoodley et al., 2004; Gotz, 2002). In order to locate a suitable surface to attach, *P. aeruginosa* uses flagellum-driven swimming motility and type IV pili-mediated twitching motility (Klausen et al., 2006). The transient attachment is mediated by gravitational and van der Waals forces, hydrogen bonding, dipole-dipole and hydrophobic interactions. Surface proteins play a role in initial attachment, of which may include fibronectin binding proteins A and B (FnBPA and FnBPB); and biofilm associated protein (Bap). The surface proteins are important in cell to cell and cell to surface interactions in *S. aureus* and *S. epidermidis* respectively (Boles and Horswill, 2011). FnBPA and FnBPB allows *S. aureus* to invade by binding to fibronectin as it is unable to directly bind to a host cell adhesion receptor (Sinha et al., 1999). Bap is involved in primary bacterial to surface adhesion as well as in the second step of biofilm formation where intercellular adhesion is important (Cucarella et al., 2001).

2.3.2.2 Robust adhesion

After initial attachment has occurred; the second stage follows where the bacterial cells begin to adhere more firmly to the surface in a process called “irreversible cell adherence ”. Irreversible attachment is mediated by various receptor and chemical reactions between the surface and bacteria. Such as polysaccharides and adhesion proteins in the cell membrane or cell wall (O’Toole et al., 2000). For staphylococcal biofilms initial adherence is mediated by microbial surface components recognising adhesive matrix molecules (MSCRAMMs) (Fey, 2010).

2.3.2.3 Microcolony formation and maturation

Stage three of biofilm development occurs when bacteria start to produce EPS and begin the process of microcolony formation. Extracellular polysaccharides are secreted when

the planktonic to biofilm phenotype change occurs; which start forming the matrix of the biofilm (Donlan, 2001). *S. epidermidis* produces polysaccharide intercellular adhesin (PIA) and or poly-N-acetylglucosamine (PNAG) that are essential for developing three-dimensional tower structures, resistance to fluid shear stress, and resistance to biocides and neutrophil dependant killing (Fey, 2010; Rohde et al., 2010). The fourth stage follows when the biofilm grows and matures.

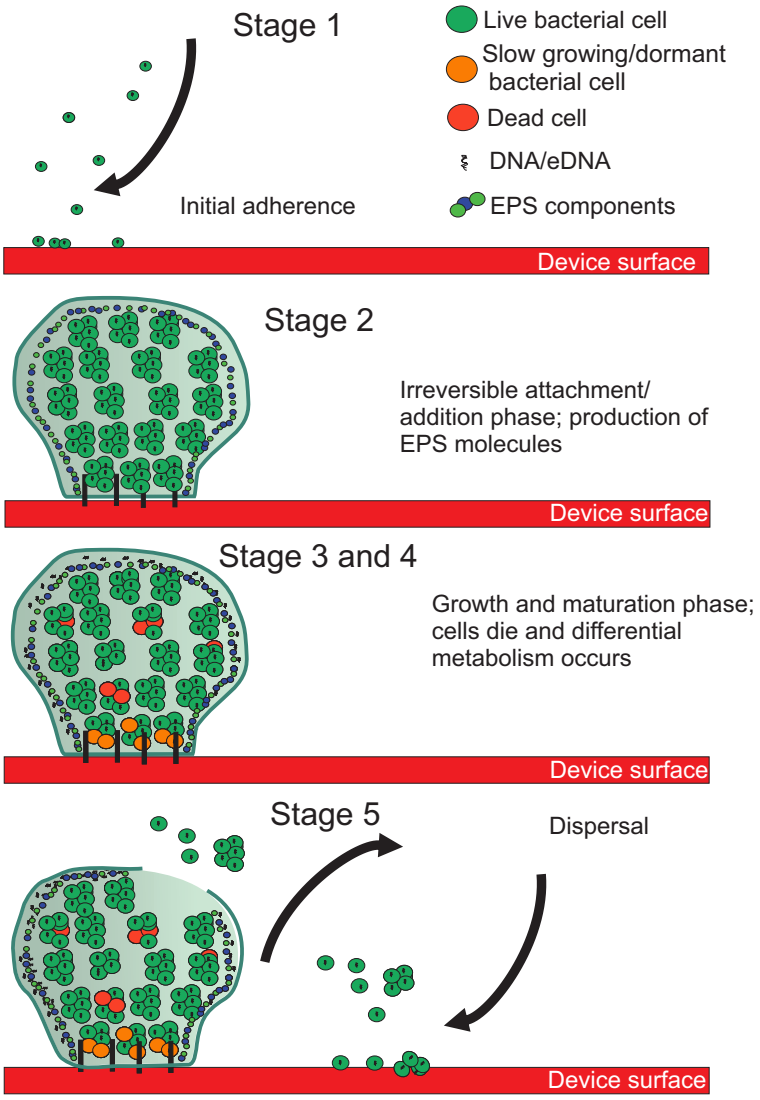

Figure 2.6: Biofilm formation. Initiation and reversible attachment, the addition and microcolony formation phase, maturation and cell death phase followed by the final dispersal stage.

2.3.2.4 Dispersal

The fifth and final stage of the cycle is dispersal or shedding of bacteria or groups of bacteria or microcolonies which are able to colonise new niches (Donlan, 2001; Prassana

and Doble, 2008; Hall-Stoodley et al., 2004). For staphylococcal biofilms dispersal is mediated by accessory gene regulator, arg, production of proteases, nucleases and modulins (Fey, 2010; Boles and Horswill, 2011). Dispersal of the biofilm may explain how chronic infection develops into periodic acute episodes (Donlan, 2002).

The time scale for biofilm formation is dependant on the properties of the device surface, the physical, chemical and biological characteristics of the overlying fluid, the flow rate of the fluid and the fluid shear stress at the solid surface interface and the concentration and species of bacterial cells within the fluid can all be important in determining the rate of cell attachment (Donlan, 2001; Hall-Stoodley et al., 2004; Costerton and Lewandowski, 1995; Donlan, 2008). Thus, the mechanisms necessary for different types of bacteria to form biofilms may differ but the pattern they follow to form the biofilm are similar. Evaluation of the steps in biofilm formation in respect to the environment that bacteria encounter within CVCs are important in understanding biofilm related infection.

2.3.3 Factors that may influence biofilm formation

Biofilm formation studies have mostly been done under *in vitro* conditions because of the associated difficulties with studying biofilms *in* or *ex vivo* (Section 2.3.3.1). Biofilm formation using *in vitro* methods may result in variations compared to biofilm formation *in vivo* there are also difference in biofilm formation between different organisms (Section 2.3.3.2). The *in vitro* biofilm formation studies may not necessarily be directly related to CVCs but they may enhance the understanding and indicate required *in vivo* studies. Thus, to account for all possible influences the environment within CVCs may have on biofilm formation both *in vitro* and clinical studies into biofilm formation are discussed. The factors from *in vitro* and *in vivo* (or *ex vivo*) studies that may influence biofilm formation on CVCs are considered separately.

2.3.3.1 *In vitro* biofilm formation and possible influence on clinical catheter use

S. epidermidis cells within a biofilm exist in four metabolic states; aerobic, fermentative growth, dead and dormant (Fey, 2010). Slow growing or dormant cells are less susceptible to antibiotic therapy which relies on metabolically active cells to inhibit or kill the bacteria. Slow growing bacteria may be able to re-propagate the biofilm similar to persister cells. So when the symptoms of infection have subsided the infection may re-occur due to the survival of slow or dormant bacterial cells.

Persister cells on the other hand may be a portion of bacterial cells that can also enter a dormant state but the cells are also phenotypically multidrug-tolerant. It has been hypothesised that persister cells can repopulate a biofilm once the patient is no longer administered with antibiotics (Lewis, 2010). When analysing catheter-biofilm colonisation

the time cultures are incubated for could initially result in false negatives due to antibiotics in the catheter. Therefore, standard twelve to twenty-four hour plate counts may need to be extended to 3 or even 4 days.

In addition, there are variants of *S. aureus* called small colony variants (SCVs, *hem B* mutant) which originate by mutations in metabolic genes (Melter and Radojevic, 2010). The *S. aureus hem B* mutant ferments sugars and is slow growing (Proctor et al., 2006; von Eiff et al., 1997). *S. aureus* SCVs are not very virulent but persists due to reduced antibiotic susceptibility (Tubby et al., 2013).

In vitro experiments on both *S. aureus* and *P. aeruginosa* biofilms have shown that glucose may play an important part in biofilm dispersal (Boles and Horswill, 2008, 2011; Parsek and Singh, 2003). When glucose is exhausted from the growth medium of *S. aureus* the accessory gene regulator (agr) system is activated. The activation of the arg system leads to the production of matrix degrading enzymes and surfactants which may cause dispersal (Boles and Horswill, 2011). *P. aeruginosa* was found to have similar phenotype but with different mechanistic pathways (Parsek and Singh, 2003). Dispersal induced by the removal or reduction of glucose may be an important contributory factor in CVCs used for total parenteral nutrition as dispersal may cause the infection to spread or become acute and fatal.

In contrast, high-glucose medium has shown to increase biofilm formation by *Candida* species (Hawser and Douglas, 1994) and has the potential to cause CRBSI in patients receiving total parenteral nutrition (Shin et al., 2002).

Stress on bacteria such as nutrient limitation, host immune responses and antibiotic treatment can lead to activation of mutation mechanisms within bacteria. These mutation mechanisms may cause phase variation and adaptive mutations which leads to genetic changes and may also cause hyperbiofilm-forming phenotypes (Parsek and Singh, 2003). Nutrient limitation could occur due to administrating total parenteral nutrition throughout the night and then stopping it during the day time.

2.3.3.2 Clinical factors influencing biofilm formation

Soon after catheter insertion fibrin sheaths can form around the catheter which can stimulate thrombogenesis and bacterial attachment. Fibrin sheath formation is of particular relevance for staphylococci (Mehall et al., 2002). Thrombus and infection are highly related which can explain the observation that CRBSI numbers go down when catheter locks containing anticoagulants are used (Chittick and Sherertz, 2010). Heparin and urokinase have been used in locks as well as heparin bonded CVCs to reduce thrombus. Heparin has the most evidence of reducing CRBSIs and catheter colonisation (Abdelkefi et al., 2005).

Using an animal model, Mehall et al. (2002) showed that the presence of a fibrin sheath significantly increased the chances of catheter related infection. By using a rat model where the animals were inoculated with *S. epidermidis* or *Enterobacter cloacae* at either day 0 (no fibrin) or day 10 (fibrin group) after catheterisation. It should be noted that in this study the rats were inoculated by a tail injection with a 1 ml bacterial suspension of 1 x 10^8 colony forming units. A 1 ml suspension of 1 x 10^8 CFUs is a high concentration for a 200 g rat and may be unrepresentative of a clinical situation. The rat-fibrin sheath study was also limited to a 3 day post infection period until the animals were euthanised and so may not be generalisable to long-term catheter use.

Biofilms on catheters can either be single or multi-species, usually depending on the dwelling time of the device (Morris et al., 1999). Dwelling time also determines where biofilms form, extraluminal colonisation of CVCs are characteristic of short dwelling time ($<$ 10 days), luminal colonisation predominated in longer dwelling times ($>$ 30 days)(Raad et al., 1993).

All the factors listed above may influence biofilm formation on CVCs and the development of sepsis for patients whom require catheter intervention. What is known about biofilm formation in an *in vitro* system should also be taken into consideration in respect to formation within CVCs.

2.4 Clinical culture diagnostic methods

Currently CRIs are most commonly diagnosed by culture. Microbial culture is the method of multiplying microbial organisms by reproduction in a culture medium under controlled laboratory conditions. In the case of clinical culture the microorganisms are removed from the CVC either by the roll plate method (Section 2.4.1), flushing the inside of the catheter (Section 2.4.2) and lastly culture by sonication (Section 2.4.3) before being plated onto an agar plate. The type of agar plates used will depend on the organisms expected to be isolated, most often blood agar is used as the most fastidious organisms grow on blood plates (Kristinsson et al., 1989). There are 3 different plating techniques to consider. Usually removing the biofilm bacteria from the catheter involve either a nutrient broth or buffer. The nutrient broth or buffer is then either mixed into molten agar (pour plate method), spread across an agar plate using a wire loop (streak plate method) or is dropped onto agar plates using the drop plate method (Herigstad et al., 2001). The drop plate method involves dropping a small amount of the liquid containing the bacteria onto the agar plate. After plating the biofilm bacteria the petri-plates are incubated at 37 ^oC, 5% CO_2 for a minimum of 12 hours.

2.4.1 The roll plate method

The semi-quantitative roll plate method remains the most commonly used diagnostic culture test for CRIs due to being easier to use and less time consuming. The tip of the catheter (4 to 5 cm in length) is rolled across an agar plate back and forth four times with a slight downward pressure (Kristinsson et al., 1989).

2.4.2 Flushing the inside of catheters

Quantitative flushing requires the lumen of the catheter tip (first 4/5 cm) to be flushed with nutrient broth. The flushed nutrient both is then mixed with molten nutrient agar and poured into a petri-dish or serial dilutions are made followed by surface plating (Kristinsson et al., 1989; Sherertz et al., 1997).

2.4.3 Culture after sonication

Quantitative culture after sonication requires the tip of the catheter to be inserted in buffer, sonicated for a determined period of time before either using the drop plate method, mixing the sonicate with molten nutrient agar or plated using a wire loop (Kristinsson et al., 1989; Sherertz et al., 1990; Herigstad et al., 2001)

2.5 Research detection methods

Microscopy biofilm detection methods are commonly used in research and include techniques such as confocal laser scanning microscopy (CLSM) and scanning electron microscopy (SEM).

2.5.1 Confocal laser scanning microscopy

The confocal laser scanning microscope (CLSM) has become an important instrument in biofilm research. CLSM is higher resolution compared to conventional light microscopy and can produce blur-free images of thick specimens at various focal depths. Single images are taken at different depths (z stacks) and are reconstructed with a computer algorithm. Using the microscope, a laser produces electromagnetic radiation (incident light) that passes through an excitation pinhole, which is reflected by a dichroic mirror which selects a specific wavelength (Fig 2.7). The excitation light is then focused by objective lenses and scans across the specimen to generate an optical section (Muller, 2006; Paddock, 1999).

In the specimen, the excitation light is absorbed by a fluorophore (either natural or from a stain) causing an electron to enter an excited state (higher energy level) (Palmer and Sternberg, 1999). The electron drops back down to its stable lower energy ground state and loses the energy which was absorbed to emit a photon of light (Lichtman and Conchello, 2005). The emitted light or fluorescence is directed in random and has a longer wavelength compared to the excitation wave. The fluorescence is focused back onto the objective which directs it to the detector pinhole aperture. The pinhole excludes fluorescence above and below the sample focal plane (out of focus light) thus producing a sharp image (Paddock, 1999).

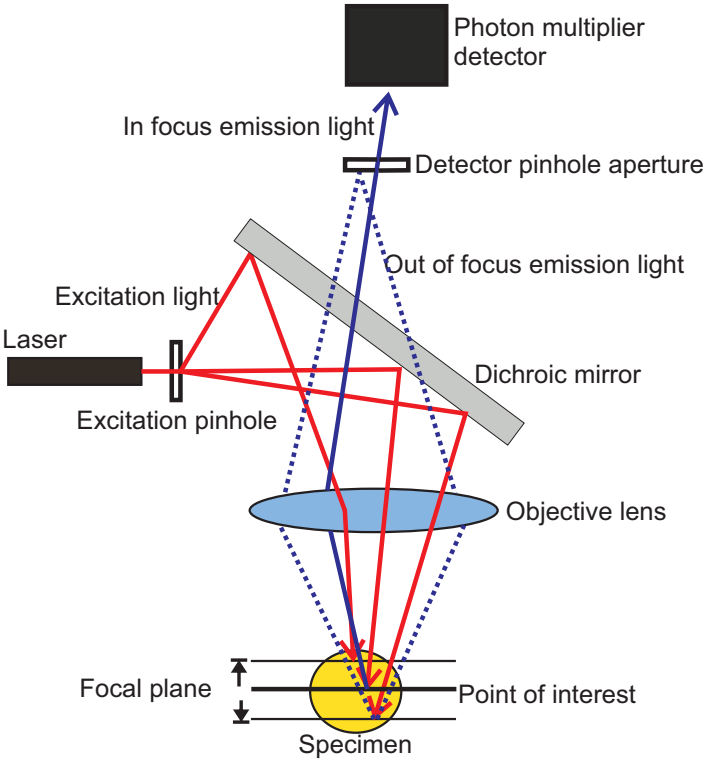

Figure 2.7: Schematic of how a confocal laser scanning microscope works. A laser produces light that passes through a pinhole after which the light is reflected by a dichroic mirror that selects a specific wavelength. The light is focused by an objective lens onto the specimen. The specimen absorbs the light and emits a photon of light. Emitted or fluorescence light is focused by an objective to the detector pinhole which selects fluorescence of interest in the focal plane.

2.5.2 Scanning electron microscopy

Modern electron microscopes can magnify objects up to two million times and is the most frequently used conventional method for visualising biofilms in catheters (Dobbins et al., 1999; Franson et al., 1984; Hachem et al., 2009). In contrast to CLSM that uses light, SEM uses electrons. A beam of high speed electrons are produced by an electron gun in vacuum (Fig.2.8). The electron gun contains a filament or electrode that is heated by

passing a current through. The cathode emits an electron cloud which is repelled from a cathode which contains a hole that leads to an anode plate to which the electrons are attracted to. This mechanism not only produces electrons but will allow the electrons to gain enough speed to produce an electron gun. The speed to the electrons is controlled by the amount of accelerating voltage is applied to the cathode and anodes.

The electrons come out of the gun in a spray pattern. In order to produce an incident electron beam a series of electromagnetic lenses. The amount of electrons travelling through the column is controlled by a condenser lens. Increasing the amount of electrons (or beam diameter) gives better signal to noise ratio but reduces the resolution. Finally, the objective lens focuses the beam onto a spot in the samples to scan across the sample.

A series of lenses control the diameter of the beam and focus on the specimen. The electron beam interact with atoms within samples resulting in energy exchange. The energy exchange results in reflected electrons or electromagnetic radiation which can be collected by a detector to produce an image.

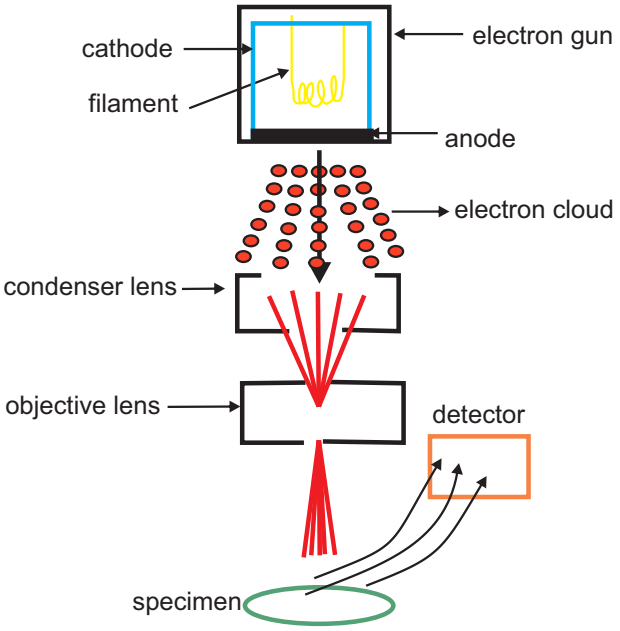

Figure 2.8: Schematic of how a scanning electron microscope works. An electron gun produces high speed electrons that passes through a condenser lens that controls the amount of electrons. The electron beam is then focused onto the specimen by the objective lens. The electron beam interact with the atoms in the specimen resulting in reflected electrons or electromagnetic radiation that is collected by the detector to produce an image.

2.6 Radiography

Conventional radiography (x-rays) is mainly used in medical diagnostics which include areas such as orthopaedics (fractures), dental (cavities), gastroenterology (barium swallow) as well as for catheter placement (Section 2.6.4).

2.6.1 X-rays

X-rays, like visible light, are a form of electromagnetic radiation. Similarly each x-ray photon has an associated energy E, which is proportional to its frequency (v) or wavelength (λ):

$$E = hv = \frac{hc}{\lambda} \tag{2.1}$$

related by the Planck constant (h, 6.63×10^{-34}J/s) and speed of light (c, 3×10^{8} m/s). But typically x-ray energy is expressed in units of electron volts (eV), where 1 electron volt is equal to 1.602×10^{-19} Joules, which is equal to the amount of energy gained or lost by an electron as it travels across an electrical potential of 1 volt.

X-rays are emitted by electrons that undergo an energy loss, occurring either when electrons transition between electron shells within an atom, or when electrons experience sudden deceleration. In both scenarios x-ray production is achieved when a target material is subjected to bombardment with high speed electrons(Hsieh, 2009).

There are two different types of x-ray radiation which can be produced in three different ways. The first type of x-ray radiation is produced (Fig. 2.9) when a high speed electron collides with an electron from an inner electron shell orbiting the atom, the inner shell electron is liberated. The empty orbital that was occupied by the liberated electron is filled with a lower energy electron from an outer shell. The energy difference created by the higher and lower energy electron transition produces characteristic x-ray radiation. Each element within the periodic table has unique shell energies, therefore x-rays produced by electron shell transitions are unique to each element and show up as distinct peaks on an x-ray emission spectrum(Ritman, 2004).

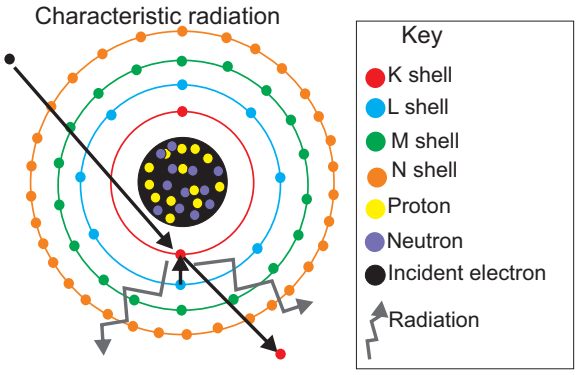

Figure 2.9: Characteristic radiation production. Electrons occupy orbits within specific quantized energy levels; the energy of characteristic radiation is the difference between the binding energy of the released inner shell electron (higher binding energy shell due to proximity to nucleus) and the binding energy of the spaced filled with the outer electron (lower binding energy shell).

The second type of radiation is produced when an electron passes close to the nucleus without a collision, the electron experiences electrostatic attraction towards the nucleus which causes electron deceleration. Kinetic energy loss by the electron produces Bremsstrahlung radiation (Fig.2.10).The amount of x-ray radiation emitted is determined by the amount of kinetic energy lost by the electron which in turn is depended on the electrostatic attraction between the incident electron and nucleus. Electrostatic attraction depends on the charge number (atomic number) of the nucleus and the distance between the passing electron and nucleus. Closer passes and elements with higher atomic numbers will produce higher energy x-rays (Ritman, 2004). This type of radiation is accountable for white radiation. Bremsstrahlung radiation can also be produced if a high speed electron directly collides with the nucleus of an atom. The electron experiences a complete loss of kinetic energy and the entire energy appears as Bremsstrahlung radiation .

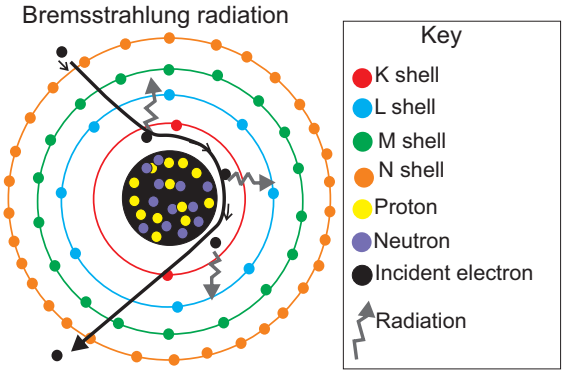

Figure 2.10: Production of Bremsstrahlung radiation. When the electron hits the target material or passes close to the nucleus the electron loses kinetic energy which transforms into Bremsstrahlung radiation .

2.6.2 X-ray production for imaging

Following Fig. 2.11 x-rays produced for soft tissue imaging are mostly composed of Bremsstrahlung radiation. A filament within the cathode is heated to release electrons. Electrons are accelerated within a vacuum by applying an electrical potential between the cathode and anode. The electrons move away from the negative cathode towards the positive anode. The positive anode attracts the electrons and serves as the target material. Collisions between the electrons and the anode result in x-ray emission. Emitted x-rays are focused towards a detector. Samples are placed in the focal path between target material and detector.

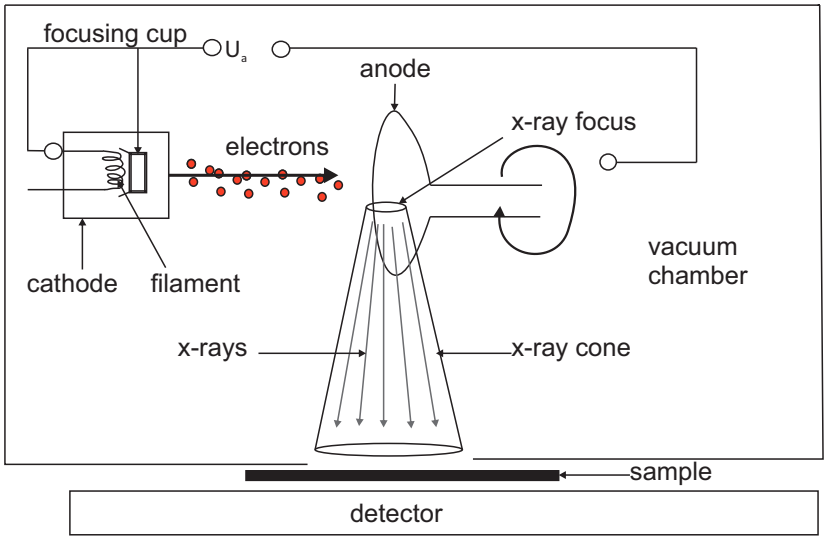

Figure 2.11: X-ray production for imaging

2.6.3 The interaction of x-rays with matter

Samples that absorb x-rays appear as bright objects on radiographs, while samples that do not absorb x-rays appear dark on radiographs. To obtain images with high contrast it is necessary to ensure that a material with suitable x-ray attenuation is selected. The attenuation of x-ray photons by materials occurs via three primary mechanisms, the photoelectric (or photoabsorption) effect, the Compton effect, and through coherent (or Rayleigh) scattering. The probability of each of these effects occurring is related to the energy of the x-ray photons as indicated by Fig. 2.12, the atomic numbers of the elements in the material as well as the thickness and density of the material.

At very low keV the photoelectric effect followed by Compton scattering has the highest probability of occurring (Fig. 2.12). When coherent scattering occurs, the x-ray photon passes through the material without energy transfer (Rockett and Wang, 2009). Coherent scattering is thus a minor contributor to x-ray attenuation by a material.

In contrast, for the photoelectric effect the energy from x-ray photons can be completely absorbed by electrons close to the nucleus of the atom (Rockett and Wang, 2009; Simpkin, 1999). Typically, the electrons are supplied with enough energy to be emitted causing ionisation of the material atom. The atom returns to a neutral state and in doing so emits an x-ray photon characteristic of the atom, which does not travel far enough (and is reabsorbed) to affect production of the radiograph. The photoelectric effect provides the best contrast in radiographs as the energy of the incoming x-ray photon is totally absorbed.

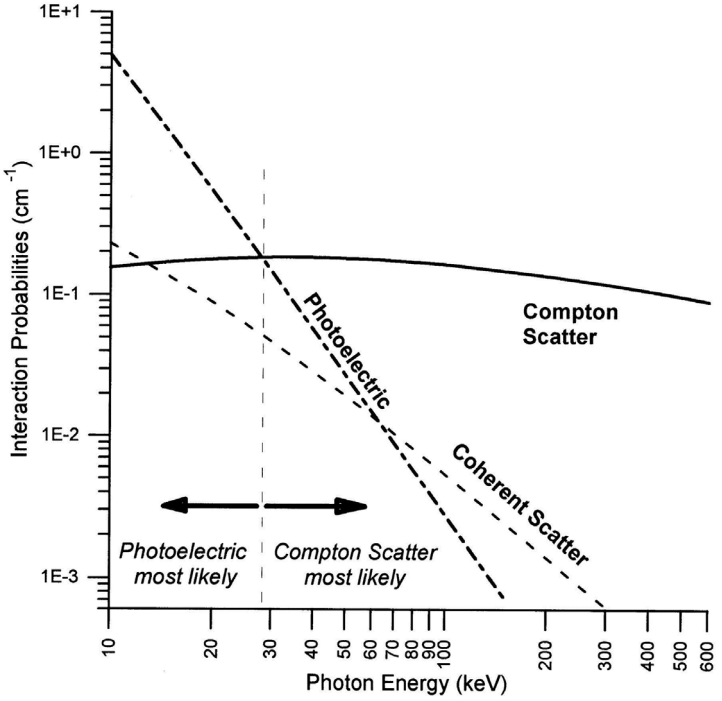

Figure 2.12: The probability of coherent scattering, photoelectric effect, and Compton scattering interactions in water (reproduced from Simpkin 1999).

By selecting atoms with a higher atomic number and subsequently more tightly bound electrons, image contrast can be increased. The photon energy required to maximise the probability of the photoelectric effect must be higher than the binding energy of the innermost electron shell surrounding the atom. However increasing the photon energy much beyond the binding energy of the innermost electron shell can actually reduce the probability of it occurring and consequently reduce contrast.

In Compton scattering, higher energy x-ray photons are scattered by the electrons in lower energy shells within the material. The electrons that interact with the incoming x-ray photons are liberated from the atom (so-called recoil electrons) by absorbing a small amount of the kinetic energy from the photons. The scattered x-ray photon can proceed to be scattered further which can lead to the effect of reducing the contrast and sharpness of the radiograph. Materials with low atomic numbers are more susceptible to Compton scattering as the binding energies of the electron shells are lower. Compton scattering can be reduced by algorithmic correction.

2.6.4 Radiography on CVCs

CVC materials are manufactured to be visible by x-rays to locate the material using photon imaging based methods should detection *in vivo* be required. The radiopaque substances embedded within the catheter materials adds another level of complexity and needs to be considered before using μCT to detect biofilms on CVC material surfaces. Different catheter manufacturers use assorted radiopaque materials and embed the substances within the catheters. Examples of catheter patents by various CVC manufacturers (Cook, Baxter) indicate that barium sulphate, bismuth subcarbonate and bismuth tricarbonate are commonly used to radio-pacify catheters for x-ray detection (Drewes and Parker, 1994; Becker and Pham, 1984). Improved radiopaque tips have also been patented which uses layering of platinum and nickel between the flexible catheter material (Pedersen and Peiffer, 2001).

Correct catheter tip positioning is important to avoid catheter migration into the heart (Vesely, 2003). An example of a situation where an x-ray was needed is highlighted in a case report by Orme et al. (2007). During an elective bimaxillary osteotomy of a 20 year old female a PICC was inserted for central venous pressure monitoring during surgery. The patient's haemoglobin levels were found to be low, after which a single unit was administered via a peripheral cannula. The patient's potassium serum dropped and potassium chloride (44 mmol diluted in 100 ml sodium chloride 0.9%) was administered over a period of 2 hours using the PICC. Thirty minutes later an elevation on the electro cardiogram (ECG) was noted and the patient complained of shoulder pain. The ECG results were consistent with a myocardial infarction. After various interventions over 4 days the treatment was unsuccessful and the patient died. Post-mortem examination confirmed death as a result of cerebral hypoxia caused by a cardiac arrest. Analysis of the pericardial fluid identified that the migration of the PICC resulted in the administration of potassium-rich fluid into the pericardium which lead to the cardiac arrest and accidental death. Due to the occurrence of the preventable death of the patient the authors recommend that chest radiography should be mandatory before fluid is administered through a catheter (Orme et al., 2007).

Therefore, the radiopaque substances embedded within the catheter wall are needed to correctly place CVCs. But to enable biofilm detection, contrast enhancement is required to differentiate between the catheter wall, biofilm and fluid phase. Therefore, the relative x-ray attenuation of the catheter needs to be compared with the x-ray attenuation of the metal stained biofilm. However, CVC manufacturers do not disclose the radiopaque substance within the different catheter types, thus the x-ray absorption has to be dealt with on a case by case basis.

2.7 Aims and objectives

The aim of this project is focused around biofilm detection methods within central venous catheters. There are four specific objectives discussed, the first and second in Chapters 3, 4 and 5, the third objective is explored in Chapter 6 and lastly the fourth in Chapter 7. The first objective is to map where biofilms form in clinical catheters. Using culture, confocal laser scanning and scanning electron microscopy imaging techniques, biofilm distribution will be examined to investigate whether deposition occurs mostly at the catheter tip, or further along the catheter line.

The second objective is to determine whether biofilms are culturable from clinical samples. Clinical culture results will be compared to confocal laser scanning microscopy and scanning electron microscopy to establish whether culture is a reliable biofilm detection method. By exploring the various detection methods results may lead to an increased understanding in the detection techniques to improve upon diagnostics.

The third objective is to determine and develop a protocol for a positive contrast stain for x-ray micro computed tomography. Staining methods will be developed to distinguish between the catheter material surface, liquid and biofilm. Contrast agent selection will be determined by using energy dispersive x-ray analysis to determine which agents will bind and be retained best within biofilm components.

The fourth and final objective is to develop x-ray micro computed tomography to detect *in vitro* grown *S. epidermidis* and clinical biofilms within CVCs non-destructively. Scanning electron microscopy will allow for validation of the x-ray μCT results.

Chapter 3

Microbial culture to detect biofilms

3.1 Introduction

The most common method used to confirm a suspected catheter related bloodstream infection (CRBSI) is to remove and culture the catheter. However, the detection and diagnosis of biofilm bacteria in central venous catheters (CVCs) using culture are difficult and problematic. Culture cannot distinguish between planktonic and biofilm bacteria. Biofilms may not be recovered using conventional culture. The detection rate may be low due to slow growing bacteria and residual antibiotics in the catheter that may initially inhibit growth leading to false negatives (Zandri et al., 2012). In addition, there are currently no bloodstream markers to specifically detect biofilm bacteria. Therefore, diagnosing CRBSIs by drawing blood through the CVC may not be reliable to recover sufficient biofilm bacteria for a 5:1 ratio to peripheral blood culture (Section 2.2.3.1) (O'Grady et al., 2011). In addition, drawing blood through the catheter limits bacterial recovery to the lumen only (Raad and Bodey, 1992). Currently all direct and indirect clinical biofilm CRI diagnostic methods are based on culture and will be discussed separately. The most commonly used method is the roll plate method (Curtis, 2009; Mermel et al., 2009, 2001), (Section 2.4.1), followed by quantitative flush or sonication culture (Sections 2.4.2 and 2.4.3).

3.1.1 Roll plate

The roll plate method (described in Section 2.4.1) is the most common clinical diagnostic method used in hospitals. However, the method only samples the external surface of the catheter which would be adequate for a recently inserted catheter. In addition, the external surface of the catheters are more likely to be colonised when indwelling for less than 15 days (Crump and Collignon, 2000; Mermel et al., 2001; Raad et al., 1993).

3.1.2 Quantitative sonication or flushing

For long term catheters (>30 days) suspected of infection, quantitative culture by sonication and vortex should be used as the technique samples the inside and the outside of the catheter lumen (Crump and Collignon, 2000). Quantitative culture of the catheter segment requires either flushing the segment with broth, or vortexing, or sonication of the sample in buffer, followed by serial dilutions and surface plating on blood agar. Flushing the catheter section using broth or buffer through the lumen allows for bacteria recovery in the lumen (Kristinsson et al., 1989). Using quantitative culture, a yield of 10^2 CFU from a catheter is indicative of catheter-related infection (or colonisation)(Chittick and Sherertz, 2010). When Raad et al. (1993) compared the toll plate method and culture by sonication, they revealed that sonication had a much higher sensitivity (65−72%) compared to the roll plate method (42−45%).

According to Kristinsson et al. (1989) flushing was just as effective as sonication. The flushing study showed that the roll plate method was not sufficient for diagnosing infection (Kristinsson et al., 1989). But the flushing culture method would not be appropriate for all types of infection because short term catheters are more likely to be colonised on the outer surface which flushing misses and may thus result in false negatives. In addition, using broth to flush catheters may cause enhanced growth and would increase the risk of contamination (Mermel et al., 2001). Growth within the media before dilutions and plating on solid agar could lead to unreliable results (artificially high CFUs) and false-positives (contamination). So if the lab is not equipped with a sonicator, buffer should be used as the flushing medium.

In contrast, Raad and Bodey (1992) showed that culture after sonication was found to be the most sensitive in predicting CRBSIs. Sonication recovers bacteria from the lumen and the outer surface of the catheter, therefore can be used for short and long term catheters as well as exit site- and catheter related bloodstream infection. Using the roll plate followed by the flushing method in combination would have to be used when dealing with short and long term catheters respectively if sonication is not possible. But even then, if the source of bacteria is due to contaminated infusion therapy, biofilm may form in the inner lumen of a short-term indwelling catheter.

But regardless of the type of CVC culture used, all methods are highly susceptible to false negative results. Residual antibiotics, viable but non culturable and slow growing biofilm bacteria may all contribute (Zandri et al., 2012; Raad et al., 1993).

3.2 Experimental approach

The goal of the current chapter was to estimate the incidence and distribution of biofilms in clinical catheters in adult and paediatric oncology patients regardless of whether there was bloodstream infection or not. However, before clinical experiments; *in vitro* experimentation was required to establish the method. A standard inoculum was used to ensure reliability (Section 3.3.3). Once the inoculum was prepared the *in vitro* biofilms were grown in CVCs (Fig. 3.1, Section 3.3.4). A clinical audit was performed to establish the CRI rate at the University Hospital Southampton NHS Foundation Trust (Section 3.3.1). After which clinical CVC (Section 3.3.2 and *in vitro* samples were collected and processed to critically evaluate culture (Section 3.3).

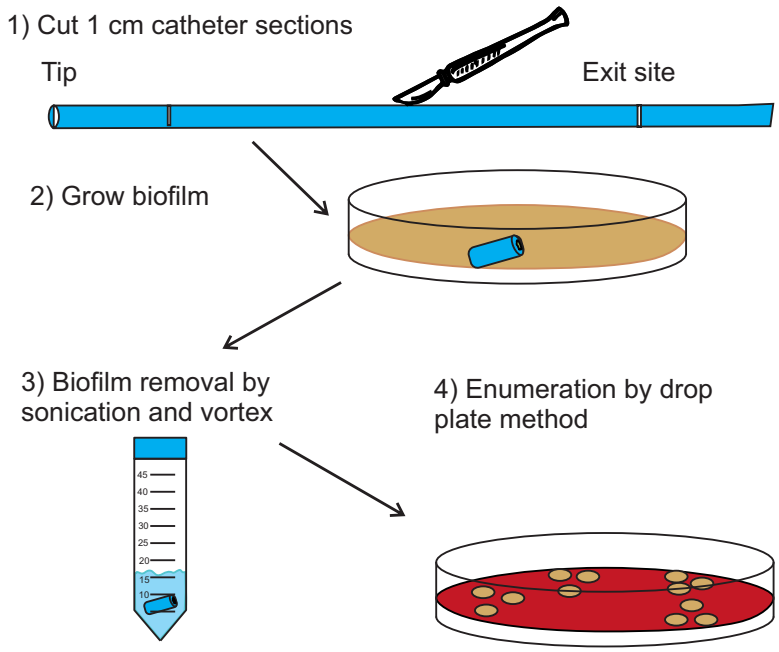

Figure 3.1: Sample processing for biofilm culture and microscopy detection. For *in vitro* experiments all steps were followed whereas for the clinical pilot experiments after sample collection, steps 1, 3 and 4 were followed. (1) showed how pieces were sectioned, (2) how *S. epidermidis* biofilms were grown, (3) biofilm removal by sonication; and (4) enumeration by the drop plate method.

3.3 Materials and methods

3.3.1 Clinical audit

As part of the collaboration with Semprus Biosciences a clinical audit was carried out by Dr. Elizabeth Calton, a National Institute for Health Research (NIHR) academic foundation doctor at the time, to investigate CVC infection rates. The adult oncology audit included PICCs inserted between 11/05/2010 to 30/12/2010 and removed between 26/05/2010 to 30/04/2011 from oncology patients at UHS. The paediatric audit included CVCs inserted between 01/01/2010 to 23/12/2010 and removed between 02/01/2010 to 31/12/2010 from paediatric oncology patients at the University Hospital Southampton.

3.3.2 Clinical pilot study

The initial research plan was to optimise new methods on clinically discarded samples in collaboration with Semprus Biosciences to formalise the protocol and full NHS Research Ethics application to perform a clinical trial on Semprus' patented new CVC technologies. However, after the pilot workup, Semprus Biosciences withdrew from infection research, concentrating on the anti-thrombotic aspect of their new CVC technologies. Clinical and laboratory teams agreed that limited laboratory pilot work could be carried out in this context (i.e. to inform a full ethics application) without formal ethical approval on non-human (i.e. plastic) material that would otherwise have been discarded.

All the samples collected were discarded CVCs removed from patients at the University Hospital Southampton NHS Foundation Trust. As this was a small pilot study, no clinical phenotype information was available.

3.3.2.1 Adult specimen removal and collection

Adult clinical CVC samples were collected from oncology and total pareneral nutrition (TPN) wards as well as from consultants and nurse practitioners from the radiology department. The nurses or clinicians removed the CVC following their standard protocol. The removed CVC was placed on a sterile tray (normal British NHS protocol sterile tray). The CVC which was outside the patient was cut off with sterile scissors and left on the tray for discard. The rest of the CVC was further sectioned into 2 pieces and placed in sterile labelled specimen containers(VWR, UK). Sample pots were stored in a UN-approved collection box for transport to microbiological lab for further processing.

3.3.2.2 Paediatric specimen removal and collection

All paediatric oncology CVCs were removed in theatre under sterile field conditions using the normal surgical protocol. The surgeon removed the CVC exit site dressing and marked on the CVC with a sterile marker approximately 1 cm distal to skin exit site of the line. The CVC was removed from the patient (with or without cut-down to the vein or cuff as clinically indicated) by the surgeon. The proximal segment (indwelling line section) was handed to the sample collector.

If the CVC was clinically indicated for culture, the tip (proximal) end of the CVC (4 cm) was cut horizontally with sterile scissors. The 4 cm section was placed in a sterile leak-proof container and was transported to the HPA (sticker on standard clinical request form). The rest of the catheter was divided into two further sections and placed in containers labelled 2 and 3 respectively to enable identification of proximal and distal ends. Sample containers were placed in a UN-approved container and was transported to the research lab as soon as possible (within 15 minutes) for processing. The present study did not interfere with the routine clinical standard operating procedure (SOP).

3.3.2.3 Clinical specimen transport and storage

Specimens were stored at 4^{o}C prior to transport or before processing if immediate sample manipulation was not possible. Immediate processing was not always possible if multiple lines were collected on the same day; paediatric samples coming from theatres were often 4 lines in the space of an hour. Transport and processing was conducted as soon as possible in a Category 2 hood at room temperature.

3.3.2.4 General clinical sample processing for all CVC types

A sterile field was prepared in a Category 2 hood, consisting of a glass cutting board sterilised with 70% ethanol and sterile forceps (Fig.3.2). The 4 cm tip section, if the tip was not sent to HPA, or the second 4 cm section was further sectioned into 1 cm parts using a sterile scalpel and forceps (Fig. 3.3). The most proximal 1 cm part of each section (of tip, middle or subcutaneous parts of the line for culture) was further subdivided into approximately 2 *mm* slices using a sterile scalpel and forceps. Slices were placed in an Eppendorf tube containing 1 ml of sterile PBS. Sliced sections in PBS were dedicated to culture (Section 3.3.7).

The next most proximal 2 cm part of the line was divided into two 1 cm sections: each placed in fixative for SEM and CLSM (described in Sections 4.3.2 and 5.2.1. The 4th most proximal 1 cm was stored without fixative at -80 ^{o}C for PCR. This method was repeated for the middle and subcutaneous (section just before the line exists the skin) sections.

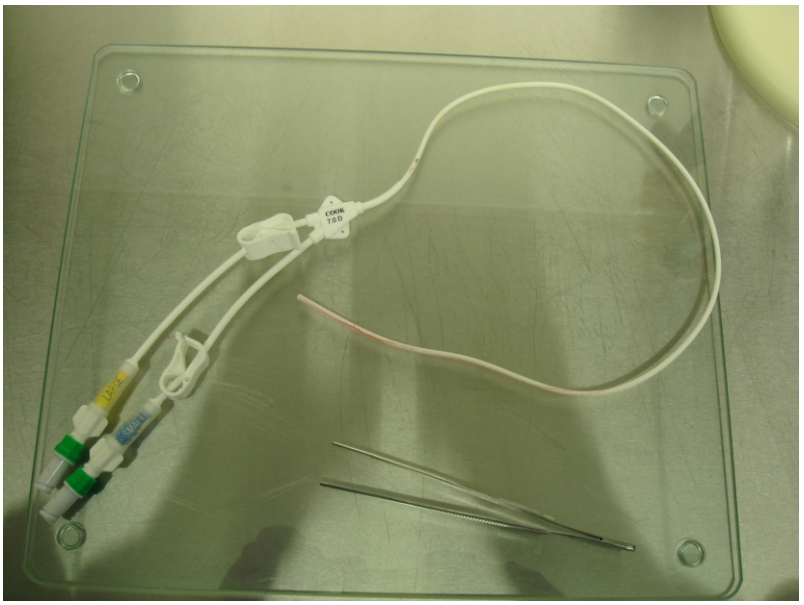

Figure 3.2: A typical PICC removed from patients during the study.

(a) Cuffed CVC

For cuffed sections of CVC (tunnelled lines only), the cuff was divided into two parts at the midpoint. 2× 1 cm segments were cut from the midpoint, one was used for culture as above and the other for SEM as above. Two further 1 cm sections were cut proximal to the cuff for PCR and CLSM.

(b) Tunnelled line subcutaneous section

For the skin exit site sections (for tunnelled lines where the subcutaneous part is not within the cuff section), sections were cut as above but the sectioning started at the distal portion (just before skin exit site) of the CVC when selecting 1 cm sections for the various procedures.

(c) Implanted port

For the port section (subcutaneously implanted CVCs only), the central silicone needle port was removed with a sterile scalpel. The needle port was sectioned vertically into two equal halves (each now semi-circular). One half was further cut into five equal parts for culture by sonication and enumeration by plating as outlined previously. The second section was cut into two halves and placed in fixative for SEM and CLSM. The attached CVC tubing was cut off at the port proximal to the end of the metal internal spur. The most distal 3 cm sections were stored for SEM, CLSM (as above) and a section without fixative at -80 ^{o}C for PCR.

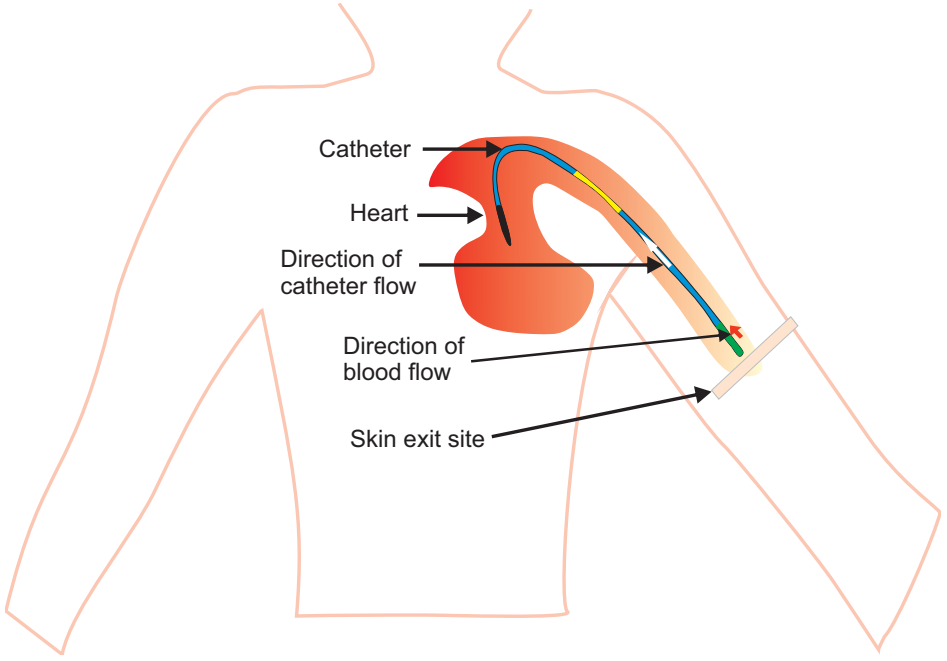

(A)

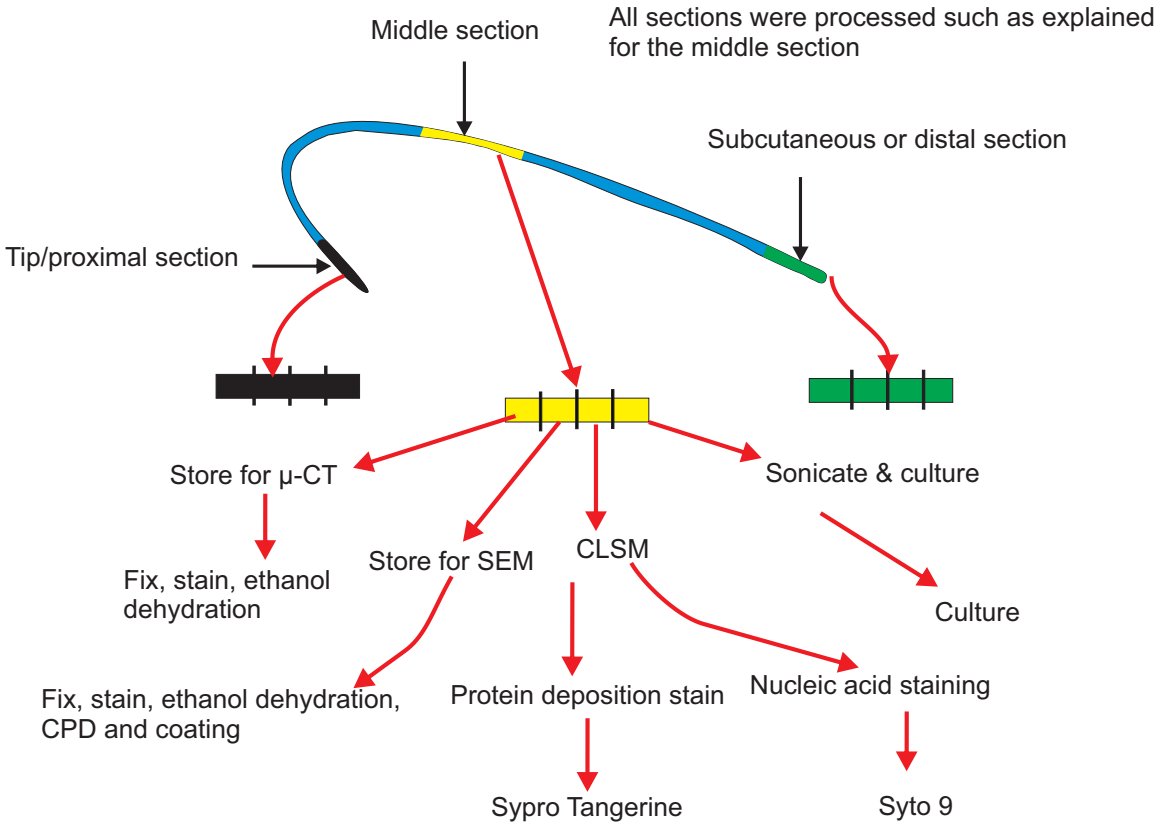

(B)

Figure 3.3: Clinical pilot specimen processing flow diagram. (A) shows the approximate positions of the tip, middle and subcutaneous sections of a PICC. (B) shows sectioning of the CVC for culture, CLSM, SEM or μCT .

3.3.3 *In vitro* inoculum preparation

All *in vitro* experiments were performed according to the following protocol. Aliquots of *S. epidermidis* bacterial stock (ATCC 35984, maintained in 1% peptone and 10% glycerol in phosphate buffered saline at pH 7.2 kept at -80^0C) were taken using a sterile 10 μl inoculation loop and mixing the looped stock with 15 ml sterile tryptic soy broth (TSB) in a 50 ml falcon tube. The overnight culture was incubated under agitation for 12 hours at 37 ^{o}C, 5% CO_2 provided by a shaker in an incubator (Fig. 3.4).

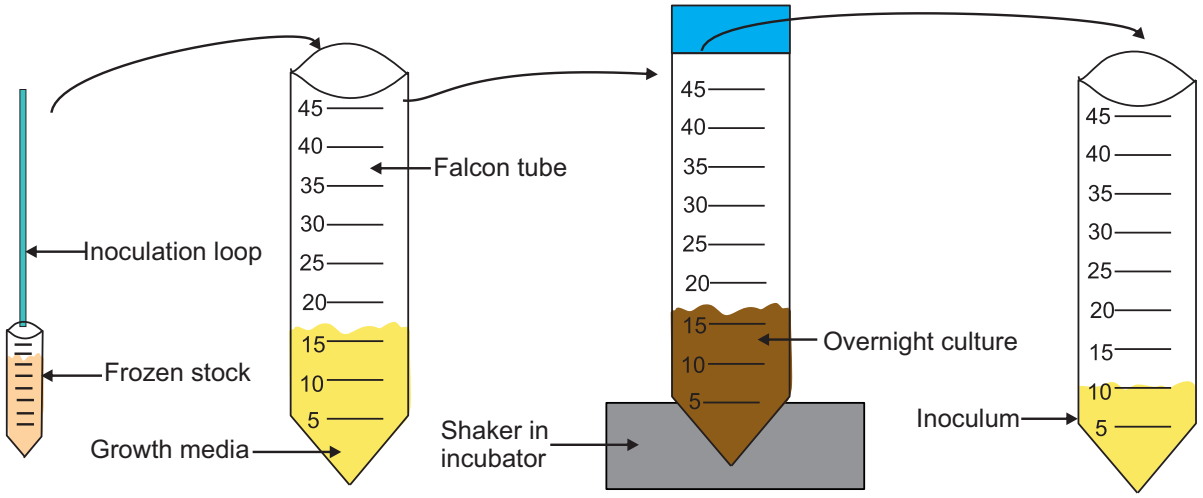

Figure 3.4: Steps to produce the inoculum. An inoculation loop is swirled in frozen stock to pick up a small amount of frozen *S. epidermidis* . The loop is dipped and mixed thoroughly in sterile media. The falcon tube containing the media and released frozen media is placed on a shaker inside a incubator for 12 hours at 37 ^{o}C, 5% CO_2. The overnight culture was diluted by mixing 10 μl into 9.9 ml of sterile TSB to produce the inoculum.

A 12 hour culture from frozen stock produced an overnight culture containing 4.76×10^8 CFUs per ml ($n = 3$). The overnight culture was diluted a thousand times by mixing 10 μl into 9.9 ml of sterile TSB to obtain a starting culture concentration of 4.76×10^5 CFUs per ml in the inoculum.

3.3.4 Growing *in vitro* biofilms

Following preparation of the inoculum, *In vitro* biofilms were grown in Lifecath 5 French polyurethane PICCs (Vygon, UK) using different growth systems depending on the aim of the experiment. Each model growth system was discussed separately.

3.3.4.1 Static *in vitro* CVC biofilm model

Using a sterile scalpel (Fisher Scientific, UK) a CVC was cut into 1 cm sections. CVC sections were injected with the inoculum (from Section 3.3.3) using a sterile needle and syringe. The inoculated sections were placed in the remainder of the inoculum. The immersed CVC sections in the inoculum were placed in an incubator at 37 ^{o}C, CO_2 for a determined time (depending on the requirements of the experiment, Fig.3.5). Thereafter, the CVC sections were either prepared for CFU determination (Section 3.3.6) or for biofilm detection by microscopy (Section 4.3 or Section 5.2).

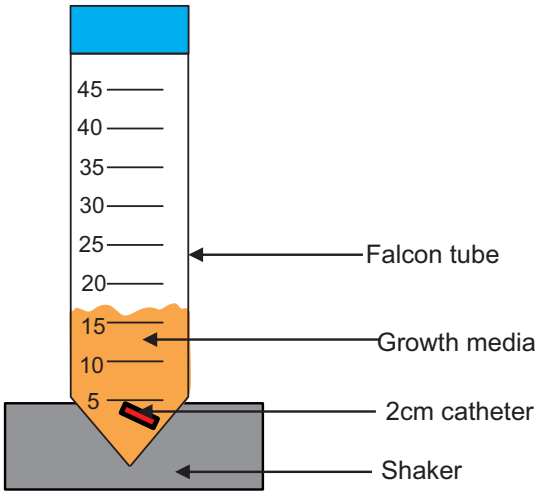

Figure 3.5: Static biofilm-CVC model. A CVC was sectioned into 1 cm sections, inoculated with 4.29 $\times 10^5$ CFUs per ml and incubated in a 50 ml falcon tube containing 10 ml of sterile TSB in a 37 ^{o}C, CO_2 for 24 hours.

3.3.4.2 *In vitro* CVC-flow biofilm model

A CVC-lumen flow model was developed to allow flow on the inside of the lumen only. 60 cm of Lifecath polyurethane, 5 French PICC was attached to 25 cm size 13 silicone Masterflex tubing (Fisher Scientific, UK) attached to a peristaltic pump at 19 revolutions per minute (RPM). The tubing and pump set-up resulted in a flow rate of 1.13 ml per minute through the CVC lumen (Fig.3.6). 100 ml of half strength TSB was used as growth medium. The growth medium was inoculated with 5 x 10^{-5} CFUs per ml as outlined previously. Tubing and growth medium was placed in an adapted incubator at 37 ^{o}C for 5 days whilst the pump was running. Tubing was flushed $\times 2$ with sterile PBS every 12 hours for 5 minutes and replaced with sterile growth medium using the same flow rate. The growth medium bottle was replaced daily. CFU determination (Section 3.3.6) by the drop plate method was performed on the spent media at 24, 48, 72, 29 and 120 hours to check for contamination.

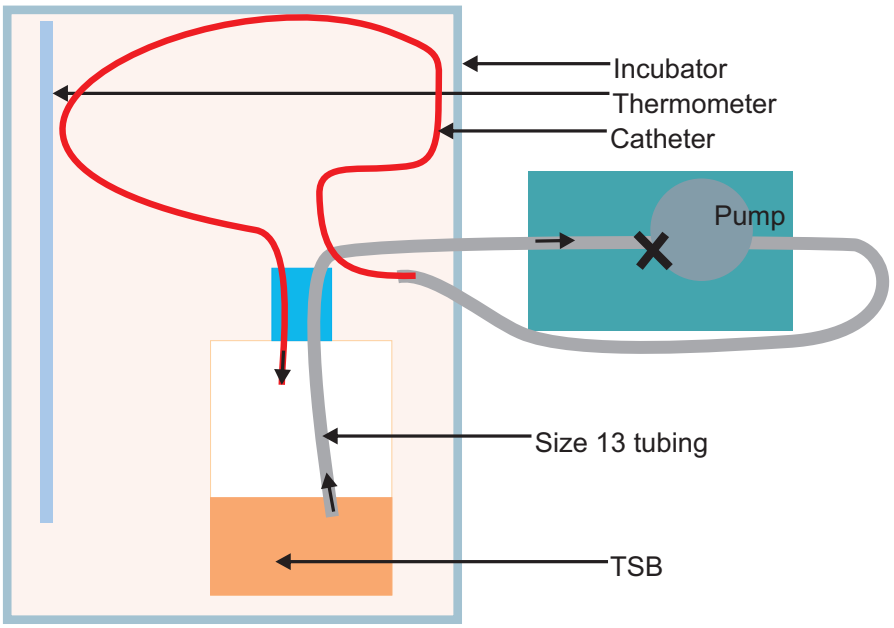

Figure 3.6: Catheter-flow biofilm model with flow in the lumen only. *S. epidermidis* biofilms were grown under flow in a 5 French PICC for 5 days. Tubing and growth medium bottle was kept in an adapted incubator at 37 ^{o}C with flow rate of 1.13 ml per minute.

3.3.5 Sonication for biofilm removal from CVCs

In order to remove biofilms from CVCs grown by using the model methods (Section 3.3.4), the literature indicated that sonication increased CFU determination (Bjerkan et al., 2009). Therefore, sonication optimisation was initially performed and was used to remove and quantify biofilm bacteria from CVC sections for all subsequent experiments.

After the growth period the 1 cm CVC sections (as prepared earlier using the static growth model, see Section 3.3.4.1) were removed from the growth medium and gently rinsed in PBS three times by aspiration. Rinsed samples were sectioned using a sterile scalpel into 1 to 2 *mm* transverse pieces. Sectioned pieces were placed in 1 ml of PBS and were either mixed by vortex (for 10 seconds) or vortexed before and after with either 30, 120, 180 or 300 seconds of sonication (Maplin, UK). The sonicate was serially diluted followed by the drop plate method, incubation and CFU determination per cm of CVC as below (Fig. 3.7 and Section 3.3.6).

Sonication time of 180 seconds was found to recover the highest number of bacteria, and therefore considered the most effective time for removing biofilm from CVCs (Fig.3.8). Statistical tests were performed at 95% confidence intervals (geometric mean $\pm$ SE) n=3 on $\log_{10}$ transformed CFUs per cm (1 cm section in 1 ml PBS) of CVC. There was a statistically significant difference between no sonication and 30 seconds (t-test, two sample two-tail,$P = 0.016$), no sonication and 120 seconds (t-test, two sample two-tail, $P = 0.020$), no sonication and 180 seconds (t-test, two sample two-tail, $P = 0.001$) and

no sonication and 300 seconds (t-test, two sample two-tail, $P = 0.002$). In contrast, there was no significant difference between 30 seconds and 120 seconds of sonication (t-test, two sample two-tail, $P = 0.390$) or 30 seconds and 300 seconds (t-test, two sample two-tail, $P = 0.188$). There was a statistical significant difference between 30 seconds and 180 seconds of sonication (t-test, two sample two-tail, P= 0.04) and between 180 and 300 seconds of sonication (t-test, two sample two-tail, $P = 0.032$). These difference suggested that 180 seconds of sonication was most efficient for recovering colony forming units from 1 cm of CVC (Fig.3.8). Accordingly, all subsequent CVC culture by sonication and agar plating used a sonication time of 180 seconds.

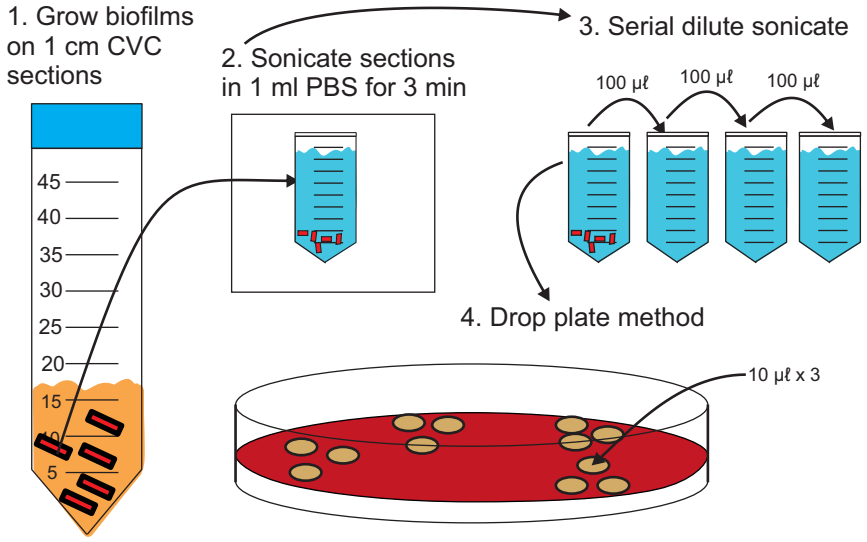

Figure 3.7: Preparation for sonication bacterial recovery from *in vitro* static CVC-biofilm model grown samples.

3.3.6 Bacteria concentration determination

Using the overnight culture (or sonicate) eight 10 fold serial dilutions were made by mixing 100 μl of overnight culture (or sonicate) into 900 μl of sterile phosphate buffered saline at pH 7.2 (PBS) and vortexing before and after every dilution. Dilutions were plated on blood agar plates (Health Protection Agency, UHS, UK) using the drop plate method (Herigstad et al., 2001). 10 μl $\times$3 drops for each dilution were dropped on agar plates and incubated for 12 hours at 37 ^{o}C, 5% CO_2.

Thereafter, colony counts were performed at the dilutions which produced between 10 to 30 colonies per 10 μl drop (Fig.3.9). The data were used to calculate the colony forming units per ml of the overnight culture. All subsequent experiments were performed to result in the same CFU concentration in the inoculum.

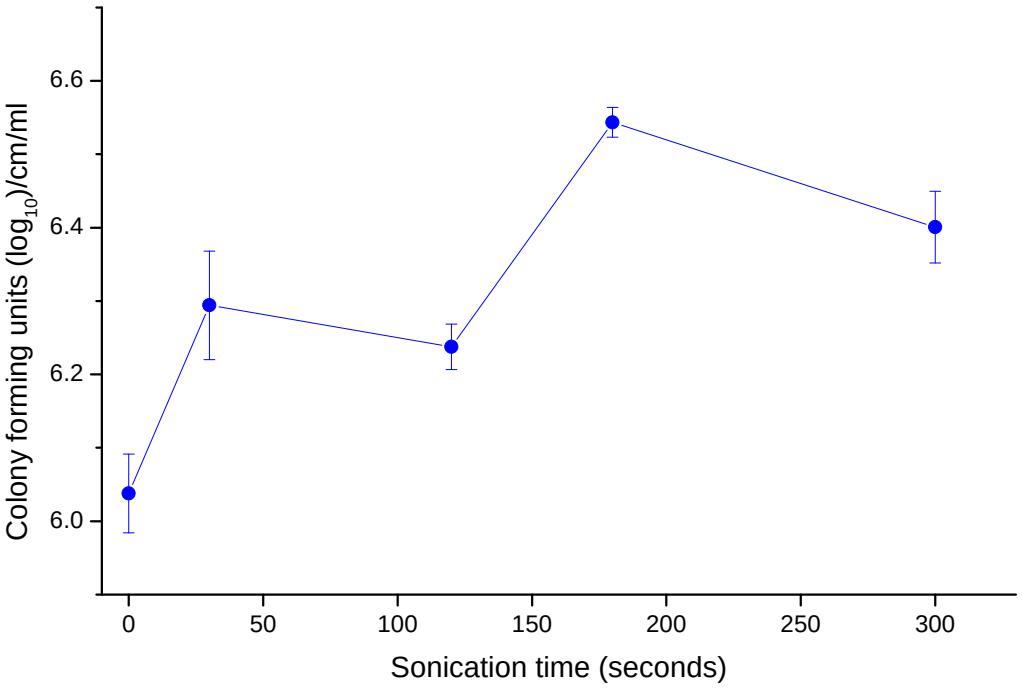

Figure 3.8: Sonication time for *S. epidermidis* biofilm removal from CVCs. The plot indicated that 180 seconds of sonication time was most the efficient for removing 24 hour *S. epidermidis* biofilms from CVCs for enumeration by culture and plating. There was a statistically significant difference between no sonication and 30 seconds (t-test, two sample two-tail,$P = 0.016$), no sonication and 120 seconds (t-test, two sample two-tail, $P = 0.020$), no sonication and 180 seconds (t-test, two sample two-tail, $P = 0.001$) and no sonication and 300 seconds (t-test, two sample two-tail, $P = 0.002$)(geometric mean ± 1 SE n=3).

3.3.7 Clinical culture by sonication

Following clinical sample collection and sectioning (Section 3.3.2) the 2 *mm* sections were placed in a sterile Eppendorf containing 1 ml of sterile PBS buffer. The Eppendorf tube was sonicated for 3 minutes (Section 3.3.5). If the CVC was suspected of infection, $3\times$ serial dilutions were made (if not suspected of infection no dilutions were made). Thereafter, the drop plate method was performed (Section 3.3.6). The agar plates were incubated for 72 hours at 37 ^{o}C, 5% CO_2. Colony counts were performed at 12, 24, 48 and 72 hours.

If a sample was culture positive, a colony was spread on the following agars: Pseudomonas isolation agar, Mannitol salt agar (MSA, Fisher Scientific, UK) and MacConkey agar (MA). If the sample was positive for *S. epidermidis* the Mannitol salt agar would become pink whereas if *S. aureus* was present the agar would turn yellow (Fig. 3.10). Therefore, depending on whether colonies grew on which agars the appropriate identification was made. Gram stain was performed on unknown cultures.

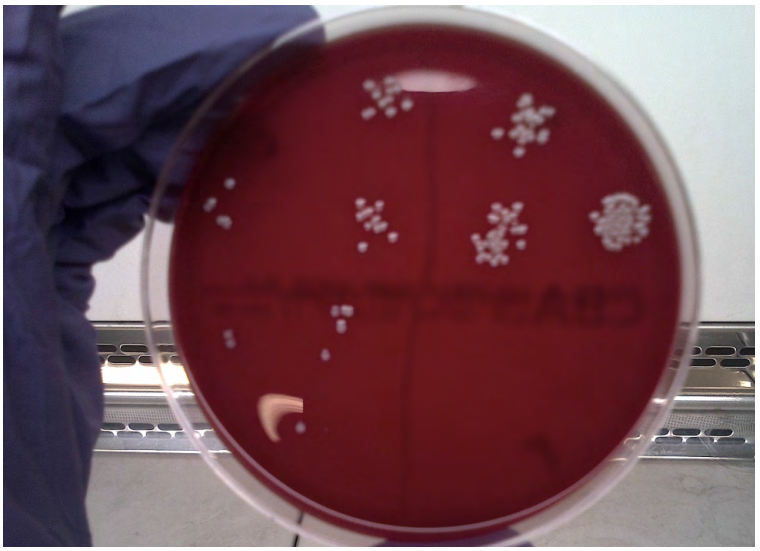

Figure 3.9: Blood agar plate with *S. epidermidis* bacterial colonies 12 hours after plate incubation. Each quarter of the plate represents a dilution factor of 10 and 3 drops of 10 μl each of a particular dilution that was dropped onto the plate.

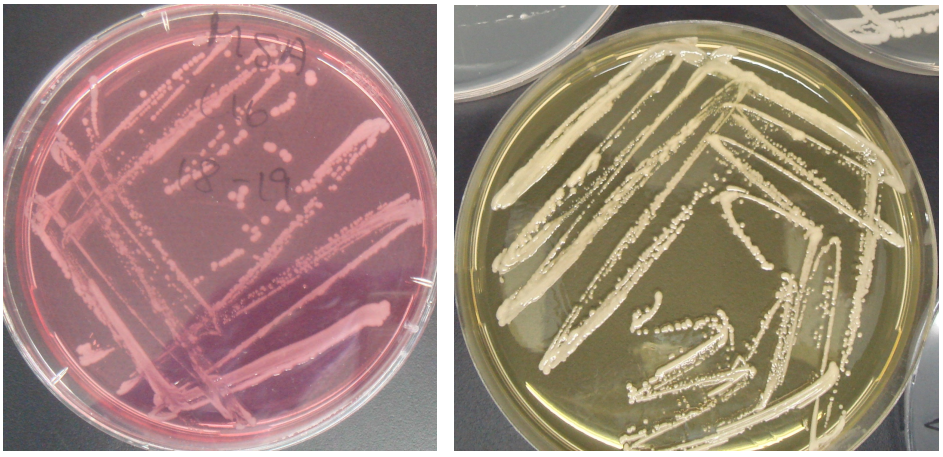

(A) *S. epidermidis* (B) *S. aureus*

Figure 3.10: Pictures of C16 and P6 Mannitol salt agar. (A) showing C16 MSA plate with *S. epidermidis* and (B) P6 MSA plate with *S. aureus* colonies

3.3.7.1 Culture positive

Culture positive was defined as $\geq$25 CFUs per cm of CVC. The culture positive definition was derived from the literature. Quantitative culture was defined as positive for colonisation when CFUs per CVC isolated was $\geq$100 (Mermel et al., 2009; Crump and Collignon, 2000). The most common clinical protocol was to send the CVC tip section (first 4 cm's from the tip) for culture by the roll tip method or flush (Curtis, 2009; Mermel et al., 2009). Therefore, due to only culturing 1 cm (clinical protocol 4 cm) from the tip the culture positive colonisation criterion was altered accordingly.

3.3.7.2 Gram stain

1) Heat fix bacterial smear. 2) Applying a primary stain (crystal violet) to the heat-fixed smear of a bacterial culture. 3) Add iodine, which binds to crystal violet and traps it in the cell. 4) De-colour with alcohol. 5) Counter stain with safranin.

3.3.8 Statistics

When the culture positive difference between the tip, middle and subcutaneous sections were compared, the nonparametric Mann-Whitney test was used because two groups were compared, the data was independent of each other and analysed as ordinal data by ranking as 1 (positive) or 0 (negative). Significant difference was established when the probability value was less than 0.05. The same was done when adult and paediatric culture results were compared (Minitab 16, US).

3.4 Results

3.4.1 Clinical audit

3.4.1.1 Adult audit

The adult oncology audit included 78 PICCs of which 66 were single and 12 double lumen lines. The most frequent indication for PICC insertion was chemotherapy followed by TPN, poor venous access and antibiotics. Average dwell time for the CVCs was 79 days with a median of 70 and mode of 128. Data included 78 PICC insertions (14 only data for insertion), 51 removals and 13 remained indwelling. The most common indication for removal was end of treatment 45%, followed by patient death 21.6%, line replacement 7.8%, blocked, displaced or venous thrombosis 5.9% (Table 3.1) and lastly; suspected ESI and suspected BSI 3.9%. Of the suspected BSI (2 CVCs), 1 was culture positive. Similarly, 2 ESIs only 1 was positive.

3.4.1.2 Paediatric audit

The paediatric oncology CVC audit included 142 CVCs, of which 70 remained indwelling. The average dwell time for the CVCs was 155.2 days with a median of 131 and mode of 365. Data included 142 CVC insertions, 72 removals and 11 assessed CVCs with 70 remaining indwelling. The most common indication for CVC removal was end of treatment 54.2% followed by mechanical failure 12.5%, suspected CABSI 11.1%, death 9.2%, blockage

5.6% and exit site infection 4.2% (Table 3.2). Of the suspected CABSIs CVCs removed 6 out of 8 were culture positive.

Table 3.1: Adult oncology PICC audit data showing type of CVC, indication for insertion

PICC insertions	Total number	Percentage of total inserted (78)
Single lumen (4 French)	66	84.6
Double lumen (5 French)	12	15.4
Insertion indication	Total number	Percentage of total inserted (78, some multiple indications)
Chemotherapy	67	85.9
TPN	5	6.4
Poor venous access	7	9.0
Antibiotics	7	7.0
Uses of line	Total number	Percentage of 78 total (some multiple uses)
Chemotherapy	67	85.9
TPN	4	5.1
Blood products	18	23.1
Antibiotics	26	33.3
Other medications	27	34.6
Removal indication	Total number	Percentage of total removed (51 removed)
Blocked	3	5.9
Displaced/fell out	3	5.9
End of treatment	23	45.1
Replaced with Hickman	4	7.8
Suspected ESI	2	3.9
Of which culture +'ve	1	1.96
Suspected BSI	2	3.9
Of which culture +'ve	1	1.96
Patient died	11	21.6
Venous thrombosis	3	5.9

ESI- exit site infection, BSI- bloodstream infection

Table 3.2: Paediatric oncology audit data indicating CVC types, CVC removal indications and infection rates

Catheter type	Total	Percentage inserted (142)
Port	22	15.6
Tunnelled CVC	116	81.7
PICC	4	2.8
Removal indication	Total removed	Percentage of removed (72)
EOT	39	54.2
Patient died with line	7	9.7
Blocked	4	5.6
Mechanical failure	9	12.5
Suspected CABSI	8	11.1
Proven CABSI	6	8.3
ESI	3	4.2
Other	2	2.8
Infection assessment	Total number	Percentage of assessed (11)
CABSI	6	54.6
Contaminant	1	9.1
Culture -'ve not suspected CRBSI	1	9.1
Culture +'ve ESI	2	18.2
Other source of infection	1	9.1

EOT- End of treatment, CABSI- catheter associated bloodstream infection, CRBSI- catheter related bloodstream infection, ESI- exit site infection

3.4.2 Clinical pilot CVC information

Single lumen CVCs were the most commonly removed adult CVC (95%) (Table 3.3). The most common indication for CVC removal for adult CVCs were also end of treatment (EOT, 52.2%), blockage (23.8%), confirmed bloodstream infection (9.5%, by blood cultures) which was suspected to be related to the CVC, mechanical damage (4.8%), uncomfortable for patient (4.8%) and for exit site infection (4.8%) (Table 3.3). 60% of the oncology CVCs removed were for EOT.

Catheter numbers P29, P30, P32 and P36 were recovered from cystic fibrosis(CF) patients. P29 and P30 was suspected of bloodstream infection, removed from patients but CVC cultures were not requested as blood cultures were positive for *P. aeruginosa*. P29 was left for 2 weeks in a sterile container and P30 for 4 days with no buffer or fixative. Due to length of time both P29 and P30 were left in the container the samples were not cultured and were immediately placed in SEM fix. P32 was removed for end of treatment. P6 was the only line that was removed due to an exit site infection. P36 was removed because

it was uncomfortable for the patient but it was not clinically suspected of infection. Half of the adult CVCs came from oncology patients, followed by 25% from TPN, 21% from cystic fibrosis patients and 5% from medical patients. The medical patient had cellulitis and was of interest because the patient was dressing the CVC themselves.

Table 3.3: Adult patient date removed, clinical area, CVC type and clinical indication for removal

Sample ID	Date removed	Clinical area	Catheter type	Removal indication
P1	31/03/2011	Oncology	Bard SL silicone PICC	EOT
P2	08/04/2011	Oncology	Bard SL silicone PICC	Broken
P3	15/04/2011	Oncology	Bard SL silicone PICC	Blocked
P4	19/04/2011	Oncology	Bard SL silicone PICC	Blocked
P5	27/04/2011	Oncology	Bard SL silicone PICC	EOT
P6	28/04/2011	Oncology	Bard SL silicone PICC	ESI
P7	04/05/2011	TPN	SL polyurethane PICC	Blocked
P9	06/05/2011	TPN	Cook SL polyurethane PICC	EOT
P18	01/06/2011	TPN	Cook SL polyurethane PICC	EOT
P21	15/06/2011	Oncology	Bard SL silicone PICC	EOT
P26	27/07/2011	TPN	Cook SL polyurethane PICC	EOT
P28	12/01/2012	Medical outpatients	Bard SL silicone PICC	EOT
P29	27/02/2012*	Respiratory (CF)	Bard SL silicone PICC	BSI
P30	27/02/2012*	Respiratory (CF)	Cook SL polyurethane PICC	BSI
P31	12/03/2012	Oncology	SL polyurethane Port	EOT
P32	27/03/2012	Respiratory (CF)	Port SL polyurethane	EOT
P33	14/06/2012	Oncology	Bard SL silicone PICC	EOT
P34	14/06/2012	Oncology	Bard SL silicone PICC	EOT
P35	15/06/2012	TPN	Tunnelled Hickman DL polyurethane cuffed	Blocked
P36	18/06/2012	Respiratory (CF)	Cook SL Port polyurethane	Uncomfortable
P38	25/09/2012	Oncology	Cook SL Port polyurethane	Fibrin sheath blockage

EOT- end of treatment, ESI- exit site infection, TPN- total parenteral nutrition, BSI- bloodstream infection, PICC, peripherally inserted CVC, SL - single lumen, DL - double lumen, CF - cystic fibrosis

The most common CVC type removed from paediatric oncology patients (Table 3.4) were tunnelled CVCs 48%, followed by leader cuffs 26%, ports 17% and Hickman CVCs 9%. These CVCs were all removed during surgery. End of treatment was the most frequent indication for CVC removal (82.6%), followed by migration (13%) and exit site infection (4.4%).

Table 3.4: Paediatric patient oncology information, date removed, CVC type and clinical indication for removal.

Sample ID	Date removed	Catheter	Indication for removal
C1	14/04/2011	Port	End of treatment
C2	28/04/2011	Tunnelled	End of treatment
C3	28/04/2011	Tunnelled	End of treatment
C4	05/05/2011	Port	End of treatment
C5	05/05/2011	Tunnelled	End of treatment
C6	19/05/2011	Hickman	Exit site infection
C7	19/05/2011	Hickman	End of treatment
C8	19/05/2011	Leader cuff	End of treatment
C9	19/05/2011	Port	End of treatment
C10	26/05/2011	Tunnelled	End of treatment
C11	02/06/2011	Tunnelled	Migration
C12	02/06/2011	Tunnelled	End of treatment
C13	02/06/2011	Tunnelled	End of treatment
C14	02/06/2011	Port	End of treatment
C15	09/06/2011	Tunnelled	Revision
C16	09/06/2011	Tunnelled	End of treatment
C17	16/06/2011	Leader cuff	End of treatment
C19	14/07/2011	Tunnelled	End of treatment
C20	14/07/2011	Tunnelled	End of treatment
C21	28/07/2011	Leader cuff	Revision
C22	28/07/2011	Leader cuff	End of treatment
C23	28/07/2011	Leader cuff	End of treatment
C24	28/07/2011	Leader cuff	End of treatment

Note, all composed of polyurethane and brand of CVCs were unknown.

3.4.3 Clinical culture by sonication

Only 4 of the 18 adult PICCs that were cultured was positive (excluding P29 and 30, Table 3.5). Of the 4 positive CVCs, 1 was positive for all sections, 2 were positive for tip and subcutaneous sections and 1 was positive at the subcutaneous region only. One (P32) of the positive CVCs were from a CF patient and 3 from oncology patients. The culture

positive variations for adult CVCs between the different sections (tip and subcutaneous) were not statistically significant (Mann-Whitney at 95% CI, $P = 0.695$, Fig. 3.11).

Table 3.5: Colony forming units/ml per cm of CVC recovered from tip, middle and subcutaneous regions from adult patients

Sample ID	CFU/cm/ml		
	Tip	Middle	Subcutaneous
P1	67 *S. epidermidis*	133 *S. epidermidis*	267 *S. epidermidis*
P2	0	0	0
P3	0	0	33 *S. epidermidis*
P4	0	0	0
P5	0	0	0
P6	33 *S. aureus*	0	133 *S. aureus* and 33 *S. epidermidis*
P7	0	0	0
P9	0	0	0
P18	0	0	0
P21	0	0	0
P26	0	0	0
P28	0	0	0
P29	HPA* *P. aeruginosa*	HPA* *P. aeruginosa*	HPA* *P. aeruginosa*
P30	HPA* *P. aeruginosa*	HPA *P. aeruginosa*	HPA* *P. aeruginosa*
P31	0	0	0
P32	133 yellow colonies Gram -'ve rods■ & 867 milky colonies	0	200 milky colonies Gram -'ve rods■
P33	0	0	0
P34	0	0	0
P35	0	0	0
P36	0	0	0

* blood culture results supplied by the Health Protection Agency, ■ Gram stain and light microscopy identification

Only 1 CVC removed from the adult oncology population that was cultured was removed due to clinical suspected exit site infection. All other CVCs were removed for end of treatment, or the CVCs were broken or blocked. Therefore, only P6 could be considered as CVC-related exit site infection. Unfortunately we did not know whether a swab of the exit site infection was taken as part of the routine clinical investigation. Accordingly, no definitive conclusions could be made regarding P6 culture results. All other culture positive CVCs were considered to be colonised. Interestingly, P32 grew two different types of bacteria at the subcutaneous section (yellow and milky colonies) whereas at the tip section only milky colonies grew (Fig. 3.12).

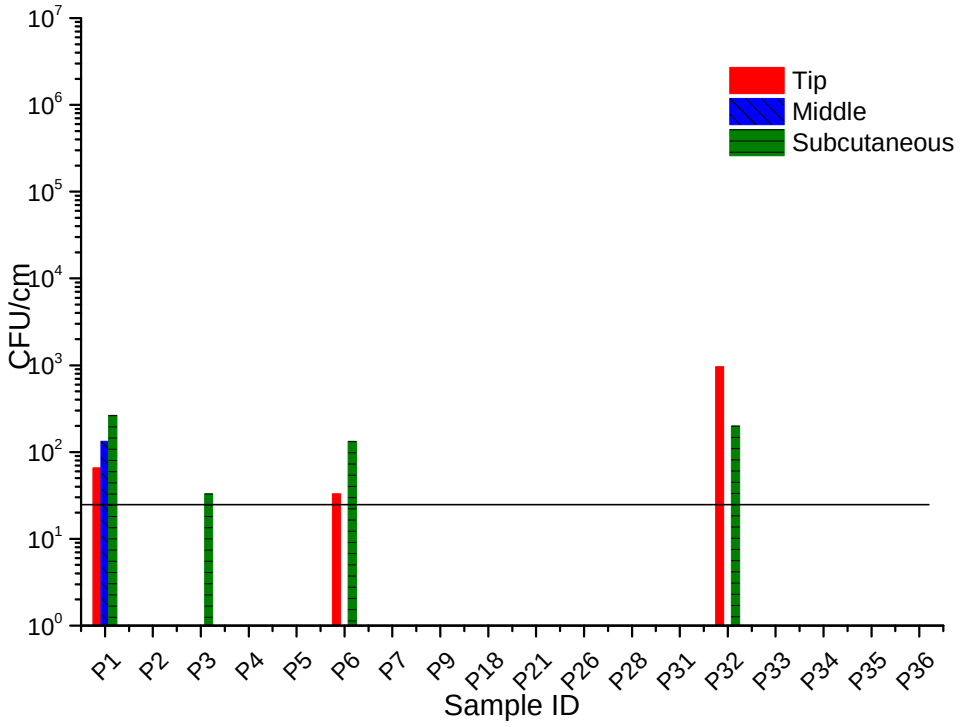

Figure 3.11: Plot comparing CFUs recovered from adult clinical samples. The plot showed CFUs/cm/ml recovered from adult CVCs recovered from the tip sections in red, the middle in blue and the subcutaneous sections in green. There were no statistically significant differences between the different sections (tip and subcutaneous, Mann-Whitney at 95% CI, $P = 0.695$).

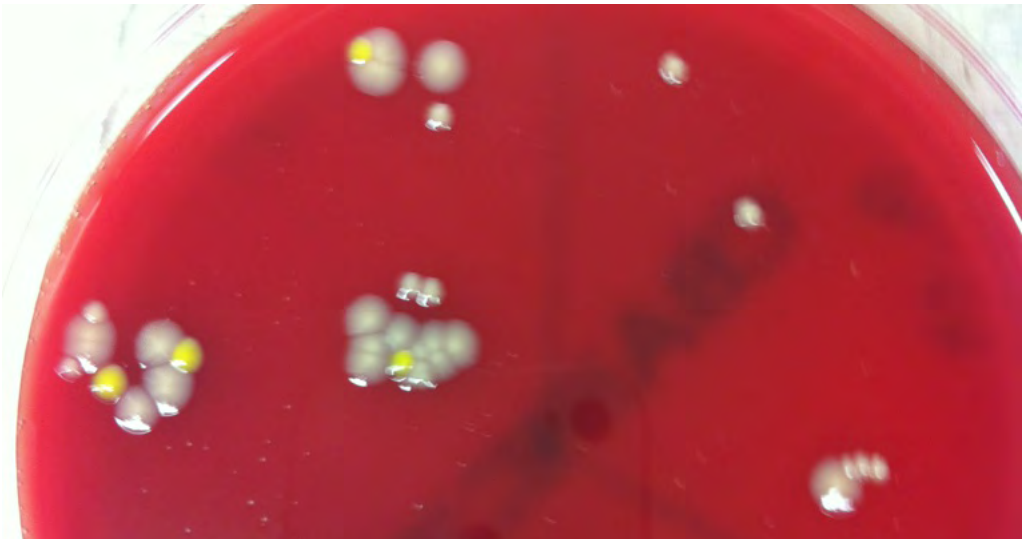

Figure 3.12: P32 enhanced culture by sonication blood agar plate. The subcutaneous section grew both yellow and milky colonies whereas the tip section only grew milky colonies.

For the paediatric CVCs, 13 out of 23 that were cultured were positive (Table.3.6). Of the 13, only 1 was positive for the tip and subcutaneous sections. Only 2 samples were positive at the tip section (this includes 1 from tip and subcutaneous sections positive) and 1 out of 11 of the middle sections were positive, whereas 12 out of 23 subcutaneous sections were positive.

Culture positive results for paediatric patients between the tip and subcutaneous sections showed statistically significant differences (Mann-Whitney at 95% CI, $P = 0.002$, Fig. 3.13). Whereas the difference between tip and middle section, and middle and subcutaneous sections were not statistically significant (Mann-Whitney, $P = 0.915$ and $P = 0.105$ respectively).

Table 3.6: Colony forming units per ml per cm of CVC recovered from tip, middle and subcutaneous regions removed from paediatric oncology CVCs.

Sample ID	CFU/cm/ml		
	Tip	Middle	Subcutaneous
C1	0	0	0
C2	0	0	0
C3	0	0	33 *S. epidermidis*
C4	33 *S. epidermidis*	0	0
C5	0	–	0
C6	–	0	600 *P. aeruginosa*
C7	1233 Not identified	–	833 *S. epidermidis*
C8	0	0	400 *S. epidermidis*
C9	0	0	0
C10	0	0	5400 *S. epidermidis*
C11	0	–	0
C12	0	–	tntc *S. epidermidis*
C13	0	–	767 *S. epidermidis*
C14	0	–	0
C15	0	100 Gram +'ve rods♦	66 Gram +'ve rods♦
C16	0	–	1400 *S. epidermidis*
C17	0	0	1700 Gram +'ve rods♦
C19	0	–	0
C20	0	–	0
C21	0	–	67 *S. epidermidis*
C22	0	0	2567 *S. epidermidis*
C23	0	–	0
C24	0	–	0

– no sample, ♦ Gram stain and light microscopy identification

Interestingly, the child CVC (C6) removed for exit site infection was culture positive at the subcutaneous end (Table 3.6). The tip of C6 was sent to the HPA lab as clinically indicated. The HPA lab did not culture anything from the tip. In contrast, we cultured *P. aeruginosa* from the opposite end of the CVC (Fig 3.14). Site selection for culture should be considered. The variability between tip and subcutaneous cultures may have been due to the type of CVCs. All paediatric oncology CVCs were tunnelled or implanted just under the skin. Only one paediatric CVC was removed for suspected exit site infection (C6), therefore the rest were considered as colonised.

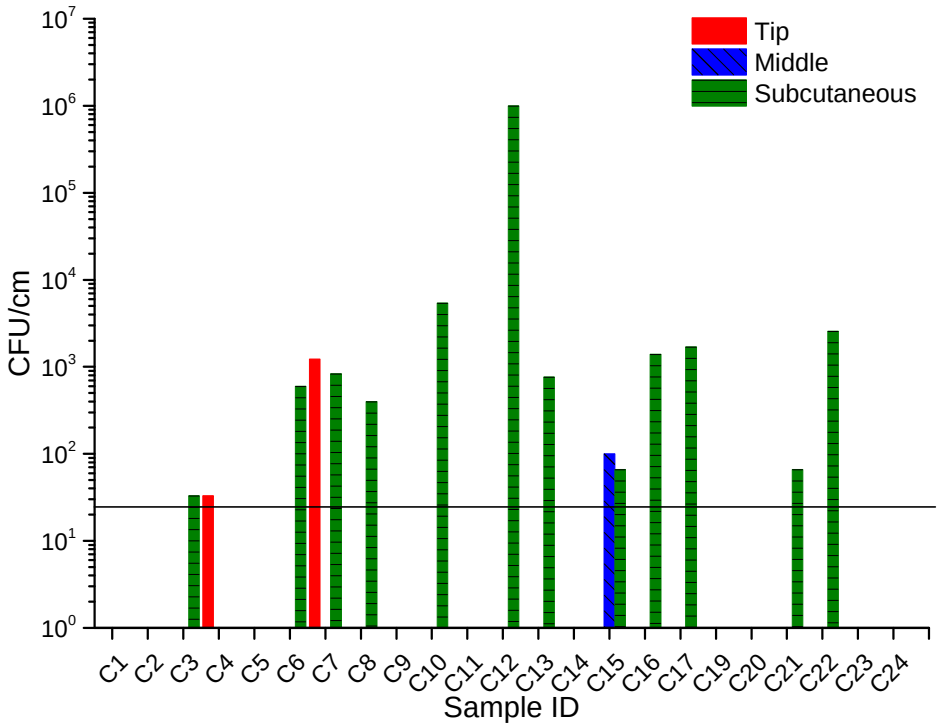

Figure 3.13: Plots comparing CFUs recovered from paediatric clinical samples. The plot showed the CFUs/cm/ml recovered from the tip sections in red, the middle in blue and the subcutaneous sections in green from paediatric oncology CVCs. There were statistically significant differences between the tip and subcutaneous sections showe (Mann-Whitney at 95% CI, $P = 0.002$). Conversely no differences between tip and middle section, and middle and subcutaneous sections (Mann-Whitney, $P = 0.915$ and $P = 0.105$ respectively).

In many of the paediatric samples, an oily residue was noticed when 10 μl of the sonicate was dropped on to blood agar plates during culture. The samples also appeared to experience slow or inhibited growth when it was culture positive. Colonies were only observed after 48 to 72 hours post incubation. The oil droplets were likely propofol (Dr. Libby Calton personal communication). Propofol was often used at UHS as the anaesthetic of choice and was administered through the CVC before removal.

C17 and P32 also appeared to contain more than one type of bacteria (Figs 3.15 and 3.12). Both species recovered from C15 and C17 were identified as Gram positive rods (Fig 3.16).

In contrast, P32 contained Gram negative rods. The bacteria at the tip and subcutaneous sections of C7 on the other contained different bacteria with the subcutaneous section containing *S. epidermidis* and the tip section unidentified small colonies (Fig. 3.17)

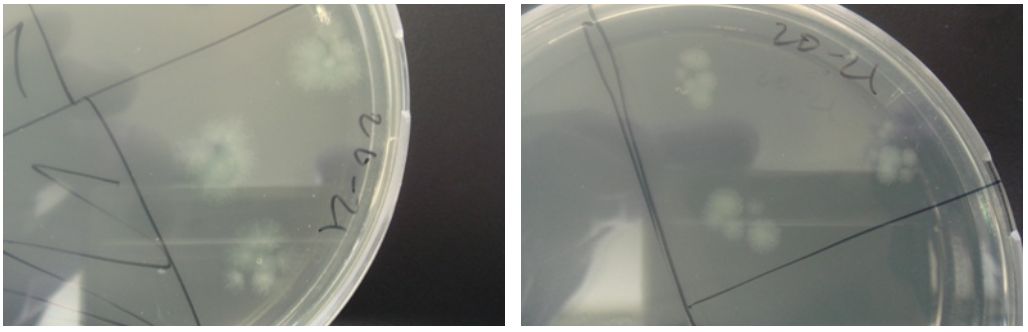

(A) C6 TSA 12 hours post culture (B) C6 PIA 12 hours post culture

Figure 3.14: C6 *P. aeruginosa* on TSA and PIA agar plates 12 hours post culture

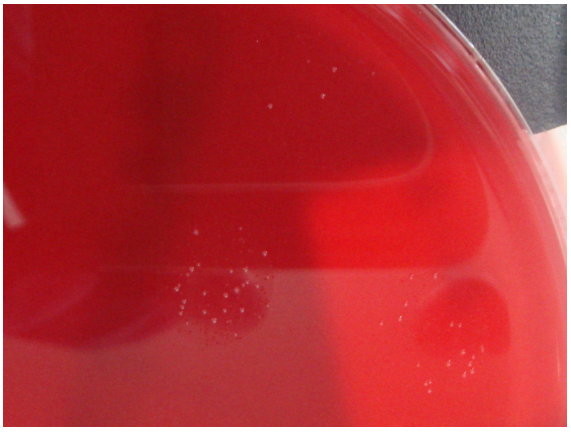

(A) C17 12 hours post culture

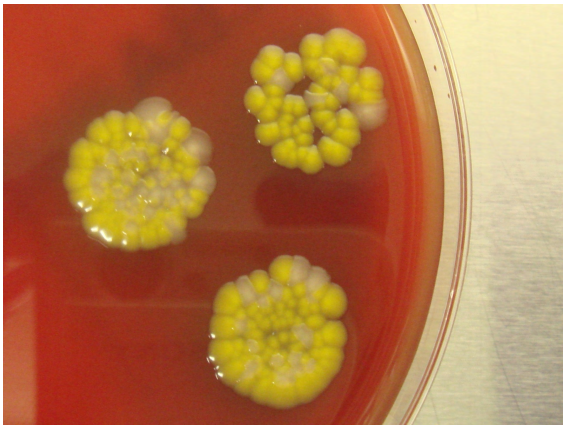

(B) C17 96 hours post culture

Figure 3.15: C17 blood agar with colonies at 12 and 96 hours post culture. (A) shows very small milky coloured colonies of bacteria and (B) shows the same plate with large yellow coloured colonies 3 days later. Gram stain on both.

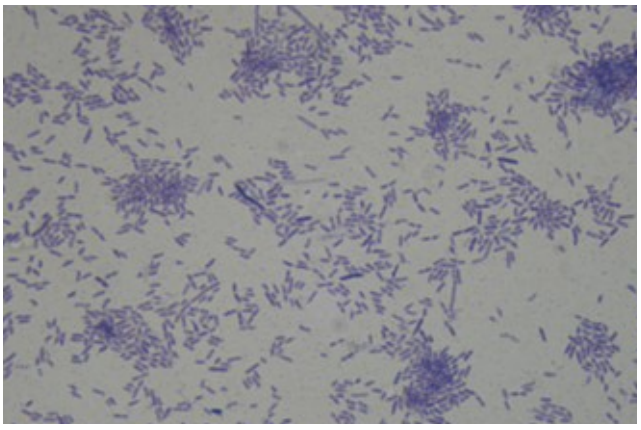

Figure 3.16: Child 17 yellow colonies are Gram positive rod imaged with light microscope.

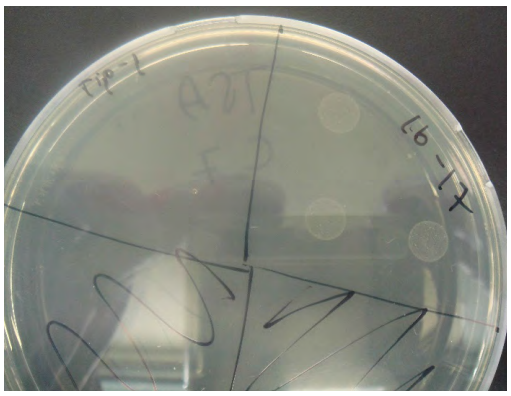

(A) 12 hours

(B) 24 hours

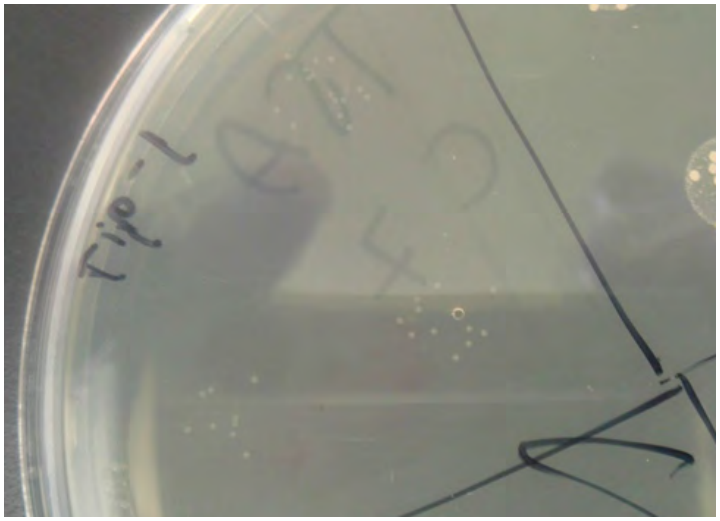

(C) Tip - 1 cm 24 hours

Figure 3.17: C7 tip and subcutaneous growth rates. (A) showing the growth of C7 12 hours post culture; (B) with *S. epidermidis* at the subcutaneous section and (C) small unidentified colonies 24 hours post culture.

When paediatric culture results were compared with adult, the difference between tip and middle sections were not significant (Mann-Whitney, $P = 0.7880$ and $P = 0.8370$ respectively). In contrast, the difference between paediatric and adult subcutaneous sections were statistically significant (Mann-Whitney, $P = 0.0237$, Fig. 3.18).

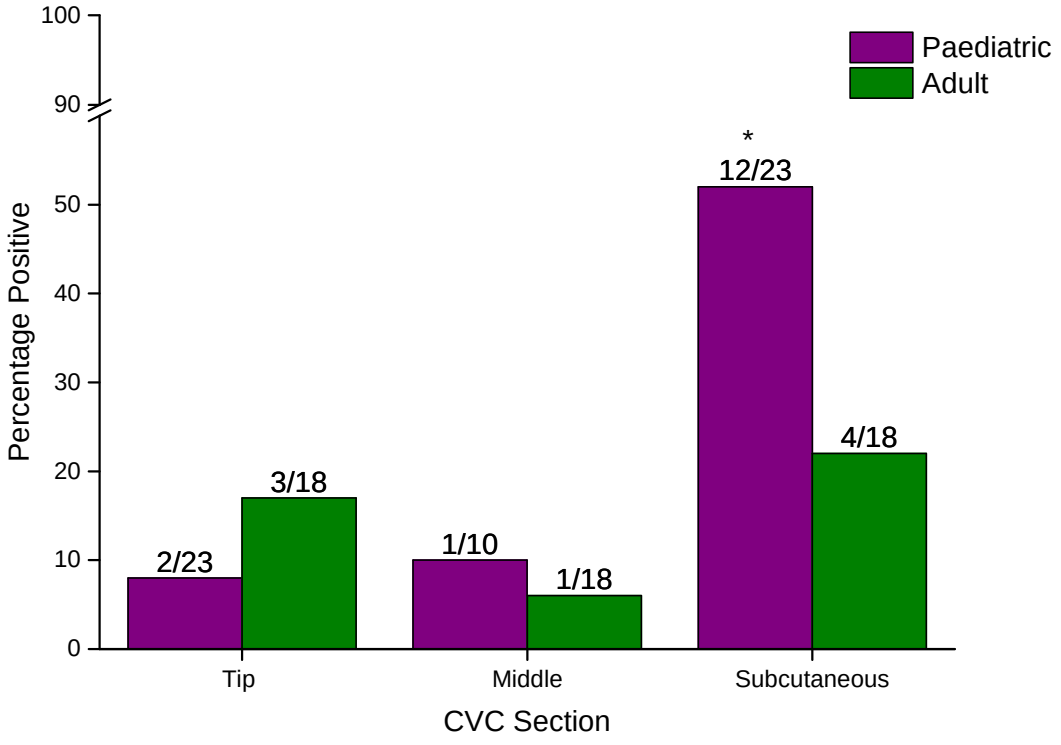

Figure 3.18: Clinical culture results for paediatric and adult CVCs. Paediatric results in purple and adults in green. This plot indicates that paediatric samples were most commonly colonised at the subcutaneous end whereas adult sections were more likely colonised at the tip or subcutaneous end. The black line represents 25 CFUs/cm of CVC The difference between paediatric and adult subcutaneous sections were statistically significant as indicated by $*$ (Mann-Whitney, $P = 0.0237$).

3.5 Discussion

Microbial results showed that paediatric oncology samples had significantly higher positive subcutaneous sections. In contrast there was no difference for the adult samples. The hypothesis for the variation will be discussed in the text below.

The clinical audit showed that the removal indications in the small clinical pilot study may have been representative of the adult and paediatric oncology population at SUHT. Using enhanced microbial culture to map where biofilms formed within the clinical pilot study samples showed that paediatric oncology CVCs formed biofilms more commonly at the subcutaneous ends. Whereas there was no significant difference for the adult CVCs.

In vitro work allowed for optimisation of known clinical and research methods used for biofilm detection within CVCs. The literature had already established that the gold standard roll plate method was not sufficient for detecting all biofilms, especially within the lumen of longer dwelling CVCs. Biofilm formation on CVCs indwelling for < 10 days were found on the external CVC surface whereas CVCs indwelling for ≥ 30 days form biofilms inside the lumen (Donlan, 2011). The audit results revealed that CVCs were left indwelling for > 15 days. Accordingly, the roll-tip would not have been a sufficient choice. SUHT HPA uses culture by vortexing and solid agar plating for detecting CRIs. Culture by sonication and solid agar plating was tested and proved to be more efficient at removing biofilms compared to vortexing and plating alone (0 seconds of sonication was vortexed).

The audit revealed the indications for CVC removal from the pilot clinical study was similar but in much greater numbers. Potentially indicating that the small pilot study was representative. The culture results from the audit was however only from catheters suspected of infection whereas the clinical pilot study cultured all catheters. Although the CDC and IDSA do not recommend routine culture of all CVCs (O'Grady et al., 2011), for the clinical pilot the objective was to map biofilm formation and test whether culture results were reliable regardless if the samples were infected or colonised. In addition, many studies have shown that colonisation of CVCs often results in infection (Raad et al., 1993) or that it leads to an increased risk for CRI (Pearson, 1996).

Similar to the literature (Section 2.2.2) for both the adult and paediatric clinical CVC samples; culture by sonication most frequently recovered *S. epidermidis* (Donlan, 2001; Weinstein, 2007; Sawyer and Leon, 2010; Lorente et al., 2006). For adult CVC samples, this was followed by *S. aureus* (P29 and P30 excluded as the data was from blood cultures) and lastly by Gram negative rod bacteria. For paediatric oncology CVC samples the second most commonly isolated organism was Gram positive rods followed by *P. aeruginosa* . Although not all the organisms listed in the literature were isolated the pattern was very similar. It should be mentioned however, that the bacteria numbers from the literature was often isolated from blood cultures. Even though the diagnoses were CABSIs there was not always corroborating evidence from CVC cultures (O'Grady et al., 2011).

Corroborating evidence from removing and culturing CVCs however, may need reviewing. The 2001 IDSA recommended that for CRIs either the catheter tip or subcutaneous sections should be cultured (Mermel et al., 2001). In contrast, the 2009 IDSA guidelines recommends that the tip rather than the subcutaneous sections should be cultured Mermel et al. (2009). Interestingly, the 2001 IDSA guidelines based their recommendation on a study that found sonication of the subcutaneous segment to be the most sensitive at detecting colonisation (Sherertz et al., 1997). Culture found significantly more positive subcutaneous compared to tip sections for paediatric samples. Because most of the paediatric CVCs were tunnelled a theory that may account for higher colonisation rates at the subcutaneous sections could be that bacteria within deeper layers of the skin could have been the source of the contamination (Costerton et al., 2004). Or because the lines were mostly tunnelled or implanted, more tissue damage may have resulted in fibrin sheath formation. Fibrin sheath formation has been show to stimulate staphylococci biofilm formation (Mehall et al., 2002; Chittick and Sherertz, 2010). Paediatric CVC sample removal was the most controlled as the samples were removed in theatres by a clinician that made every effort to ensure none of the sections were contaminated. The tip (first 4/5 cm) of C6 was sent to the HPA for culture as the paediatric patient had an exit site infection. The tip section came back as culture negative. We cultured the middle and subcutaneous sections of C6. The middle section was culture negative but most importantly was that the subcutaneous section was culture positive for *P. aeruginosa* . Oncology patients are immune compromised and not knowing which organism caused the infection may have compromised the treatment route chosen by the clinician. In addition, sample P6 which was removed from an adult oncology patient due to an exit site infection (sample not sent for culture by clinician) cultured *S. epidermidis* and *S. aureus* from the subcutaneous section.

In many of the paediatric samples, an oily residue was noticed when 10 μl of the sonicate was dropped on to blood agar plates during culture. The samples also appeared to experience slow or inhibited growth when it was culture positive. The oil droplets were likely propofol. Interestingly, the literature has established that propofol emulsion supports the growth of *Escherichia coli*, *C. albicans* , *S. aureus* and inhibits the growth of *P. aeruginosa* (Wachowski et al., 1999; Tessler et al., 1999). Gocmen et al. (2012) administered propofol using CVCs and found that eighteen out of twenty five patient isolated *S. epidermidis* strains to be positive for slime production. The researchers did state that this could have been due to the drug additives (propofol contained soy bean oil, egg lecithin and glyceryl).

Culture might be less time consuming and cheaper than imaging methods for clinical diagnostics; but culture can suffer from false positives due to contamination during CVC removal. Imaging techniques would be less susceptible to result in false positives as contaminating bacteria may be less likely to be in a biofilm form, thus would not be biofilm positive. In addition, culture may suffer from false negatives. This may be because

biofilms can exist in a viable but non culturable state (Zandri et al., 2012; Raad et al., 1993). Using culture by sonication and solid agar plating may improve results compared to the roll plate method but the method is unable to pinpoint where the infection is coming from (luminal or on the outside surface) thus more difficult to determine contamination. Another limiting factor for this specific work regarding culture by sonication and solid agar plating was only using a 1 cm section for culture. During the clinical study, biofilms within the CVCs were found to be very heterogeneous, thus there could have been many false negative culture results. The reason behind only using a 1 cm section of CVC (of the tip, middle and subcutaneous) was because other techniques were compared to culture; the sections had to be as close as possible to ensure that comparisons were fair.

Chapter 4

Confocal laser scanning microscopy to detect biofilms

4.1 Introduction

Confocal laser scanning microscopy (CLSM, explained in Section 2.5.1) allows for nondestructive, in situ analysis of living, fully hydrated biofilms without the need for harsh chemical fixation or embedding techniques (Costerton and Lewandowski, 1995; Surman et al., 1996). For central venous catheters (CVCs) however, CLSM is destructive as the CVC has to be sectioned in order to expose the biofilm for imaging.

CLSM is commonly used to study biofilms using fluorescently labelled stains (Flemming and Wingender, 2010; Coenye and Nelis, 2010; Neu et al., 2010). Fluorescent stains allow for direct *in situ* biofilm detection using different fluorophores (Hall-Stoodley et al., 2006; Nistico et al., 2011). *In vitro* experiments of biofilm architecture and matrix components using CLSM have elucidated how three dimensional structures are formed by various biofilm bacteria (Lawrence et al., 2003). From the mushroom structures formed by *P. aeruginosa* to the impact the accessory gene regulator, Agr have on *S. aureus* biofilms (Hall-Stoodley et al., 2004; Periasamy et al., 2012). Nevertheless, repeated laser scans can cause bleaching or fading of the fluorescent signal (Costerton and Lewandowski, 1995).

Although CLSM is a common biofilm imaging technique not many papers in the literature use CLSM for catheter biofilm studies. Often catheter biofilm studies make use of animal models and either do not use clinical CVCs or only culture the CVCs and perform CLSM on other surfaces (Periasamy et al., 2012; Andes et al., 2004). For example, Andes et al. (2004) used polyethylene tubing with no additives implanted into rats.

4.2 Experimental approach

The objective for this chapter was to determine whether biofilms can be detected and location mapped within clinical CVCs using CLSM. Before any clinical samples could be analysed using CLSM, a sectioning and staining protocol had to be developed. During these experiments significant amounts of CVC material autofluorescence were encountered. Therefore, in order to continue, the material autofluorescence had to be tested. Once the levels of autofluorescence was determined, biofilm and protein stains were considered as well as determining whether image analysis using the fluorescence strength could be determined. Lastly, the definition of a biofilm positive clinical CVC sample was considered before the samples were analysed.

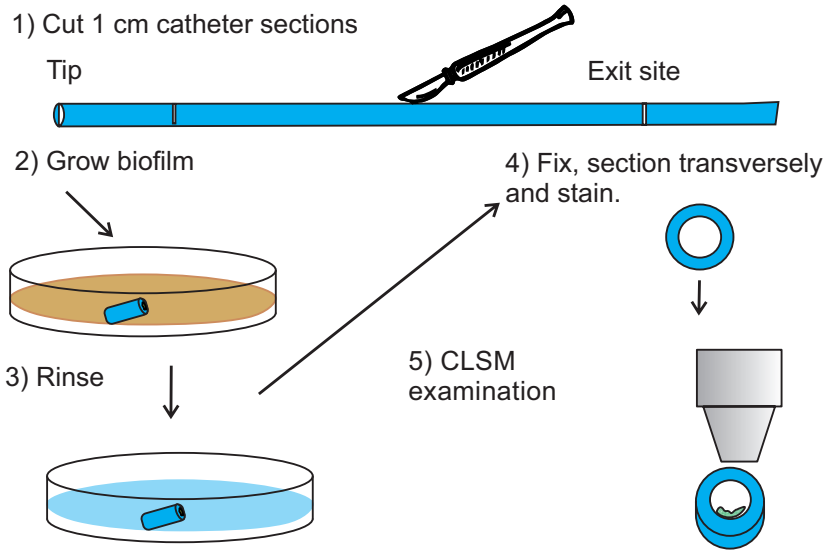

Figure 4.1: Sample processing for biofilm culture. For *in vitro* experiments all steps were followed whereas for the clinical pilot experiments after sample collection, steps 1, 3, 4 and 5 were followed. (1) showed how pieces were sectioned, (2) how *S. epidermidis* biofilms were grown, (3) rinsing (4) fixing, sectioning and staining; and (5) microscopy.

4.3 Materials and methods

All materials were purchased from Sigma Aldrich UK unless stated otherwise.

4.3.1 Catheter material autofluorescence

In order to assess auto-fluorescence produced by polyurethane and silicone CVC materials (containing various dyes depending on the manufacturer) lambda scans were performed

on sterile CVCs. Lambda scans were used to determine the emission spectra produced by the materials. CVCs that were tested included, polyurethane (Cook and Health Line International) and silicone (Bard) PICCs.

Sterile CVC sections were cut cross-sectionally, placed in a drop of Citifluor (mixture of glycerol and PBS) and placed under the confocal laser scanning microscope (CLSM, Leica SP5). Lambda scans were performed with the following laser lines: 405 nm, 485 nm, 476 nm, 488 nm, 496 nm, 514 nm, 561 nm, 594 nm and 633 nm. Emission data was collected from 410 to 780 nm. Optics were set at $\times$ 63 magnification, lasers were kept at 25% power and the photon multiplier (gain) at 25%. In order to evaluate the significance of the CVC material fluorescence, the minimum fluorescence intensity (FI) for stained biological deposits from clinical samples were measured and compared to the material autofluorescence.

4.3.2 Sample preparation prior to sectioning

After *in vitro* CVC samples were grown (Section 3.3.4) and clinical samples collected and processed (Section 3.3.2.4) the samples were rinsed with PBS buffer and fixed in general fixative (SEM fix, 3% glutaraldehyde, 4% formaldehyde in $0.1M$ piperazine-N,N-bis 2-ethanesulfonic acid buffer (PIPES) at pH 7.2) or alcian fixative (alcian blue, 3% glutaraldehyde in $0.1M$ cacodylate buffer at pH 7.2) to fully cover the sections of CVC and were incubated in the dark at 4^oC for 12 hours using a refrigerator. Thereafter, the fixed sections were rinsed twice by gently flushing the sample container with PBS for 10 seconds each.

4.3.3 Sectioning

Before CVC sections could be stained the samples had to be sectioned in two different ways. CVC were sectioned using a sterile scalpel into small transverse ('doughnut') slices at an angle of approximately 30 degrees without creating any rough edges. Longitudinal samples were sectioned along the midsection but it was difficult due to the small diameter of the CVCs. Imaging the longitudinal surface using CLSM (Fig.4.2, (A) and (B)) resulted in ambiguous micrographs. The presence or absence of biofilms on these sections could not be established. The transverse ('doughnut') sections allowed for discrimination between the CVC material and the biofilm cells (Fig.4.2, (E) and (F)) because the cells protrude beyond the edge. Cutting the slices into 1 to 2 *mm* length at an angle of approximately 30 degrees increased how far into the slice micrographs could be taken. Subsequently, all experiments using CLSM to examine CVC samples were cut transversely at an angle of 30^0. 5 *mm* sections from the *in vitro* prepared samples were also examined by SEM. The negative control (Fig.4.2C) contained no biofilm. The positive 24 hour *S. epidermidis* biofilm sample

(Fig.4.2D) did contain cocci biofilm. SEM was used to corroborate whether biofilm were present or absent in the respective CLSM samples. Accordingly, all CLSM sectioning was performed on rings of 1 *mm* depth cut at an angle of approximately 30 degrees.

4.3.4 Sample staining

After samples were sectioned, slices stained with SYPRO Tangerine (a protein stain) and SYTO 9 (a nucleic acid stain for all cells). The two fluorescent stains had similar excitation waves (SYTO 9, 470-490 nm and SYPRO Tangerine, 450-490 nm) but different emission spectra (SYTO 9, 520-550 nm, SYPRO Tangerine, 630-670 nm). SYPRO Tangerine was prepared by adding 1 μl of the stain to 5 *ml* of sterile PBS (made according to manufacturer recommendations). 1 *ml* of stain per well was added into a 24 well plate. 1 to 2 *mm* CVC sections were placed into the respective wells and were covered in aluminium foil and incubated for 30 minutes. SYTO 9 was prepared by adding 2 μl of SYTO 9 into 1 *ml* of PBS-SYPRO stain which had been previously dispensed to respective wells in a 24 well plate. The two stains were mixed gently pipetting up and down 6 times. The plate was covered with aluminium foil and incubated for a further 15 minutes at room temperature.

4.3.5 Effect of stain order

To assess whether the order of staining with two stains had an influence on the staining efficacy a second procedure was used. For the second procedure (first procedure outlined previously) SYTO 9 was added first, staining for 15 minutes in the dark followed by staining with SYPRO Tangerine for 30 minutes. In addition, the stains were also added simultaneously or the first stain removed, rinsed and stained with the second stain separately.

No visible differences were observed between adding SYTO 9 or SYPRO Tangerine first. Therefore, due to the different stain time recommendations for the two stains (SYPRO Tangerine 35 minutes and SYTO 9, 15 minutes) SYPRO Tangerine was added for 20 minutes first followed by the addition of SYTO 9 for a further 15 minutes.

4.3.6 Microscopy

Samples were placed in microscopy dishes with one drop of Citifluor (mixture of glycerol, PBS and antifadent, Agar Scientific, UK) to immobilise the samples and to prevent stain bleaching. Stained samples were examined by an inverted Leica confocal laser scanning microscope using a 63$\times$ oil immersion objective. The 488 nm and 496 nm lasers were used to excite SYTO 9 and SYPRO Tangerine. The sensitivity of the detector (gain) was adjusted to minimise autofluorescence and the lasers were kept at 25% power.

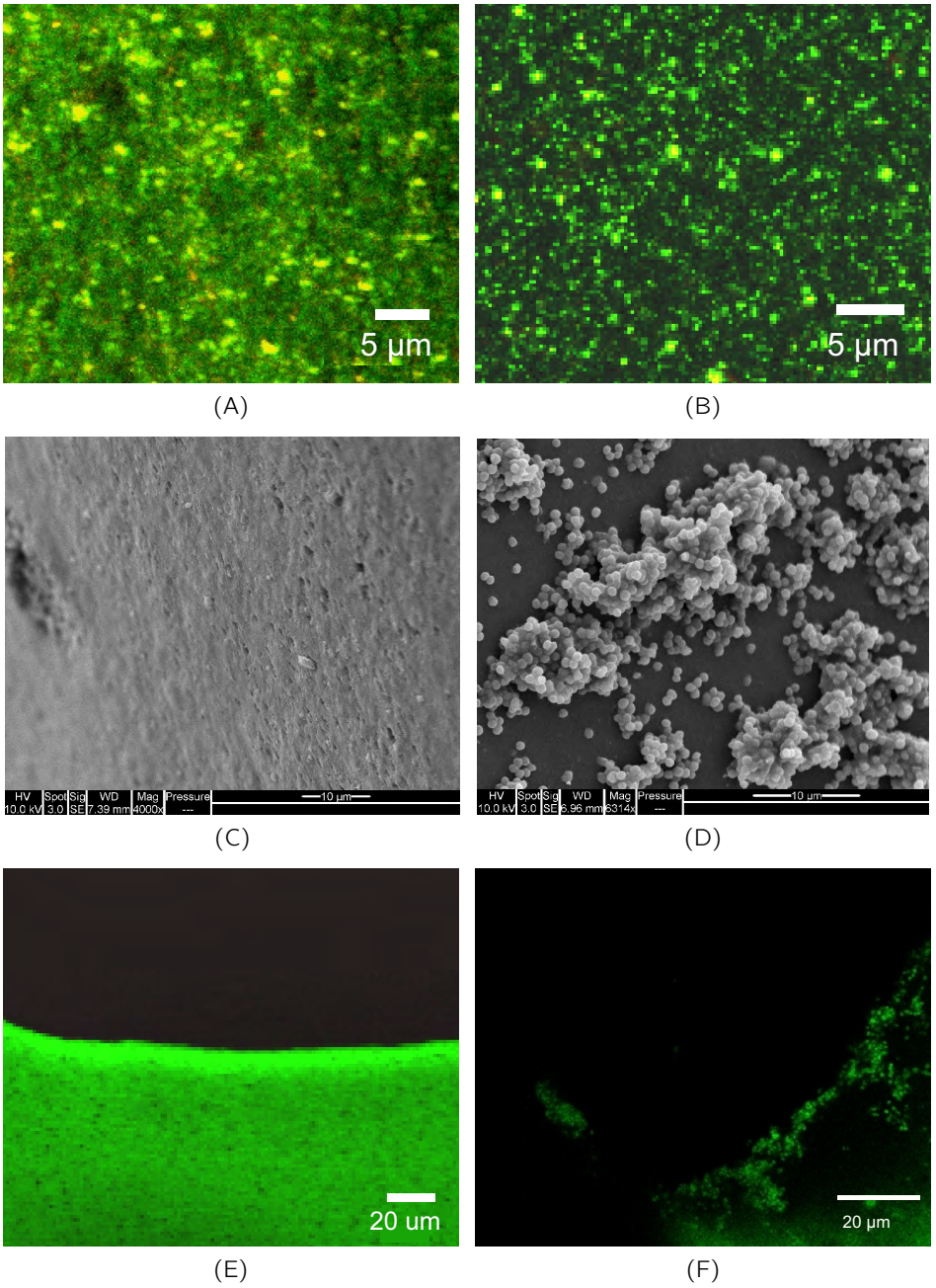

Figure 4.2: CLSM and SEM micrographs of static CVC-biofilm model grown and control samples to illustrate the different section methods. (A), CLSM micrograph of an untreated control CVC sectioned longitudinally and imaged using the 488 and 496 nm laser line. (B), CLSM micrograph of a *S. epidermidis* static CVC-biofilm sample grown on a section of Lifecath PICC sectioned longitudinally and imaged using the 488 and 496 nm laser with an emission of 500 and 640 nm (scale bar = 5μm). (C) SEM micrograph of the control CVC with no biofilm and (D) SEM micrograph of the *S. epidermidis* static CVC-biofilm sample showing evidence of biofilms (scale bar = 10 μm). (E), CLSM micrograph of the control sample sectioned transversely showing no evidence of a biofilm (scale bar = 20 μm) and (F), the *S. epidermidis* static CVC-biofilm sample grown on a section of Lifecath PICC indicating evidence of a biofilm (scale bar = 10 μm).

4.3.7 Image analysis

To determine whether deposit quantification was possible by applying a fluorescence intensity threshold, CVC material autofluorescence and stained deposit fluorescence intensities were compared. Using Fiji software, a straight line of 100 pixels were drawn on clinical deposit and CVC surfaces (as indicated by red circles in Fig. 4.3) of 5 different CVCs using confocal micrographs. The fluorescence intensity profile plots of the lines were determined. The fluorescence intensities were calculated for polyurethane and silicone CVCs, and included separate measurements for SYPRO Tangerine and SYTO 9 emission channels.

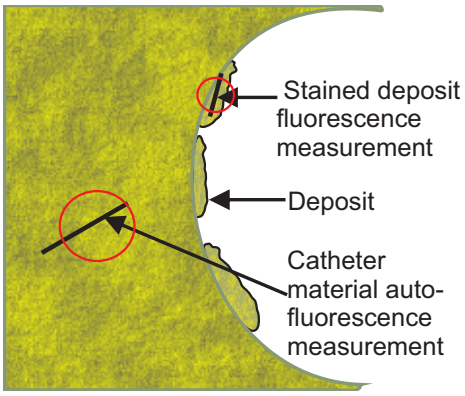

Figure 4.3: Representative illustration of the transverse confocal microscopy view of a CVC section. Profile plots of CVC material-autofluorescence and deposit fluorescence were measured and compared by using Fiji software to draw a straight line of 100 pixels in green (SYTO 9) and red (SYPRO Tangerine) channels, plotting the fluorescence profiles and calculating the means .

4.3.8 CLSM biofilm positive

In order to determine whether a biofilm was present using CLSM a clear definition in relation to the work was developed. For a CVC to be positive for a biofilm using CLSM, evidence of two or more bacteria attached to a surface with or without EPS (surface could be CVC or other deposits that were attached to the CVC) had to be present.

4.3.9 Statistics

When the differences between mean fluorescence intensity between the CVC material and deposits were compared the parametric two-sample two-tailed t-test was performed at 95% confidence intervals (Minitab, US). The t-test was used because the data was continuous, means from two independent groups were compared. To compare tip, middle and subcutaneous sections of the adult and paediatric CVC samples the Mann-Whitney

test was used at 95% confidence intervals. The Mann-Whitney test was used because two independent groups with ordinal data that were ranked (1 for evidence of biofilms and 0 for no evidence of biofilms) were compared. The degree of biofouling was also ranked (as explained in Section 4.3.7). Significant difference was established when the probability value was less than 0.05 (Minitab 16, US).

4.4 Results

4.4.1 CVC material autofluorescence

The assorted CVC types all showed autofluorescence using the different laser lines across the spectrum at varying intensities (Fig.4.6). The minimum fluorescence intensity (FI) for stained biological deposits from clinical samples were measured as 20 FI, (mean ± SE, n=5). However, the material auto-fluorescence intensities (obtained from lambda scans) were shown to be significant as the material FI was much greater than the minimum FI for stained biological deposits (Fig.4.4).

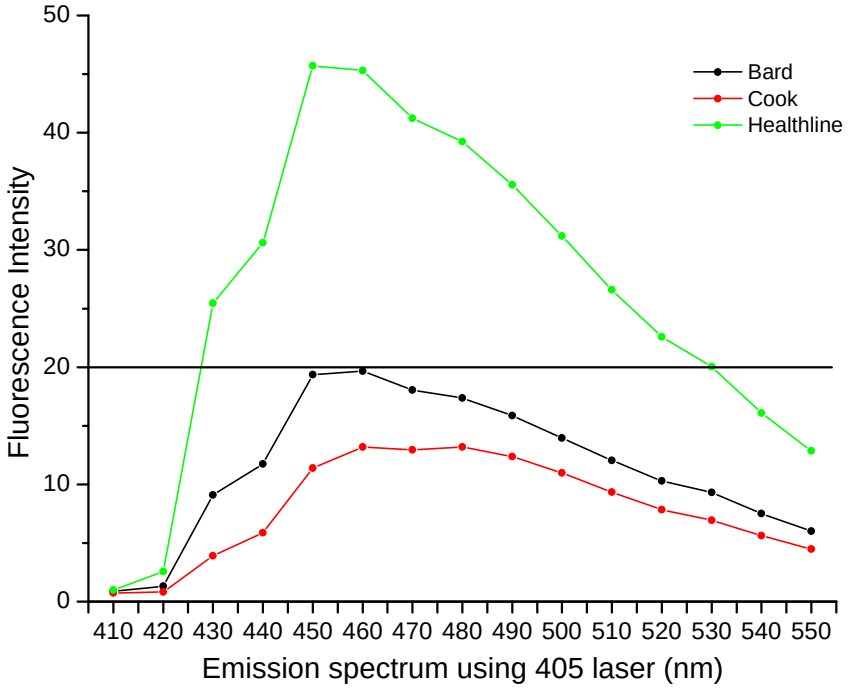

Figure 4.4: Comparison of the mean emission fluorescence intensities (410 to 550 nm) of different CVC brands using the 405 nm laser line. The black line represents the lowest mean fluorescence intensity of deposits found on clinical samples (20, mean, n=5).

Using the 405 nm laser line the Health Line polyurethane PICC auto-fluoresced at 2.3 times as high intensity as the Bard silicone PICC and 3.5 times more intense compared to the Cook polyurethane PICC with emission spectrum between 410 to 550 nm (Fig.4.4).

The polyurethane (Cook) PICCs had the highest mean fluorescence intensity using the 561 and 633 nm laser lines with emission spectra between 600 to 800 nm using the 561 and 633 nm laser lines (Fig.4.6A). The silicone (Bard) PICCs also had autofluorescence at the same emission range using the same laser lines but was 50% less intense (Fig.4.5 and 4.7). Therefore, to avoid autofluorescence all subsequent CLSM experiments used the 488 and 496 nm laser lines to excite SYTO 9 and SYPRO Tangerine respectively.

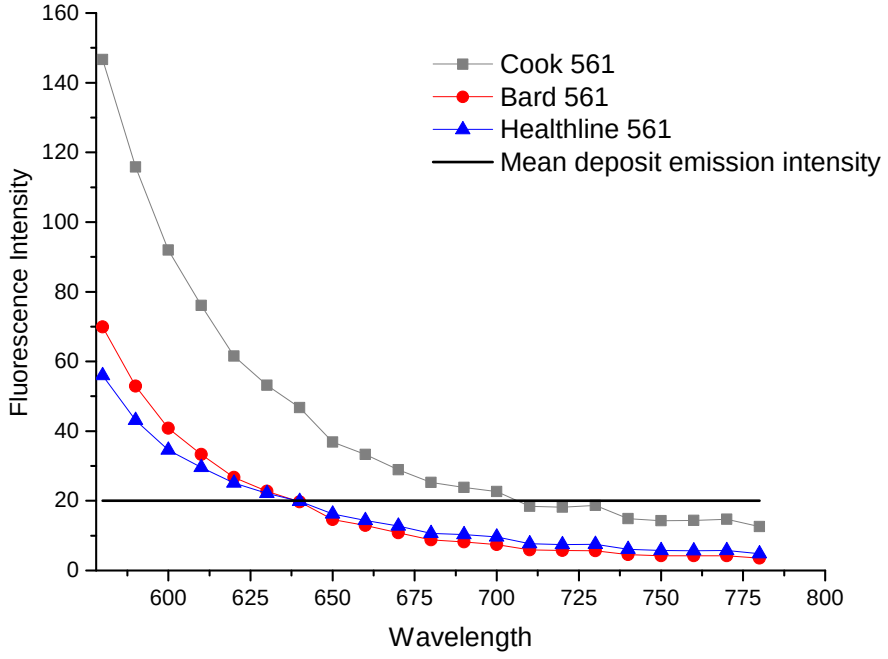

Figure 4.5: Comparison of the mean emission fluorescence intensities (580 to 780 nm) of different CVC brands using the 561 nm laser line. The black line represents the lowest mean fluorescence intensity of deposits found on clinical samples (20, mean, n=5).

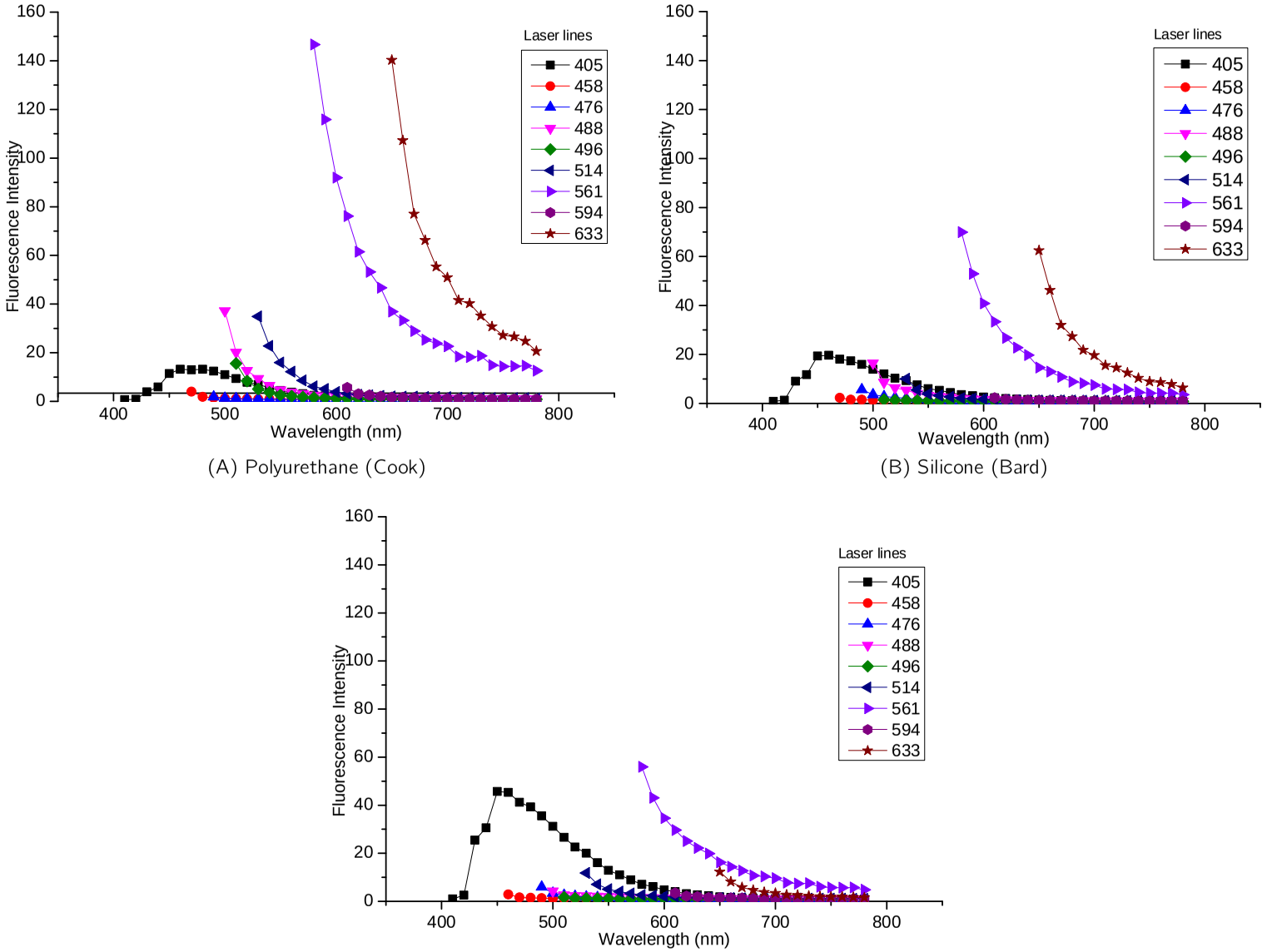

(A) Polyurethane (Cook)

(B) Silicone (Bard)

(C) Polyurethane (Health Line International Corporation)

Figure 4.6: Comparisons between the mean autofluorescence intensity produced by different CVC types. Plot (A) showed the autofluorescence produced by a polyurethane CVC, (B) showed autofluorescence from a silicone CVC, (C) autofluorescence from polyurethane Health Line International Corporation CVCs.

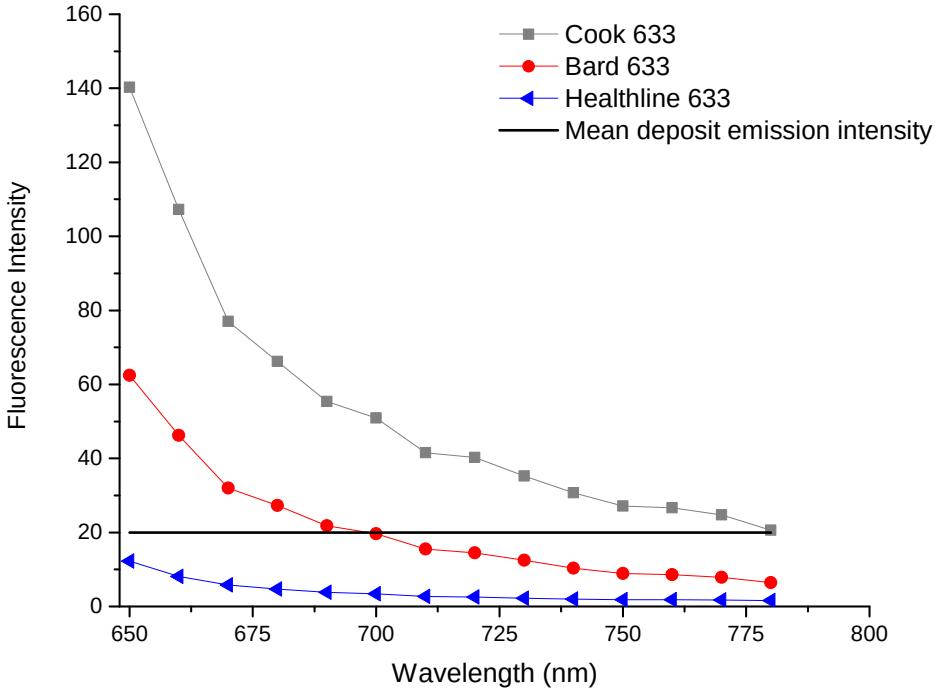

Figure 4.7: Comparison of the mean emission fluorescence intensities (650 to 780 nm) of different CVC brands using the 633 nm laser line. The black line represents the lowest mean fluorescence intensity of deposits found on clinical samples (20, mean, n=5).

4.4.2 Effect of autofluorescence on stain fluorescence

The significance of CVC material autofluorescence was examined by comparing the mean fluorescence intensities between the CVC material and stained deposit from clinical data (Fig.4.8). The mean fluorescence intensities for deposit and CVC material were of a similar level to the autofluorescence that was determined in the lambda scan plots (Fig.4.2).

There was no significant difference at 95% CI for mean fluorescence intensities between CVC surfaces and deposits for silicone green and red wavelengths ($P = 0.425$ and $P = 0.613$ respectively) (5 readings for each patient CVC for 3 patients in each group) and for polyurethane green and red channels ($P = 0.504$ and $P = 0.637$ respectively). CLSM biofilm positive samples could only be determined based on cell morphology.

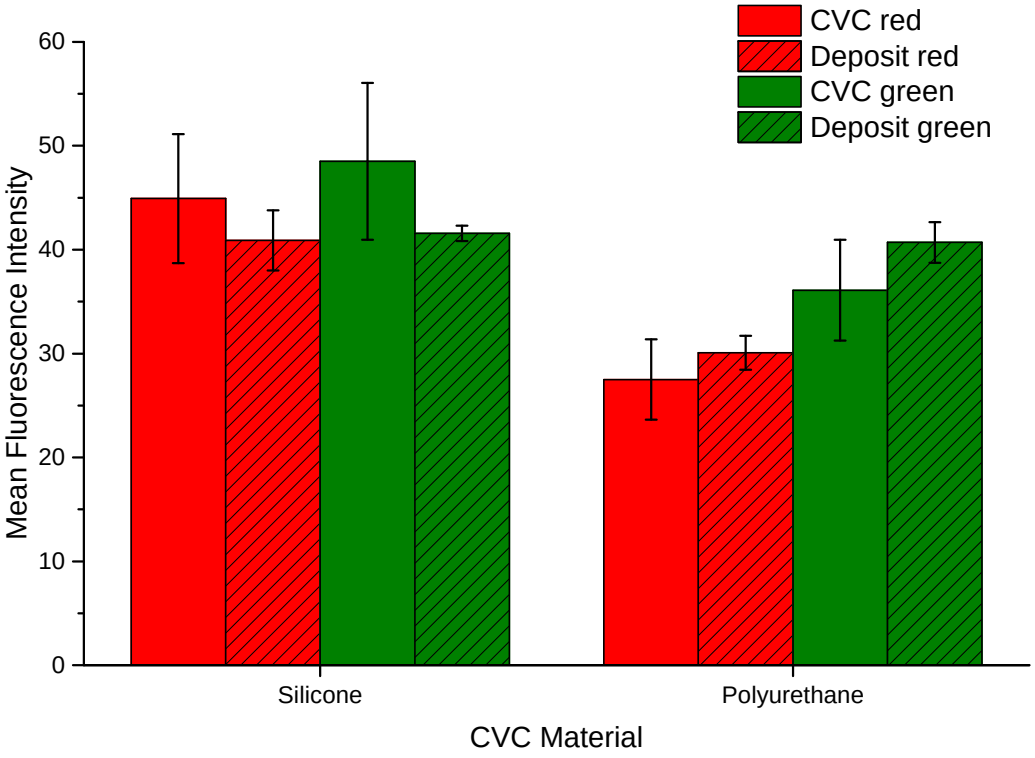

Figure 4.8: Plot of mean fluorescence intensity of CVC-autofluorescence and deposit stained with SYPRO Tangerine and SYTO 9 from clinical CVCs. Red bars represented the SYPRO Tangerine channel and green the SYTO 9 channel. Solid bars were deposits and striped were CVC surface auto-fluorescence intensity. There was no significant difference at 95% CI using the t-test for mean fluorescence intensities between CVC surfaces and deposits for silicone green and red wavelengths ($P = 0.425$ and $P = 0.613$ respectively) and for polyurethane green and red channels ($P = 0.504$ and $P = 0.637$ respectively, Mean $\pm$1SE, n=3 samples in each group, 5 readings per sample).

4.4.3 Biofilm detection in clinical CVCs

When imaging deposits on sections of clinical CVC, it was not always clear whether there were any bacterial cells present due to the significant material autofluorescence (Fig.4.9, (A) and (B)). Clusters of biofilm cells were observed but due to non-biofilm biological deposits and CVC material autofluorescence it was difficult to establish whether these were microbial in origin. When micrographs were post processed and digitally enhanced bacterial cells were detected (Fig.4.9C). Detection of biofilms composed of bacilli and rod shaped bacteria were easier to detect due to discernible morphology, distinctly different to autofluorescence as well for heavily colonised CVCs with less unknown biological deposit as seen in Fig. 4.10.

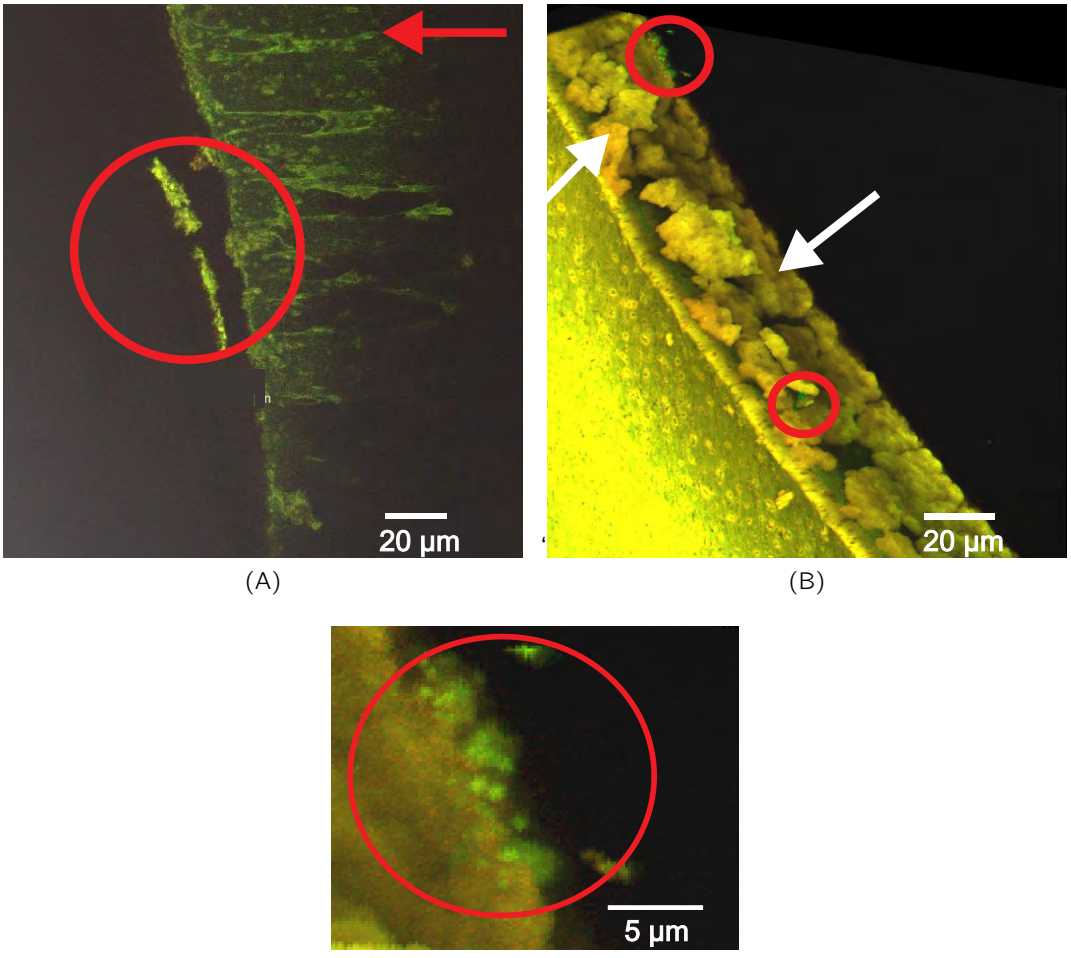

(A) (B)

(C)

Figure 4.9: Transverse confocal laser scanning micrographs of subcutaneous sections from C5 and C22 showing biofilms attached to the inner lumen of a section of CVC. (A) C5 with possible biofilm lifted from the material surface (red circle) and smeared biofilm on the CVC material (red arrows scale bar=10μm). (B), C22 showing significant CVC autofluorescence and significant amounts of protein (white arrows, scale bar=20μm). (C), zoomed in micrograph from the top red circle of (B) indicating the presence of cocci bacterial cells(scale bar=10μm).

4.4.4 Sample sectioning and heterogeneity

Due to the properties of silicone and polyurethane materials that CVCs were made from, sectioning was often a problem. The material compressed during cutting and thus experienced a large shape deformation when sectioned. Due to deformation and small diameters of the tubing (often less than 1 *mm*), sectioning resulted in substantial sample destruction. Transverse sectioning was difficult due to requiring precise clean edges. If a polyurethane CVC was processed immediately after receiving the sample and it was still 'warm', transverse sectioning for polyurethane CVCs were more precise compared to silicone CVCs. If the polyurethane CVC was cold the material stiffened and required more

cutting force which often resulted in jagged edges. For silicone CVCs, a thin sharp scalpel blade was required for precise sectioning but substantial tube compression occurred.

The heterogeneity that was observed by CLSM for clinical specimens using transverse sectioning was illustrated by low magnification using tile scanning images (Fig.4.11). The micrographs showed distinctive variation between the different sections from the same patient CVC. The tip region removed from the P29 (Fig.4.11A) showed no evidence of bacterial cells. In contrast, the subcutaneous region (Fig.4.11B) was classed as positive for biofilm as bacterial cells were identified based on size at higher magnification (Fig.4.11D).

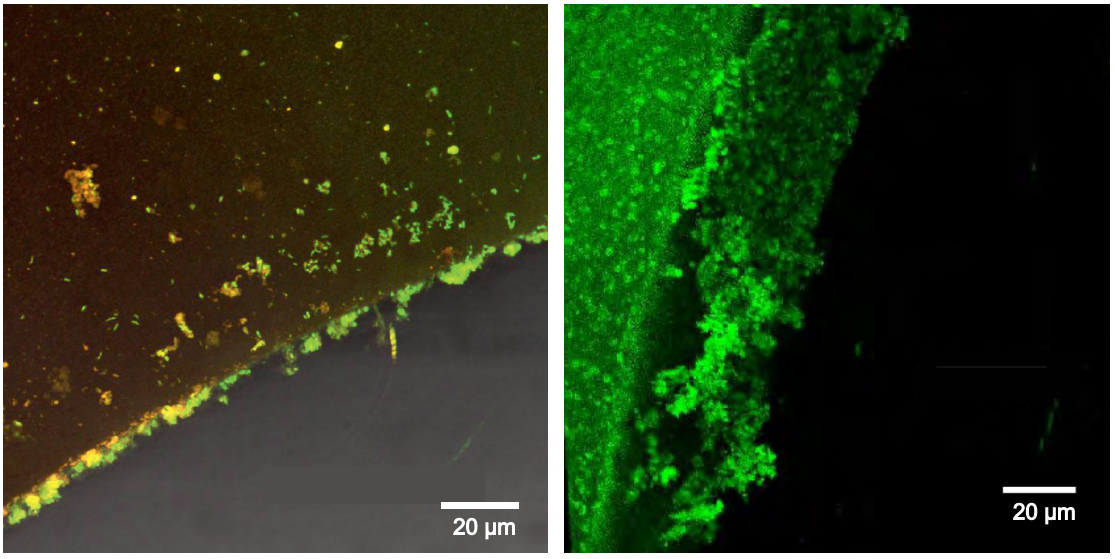

(A) (B)

Figure 4.10: Confocal laser scanning micrographs of rod and cocci shaped bacterial cells on CVC sections. P30 subcutaneous section (A) showing rod shaped cells and C3 subcutaneous section (B) cocci towers (scale bars=20μm).

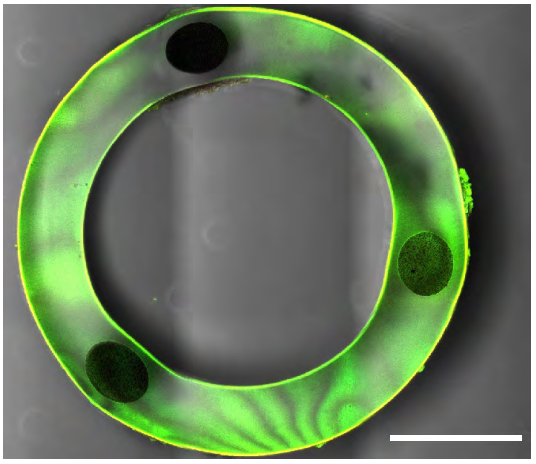

(A) P29 tip tile micrograph

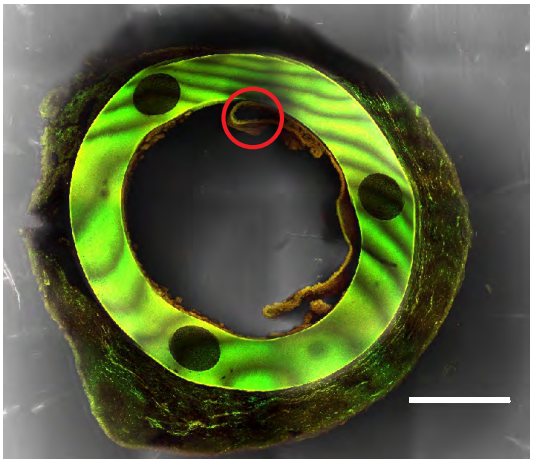

(B) P29 subcutaneous tile micrograph

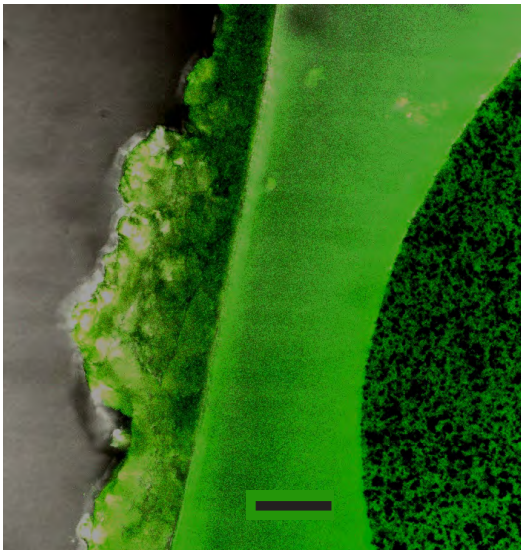

(C) P29 tip × 63 micrograph

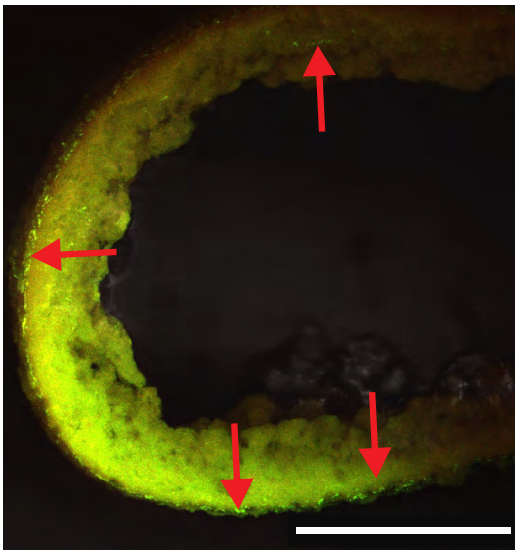

(D) P29 subcutaneous × 63 micrograph

Figure 4.11: (ii) CLSM micrographs of tip and subcutaneous PICC regions removed from patient 29. (A), showed the tip section tile scan with no biofilm morphological evidence, showed by a higher magnification micrograph (C) (scale bar= 20 μm). In contrast, (B) the subcutaneous section was positive for biofilms (scale bars = 500 μm) illustrated in the higher magnification micrograph of the red circle, (D), showed bacterial cells (in green) embedded within a protein deposit (in yellow, scale bar= 50 μm), image enhanced to emphasize green.

4.4.5 Data and statistics

The tip and middle sections from the adult samples had higher percentages of biofilm positive using CLSM results compared to the paediatric samples (Table 4.1 and 4.2). There was no statistical difference between different confocal biofilm positive sections in the adult (Mann-Whitney test, CI at 95%,P = 0.5045) or paediatric sections (Mann-Whitney test, CI at 95%, P = 0.248, Fig.4.12).

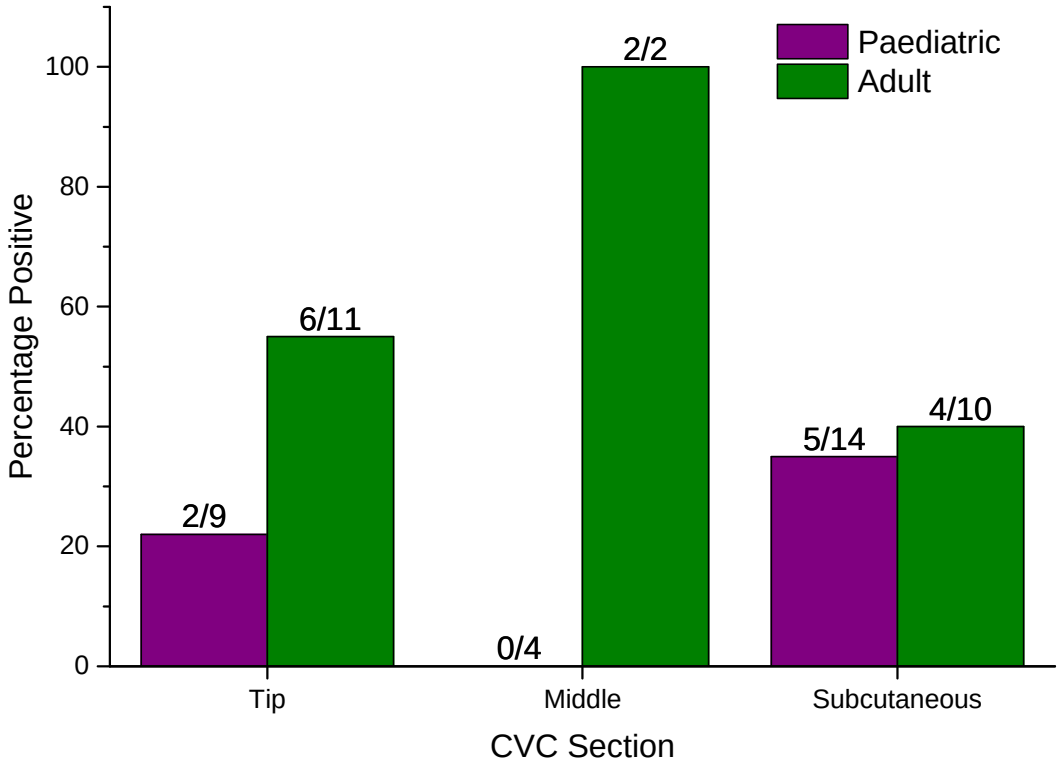

Figure 4.12: Plot showing percentage positive clinical CLSM for paediatric and adult CVCs. Paediatric positive bars in purple and adult positive bars in green. The tip is the section closest to the heart and the subcutaneous is the section just before the CVC exits the skin. There was no statistical difference between different confocal biofilm positive sections in the adult or paediatric sections (Mann-Whitney test, CI at 95%,P = 0.5045 and P = 0.248 respectively).

Table 4.1: Confocal laser scanning microscopy results for CVCs removed from adult patients.

Sample ID	Tip	Middle	Subcutaneous
P4	P	–	N
P5	N	–	N
P9	N	–	N
P18	P	–	P
P21	P	P	N
P26	P	–	N
P29	N	P	P
P30	N	–	P
P31	P	–	–
P32	N	–	N
P36	P	–	P
Percentage +'ve	54.55%	100%	40%

P denoted evidence for biofilm, N no evidence of biofilm and – no sample.

Table 4.2: Confocal laser scanning microscopy results for paediatric oncology patients.

Sample ID	Tip	Middle	Subcutaneous
C2	P	–	N
C3	N	N	P
C4	N	–	–
C5	–	–	P
C6	–	N	N
C7	N	–	N
C8	P	N	P
C11	N	–	N
C12	N	–	N
C13	N	–	P
C14	N	–	N
C15	–	N	N
C16	–	–	N
C17	–	–	N
C22	–	–	P
Percentage +'ve	22.22%	0%	35.71%

P denoted evidence for biofilm, N no evidence of biofilm and – no sample.

4.5 Discussion

In the current chapter, CLSM revealed that the tip sections of the adult CVC samples had higher biofilm positive results compared to the subcutaneous sections. In contrast, CLSM found more evidence of biofilms in the subcutaneous sections for paediatric samples compared to the tip sections. The difference in both cases however, were very small.

Whether the slightly higher percentage of subcutaneous sections for the paediatric CVC samples were because the samples were mostly tunnelled was not known. Nonetheless, CVC sample removal from the patient and processing with forceps probably caused significant destruction of any biological deposits on the CVC outer surface. Regardless, there was significant heterogeneity throughout the CVCs, often with one end containing thick biological films and the other end almost nothing (Fig. 4.11).

However, CLSM proved to be a difficult method for detecting biofilms on CVC surfaces. Sample sectioning, material autofluorescence and equipment limitations (focal depth) limited the accuracy. Interestingly, one of the common radiopaque CVC material fillers used is bismuth subcarbonate. Huang et al. (2014) found that bismuth subcarbonate is photo-luminescent at room temperature with an excitation spectrum in the range of 330–490 nm and emission spectra between 560–640 nm with maximum fluorescence at 613 nm. Therefore, it is hypothesised that the radiopaque compounds used in CVC materials may cause fluorescence during confocal microscopy. Clinical CVCs are not only manufactured to be radiopaque but also comes in a variety of colours. The pigments used to create these colours may also have played a part responsible for the fluorescence but that is only speculation.

CLSM method may have had significant operator bias since the method relied on operator experience and how well the CVC pieces were sectioned. This was because identifying bacteria was based on cell morphology and if any slices had uneven edges it was not possible to focus on that particular sample. In addition, CLSM is also limited regarding depth of field, even more so due to sectioning method that had to be used in this study.

Identifying biofilms based on morphology could've been resolved by using a method such as fluorescent *in situ* hybridisation (FISH) (Nistico et al., 2011). FISH was not attempted due to the method being very time consuming and would've required extensive development. In addition, due to the widespread CVC material autofluorescence the number of fluorescent probes available would've restricted the ability to identify different types of bacteria. To avoid material autofluorescence, scanning electron microscopy was done on neighbouring CVC sections.

Chapter 5

Scanning electron microscopy for biofilm detection

5.1 Introduction

Scanning electron microscopy (SEM) has shown that virtually all indwelling CVCs are colonised by microorganisms embedded in a biofilm matrix (Donlan, 2001; Raad, 1998; Raad et al., 1993; Marrie and Costerton, 1984) Although SEM (Section 2.5.2) has much higher resolution compared to CLSM, sample preparation in the form of fixation, dehydration and staining is required (Chang and Ritman, 1986). As a biological material, bacterial biofilms tend to be sensitive to the harsh treatments required for visualisation with scanning electron microscopes (Surman et al., 1996). Care must be taken when interpreting electron micrographs as sample preparation often results in the inclusion of artefacts (Richards and Turner, 1984). For example, fixatives such as glutaraldehyde was shown to cause fibrillar mesh work which was considered an artefact because the comparative sample that was not fixed with glutaraldehyde but prepared using a Sputter-Cryo technique showed bacterial shapes outlined in a slime layer (Richards and Turner, 1984). In addition, significant biofilm loss has also been shown to lead to biased conclusions about the amount and type of attached biofilm (Richards and Turner, 1984; Chang and Ritman, 1986). All the preparation required also results in more investment of time (Surman et al., 1996). Although, some CLSM techniques such as FISH can also be very time consuming (Hall-Stoodley et al., 2006; Nistico et al., 2011).

Although SEM is used for biofilm research, interestingly it was noticed that for CVC related biofilms SEM is used much more frequently compared to CLSM (Marrie and Costerton, 1984).

5.2 Materials and methods

All materials were purchased from Sigma Aldrich UK unless stated otherwise.

5.2.1 Sample preparation

After growing the CVC sections or clinical collection as described before, samples were incubated in general (SEM fix, 3% glutaraldehyde, 4% formaldehyde in 0.1M piperazine-N,N-bis 2-ethanesulfonic acid buffer (PIPES) at pH 7.2) or alcian fixative (alcian blue, 3% glutaraldehyde in 0.1M cacodylate buffer at pH 7.2) fix for a minimum of 12 hours. After fixing samples were submerged in PIPES buffer for 10 minutes.

5.2.2 Sectioning

Sample sectioning for SEM caused biomaterial loss and smearing. Initially transverse and longitudinal sections were cut. The sectioning step during sample processing which caused the least biomaterial loss had to be determined. Samples were sectioned before the fixing step, after fixing, before the ethanol dehydration series and lastly after critical point drying.

By visual inspection sectioning after fixation resulted in the least sample destruction. Precise sectioning for SEM samples were less critical compared to slices required for CLSM. Transverse sectioning could not be used for quantification and was very limited for biofilm detection and was thus not pursued further (Fig.5.1). Therefore, all SEM samples were sectioned longitudinally.

5.2.3 Ethanol dehydration series

The rinsed and sectioned samples were dehydrated using an ethanol series. PIPES buffer was exchanged with 30% ethanol for 10 minutes. The 30% ethanol was exchanged for 50% ethanol for 10 minutes, followed by 70% ethanol for 10 minutes, 95% ethanol for 10 minutes (this step was done twice) and lastly absolute ethanol for 20 minutes to complete the ethanol dehydration.

5.2.4 Critical point drying, stubbing and coating

Ethanol dehydrated samples were critical point dried (CPD) using carbon dioxide, stubbed and coated with gold-palladium.

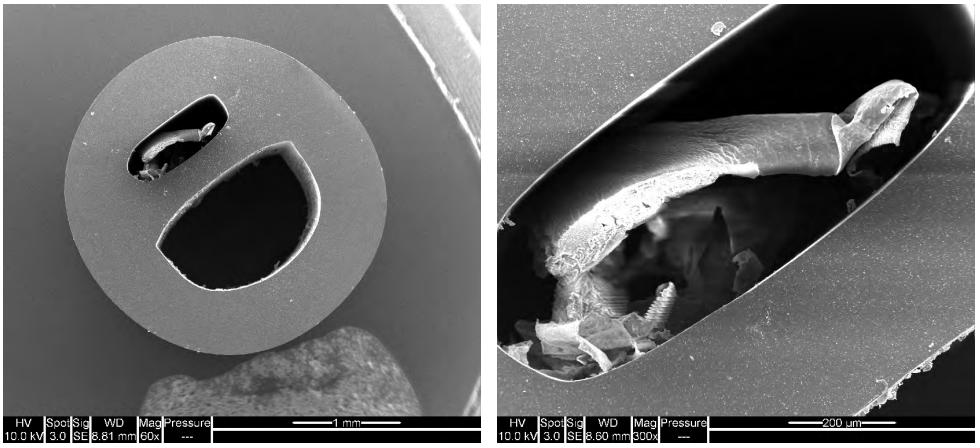

(A) (B)

Figure 5.1: Micrographs showing the limited use of transverse sectioning for SEM samples. (A) shows a transverse section of CVC removed from C2, a paediatric oncology patient. (B), a higher magnification micrograph of (A) showing CVC occlusion. The micrographs illustrate the limits of transverse sectioned clinical samples.

5.2.5 Microscopy

Coated samples were placed in a scanning electron microscope (SEM FEI Quanta 2000, USA) in full vacuum. SEM energy was set to 10 keV with a spot size of 3. The working distance was changed depending on the object being imaged but it was generally kept at circa 7 *mm*.

5.2.6 Image analysis

In order to quantify the clinical scanning electron micrographs a scoring system was developed to evaluate the degree of fouling on the CVC surfaces. A used CVC with little to no deposit (<10%) was scored at 1, 10 to 30% surface fouling was given a score of 2, 30 to 70% scored 3 and complete occlusion or very large pieces of deposit scored 4 (Fig. 5.2).

Score	Threshold		
1	0-10%	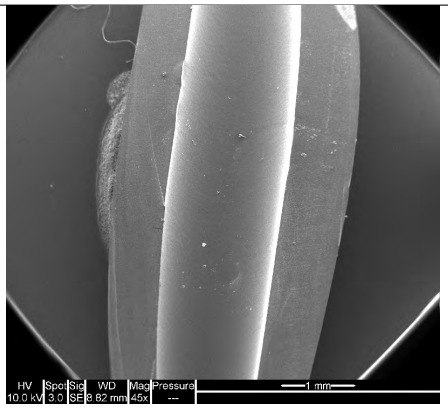	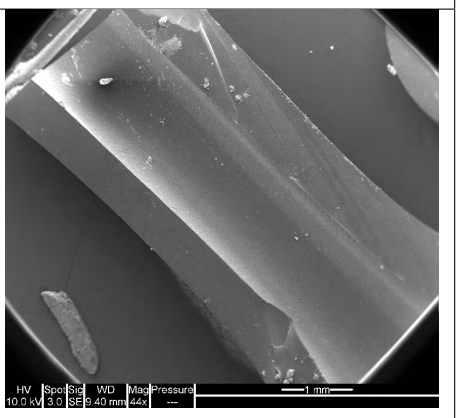
2	10-30%	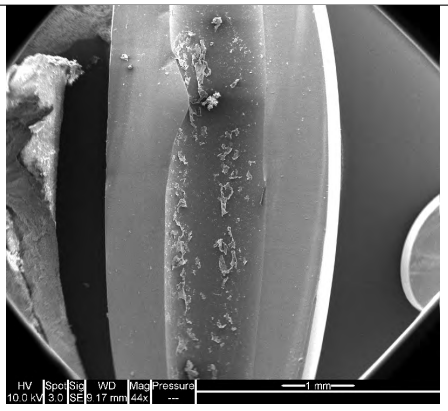	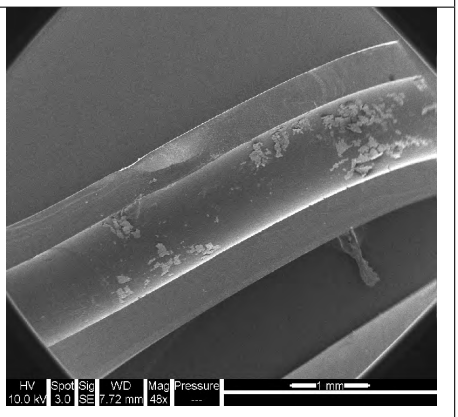
3	30-70%	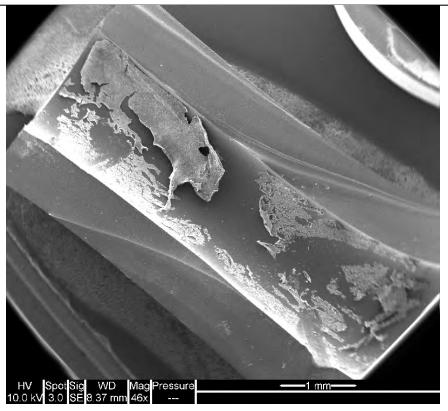	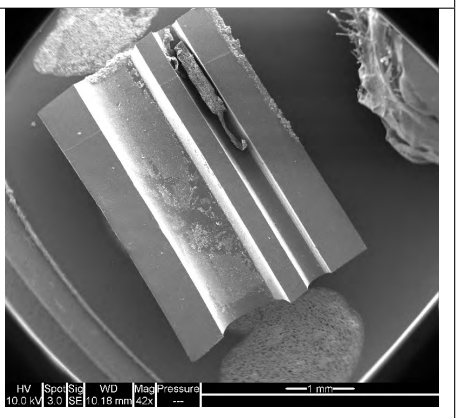
4	70-100%	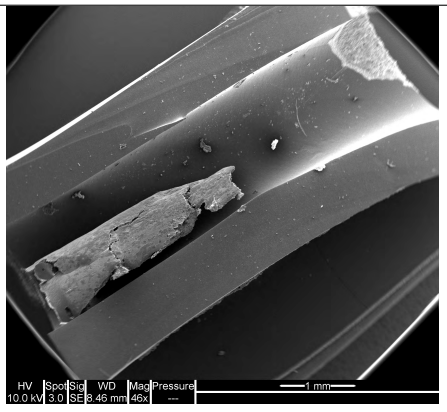	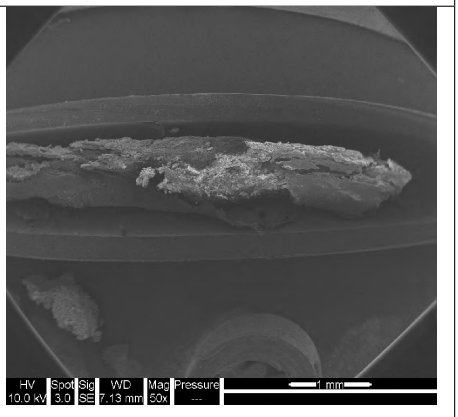

Figure 5.2: Scorecard for SEM analysis of bio-deposition in CVCs. The scorecard was developed using patient samples to quantify the degree of deposit. A small amount of deposit (<10%) scored 1, 10 to 30 % of surface fouled was given a score of 2, 30 to 70% scored 3 and complete CVC occlusion or very large pieces of deposit was scored at 4 (scale bars=1 *mm*).

5.2.7 Clinical biofilm positive

CVC sections that were examined using SEM required biofilm identification based on morphology. Human and bacterial cells differ in size and shape as outlined in Table 5.1. If cells were suspected as bacterial or fungal of origin, the diagnosis (diagnosis only as positive and not bacterial type) was made based on cell size and shape. Once a cell was identified as bacterial or fungal, a biofilm was diagnosed if there were two or more cells attached with/without visible EPS.

Table 5.1: Human blood, bacterial and fungal cell types and approximate sizes

Cell types	Size (μm)
Thrombocyte	2 - 3 (not regular in shape)
Red blood cell	6 - 8
Monocyte	7 - 10
Lymphocyte	7 - 15
Neutrophil and Eosinophil	10 - 12
Basophil	12 - 15
Macrophage	circa 21
P. aeruginosa	0.5 - 1 wide, 1-5 long
S. epidermidis and *S. aureus*	0.5 - 1.5
K. pneumoniae	0.5 wide, 2 long
C. albicans	3 - 4

5.2.8 Statistics

For comparing the evidence of biofilms at the tip, middle and subcutaneous sections and the degree of biofouling for the adult and paediatric CVC samples the Mann-Whitney test was used at 95% confidence intervals. The evidence of biofilms were ranked with 1 if there was evidence and 0 if no biofilms were found. The degree of biofouling was also ranked and compared using the Mann-Whitney test (Section 5.2.6). Significant difference was established when the probability value was less than 0.05 (Minitab 16, US).

5.3 Results

Scanning electron microscopy was used to ascertain whether biofilms were present on the *in vitro* model-grown and clinical CVC surfaces.

5.3.1 SEM on static *in vitro* model samples

In an *in vitro* system there was no added variables such as blood products, protein deposits or crystal structures (which may have been formed by medications). The only deposits on the CVC surface were the biofilms (Fig.5.3). However, processing required for SEM was extensive and may have produced artefacts such as cracks in the biofilms (Fig.5.3B), shrinkage and biomaterial loss similar to what was found in the clinical samples. The static CVC biofilm model had the most uniform growth and was thus used for all *in vitro* method development experiments (Sections 5.3.1 and 7.4.3).

5.3.2 SEM on *in vitro* CVC-flow biofilm model

The flow model proved to be successful and showed different amounts or thickness of biofilms along the CVC (Fig.5.4 and Fig. C.4). The heterogeneous spread of biofilms showed the heaviest growth at the tip section (Fig.5.4E and F) of the model compared to the middle (Fig.5.4C and D) and subcutaneous section (Fig.5.4A and B).

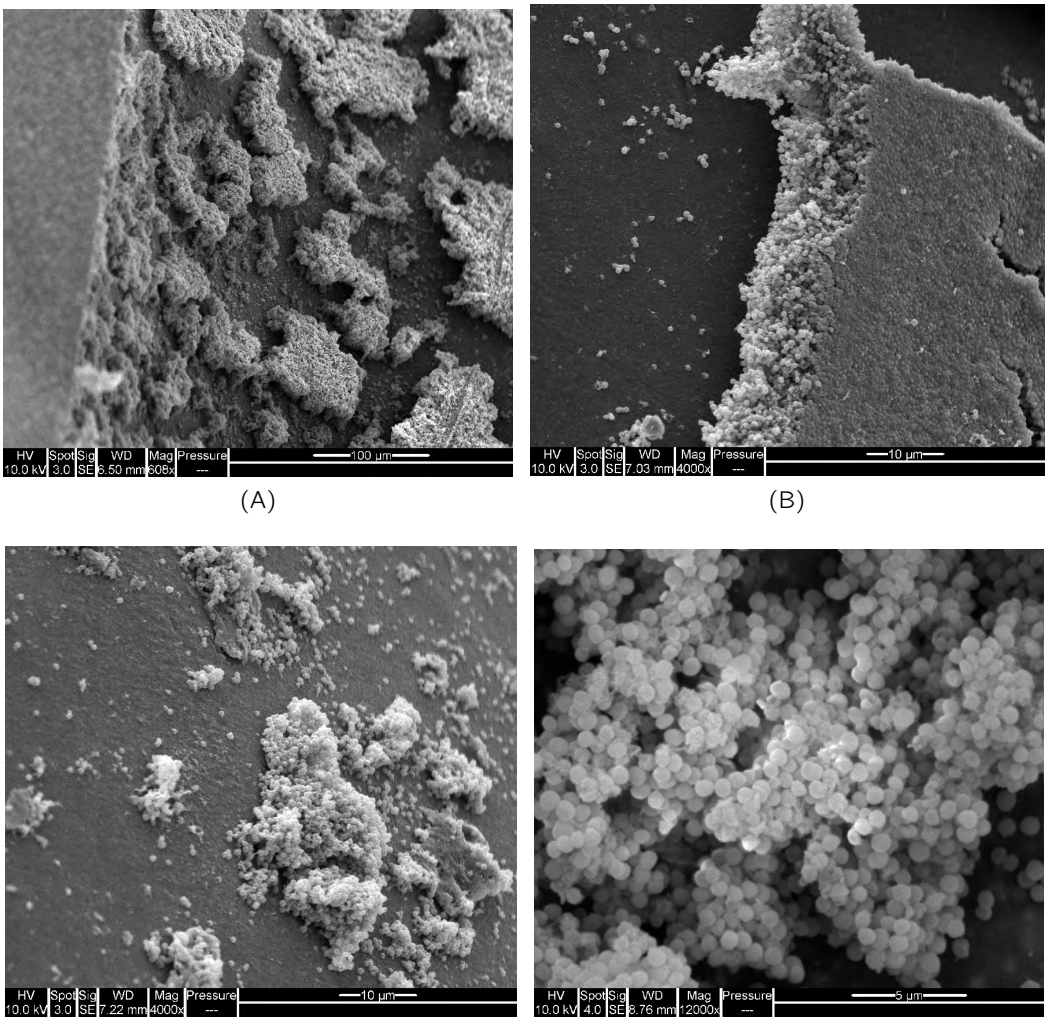

(A) (B)

(C) (D)

Figure 5.3: SEM micrographs of static *S. epidermidis* CVC-biofilm model samples. (A) showing biofilm growth in distinct clusters on the luminal CVC surface (scale bar=100 μm). (B) showing a biofilm with the drying effects evident by cracking of the film (scale bar=10 μm). (C) indicated that the biofilm grew in distinct clusters in areas on the outer surface as well (scale bar=10 μm) and, (D) higher magnification micrograph showing closely associated cocci (scale bar=5 μm).

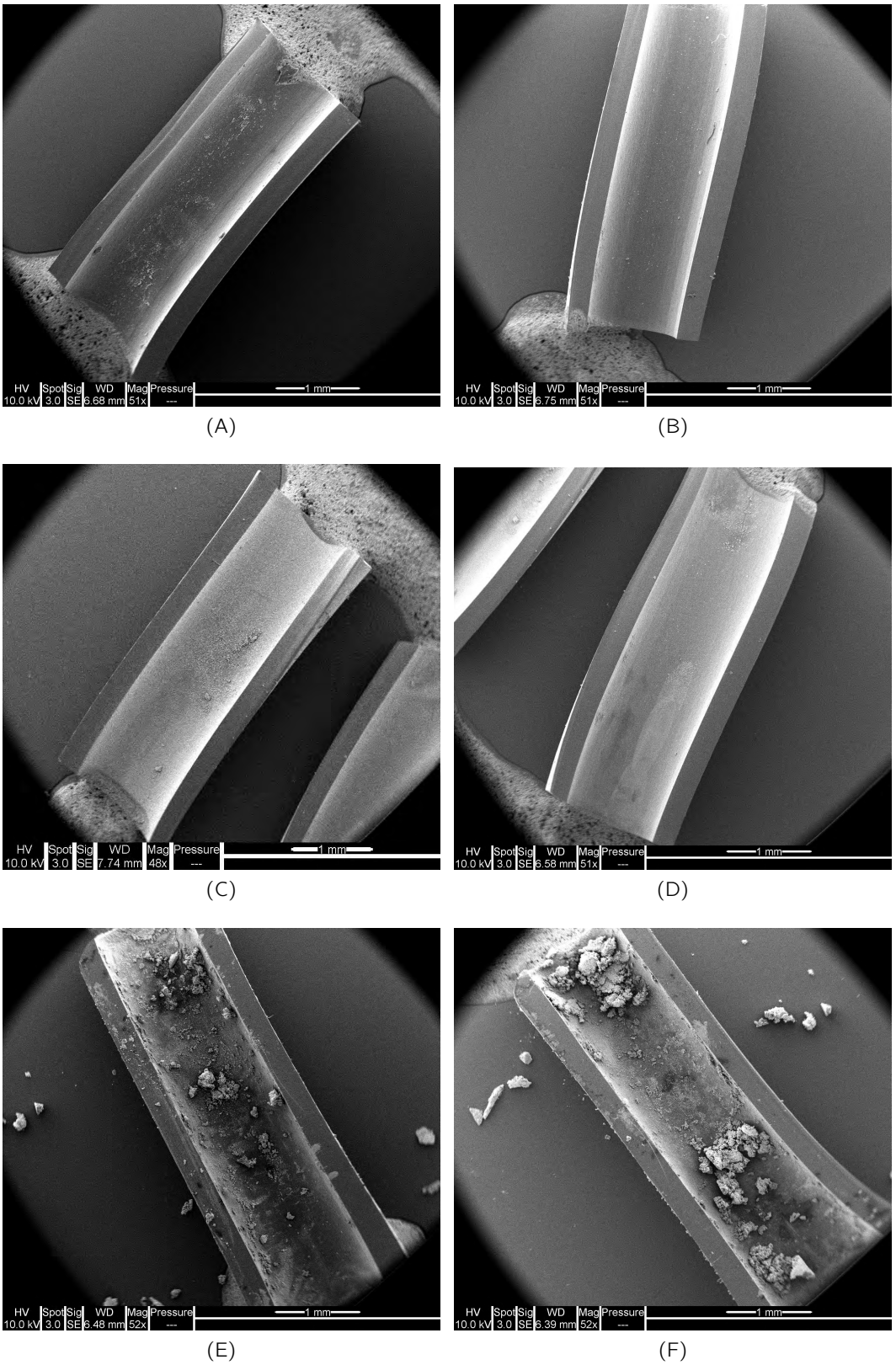

Figure 5.4: Scanning electron micrographs of CVC sections grown in the CVC-vein model. (A) and (B) were removed from the section of CVC closest to what would be the exit site. (C) and (D) were removed in the middle section and (E) and (F) was removed from the section of CVC closest to the media bottle (or the 'tip' region). Note in (E) and (F) the pieces of biofilm that fracture from the CVC surface.

5.3.3 Sample sectioning and heterogeneity of clinical samples

As discussed in Section 4.4.4 properties of the material the clinical CVCs were made from, silicone and polyurethane sectioning often resulted problematic sectioning. Silicone single lumen CVCs were more difficult to section longitudinally compared to single and double lumen polyurethane CVCs because polyurethane is much stiffer.

The biofilm distribution within the CVC lumens were highly heterogeneous when examined using scanning electron microscopy (Fig.5.5). To illustrate the heterogeneity, Fig.5.5 shows two micrographs of neighbouring subcutaneous sections removed from patient C5. Fig.5.5A was sampled at 15.5 cm away from the tip and illustrated evidence of a mixed species biofilm. Based on the cell shape and size, the mixed species biofilm appeared to contain cells of $< 5\ \mu m$ (yellow arrow) indicative of fungal origin and cocci shaped cells of 1 μm and 2 μm (red arrows) indicative of bacterial origin (see Table 5.1) In contrast, Fig. 5.5B was sampled at 16.5 cm from the tip and did not show evidence of a biofilm. The filamentous structures in Fig.5.5B may have indicated the presence of fungal hyphae. The sections of CVC did however not appear similar and highlights the heterogeneity which may contribute to false negative results.

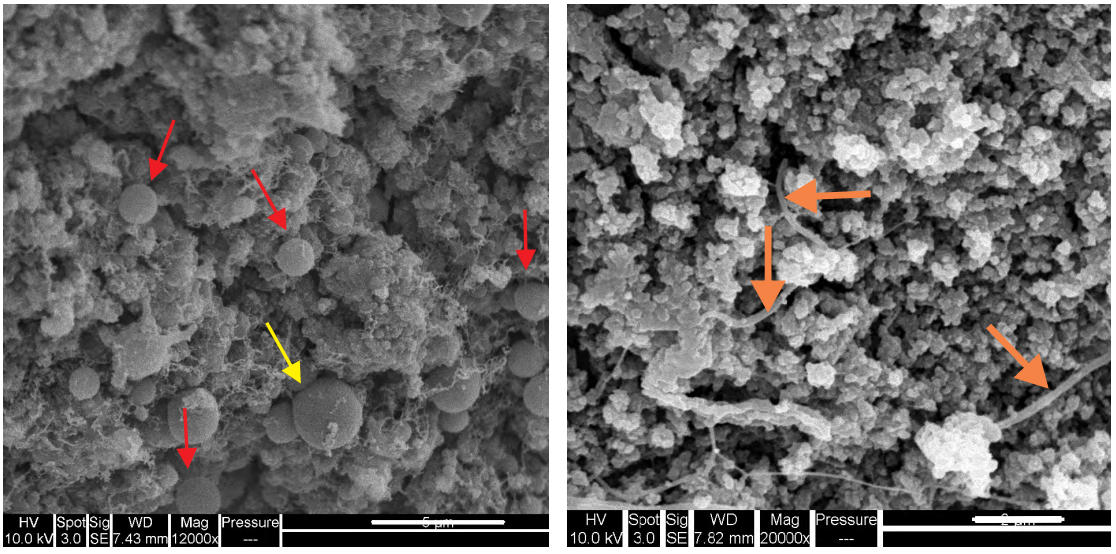

(A) C5 15.5 to 16.5 cm (B) C5 16.5 to 17.5 cm

Figure 5.5: Scanning electron micrographs of subcutaneous CVC sections from C5. (A) sampled at 15.5 to 16.5 cm from the tip(scale bar= 5 μm), showing a mixed species biofilm with cocci (red arrows) and possible yeast (yellow arrow). (B) sampled 16.5 to 17.5 cm from the CVC tip showing little evidence of a biofilm, with possible hyphae (orange arrows, scale bar= 2 μm).

The section cultured from C5 sampled at 17.5 to 18.5 cm away from the tip was culture negative (Table 3.6). A small slice of the section 15.5 cm away from the tip was also examined using CLSM and showed evidence for biofilm (Table A.2).

5.3.4 Data and statistics

There was no statistically significant difference for SEM biofilm positivity between the tip, middle or subcutaneous sections for adult (Mann-Whitney, CI at 95%, $P = 0.301$, $P = 0.398$, $P = 0.064$) and paediatric samples (Mann-Whitney, CI at 95%, $P = 0.313$, $P = 0.313$, $P = 1$, Fig.5.6). There was also no significant difference between adult and paediatric tip and subcutaneous section biofilm positivity (Mann-Whitney, CI at 95%, $P = 0.398$, $P = 0.693$ Tables 5.2 and 5.3)

Scanning electron micrographs were also analysed regarding the degree of deposition (Tables 5.2 and 5.3). Paediatric CVC sections had higher mean scores compared to adult sections (between 2.6 to 3.2 and 1.8 to 2.1 respectively). There was no statistical significant difference for SEM deposit scores between tip, middle and subcutaneous sections for adult ($P = 0.541$, $P = 0.541$ and $P = 1$ respectively) and paediatric samples ($P = 0.897$, $P = 0.737$ and $P = 0.479$ respectively). In contrast, there was a significant difference for deposit scores between paediatric and adult subcutaneous sections ($P = 0.011$).

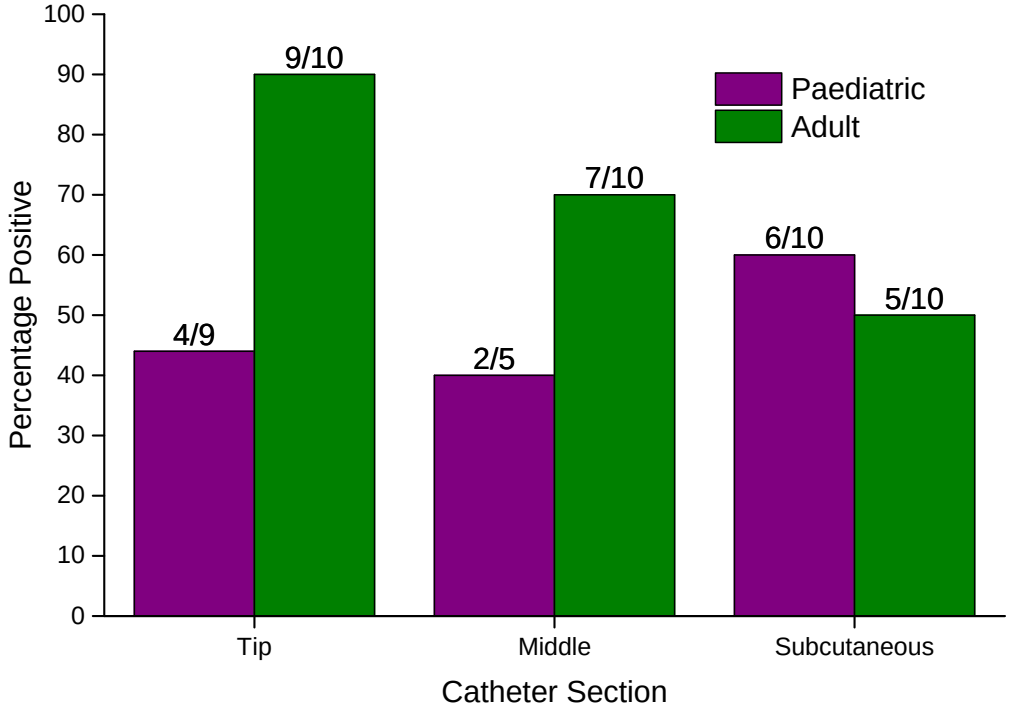

Figure 5.6: Plot for SEM percentage positive sections from adult and paediatric clinical samples. Paediatric bars were in purple and adult bars in green. Adult tip sections had higher percentage of positive sections compared to the paediatric samples and the opposite was true for the subcutaneous sections.There was no statistically significant difference for SEM biofilm positivity between the tip, middle or subcutaneous sections for adult or paediatric samples (Mann-Whitney, CI at 95%, $P = 0.301$, $P = 0.398$, $P = 0.064$ and $P = 0.313$, $P = 0.313$, $P = 1$ respectively).

Table 5.2: Scanning electron microscopy scores and evidence for the presence biofilm for CVCs removed adult patients. Catheters were scored from 0 to 4 for degree of deposit. The CVCs were also examined for the presence of biofilm.

Sample ID	Tip		Middle		Subcutaneous	
	Score	Biofilm	Score	Biofilm	Score	Biofilm
P1	1	P	1	P	1	P
P2	4	P	4	P	2	N
P3	1	P	2	P	3	N
P4	3	P	2	N	2	P
P5	2	P	2	N	1	N
P6	2	P	2	P	2	P
P7	1	N	4	N	1	N
P9	1	P	1	P	4	N
P18	1	P	1	P	1	P
P21	2	P	2	P	1	P
Mean score & percentage	1.8	90%	2.1	70%	1.8	50%

P denoted positive evidence for biofilm, N no evidence of biofilm.

Table 5.3: Scanning electron microscopy results of scores and evidence of biofilms on CVCs removed from paediatric oncology patients. The CVCs were also examined for the presence of biofilm.

Sample ID	Tip		Middle		Subcutaneous	
	Score	Biofilm	Score	Biofilm	Score	Biofilm
C1	4	N	4	N	4	N
C2	4	N	3	N	3	N
C3	3	P	–	–	–	–
C4	2	N	–	–	3	P
C5	3	P	–	–	3	P
C6	–	–	1	P	2	P
C7	1	P	–	–	4	P
C8	4	N	3	N	3	P
C9	1	N	–	–	1	N
C10	3	P	3	P	3	P
Mean score & percentage	2.6	44%	2.8	40%	3.125	67%

P denoted positive evidence for biofilm, N no evidence of biofilm and – no sample.

5.4 Discussion

In the current chapter, SEM found evidence in most of the adult (90%) and the majority of the paediatric CVC samples (70%). However, not all of the sections had evidence of biofilms which are discussed further in the text below.

Examining CVCs using SEM, similar to Raad et al. (1993), found evidence of biofilms in nearly all adult and paediatric CVC samples (90% and 70% respectively). The adult CVC samples had the most evidence of biofilms at the tip sections whereas the opposite was true for the paediatric samples. In addition, the scorecard showed that the subcutaneous sections of paediatric CVCs were much more fouled compared to the adult subcutaneous sections. Again, this may have been due to the fact that most of the paediatric samples were tunnelled CVCs and thus more than likely the amount of fibrin sheets formed were higher due to more tissue damage. Increased fibrin sheets may also have accounted for higher culture positive rates (Mehall et al., 2002; Chittick and Sherertz, 2010; Abdelkefi et al., 2005).

It should be mentioned however that only the inner lumen of the CVCs were inspected. This was because processing required the sample to be mounted and thus the sample could not be turned around. However, only the inner lumen was considered because the outer surface of the CVC may have been damaged during retrieval from the patient, handling with forceps as well as sectioning. Therefore, biofilms may have been missed if it was located on the external CVC surface. In the material and methods section of Raad et al. (1993), the protocol was to examine the luminal (inner) and external surfaces of each specimen. Yet they also critical point dried and sputter coated their samples with gold. So it would not have been possible to examine both the inner and outer CVC surfaces. They could have detached the sample from the stub and re-stubbed and coated the samples but significant sample destruction would have occurred where the samples were mounted to the initial stub. In addition, removing flexible material after it was probably also mounted onto carbon stickers would have caused extreme damage and loss (crumbling, cracking from the surface etc.) of any biomaterial on the sample (Chang and Ritman, 1986).

One issue which spans all the methodology in this project was heterogeneity within CVCs. Sections right next to each other was found to look completely different (Fig. 5.5). Therefore, false negatives from any of the methods may have been due to missing the section containing the biofilm. Although sample sectioning and SEM specific sample processes were problematic and caused biomaterial loss, electron microscopy suffered fewer limitations compared to CLSM. However, one of the limitations SEM shared with CLSM was that biofilm detection was based on cell morphology, and although there was no autofluorescence which significantly influenced CLSM the method was still biased. The biggest limitation for SEM was that patient protein (such as fibrin and fibrinogen) may have caused an initial deposit on the CVC surface and bacteria may have adhered to the

protein layer but may also have been covered by additional biological deposits which may have resulted in not being able to see the biofilms. *S. aureus* have been shown to bind to fibronectin, fibrinogen and laminin (Lowy, 1998). So because SEM only scanned the sample surface if biofilms were covered with anything the section would've resulted in a false negative diagnosis.

SEM was done on two neighbouring sections of CVC (C5 subcutaneous sections) where the one section showed evidence of a bacterial biofilm and the other did not contain bacteria but may have had fungal hyphae. So it could be that the disagreements between the different detection methods were not due to the one method being superior over the other but that the particular section did not contain any biofilm but the next section that was analysed with another method did.

False negatives could have been caused by fixatives such as glutaraldehyde which was shown to cause fibrillar mesh work that was considered an artefact because the comparative sample prepared using a Sputter-Cryo technique showed bacterial shapes outlined in a slime layer (Richards and Turner, 1984).

In order to reduce false negatives from culture, biofilm fracture and loss caused by sectioning and CPD for SEM processing and potentially missing biofilms due to being covered by other deposits x-ray micro computed tomography was developed next.

Chapter 6

Contrast stain for x-ray μCT

6.1 Introduction

Similar to water and soft tissues biofilms do not attenuate x-rays very much. In order to visualise biofilms using x-rays, a contrast enhancing stain with a higher x-ray attenuation coefficient may be required. Complimentary to the CT scanner settings, the best possible contrast agent will depend on the sample thickness as well as the atomic number and density of the stain.

The sample composition needs to be considered in relation to the stain chosen. The biological target abundance has to be evaluated as the efficiency of the stain will increase if more of the target is available. When staining biofilms, the EPS and bacterial cell composition are the stain targets. Biofilms are mainly composed of water, carbohydrates (EPS), DNA, lipids (cell membranes) and proteins (cell contents).

6.1.1 Attenuation coefficient of the sample

The attenuation coefficient, μ is the fraction of incident photons absorbed from the x-ray beam in a unit of distance. The attenuation coefficient of matter increases with density and increasing atomic number (Wildenschild and Sheppard, 2013; Bayaraktar et al., 2008). Atomic number matters because as the x-ray beam penetrates the material the more atoms there are the more the beam will be attenuated. In table 6.1, the atomic number and densities of well known metals used in histology stains as well as some other common elements and catheter material elemental components are summarised.

In the soft x-ray range, the attenuation decreases with increasing photon energy (keV) of the x-ray beam (Kalender, 2011; Hubbell and Seltzer, 2014). The exception is at a K-edge of an element, where the attenuation will increase rapidly with an increase in photon energy.

Table 6.1: Metal stain candidates. Atomic number and densities of heavy metals, common elements and elemental components of catheter material

Metal component of stain	Atomic number	Density at r.t. (g/cm^3)
Silver	47	10.501
Gold	79	19.2828
Tungsten	74	19.25
Silicon	14	2.3296
Barium	56	3.594
Carbon	6	2.267
Oxygen	8	0.001429
Calcium	20	1.55

The Beer-Lambert law describes the relationship between light transmitted and absorbed in terms of attenuation coefficient and sample length, given by equation:

$$I = I_0 e^{-\mu L} \tag{6.1}$$

where I is the incident and I_0 is the transmitted x-ray intensities; L is the thickness of the material (1 cm) and μ is the linear attenuation coefficient of the material.

At an energy of 30 keV, the value of μ for 1 cm of bone is 1.6 cm^{-1}, so the fraction of photons transmitted through bone is $e^{-1.6}$ or 0.20 (20%). For soft tissue the mean μ is 0.38 cm^{-1} at 30 keV, so 68% of the photons are transmitted through 1 cm of soft tissue. At 30 keV the μ value for water is 0.37 cm^{-1}, so 69% of the photons are transmitted through 1 cm of water. Therefore, in the reconstructed tomograph there would not be any contrast between water and soft tissue.

The linear attenuation of gold, silver, tungsten and silicon is summarised in Figure 6.1. When a CT scanner with a polychromatic x-ray source at 70 keV would have an average keV of circa 35 keV (Siemens, 2014). At 35 keV, gold would have the highest linear attenuation coefficient compared to tungsten and silver.

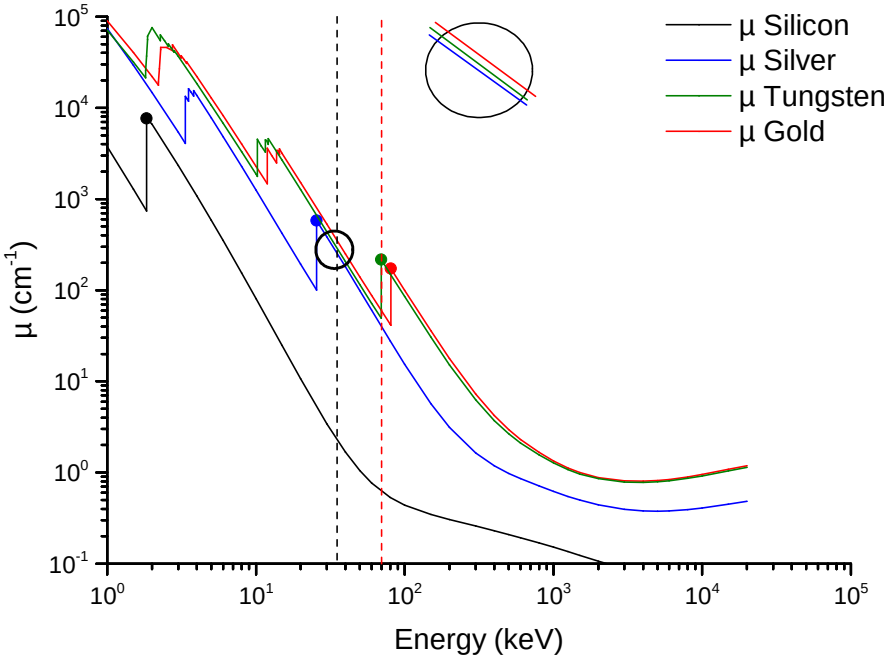

Figure 6.1: Linear attenuation coefficient plots of gold, silver, tungsten and silicon. The keV of the scanner is the dashed black line (70) with the average flux the red dashed (35). Where the red line intersects the graph at Y is the theoretical linear attenuation of each metal at 35 keV. Gold has the highest theoretical linear attenuation at 35 keV followed by tungsten and silver. Attenuation coefficient data from (Hubbell and Seltzer, 2014).

Therefore, a metal contrast agent in the form of a stain would be required to increase the contrast and allow the distinction of biofilms from water. To evaluate contrast agents, the elemental composition of the stain, atomic number, density of the stain and the thickness of the sample needs to be taken into consideration.

6.1.2 Heavy metal stain selection

X-ray μCT has been used extensively to study small animals. Metscher (2009) wrote an in-depth review about using different stains to compare the ability to distinguish between different tissues. Stains that have been used in x-ray μCT for small animals include phosphotungstic acid (PTA), phosphomolybdic acid (PMA), potassium iodide (KI), iodine (I_2), osmium tetroxide (OsO_4), phosphotungstic acid (PTA) (Metscher, 2009). With PTA and inorganic iodine deemed the most broadly useful.

Metscher (2009) goes on to conclude that OsO_4 is the most commonly used contrast stain for x-ray μCT of soft tissues due to strong x-ray absorption. Osmium tetroxide is however highly toxic, expensive to dispose of, does not stain well if samples had been in ethanol

and slow to penetrate specimens. Although PTA also penetrates slowly, it is less toxic, easier to use and will stain samples that have been stored in alcohol (Metscher, 2009). In addition, Metscher (2009) has shown that inorganic iodine penetrates all soft tissues they tested and was shown to be versatile and robust.

Davit et al. (2011) also used iodine to validate that a medical suspension of barium sulphate used as a negative stain did not penetrate the biofilm. The suspension of barium sulphate was used to differentiate between aqueous, biofilm phase and polyamide beads to model porous media for x-ray μCT . The authors were able to visually observe the 3 different phases and the non stained biofilm phase was validated by staining the biofilm with iodine solution followed by another CT scan. The areas darker than the barium sulphate and lighter than the beads disappeared when stained with iodine so the authors concluded that the 3rd visible phase were biofilm. The authors were able to conclude that only a very small quantity of barium sulphate penetrated the EPS.

In contrast, Iltis et al. (2011) did not use any contrast agents but deposited silver coated glass microspheres of 5 to 15 μm in diameter on to a biofilm surface when they used synchrotron CT to examine biofilms in modelled porous media. Due to the large size of the silver beads (5 to 15 μm) the detailed biofilm structure may have been missed or very small aggregates may have appeared larger if the bead attached to an aggregate smaller than 10 μm. The authors used larger beads so that the beads did not penetrate the biofilm but whether the beads did penetrate remains unknown.

Clinically used metal based transmission electron microscopy stains were considered selected based on their ability to bind to organic matter, density, atomic number and most importantly, user safety (Table 6.2). Initially, traditional and more toxic stains that were considered included; osmium tetroxide, mercuric chloride, uranyl acetate, Reynold's lead and iodine. Osmium tetroxide reacts moderately with proteins but progressively weakens with time, it reacts strongly with phospholipids and unsaturated fats and reacts weakly with saturated fats. Lead salts react strongly with nucleic acids, proteins, phospholipids and glycogen. Uranyl acetate reacts strongly with nucleic acids and protein and reacts weakly with phospholipids, polysaccharides and fats. Mercuric chloride stains some proteins and Iodine stain starch. Gold (nano gold at 10 *nm* and/or 60 *nm* gold) is inert and stains biological material by sticking to the surface, nano gold is also commonly used in clinical diagnostic tests (Wilson, 2008). Phosphomolybdic acid stains proteins strongly (Metscher, 2009). Silver nitrate stains proteins as well as nucleic acids (Klug et al., 2000). The organic materials are all found within biofilms and were potential candidates.

Table 6.2: Metal stains analysed using EDS for potential x-ray contrast agents.

Metal stain	Metal	Atomic number	Density (g/cm^3)	Safety
Uranyl Acetate	Uranium	92	18.95	Radioactive and toxic
Reynold's Lead	Lead	82	11.34	Toxic
Mercuric Chloride	Mercury	80	13.456	Highly toxic
Gold	Gold	79	19.32	Nontoxic and non-irritating
Osmium Tetroxide	Osmium	76	22.4	Highly toxic
Phosphotungstic Acid	Tungsten	74	19.3	Mild irritant
Iodine	Iodine	53	4.93	Irritant
Silver nitrate	Silver	47	10.501	Irritant
Phosphomolybdic Acid	Molybdenum	42	10.22	Irritant

6.2 Experimental approach

In order to determine which stains are best retained by biofilms and would be more likely to absorb x-rays, energy dispersive x-ray analysis (EDS) was used. EDS evaluates elemental content of samples by detecting characteristic radiation produced by different elements within the sample (Lünsdorf et al., 1997). Radiation travels through space as individual photons, therefore, eventually the photon is absorbed by transferring the energy back to an electron. The chance of the energy absorption from the photon to the material electron is greatly enhanced if the photon encounters a material with electron energy levels close to the photon energy content. Consequently, EDS indirectly measures the ability of the contrast agent to absorb x-ray radiation.

EDS analysis was firstly done on *S. epidermidis* biofilms stained with a single metal stain (Section 6.3.5). Initially EDS was done on traditional more toxic stains; because the final goal would be to use the stains *in vivo* , less toxic single stains were tested and focused on. However, because it is commonplace to use more than one stain for increased metal loading for microscopy enhancement (Lackie, 1996; Scopsi et al., 1986; Lackie et al., 1985) we analyses samples with dual stains (Section 6.3.6).

For EDS counts per second and weight percentage composition (of each element) was used to semi quantitatively compare staining efficiency. The hypothesis was that the stain which produced the highest counts per second (signal, thus greatest percentage of the element present), along with the atomic number and density would result in the best contrast enhancing stain for x-ray μCT .

6.3 Materials and methods

All materials were purchased from Sigma Aldrich UK unless stated otherwise.

6.3.1 Biofilm growth on glass slides

To test the metal stains using EDS, 10 *mm* circular glass microscopy coverslips were placed in a 24 well plate and inoculated with 1 *ml* of *S. epidermidis* (strain ATCC 35984) at 4.76 $\times$ 10^5 CFUs per *ml* in tryptic soy broth (inoculum as prepared in Chapter 3, Section 3.3.3) for 5 or 3 days at 37 ^{o}C, 5% CO_2 in an incubator (Fig. 6.2). Tryptic soy broth medium was changed daily by using sterile plastic pipettes. Coverslips with biofilms were fixed overnight in 1 *ml* of general fix (3% glutaraldehyde, 4% formaldehyde in 0.1 *M* piperazine-N,N-bis 2-ethanesulfonic acid buffer (PIPES) at pH 7.2.). Fixed coverslips were gently immersed in 1.5 *ml* of PIPES buffer for 10 minutes twice.

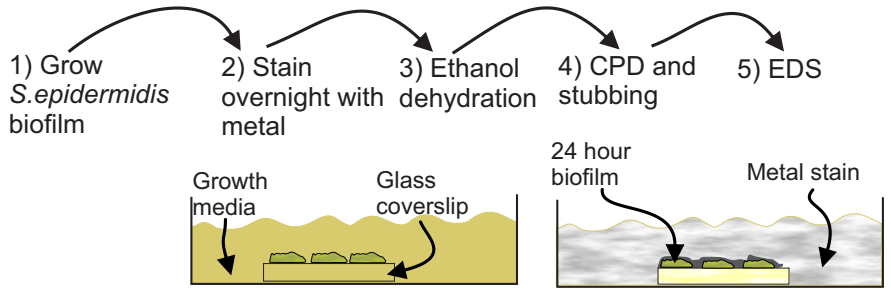

Figure 6.2: EDS sample preparation. Samples were prepared for EDS analysis according Sections 6.3.1, 6.3.4 and 6.3.5 by staining with a metal after biofilm growth, ethanol dehydration and critical point drying.

6.3.2 Stain preparation

6.3.2.1 Traditional stains

Initially samples grown on 10 *mm* microscopy slides for 3 days were stained with 4% aqueous osmium tetroxide, 2% uranyl acetate, 10% mercuric chloride, 10% phosphomolybdic acid, 3% phosphotungstic acid or 1% iodine.

Osmium tetroxide was prepared by the Southampton University Biomedical Imaging Unit by dissolving apules in distilled water. 2%(w/v) Uranyl acetate was prepared by adding 2 g to 100 m*l* of 50% ethanol. Uranyl acetate solution was left in the fridge overnight at 4^{o}C. 10% Aqueous (w/v) mercuric chloride and phosphomolybdic acid (saturated and filtered) were individually prepared by dissolving in distilled water. Phosphotungstic acid at 3% was prepared by making a 10% stock of 10 g PTA in 100 *ml* distilled water. In order

to improve penetration into cells, 30 *ml* of the stock was mixed with 70 *ml* of absolute ethanol to make 3% PTA in 70% ethanol. Iodine solution was prepared by mixing 0.2 *g* of iodine to 20 *ml* of absolute ethanol to produce 1% concentration of iodine (w/v).

6.3.2.2 Safer stains

Less toxic stains prepared included nano gold, silver nitrate and phosphotungstic acid. The nano gold (10 and 60 *n*m, BBI Solutions, UK) stains did not require any preparation and was used at full concentration. 10 *nm* Gold had 5.70×10^{12} and 60 *nm* gold 2.60×10^{10} particles per *ml*. Phosphotungstic acid was prepared as above. To make a 3% silver nitrate staining solution, acetate buffer (pH 5.6) was prepared by making stock solutions of 0.2 M acetic acid (stock A) and 0.2 M sodium acetate (stock B). For stock A, 1.2 *ml* glacial acetic acid was mixed in 100 *ml* distilled water and for stock B, 1.64 g sodium acetate anhydrous was dissolved in 100 *ml* distilled water. To complete the sodium acetate buffer, 4.8 *ml* of stock A and 45.2 *ml* of stock B was mixed and made up to 100 *ml* with distilled water. A 10% aqueous silver nitrate stock solution was prepared by dissolving 10 g of silver nitrate in 100 *ml* distilled water. For the finished silver solution, 10 *ml* of the acetate buffer, 3 *ml* of the aqueous silver nitrate and 87 *ml* of distilled water was mixed by shaking.

6.3.3 Sample staining

After rinsing the coverslips (from Section 6.3.1) with buffer the samples were also rinsed in distilled water. The samples destined for PTA staining firstly had to go through an ethanol dehydration series. The samples were bathed in approximately 1 *ml* of 30, 50 and 70% ethanol for 10 minutes each (Section 5.2.3). Thereafter, the partially dehydrated samples were immersed in PTA in a fume hood overnight. All other samples were placed in the stains without other preparation and left in the fume hood overnight. The container that had the samples stained with silver nitrate were covered with aluminium foil (to prevent light reaction).

6.3.4 Washing, ethanol dehydration and critical point drying

After staining, the osmium tetroxide, uranyl acetate, nano gold and silver nitrate stained samples were washed twice for 10 minutes with 1.5 *ml* 0.1 M PIPES buffer and phosphomolybdic acid and iodine samples with 70 and 100 % ethanol respectively. PIPES washed coverslips were dehydrated by an ethanol dehydration series by submersing the samples in 1 *ml* of 30, 50, 70, 95 and finally 100% ethanol for 10 minutes each. And phosphomolybdic acid samples were dehydrated from 70 to 100% ethanol. Ethanol

dehydrated coverslips were stubbed on aluminium stubs using carbon self adhesive stickers followed by critical point drying using carbon dioxide before SEM and EDS analysis

6.3.5 EDS on single stains

6.3.5.1 EDS on traditional single stains

The first set of stubbed, more toxic samples were coated with a thin layer of carbon before being placed in the SEM at full vacuum at 10 mm working distance, 20 keV, spot size of 4.5 μm, pressure of 10^{-5} Torr at $\times$1000 magnification with an approximate 1900 counts per second and dead time of around 20%. Coverslips were scanned using energy dispersive x-ray analysis and analysed with Genesis Spc (SEM FEI Quanta 2000, USA). Counts per second for each metal was normalised against the total counts of all elements.

6.3.5.2 EDS on safer single stains

Because the thin layer of carbon could have affected results and artefacts from using full vacuum, another SEM was found. The stubbed and dried samples and placed in an SEM in wet mode with low vacuum (environmental mode) at 10 keV with spot size of 4.5 μm, pressure of 0.6 Torr and count rate of 5000 to 6000 and dead time of 20% and analysed with NSS X-ray Microanalysis (Phillips FEI XL30 ESEM, USA). In order to account for varying amounts of biological matter and the semi-quantitative nature of EDS on biological matter (imperfect surface) the counts collected by the detector in the spectra for the samples were compared as weight percentages of the total count of all elements detected as a standard method.

6.3.6 EDS on dual stains

Samples were stained and prepared identically to the safer single stained samples (including concentrations). The only difference was that after the washing steps (Section 6.3.5) the samples were stained with a secondary metal stain for another 12 hours (Table 6.3).

6.3.7 Sonication culture of glass slides

EDS data was compared to culture by sonication and solid agar plating. Biofilms grown for 5 days on 10 *mm* glass slides (described previously in Section 6.3.1). Each slide was washed in buffer and gently broken into 2 or 3 pieces and placed in 1 *ml* of PBS buffer in an Eppendorf tube. Each tube was vortexed for 10 seconds before sonication for 3 minutes.

Table 6.3: Heavy metal stains used to enhance contrast for x-ray μCT scans between CVC material, biofilm and liquid phase

Primary stain	Secondary stain
10 *nm* Gold	Silver nitrate
60 *nm* Gold	Silver nitrate
10 *nm* Gold	Phosphotungstic acid
60 *nm* Gold	Phosphotungstic acid
Silver nitrate	Phosphotungstic acid

After sonication the Eppendorf was vortexed again for 10 seconds and serial dilutions were made (vortex of 10 seconds between each dilution). Thereafter, 3×10 μl drops were placed on an agar plate quartile for each dilution. The plates were incubated for 12 hours at 37 ^{o}C, 5% CO_2. Colony counts were performed after 12 hours of incubation.

6.3.8 Statistics

The data produced by EDS analysis was continuous. In each test, the means of two groups stained with different metals were compared to each other. Because the samples all had *S. epidermidis* biofilms grown under the same conditions but were stained with different metals the two-sample, two-tailed t-test was performed on both single and dual stained experiments at 95% confidence intervals. Significant difference was established when the probability value was less than 0.05 (Minitab 16, US).

6.4 Results

Energy dispersive x-ray analysis determined that dual stain (Section 6.4.2) gave better signal to the single stains (Section 6.4.1.2).

6.4.1 EDS on single stains

6.4.1.1 EDS on traditional single stains

The micrographs of areas analysed with full vacuum EDS showed that biofilms were morphologically similar regardless of the stain (Fig.6.5). It was noted that mercuric chloride staining resulted in crystal formation (Fig.6.5D and Fig.6.3). The micrographs showed bands of light and dark streaks. Streaking was caused by charging. Charging can be reduced by the use of gold-palladium sputter coating. However, gold-palladium would interfere with the signals from the metal stains. In this experiment, the purpose was to

compare the arbitrary amounts of metal in the stained biofilm rather than imaging. The micrographs were difficult to obtain as the samples were coated with carbon instead of metal. Carbon coating was used so that there was no interference from the coating when performing the EDS scans. As a result when the micrographs were being taken the biofilm section immediately started to degrade. Sample degradation was observed once the EDS scans were complete and the magnification was reduced. The shape of the electron beam was visible, similar to what is known as electron beam-induced etching. Carbon coating also reduced the sample conductivity which increased electrostatic charge at the sample surfaces. Sample charging explained why the micrographs were bright in some areas and dark in others in a streak pattern. It is believed that mercuric chloride fixes some proteins but in this instances it formed crystals as seen in fig.6.3.

There was a statistical difference detected between the percentage silver, osmium ($P = 0.01$), uranyl ($P = 0.009$), lead ($P = 0.027$), iodine ($P = 0.008$), PTA ($P = 0.036$) as well as PMA ($P = 0.008$). The difference between the percentage of osmium and PTA detected was not statistically significant ($P = 0.116$ Fig. 6.4). In contrast the differences for PTA and mercury ($P = 0.002$), uranium ($P = 0.003$), lead ($P = 0.001$), iodine ($P = 0.0001$) and PMA ($P = 0.0001$) was statistically significant.

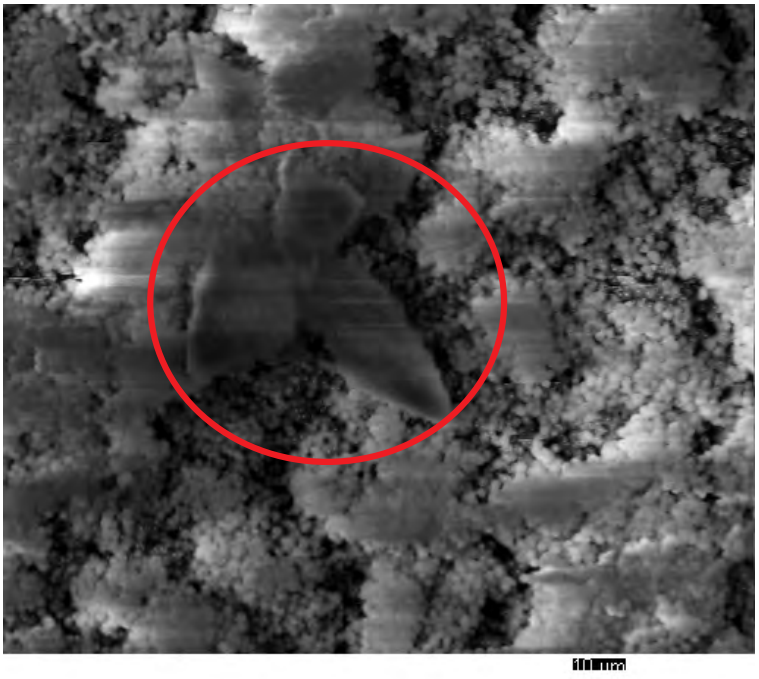

Figure 6.3: A scanning electron micrograph of mercuric chloride crystals on 24 hour *S. epidermidis* biofilm grown on a glass coupon. The red circle highlights a crystal that was formed when mercuric chloride was used as a stain. The individual cocci in the biofilm clusters can also be observed(scale bar= 10 μm).

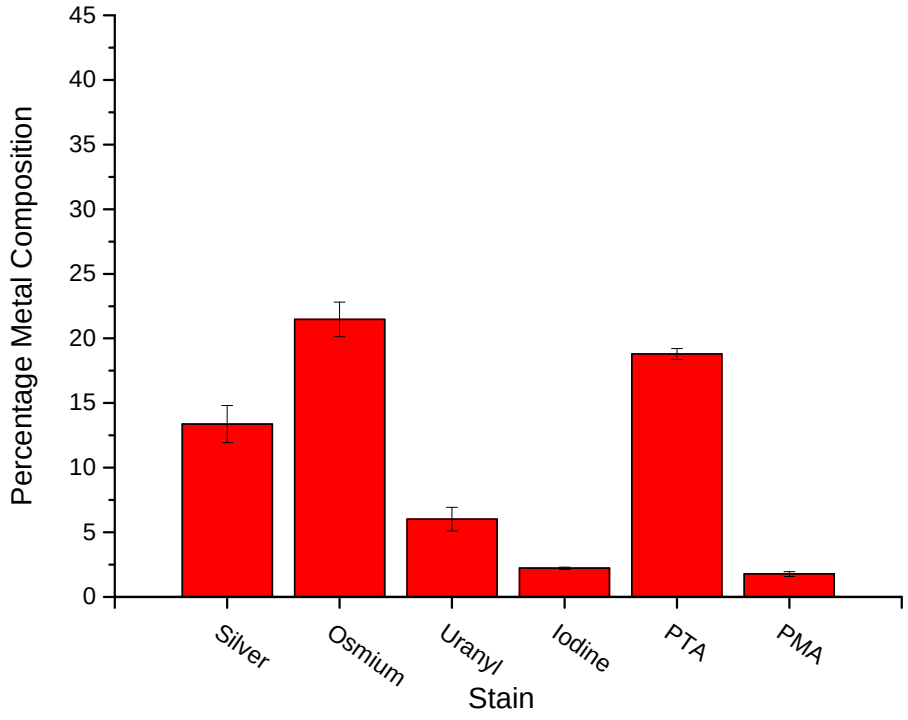

(A)

Figure 6.4: EDS percentage of metal detected in single metal stains. The plot showed that Phosphotungstic acid and Osmium tetroxide were the highest stain constituents detected in the scans. There was a statistical difference using the t-test between the percentage silver, osmium ($P = 0.01$), uranyl ($P = 0.009$), lead ($P = 0.027$), iodine ($P = 0.008$), PTA ($P = 0.036$) as well as PMA ($P = 0.008$).

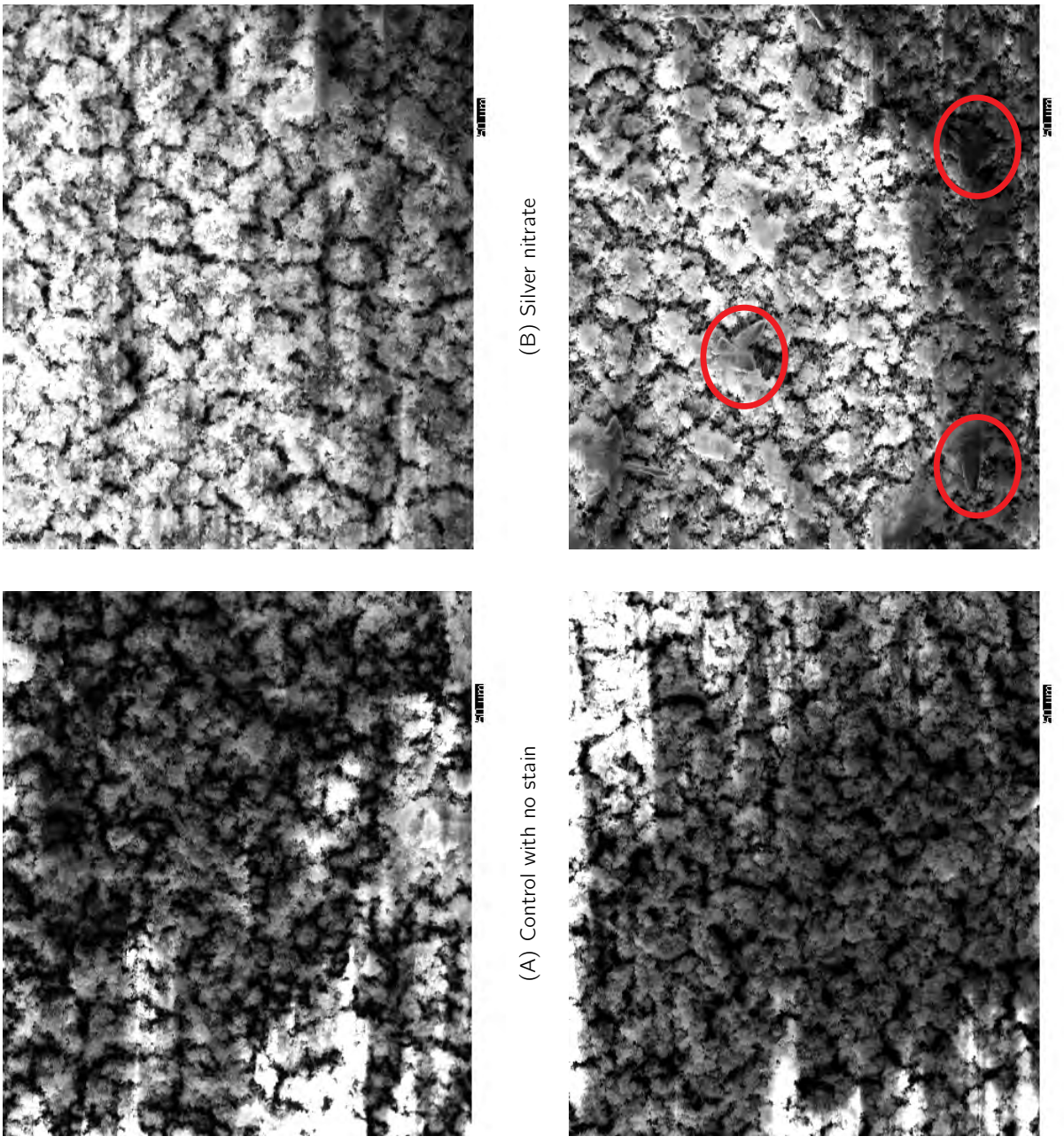

(A) Control with no stain (B) Silver nitrate (C) Osmium tetroxide (D) Mercuric chloride

Figure 6.5

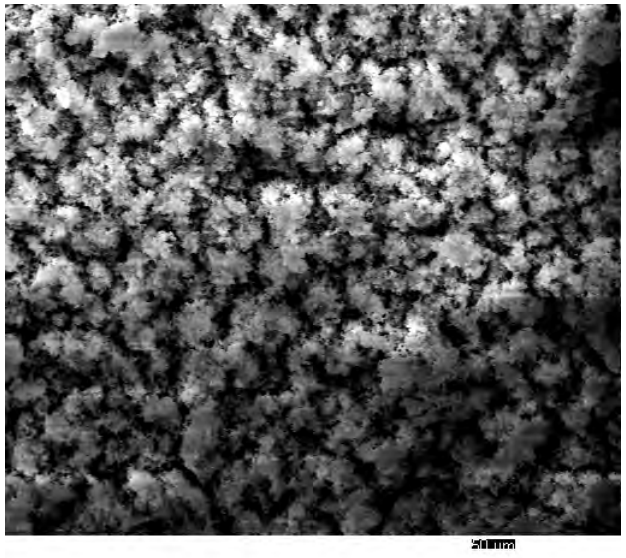

(E) Uranyl acetate

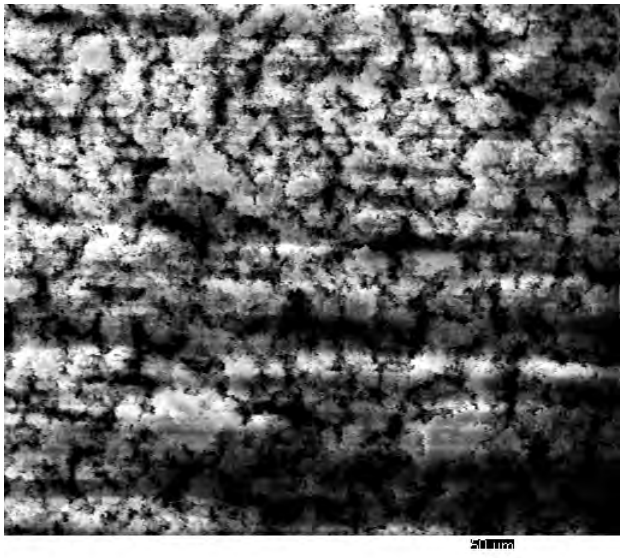

(F) Reynold's lead

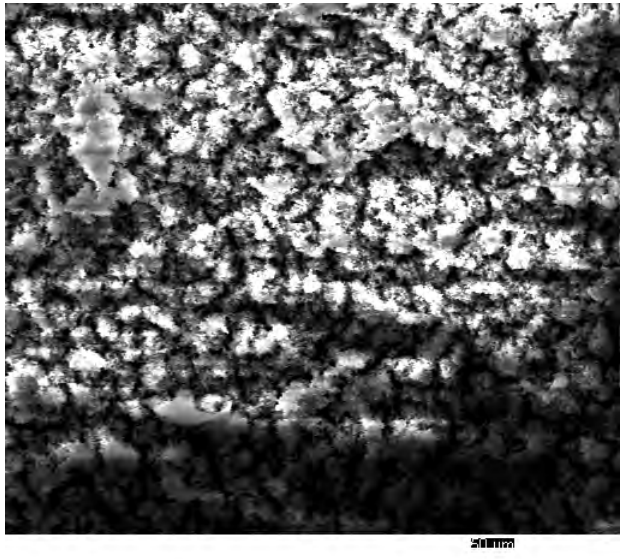

(G) Iodine

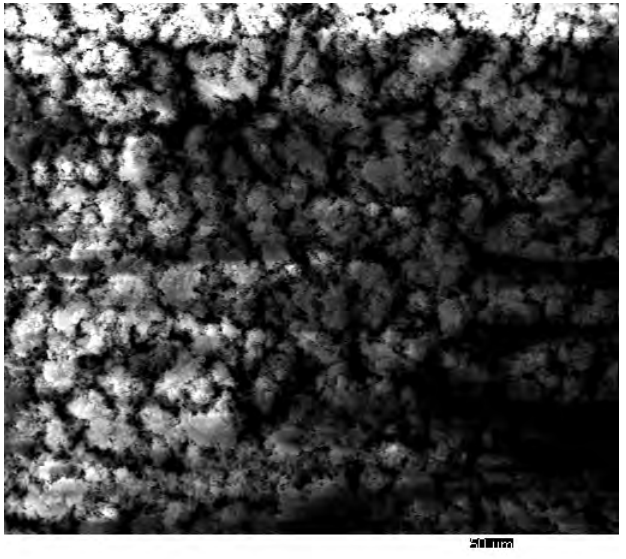

(H) Phosphomolybdic acid

Figure 6.5: (ii) Micrographs of biofilms grown on glass slides analysed with EDS. The micrographs showed that biofilm coverage were similar for all heavy metal samples that underwent EDS analysis (scale bars = 50μm).

6.4.1.2 EDS on safer single stains

The micrographs of the biofilm positive glass slides on which environmental EDS was performed showed the presence of biofilms (Fig. 6.6). All samples showed similar morphology (Fig. 6.7, (B), (D) and (F)). The EDS spectra collected from the samples which contained biofilm (Fig. 6.8B) showed a bigger carbon peak and smaller silica peak compared to the negative control (Fig. 6.8A) showing the presence of biological matter corroborating the micrographs.

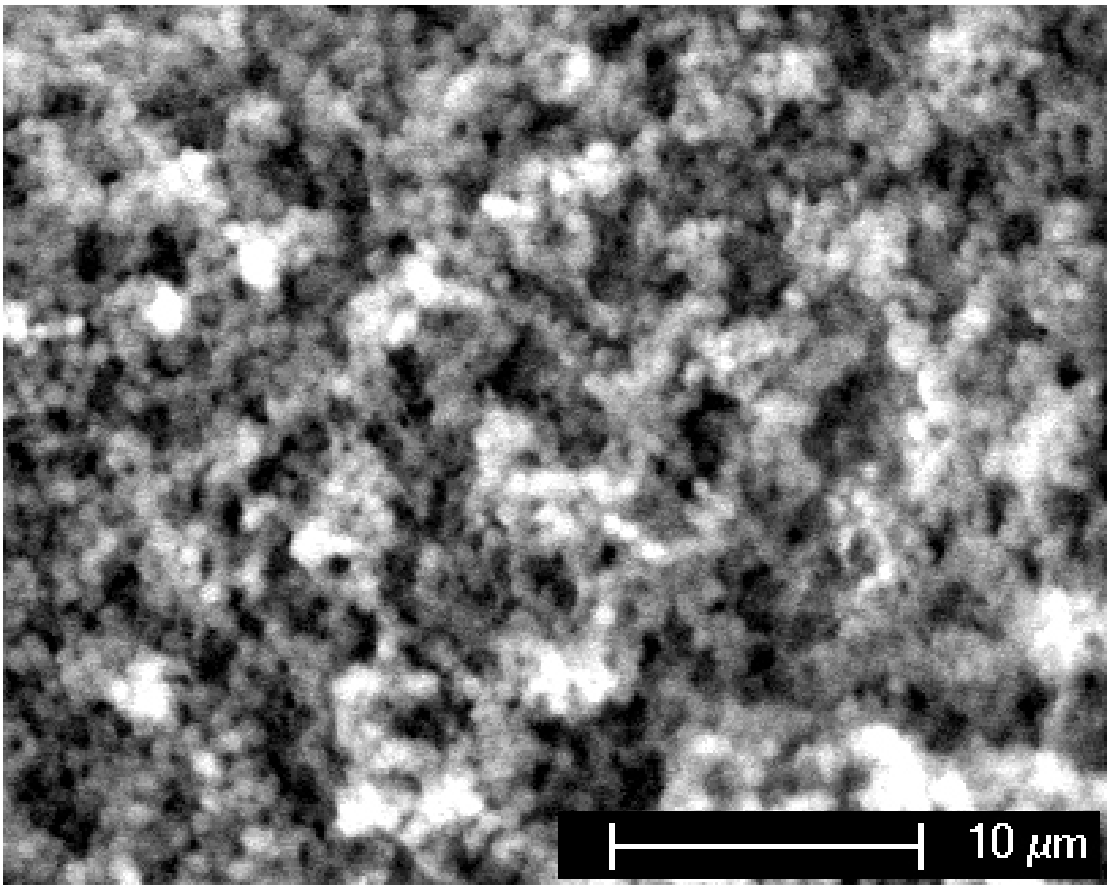

Figure 6.6: High magnification electron micrograph of a biofilm positive glass slide stained with nano gold used for EDS showing the presence of biofilm.

EDS on the biofilm negative samples stained with single stains showed that the metals did not bind to the glass slides (Fig. 6.7(A), (C) and (E)). Some material was visible on the biofilm negative stained controls. However, the EDS spectra collected from the biofilm negative control samples only showed evidence of glass (Fig. 6.8A). Elements detected which form constituents of glass include silica at 1.74, 1.83 and 1.84 keV from silicon dioxide, oxygen at 0.52 and 0.53 keV, sodium at 1.04, and 1.07 keV from sodium oxide and aluminium at 1.49, 1.5 and 1.6 keV from aluminium oxide (Fig. 6.8). Therefore, due to the nature of the processing required and no elements detected other than glass constituents (similar to what would be found in sand or dust) the material may have contained particles from dust contamination.

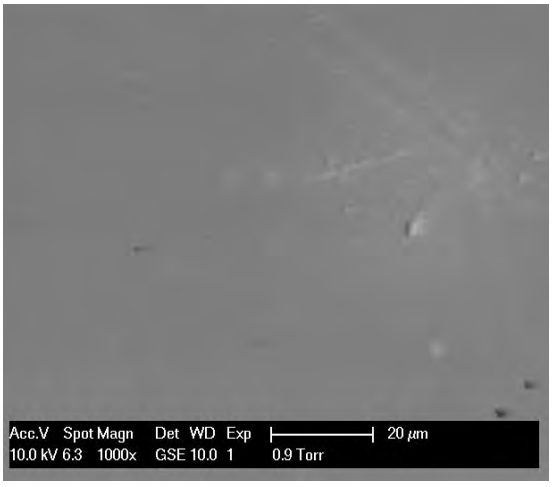

(A) Gold control

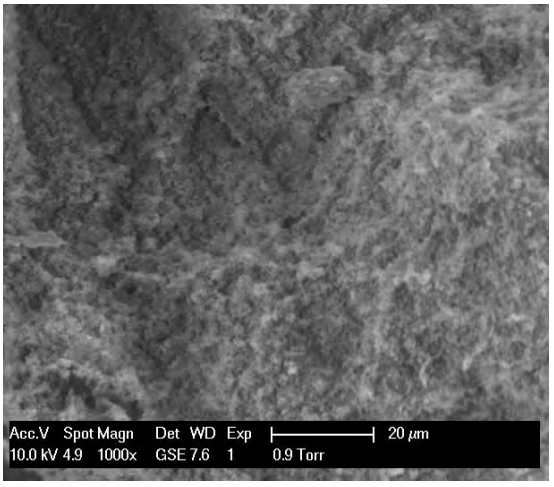

(B) Nano gold

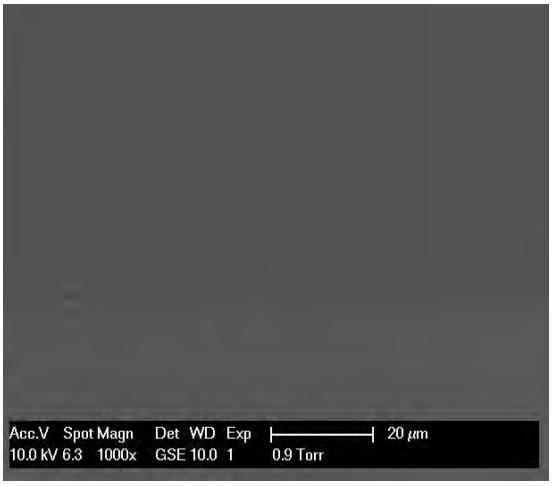

(C) Silver nitrate control

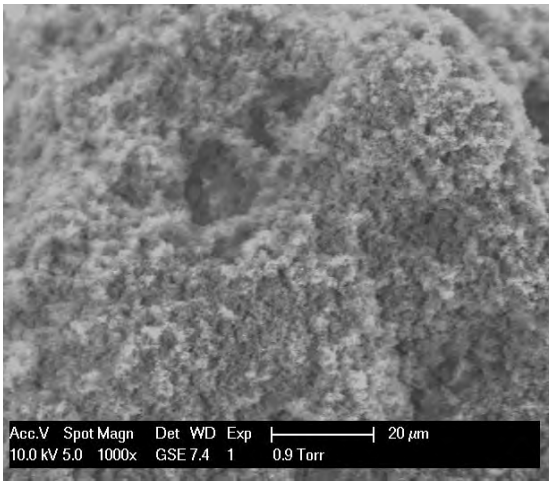

(D) Silver nitrate

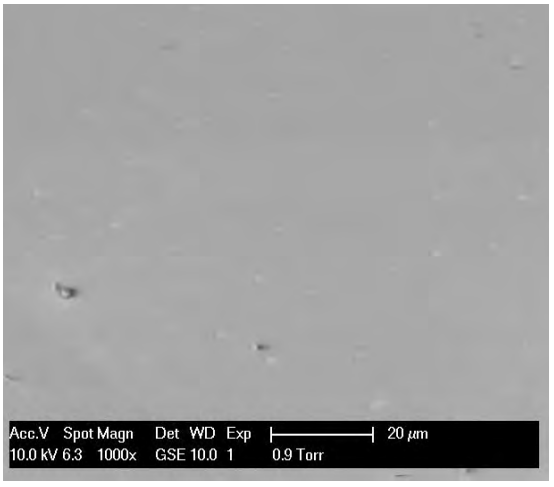

(E) PTA control

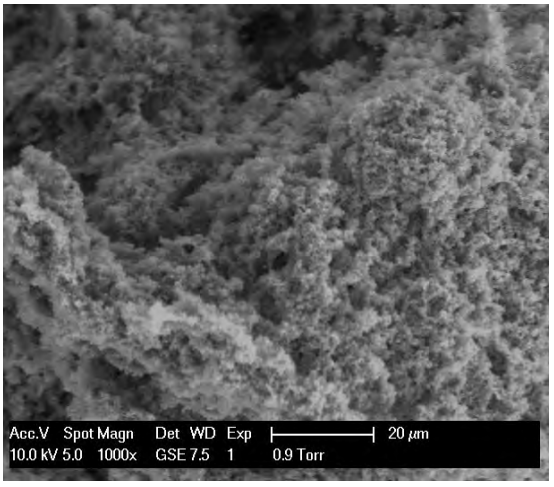

(F) PTA

Figure 6.7: Micrograph of biofilm grown on a glass slide and analysed with EDS. The micrograph showed that biofilm coverage were similar to the dual stained heavy metal samples that underwent EDS analysis (scale bars = 20μm).

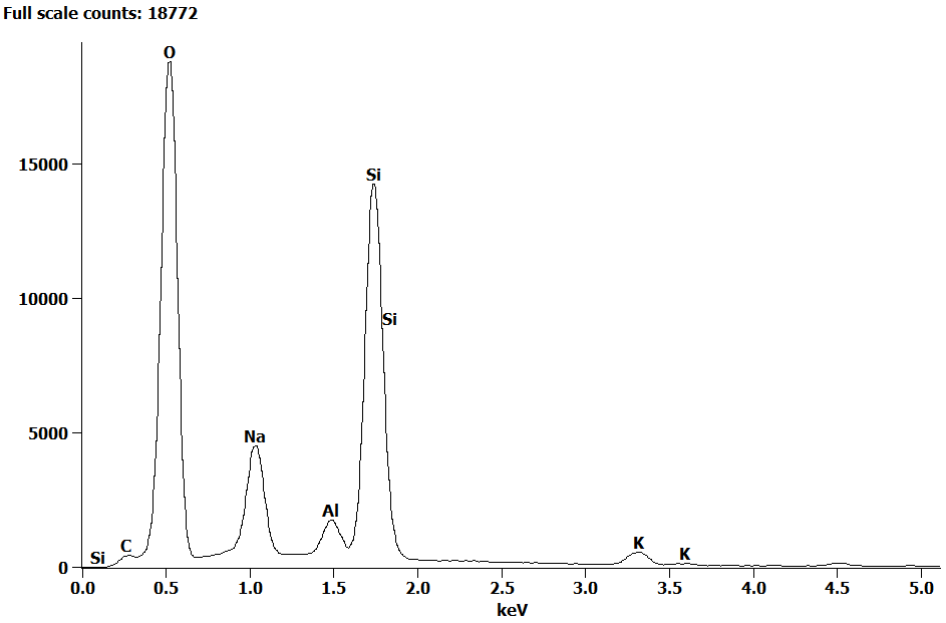

(A) Gold stained −'ve control

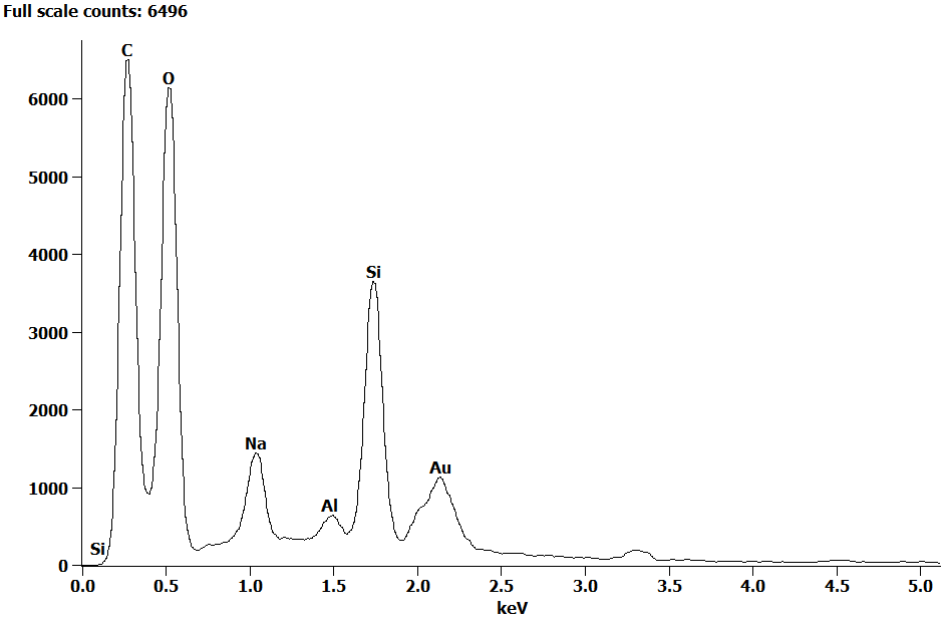

(B) Gold stained

Figure 6.8: Spectrum produced after energy dispersive x-ray analysis on single metal stains. (A) showed the spectrum of a biofilm negative control stained with gold. There were no gold peaks in the spectrum and a very low carbon peak, indicative of glass slides with no biological matter. (B) was a biofilm glass slide sample stained with gold showing a clear gold peak between 2 and 2.5 keV and a much higher carbon peak.

Because biological samples are imperfect for EDS analysis, the results are semi-quantitative. Therefore, the normalised elemental weight percentage was used (Fig. 6.9). When the weight percentage metal composition in the stains were compared there was statistical difference between gold and silver ($P = 0.003$) gold and tungsten ($P = 0.0001$); and silver and tungsten ($P = 0.0001$).

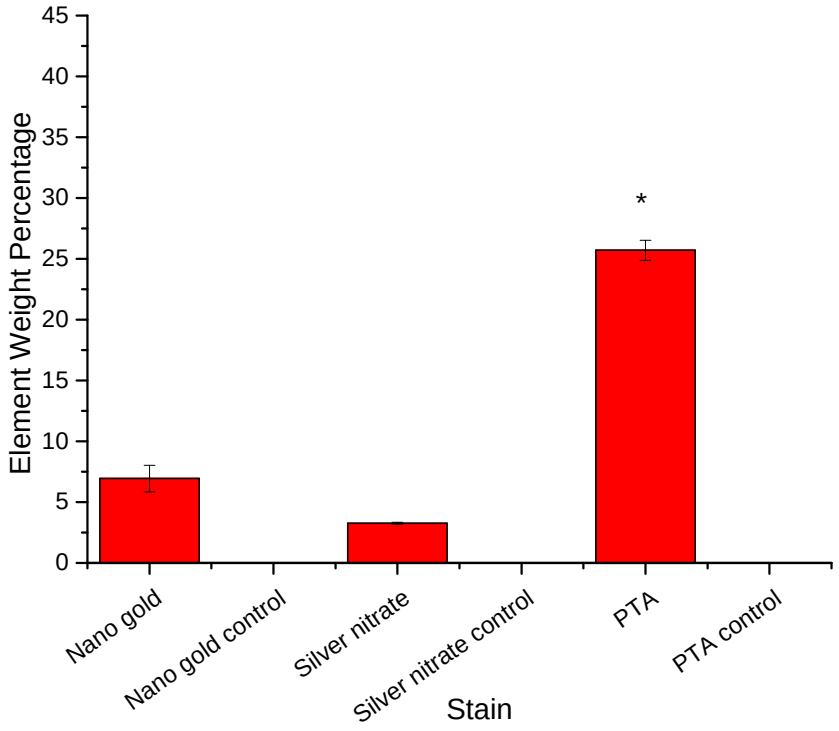

Figure 6.9: Plot comparing element weight percentage metal composition in biofilm samples using EDS. No metals were detected in the stained negative controls. PTA resulted in the highest metal load within the biofilm. The weight percentage metal composition in the stains were compared using the t-test and there was statistical difference between gold and silver ($P = 0.003$) gold and tungsten ($P = 0.0001$ as indicated by $*$); and silver and tungsten ($P = 0.0001$ as indicated by $*$).

6.4.2 EDS on dual stains

A representative high magnification micrograph (Fig. 6.10) showed that the biofilm positive glass slide samples contained bacteria. The micrographs taken during EDS analysis also showed that the biofilm positive samples stained with 10 *nm* gold and silver nitrate, 60 *nm* gold and silver nitrate, 10 *nm* gold and PTA, 60 *nm* gold and PTA; and silver nitrate and PTA all appeared similar in morphology (Fig.6.11). The samples looked slightly different to that of the single stains (Fig.6.7) which may have been due to enhanced fixing from using two stains. The appearance of more detail for the dual stained samples could also

have been due to a heavier metal load which increased conduction and reduced scattering artefacts (SEM was in environmental mode with no coating, Section 6.3.5).

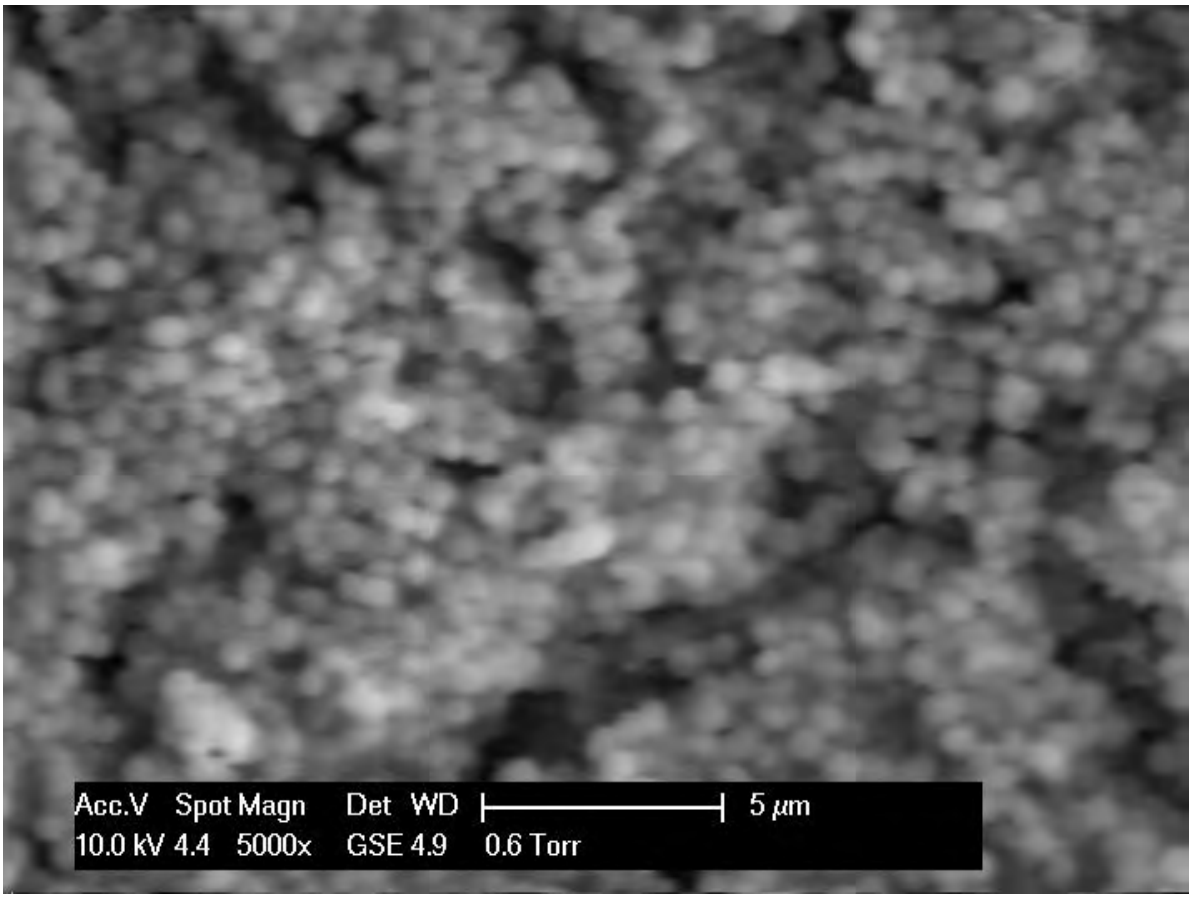

Figure 6.10: High magnification micrograph of a biofilm positive glass slide used for dual stain EDS showing the presence of bacteria.

Similar to the biofilm negative samples stained with single metal stains, the dual metal stains did not bind to the glass slides either (Fig. 6.11) but had unidentified substance. Again, the EDS spectra collected during analysis for the biofilm negative control samples stained with the various dual stain combinations showed no sign of the elements contained within the stains (Fig. 6.12A). There was a very small carbon peak near 0.27 keV indicating little to no biological matter.

All the samples which contained biofilm (Fig. 6.12B) showed significantly bigger carbon peaks and smaller silica peaks. As an example of the data, the sample stained with 10 *nm* nano gold and silver nitrate showed a gold peak seen at 2.12 keV and a silver peak at 3.35 keV showing that the stains were retained within the biofilm. The higher count rate seen in the control sample was because EDS works best on smooth, polished samples thus the x-rays received from 'non perfect' biofilm samples do not give such high signals. For this reason, the count rate could not be used, and the data was analysed by element weight percentage as seen in Figure 6.13. The mean CFU per 13 mm glass slide was 6.9×10^7 with no statistical significant difference between the replicates ($0.063 \leq P \leq 0.270$).

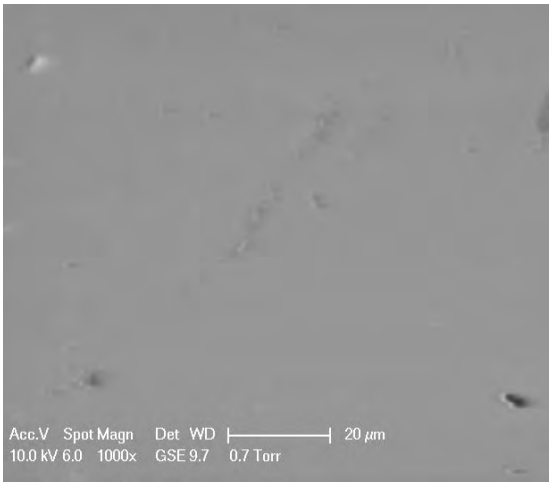

(A) 10 *nm* Gold and silver nitrate control

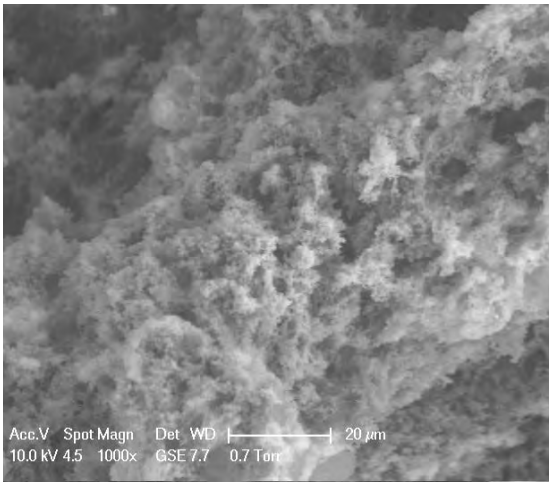

(B) 10*nm* Gold and silver nitrate

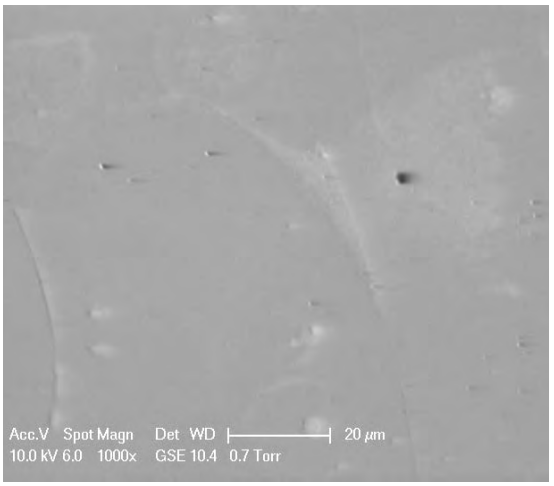

(C) R60 *nm* Gold and silver nitrate control

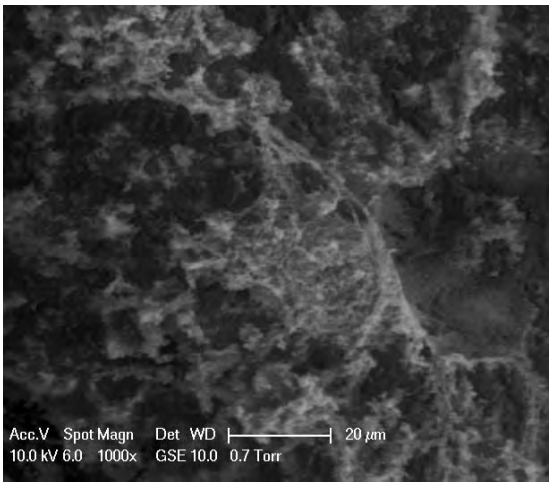

(D) 60*nm* Gold and silver nitrate

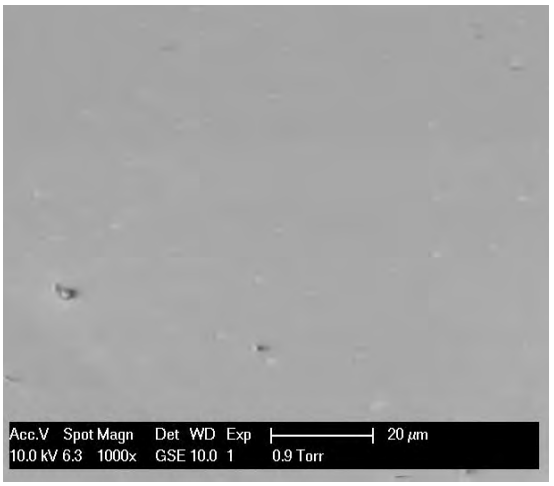

(E) 10 *nm* Gold and PTA control

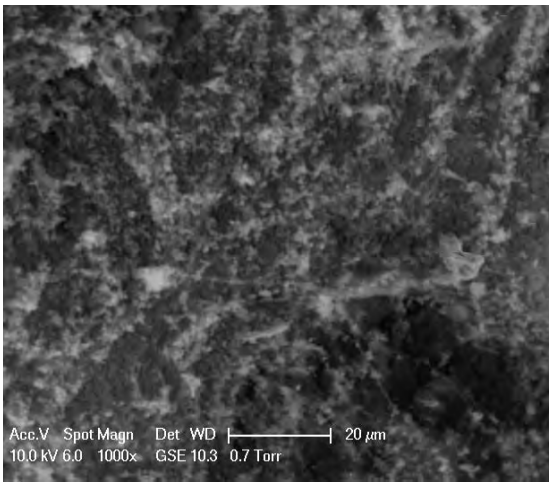

(F) 10*nm* Gold and PTA

Figure 6.11: (i)

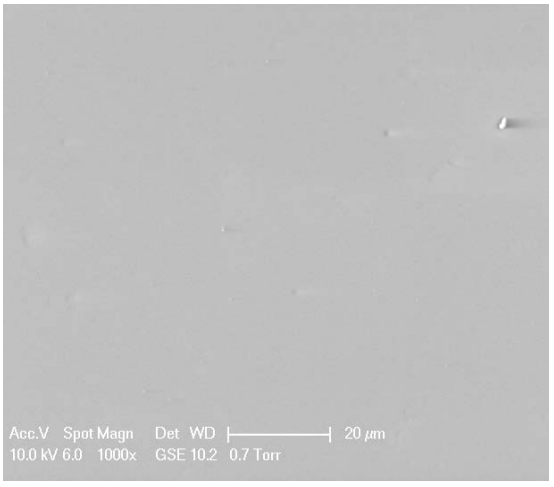

(G) 60 *nm* Gold and PTA control

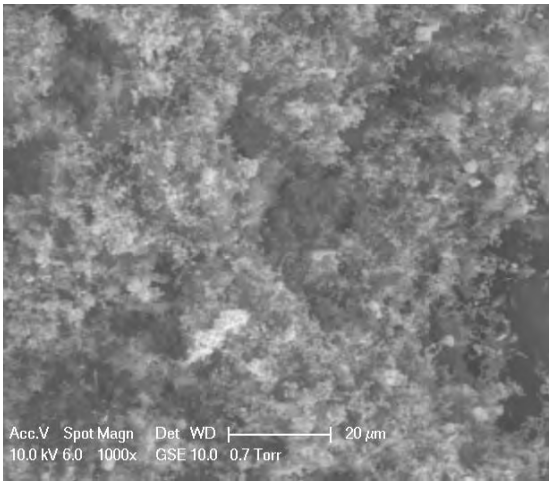

(H) 60*nm* Gold and PTA

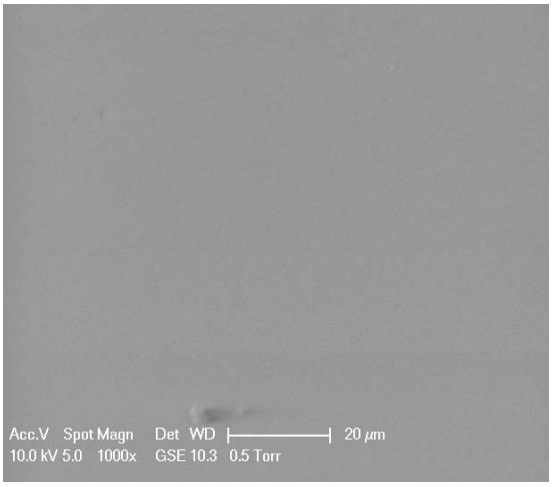

(I) Silver nitrate and PTA control

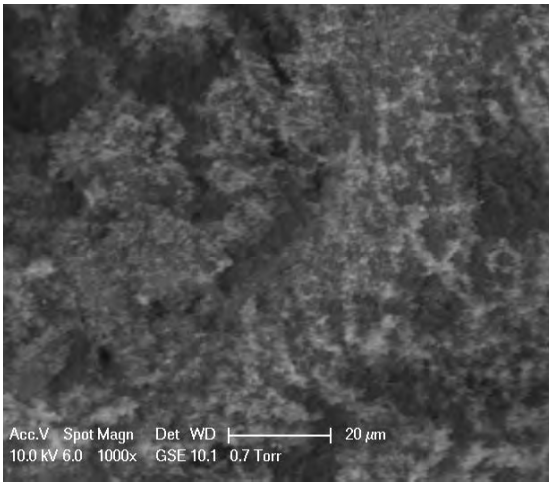

(J) Silver nitrate and PTA

Figure 6.11: (ii) Micrographs of biofilms that were grown on a glass slides, stained with two metal stains and analysed with EDS. (A), (C), (E), (G) and (I) were biofilm negative control samples and (B), (D), (F), (H) and (J) biofilm positive samples stained with 10 *nm* gold and silver nitrate, 60 *nm* gold and silver nitrate, 10 nm gold and PTA, 60 nm gold and PTA and silver nitrate and PTA respectively. The biofilm negative stained samples showed that the stains did not adhere to the glass slides. The biofilm positive samples showed similar biofilm growth across all (scale bars = $20\mu m$).

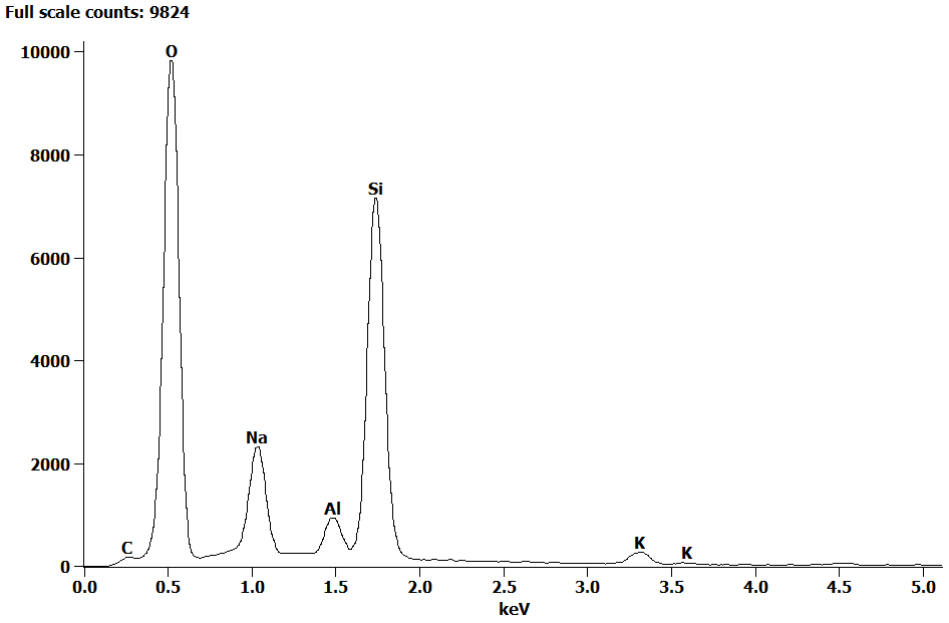

(A)

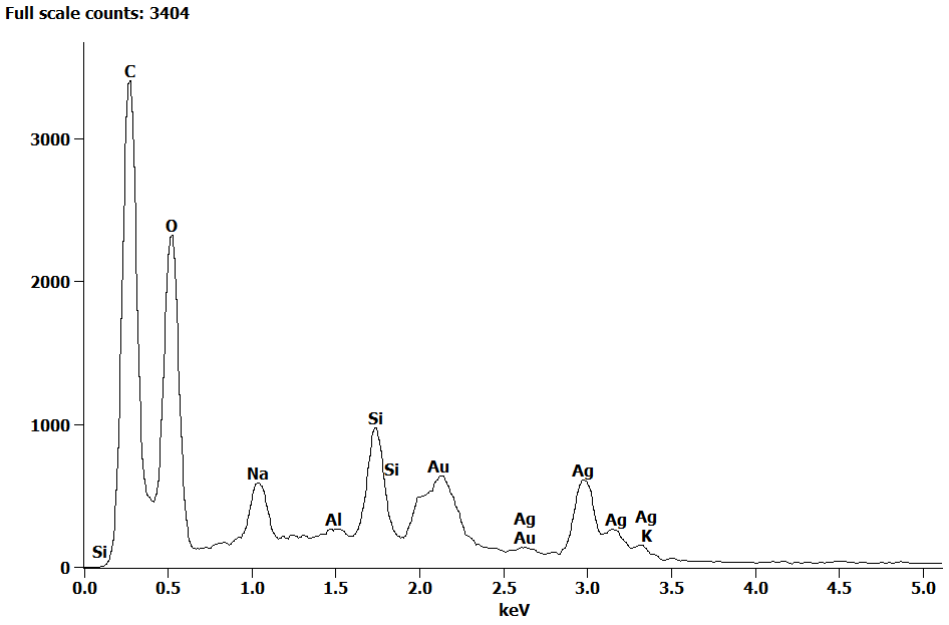

(B)

Figure 6.12: Spectrum produced after energy dispersive x-ray analysis on samples stained with 10 *nm* gold and silver nitrate. (A) was a biofilm negative control and (B) was a biofilm positive sample, both stained with 10 *nm* nano Gold and silver nitrate. A very small carbon peak near 0.27 keV and no gold or silver peaks were detected in (A), indicative of a sample without biofilm and no stain. In contrast, (B) had a very large carbon peak at 0.27 keV along with a gold peak at 2.12 keV and silver peaks at 3.35 and 3.53 keV showing evidence of biofilm and the stains.

Figure 6.13, showed that 10 *nm* gold and silver nitrate had a much higher total stain element weight percentage. There was a statistically significant difference between percentage of total metal detected for 10 *nm* gold and silver nitrate compared to 60 *nm* gold and silver nitrate ($P = 0.0.016$), 10 *nm* gold and PTA ($P = 0.006$) and 60 *nm* gold and PTA ($P = 0.007$). In contrast, the percentage of metal detected in the biofilm sample stained with 60 *nm* gold and silver nitrate was not statistically different compared to 60 *nm* gold and PTA ($P = 0.815$), 10 *nm* gold and PTA ($P = 0.899$) or silver nitrate and PTA ($P = 0.942$).

There was no statistical difference between the all primary stains (P ranged from 0.5 to 0.9), apart from 10 *nm* and 60 *nm*, gold and silver ($P = 0.0001$ for both). Whereas there was statistically significant difference between the secondary stains detected in the sample stained with 10 *nm* gold and silver nitrate and 60 *nm* gold and silver nitrate ($P = 0.008$); 10 *nm* gold and silver nitrate and 10 *nm* gold and PTA ($P = 0.003$); 10 *nm* gold and silver nitrate and 60 *nm* gold and PTA ($P = 0.004$).

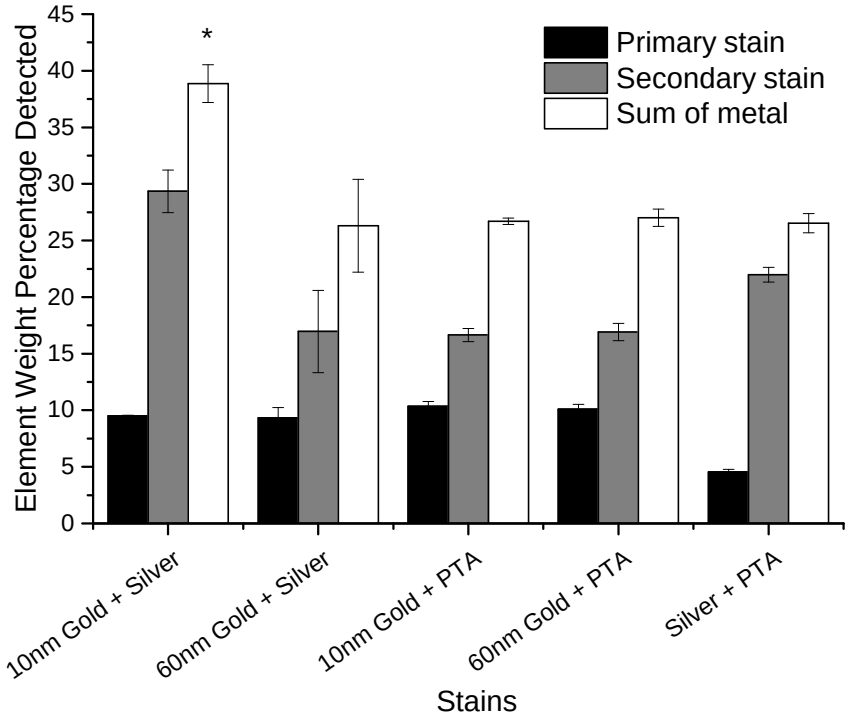

Figure 6.13: EDS mean elemental weight percentage composition of metal detected in the sample. The black bars show the average elemental weight percentage of the primary metal detected in the sample, grey indicating percentage of the secondary stain and white the sum total of metal deposited by the various stains as indicated by the x-axis (n=3 intendant repeats). Note, all samples had clean, stained controls where no stain metals were detected and was omitted from the graph. There was a statistically significant difference between percentage of total metal detected for 10 *nm* gold and silver nitrate (as indicated by $*$) compared to 60 *nm* gold and silver nitrate (t-test, $P = 0.0.016$), 10 *nm* gold and PTA ($P = 0.006$) and 60 *nm* gold and PTA ($P = 0.007$).

6.5 Discussion

Energy dispersive x-ray analysis (EDS) was able to differentiate between elements using x-ray detection and exploiting the distinct ionisation energies from each element. EDS determined that 10 *nm* nano gold and silver nitrate was best suited of the stains tested as the contrast agent for detecting biofilms within CVCs (Section 6.4.2).

Barium sulphate used by Davit et al. (2011) was considered but because the samples were stacked on top of each other and were scanned 2 samples at a time for about an hour each, movement of barium sulphate was a high probability. If any movement occurred during any of the μCT scans the centre of rotation could not be calculated and the data could not be reconstructed to produce three dimensional data. In addition because EDS required ethanol dehydration and critical point drying a barium sulphate suspension would not have been possible. Potassium iodide was used in the infancy of testing x-ray μCT for biofilm detection within CVCs but did not provide sufficient contrast (data not shown). Iodine in ethanol was also tested using EDS but again did not result in a high count rate. Iltis et al. (2011) on the other hand used silver coated microspheres to provide contrast. The microspheres had an average diameter of 10 μm which was considered too large and therefore was not considered for this study. Gold particles with a diameter of 10 *nm* were used instead.

Initially single metal contrast stains were tested and PTA outperformed nano gold and silver nitrate. However, because of common practice to use more than one stain for enhancement in microscopy (Lackie, 1996; Scopsi et al., 1986; Lackie et al., 1985) we decided to apply two stains. Applying two stains resulted in higher signals with 10 *nm* gold and silver nitrate producing the highest x-ray signal. 10 *nm* gold as a primary stain gave the same signal compared to 60 *nm* gold, and yet 10 *nm* gold resulted in 1.73 times as much silver as the samples with 60 *nm* gold as a primary stain. The difference may have been because more 10 *nm* gold particles could be deposited which would've created a bigger surface area for the silver to deposit.

If more experiments could have been performed additional dual stain combinations that would have made the comparison fairer would have included testing PTA and 10 *nm* and 60 *nm* gold with PTA as the primary stain. The reason why PTA was only used as a secondary stain was because the samples had to be partially ethanol dehydrated to 70% whereas gold and silver nitrate did not. Samples designated to be stained with PTA required ethanol dehydration due to poor PTA penetration. Using PTA as a secondary stain may have resulted in reduced penetration. When looking at both the single (Fig. 6.9) and dual (Fig. 6.13) stain EDS data this could have been the case. Using PTA as a single stain resulted in 25.7% tungsten element weight whereas for dual stained samples 10 *nm* gold as a primary stain resulted in 16.65% of tungsten by weight, 60 *nm* gold as primary resulted in 16.93%. Hypothetically if the tungsten levels of PTA as a secondary stain was the

same for using PTA as a single stain, for 10 *nm* gold and (hypothetical) PTA, the total metal weight percentage would have been 36.06%, still less than 10 *nm* gold and silver nitrate (38.87%). Nonetheless, this hypothetical theory could only be elucidated if more experiments were performed.

We could argue however that further experimentation was not required because we were able to segment the biofilm from the inner surface of the CVC by staining the biofilm with 10 *nm* gold and silver nitrate (as discussed in Chapter 7).

Chapter 7

X-ray μCT for CVC-biofilm detection

7.1 X-ray computed tomography theory

Clinical CT or CAT (computed axial tomography) scans have enabled detailed imaging of soft tissues which conventional radiography cannot achieve. As such clinical CT scans are used to detect soft tissue abnormalities such as tumours, abscesses and abnormal blood vessels. The use of clinical CT scanners is long-established, the first being used at the Atkinson-Morley hospital in London as early as 1971. Conventional radiography (x-ray) is used on a sample fixed in position to produce a single radiograph containing a two-dimensional image. In a tomographic approach a series of radiographs (or slices) are taken at different positions and angles along the sample, therefore providing more information for analysis. Research μ computed tomography (μCT) scanners are less-established but are capable of producing higher-resolution images (Kalender, 2011). Similar to clinical CT, in μCT radiograph slices of the sample are captured, however the radiograph slices are instead stitched together using computer algorithms to produce a digital three-dimensional image that can be manipulated (Bayaraktar et al., 2008; Landis and Keane, 2010).

7.2 X-ray μ computed tomography

In the last few years it was shown that synchrotron x-ray μCT could detect model grown porous media biofilms when silver coated glass beads were deposited on the surface (Iltis et al., 2011). However, this was only using a very high resolution approach which is not readily available. Benchtop x-ray μCT could also discern model porous media biofilms from polyamide beads when a negative staining approach was taken using a barium sulphate suspension (Davit et al., 2011). Both of these approaches were to study porous/soil media

alongside biofilms using beads to model soil. Taking knowledge from electron microscopy, radiography, clinical CT approaches, x-ray μCT on small animals and the work by Iltis et al. (2011) and Davit et al. (2011) that the proposed objective was to develop a novel approach to detect biofilms within CVCs in a nondestructive manner and is discussed in the sections that follow.

7.2.1 X-ray μCT on small animals and invertebrates

X-ray computed tomography have been conducted on small animals. Using various heavy metals (for contrast), critical point dried samples, samples embedded in resin as well as samples suspended in ethanol (Metscher, 2009) has improved the resolution and contrast between soft tissues. The aim of x-ray CT on animals were to enable nondestructive, whole volume imaging for comparative, developmental and quantitative studies of morphology. Contrast agents were used to distinguish organs and various tissues in these animals (Metscher, 2009).

7.2.2 X-ray μCT on biofilms

Previous work relating to bacterial habitat within soils were investigated by Thieme et al. (2003) and Nunan et al. (2006). Using synchrotron transmission x-ray microscopy at very low energy x-rays, Thieme et al. (2003) was able to visualise model colloidal flocculates associated with bacteria in a cryogenic state at the Advanced Light Source (Berkley). The bacteria associated flocculates were not stained with contrast agents as the natural absorption contrast between proteins and water of about 0.5 keV photon energy was exploited and resulted in 45 nm pixel resolution. Although the transmission x-ray microscopy technique employed by Thieme et al. (2003) was able to resolve individual bacteria and soil particles by using synchrotron transmission x-ray microscopy at very low x-ray energies (0.5 keV). The model samples had to be frozen and the maximum sample diameter size was 6 μm. The sample diameter limit would not have been suitable for investigating biofilms in CVCs.

Conversely, Nunan et al. (2006) used synchrotron micro-computed tomography at the Advanced Photon Source (Argonne National Laboratory) to visualise cleaved *ex situ* air dried soil aggregate samples to which the bacteria was adhered. The bacteria were not visualised but the habitat surrounding the bacteria was investigated.

Nunan et al. (2006) used synchrotron based x-ray tomography similarly to Davit et al. (2011) without imaging bacteria but the soil associated with the bacteria instead. The author's method involved air-drying the samples which may not have been optimum for preserving the bacterial soil habitat. The possible lack of structure preservation may also

explain why Nunan et al. (2006) did not find significant differences between untreated and treated soil samples.

Two papers report using x-ray μCT to image biofilms on porous media, Davit et al. (2011) and Iltis et al. (2011). Both papers were able to image biofilms successfully within their model porous media and highlighted the significance of this method as x-rays can image biofilms within an artificial porous-media structure in a non-destructive manner. Davit et al. (2011) used a Skycan CT scanner with a pixel resolution of 9 μm whereas Iltis et al. (2011) had pixel resolution of 4.5 μm using synchrotron at Advanced Light Source. The pixel resolutions reported in these two papers would allow for biofilm resolution but not single cells.

The synchrotron data produced by Iltis et al. (2011) although a critical research tool would not be conducive to high-throughput and is not readily available for use. Although scan times for synchrotron is much faster, time available for experiments are limited due to the existence of only a handful of synchrotron facilities (five in the UK, approximately 56 worldwide) and widespread application in many fields.

The work from both Iltis et al. (2011); Davit et al. (2011) highlighted the potential use for μCT in biofilm-porous media studies but due to the composition of soil and corresponding material x-ray attenuation coefficient (soil have varied x-ray attenuation coefficients depending on mineral composition) thus far there is no x-ray CT 3 dimensional data to visualise biofilm on natural, soil based porous media.

7.3 Experimental approach

After EDS determined the best stain, samples were prepared for x-ray μCT (Section 7.4.1) by using information obtained from EDS results. Optical profilometry was used on clean samples to determine CVC surface roughness to enable the development of semi-automated image analysis (Section 7.4.2). To assess the sensitivity and degree of correlation between μCT and amount of biofilm, biofilms were grown for various time points to achieve different surface concentrations of cells so that CFU could be compared with biofilm volume detected by μCT (Section 7.4.3). Lastly, clinical samples were scanned by x-ray μCT (Section 7.4.4).

7.4 Materials and methods

All materials were purchased from Sigma Aldrich UK unless stated otherwise.

7.4.1 Sample preparation

In vitro S. epidermidis biofilms (strain ATCC 35984) in CVC samples were grown statically for x-ray μCT (as described in Chapter 3, Section 3.3.4.1).

7.4.1.1 Dual contrast enhancing stain

Initially samples grown in CVCs for x-ray μCT were stained with Osmium Tetroxide and Uranyl Acetate (Appendix C, Section C.1). Although the stains did improve contrast, due the toxicity, other stains were investigated to move the research toward the possibility of *in vivo* staining (Section 6.1.2).

Osmium Tetroxide was prepared by the Southampton University Biomedical Imaging Unit by dissolving ampoules in distilled water. 2%(w/v) Uranyl Acetate was prepared by adding 2 g to 100 m*l* of 50% ethanol. Uranyl Acetate solution was left in the fridge overnight at 4^oC.

Using the newer, safer contrast agents in a more targeted approach the best dual stain was obtained during EDS analysis (Section 6.4.2). Dual staining was used in order to produce the best contrast of the biofilm for x-ray μCT scans. Nano gold, silver nitrate and phosphotungstic acid stains were prepared as described in the contrast agent Chapter 6, Section 6.3.2. The samples were then stained, washed and put through an ethanol dehydration series identical to the EDS glass slide preparation in Sections 6.3.3 and 6.3.4. The stained and ethanol dehydrated *S. epidermidis* CVC samples were lastly placed in carbon fibre tubes to hold the CVC sections steady during imaging as outlined below.

7.4.1.2 X-ray μCT sample holder

The inner diameter of the carbon fibre tube was selected depending on the outer diameter of the CVC sections to reduce the probability of horizontal movement (Fig. 7.1). Carbon fibre was chosen due to the material stiffness and although higher x-ray absorbent compared to plastic, the absorbency was still low enough to reach the CVC samples. Absolute ethanol was used to avoid bubble formation when inserting samples or during the x-ray μCT scan. If the sample moved during the x-ray μCT scan, the data for that scan could not be used as the centre of rotation could not be determined. According to literature absolute ethanol

not only held fewer bubbles due to lower surface tension but also gave better tissue contrast compared to water (Metscher, 2009).

7.4.1.3 Sample set up and scanner settings

The samples that were stack on top of each other within the carbon fibre tube (Mainly Planes n trains, UK) was sealed with a combination of blue tack and parafilm. The sealed carbon fibre sample holder was screwed into place with a custom built insert for the sample stage. The samples in the carbon fibre tube were scanned two at a time (to save time and costs) with either a custom-built Nikon Metrology HMX CT scanner (Fig. 7.1) or the ZEISS Xradia VERSA. Energy was kept between 60 to 70 keV with a current of between 116 to 148 μA and focal spot size of 3 μm.

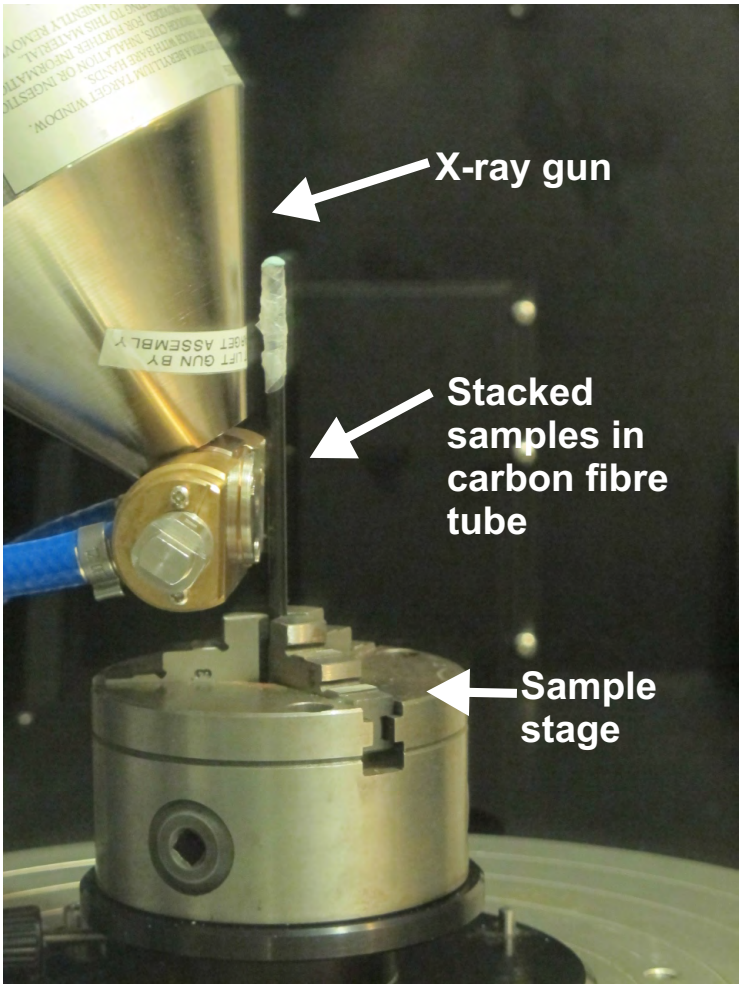

Figure 7.1: Sample set-up in Nikon Metrology HMX scanner. Catheter samples were suspended in absolute ethanol, stacked on top of each other inside a carbon fibre rod and sealed with para-film.

7.4.2 Image analysis

Before image or data analysis, the data file produced by the HMX x-ray μCT scans were loaded into CT Pro software (Nikon Metrology, US). The centre of rotation was determined (automatically or manually). The centred sample data was reconstructed using CT agent. The VERSA scanner had proprietary software that reconstructed the raw data files semi-automatically after the scans. Due to initial low contrast between the CVC and biofilm, segmentation was initially performed manually using Avizo Fire 7.0 (Visualization Sciences Group, France) (before optimisation, see Appendix C, Section C.2).

7.4.2.1 CVC roughness for automated segmentation

After improving the contrast, image segmentation of *in vitro* grown *S. epidermidis* biofilms attached to the inner wall of the CVC tube was achieved using a MATLAB script (Fig. C.2). In order to develop the MATLAB script (Section 7.4.2.2), the CVC roughness had to be determined to establish whether the μCT scanner would be able to include CVC material as an artefact.

Optical profilometry is a non-contact interferometric based method for characterising surface topography. Optical profilometry was used to establish the CVC material roughness and to ensure that μCT processing excluded any CVC material. Optical profilometry (Alicona Infinite focus, US) was performed on the inside sections from 5 sterile Lifecath CVCs to determine CVC surface roughness using an Alicona Infinite Focus using × 100 magnification.

7.4.2.2 Semi-automated segmentation

After improving the contrast by using a dual metal based stain, image segmentation of *in vitro* grown *S. epidermidis* biofilms attached to the inner wall of the CVC tube was achieved using a MATLAB script (Fig. C.2 and Fig. 7.8). This approach was utilised because segmentation by global thresholding was too difficult because radiopaque substances within the CVC material was often at a similar grey level (see Chapter 2, Section 2.6.4.

1. The MATLAB script processed cross-sectional slices by determining the centre point of the CVC by using the outer radius of the CVC (Fig. 7.2).

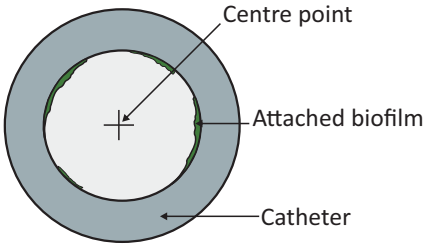

Figure 7.2: Calculating the centre point during MATLAB segmentation.

2. The average and standard deviation of the inner radius of the CVC including the attached biofilms for a given slice was calculated (Fig. 7.3). The standard deviation accounted for variations to the inner radius of the CVC due to the presence of biofilms.

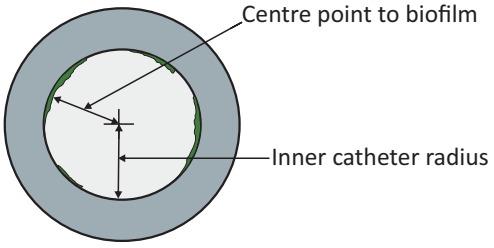

Figure 7.3: Calculating the average and standard deviation of the inner CVC radius during MATLAB segmentation.

3. To extract the biofilms from the wall of the CVC, the script created a circular mask centred on the calculated centre point with a radius consisting of the calculated average radius plus three standard deviations (Fig. 7.4).

Figure 7.4: Creating the mask during MATLAB segmentation.

4. Any biofilms on the outer wall of the CVC was removed, thus leaving the mask of r = radius in pixels + 3 SD centred at the centre point (Fig. 7.5).

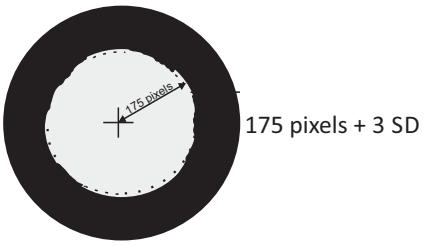

Figure 7.5: Removing the outer biofilms from the MATLAB mask

5. A grey scale threshold of 150 to 254 was applied to the data.

6. The mask retained the biofilm plus 1 pixel of the CVC caused by occasionally irregular shaped CVCs (Fig. 7.6) .

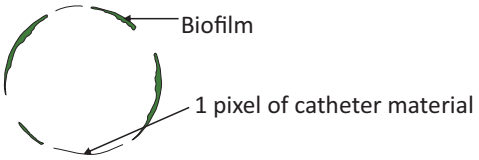

Figure 7.6: The segmented data from the MATLAB segmentation script before a 2 pixel median filter is applied.

7. A 2 pixel median filter was applied to remove the CVC tube features. Consequently, resulting in the final extracted biofilm (Fig. 7.7 and Fig. 7.8)

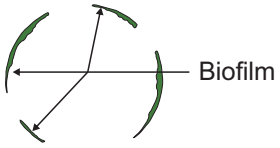

Figure 7.7: The final biofilm segmented from the CVC using the MATLAB segmentation script.

After the biofilm was segmented from the CVC the data was imported into Avizo Fire 7.0 where the data was analysed for volume and particle distribution (as shown in Results, Fig. 7.12).

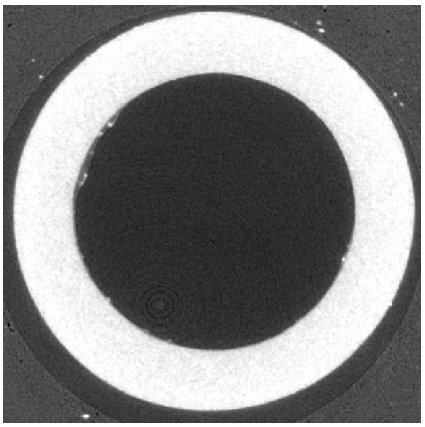

(A) 8 Bit Data

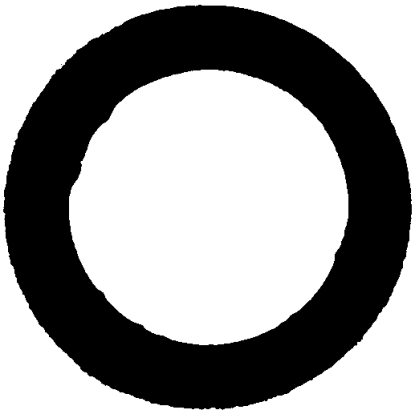

(B) Binary Mask

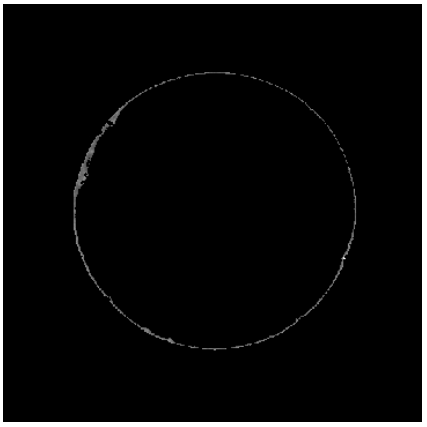

(C) 2D Segmented Biofilm

Figure 7.8: Two dimensional cross section slices from a 5 day old *S. epidermidis* biofilm in a CVC stained with nano gold and silver nitrate to illustrate the output steps from the MATLAB segmentation script. (A) showing the 8 bit input data, (B) the binary mask and (C) the final segmented biofilm.

7.4.3 X-ray μCT biofilm sensitivity

The sensitivity of x-ray μCT to detect biofilms was established by performing culture by sonication and enumeration by solid agar plating samples of CVCs that were prepared alongside μCT samples. Biofilms were grown statically for 0, 2, 12, 72 and 120 hours on CVC sections. After growth half of the samples were washed twice with PBS followed by fixation with general fix (3% glutaraldehyde, 4% formaldehyde in 0.1 *M* piperazine-N,N-bis 2-ethanesulfonic acid buffer (PIPES) at pH 7.2.), ethanol dehydration series and dual staining with nano gold and silver nitrate. The other half of the samples were washed twice with PBS but were further processed for culture by sonication and enumeration by solid agar plating as explained in detail in Chapter 3, Section 3.3.

7.4.4 X-ray μCT on clinical samples

Clinical samples saved for SEM (Chapter 3, Section 3.3.2) in general fix (3% glutaraldehyde, 4% formaldehyde in 0.1 *M* piperazine-N,N-bis 2-ethanesulfonic acid buffer (PIPES) at pH 7.2.) were gently immersed in PIPES buffer for 10 minutes twice. After the washing step the samples were stained (Sections 6.3.3 and 6.3.6) and put through an ethanol dehydration series (Chapter 5, Section 5.2.3) before being stacked in a carbon fibre tube (Section 7.4.1.2) and placed in the x-ray μCT scanner (Section 7.4.1.3).

7.4.5 Statistics

The data for the CVC roughness was continuous and the means of more than two identical CVC sections were compared. Therefore, One-Way ANOVA at 95% confidence interval was used (Minitab 16, US).

When the volumes of the manual and semi-automated samples were compared, the samples were compared to themselves but had undergone different analysis treatments. The non-parametric, Man-Whitney test was used because the test determines whether there is difference between groups by looking whether one group had higher values compared to the other. The data is continuous but also ordinal because the size of biofilm cab be ranked. The Mann-Whitney test was used because median rather than means are compared. Due to the extreme differences in biofilm sizes the mean would be affected by outliers.

In order to test whether the sum volume detected by x-ray μCT had a linear association to enhanced culture by sonication and solid agar plating the Pearson Correlation Coefficient was calculated using the $\log_{10}$ values of culture at the x axis and the sum volume on the y-axis. Whereas to test the difference between the sum volumes and percentage volume occlusion detected by x-ray μCT at the different growth time points the two-sample two-tailed t-test at 95% confidence intervals were used because the data was continuous and two different, independent groups were compared. Significant difference was established when the probability value was less than 0.05 (Minitab 16, US).

7.5 Results

The semi-automated MATLAB segmentation script was shown to be more accurate to digitally separate the biofilm from the CVC and ethanol compared to manual segmentation (Section 7.5.1). The sensitivity of x-ray μCT was determined and showed to be as sensitive as the gold standard culture method for biofilm diagnostics at as little as 2 hours (Section 7.5.2). Once the sensitivity was established, the potential of x-ray μCT as an *in vivo* diagnostic method had to be illustrated. Proof of concept was established by scanning *ex situ* clinical samples with an x-ray μCT scanner (Section 7.5.3). Lastly culture, confocal laser scanning and scanning electron microscopy methods (from Chapters 3, 4 and 5 respectively) were compared to x-ray μCT (Section 7.5.3.1).

7.5.1 Image analysis

Initially to analyse scanned samples a manual biofilm-CVC segmentation approach was used because global thresholding was not possible (Appendix C, Section C.2). Manual segmentation however was time consuming and could take weeks to complete one sample. To improve image analysis for x-ray μCT a semi-automated method was considered. The semi-automated segmentation method firstly required determining the CVC roughness (Section 7.5.1.1) in order to develop the semi-automated MATLAB script (Section 7.5.1.2).

7.5.1.1 CVC roughness for automated segmentation

Optical profilometry revealed that the polyurethane Lifecath CVC (Fig.7.9) used for *in vitro* experiments had an average roughness of 206.41 *nm* (+/- SD, n = 5 CVCs × 3 FOV). There were no statistically significant difference between the means of any of the CVC sections (One-Way ANOVA at 95% CI, $P = 0.211$). Due to the low roughness of the Lifecath PICC we could assume that applying a 2 pixel median filter during x-ray μCT image analysis would remove any CVC material in the MATLAB segmented biofilm (Section 7.4.2, Step 7).

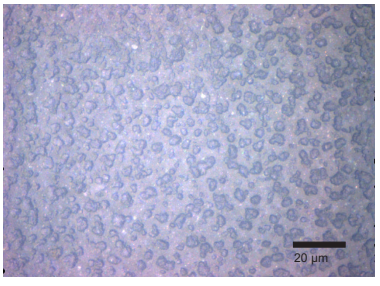

Figure 7.9: Optical profilometry micrograph showing the roughness of a Lifecath CVC (scale bar = 20 μm)

7.5.1.2 Semi-automated segmentation

Once the CVC roughness was determined, an automated segmentation process was considered. A dataset which was manually and semi-automatically segmented was compared (Fig. 7.10). The MATLAB script was specifically developed for CVC-biofilm segmentation in collaboration with Dr.D.J.Bull). By visually comparing the x-ray μCT tomographs and scanning electron micrographs the MATLAB segmented samples appeared to be more accurately segmented. When the volumes for the manual and MATLAB segmented biofilms were compared all were statistically significant ($P = 0.00001$). When comparing the manual and matlab segmented data (Fig. 7.10A and (B)) and compare the images to the scanning electron micrographs (Fig. 7.10C and (D)) it appeared as though the manually segmented biofilm that relied upon global thresholding and manual intervention was only able to select the thickest parks of the biofilm (which cracked from the CVC during SEM preparation, see red circles.)

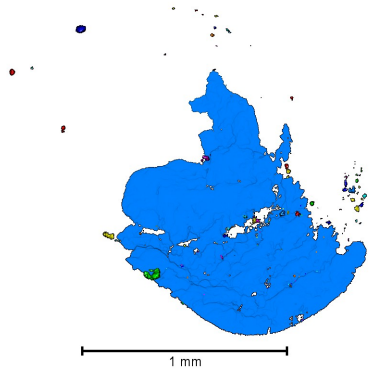

(A) Manually segmented

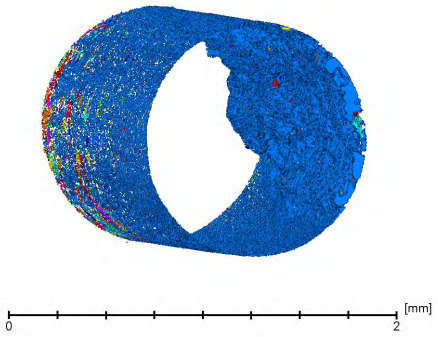

(B) MATLAB segmented

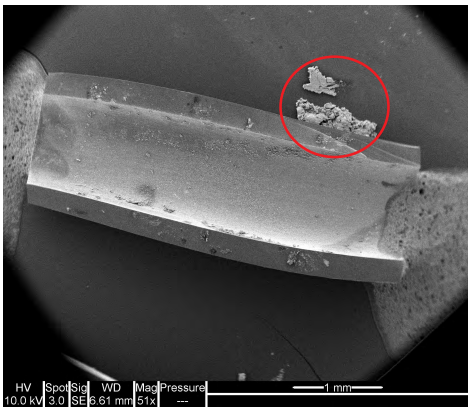

(C) SEM

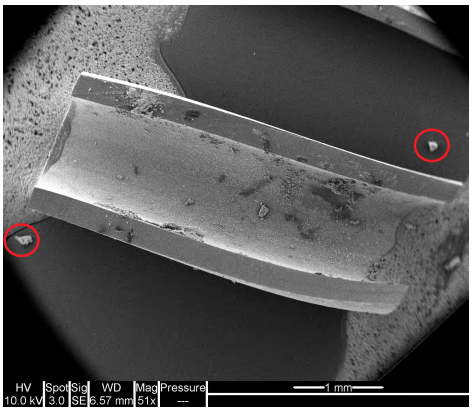

(D) SEM

Figure 7.10: Manual and semi-automated MATLAB biofilm-CVC segmentation of x-ray μCT scanned CVC-flow biofilm model samples and corresponding scanning electron micrographs. (A) was manually segmented, (B), was segmented using the MATLAB script and; (C) and (D) were the scanning electron micrographs. The scanning electron micrographs showed that the MATLAB script segmented sample appeared more closely matched. Note that in (D) a big chunk of biofilm fell out of the CVC section.

7.5.2 X-ray μCT biofilm sensitivity

X-ray μCT was able to detect biofilms as early as 2 hours after inoculation (Fig. 7.11 and Fig. 7.12C). X-ray μCT and SEM showed an increasing amount of biofilm with increasing growth time (Fig. 7.12).

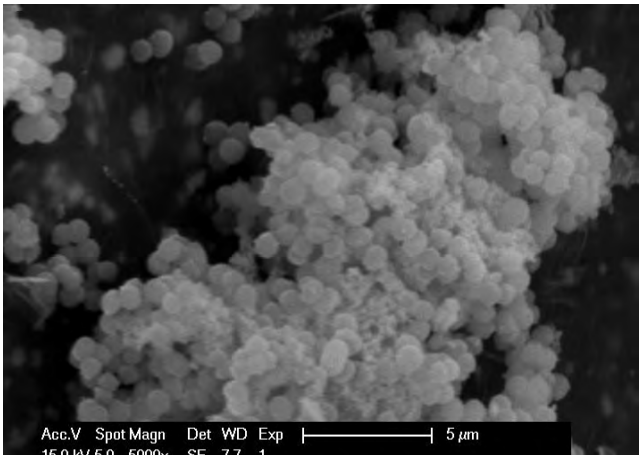

Figure 7.11: Scanning electron micrograph of a static *S. epidermidis* CVC-biofilm grown for 2 hours. Cocci are visible indicating that *S. epidermidis* biofilms did grow on the 2 hour samples.

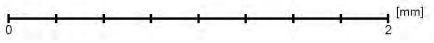

(A)

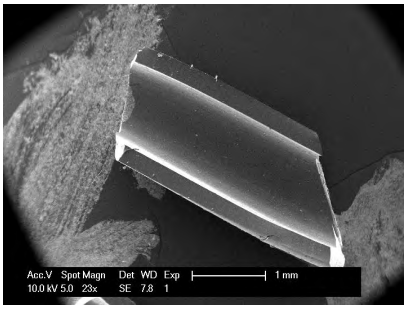

(B)

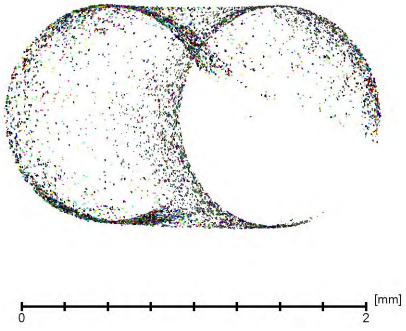

(C)

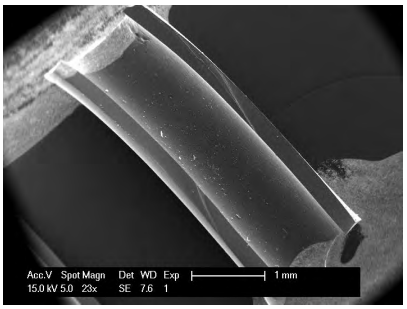

(D)

Figure 7.12: (i)

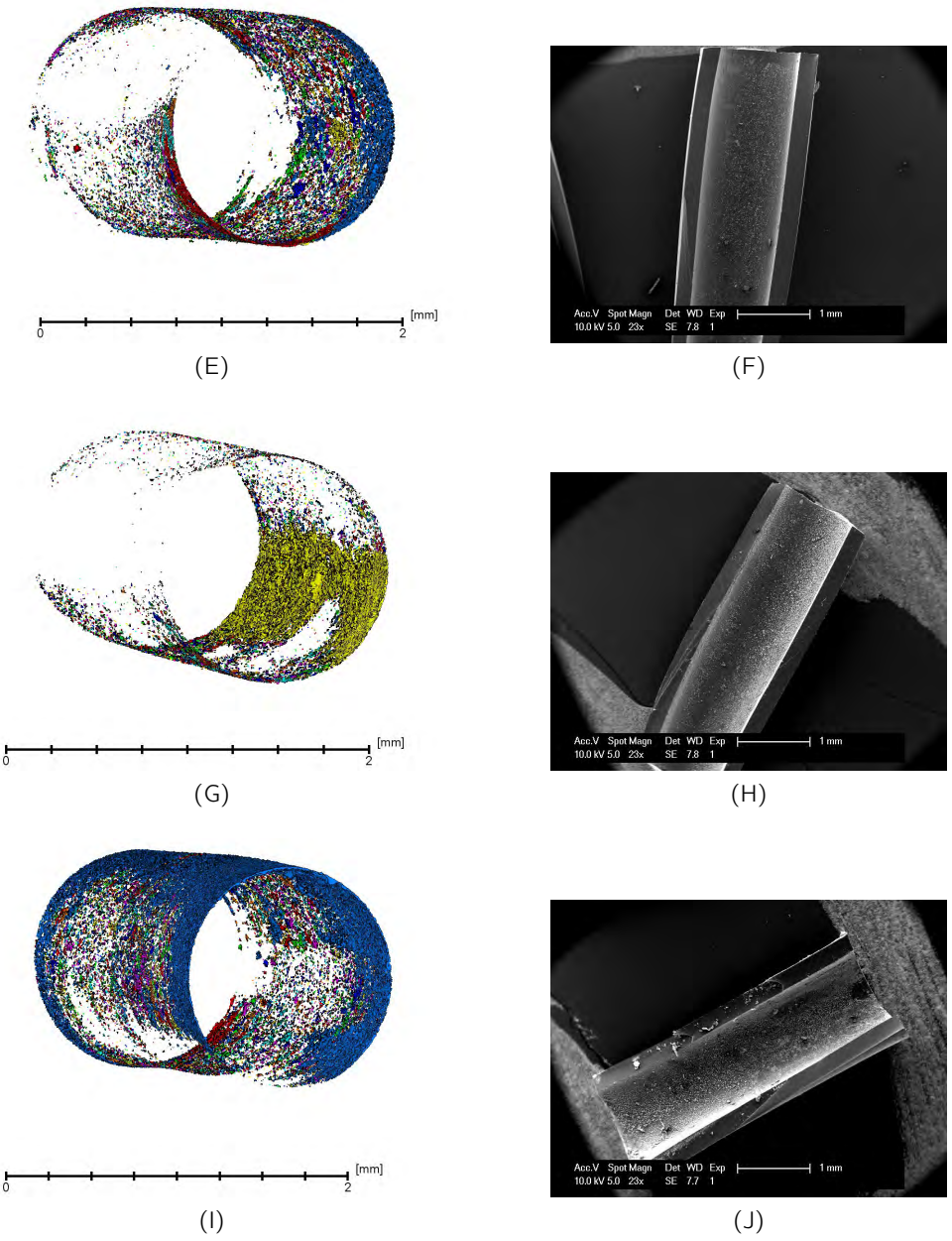

Figure 7.12: (ii) X-ray μCT reconstructed and analysed tomographs and SEM micrographs of scanned samples. (A), (C), (E), (G) and (I) showed an increase in total biofilm volume and was substantiated by (B), (D), (F), (H) and (J).

Looking at Figure 7.13 it appears as though x-ray μCT has picked up signals from the biofilm negative control (Fig. 7.13, black circle). When the controls were examined closer by SEM (Fig. 7.14) it was evident that there were unknown debris on the surface. At time points, 2, 12 and 72 hours x-ray μCT detected up more biofilm volume compared to culture.

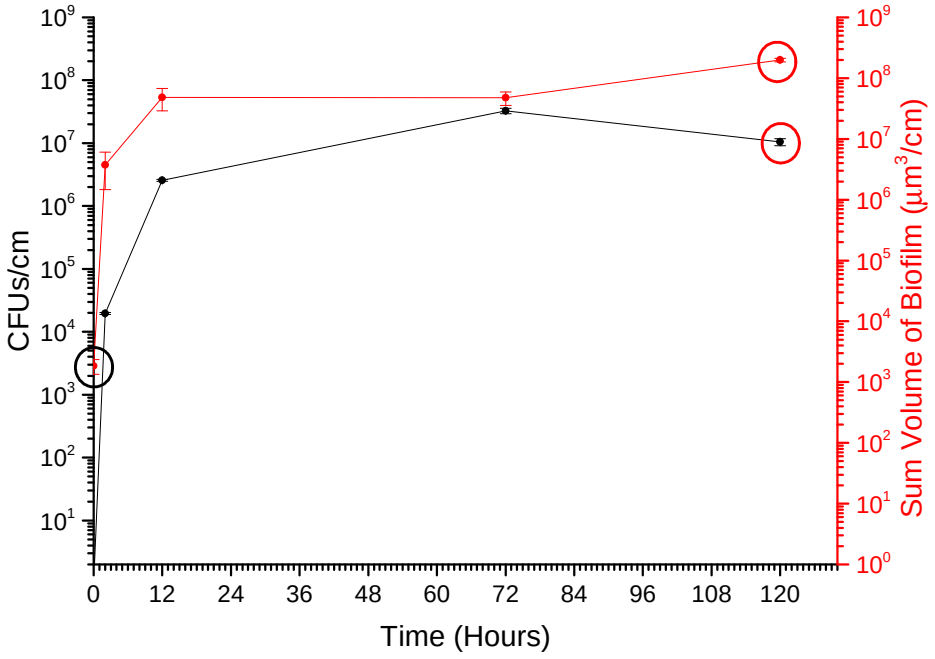

Figure 7.13: Plot comparing culture, CFUs/cm and x-ray μCT , sum volume in $\mu m^3/cm$ of CVC over time. At 0, there was a signal detected by x-ray μCT but not for culture. At each time point μCT detected more sum volume of biofilm compared to culture which may have accounted for biofilm EPS.

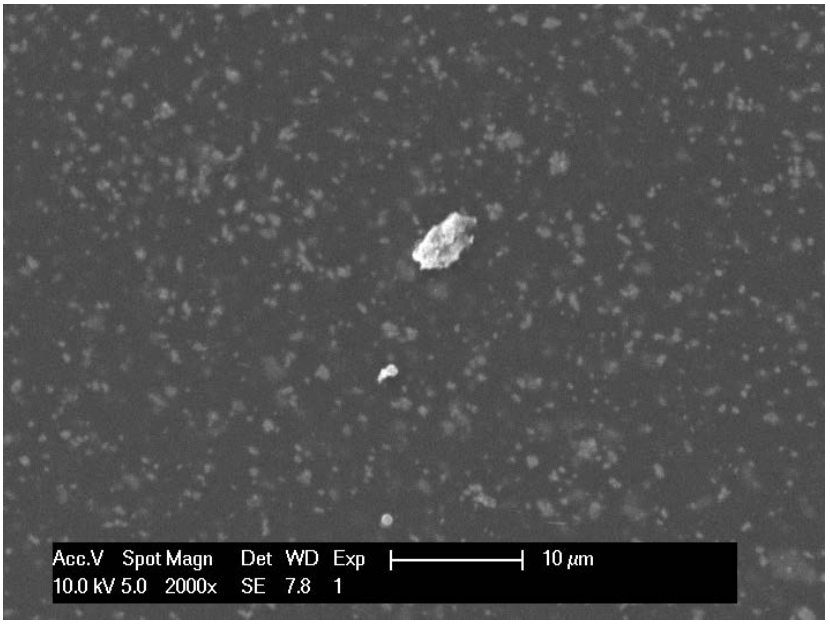

Figure 7.14: Scanning electron micrograph of a biofilm negative control showing non-biofilm debris.

When culture $\log_{10}(\mathrm{CFU}/cm)$ was plotted against the sum volume $\log_{10}$ $(\mu m^3/cm)$, the data was shown to have strong positive correlation (Fig. 7.15, Pearson Correlation Coefficient R = 0.9828, R^2 = 0.9659 and P = 0.003).

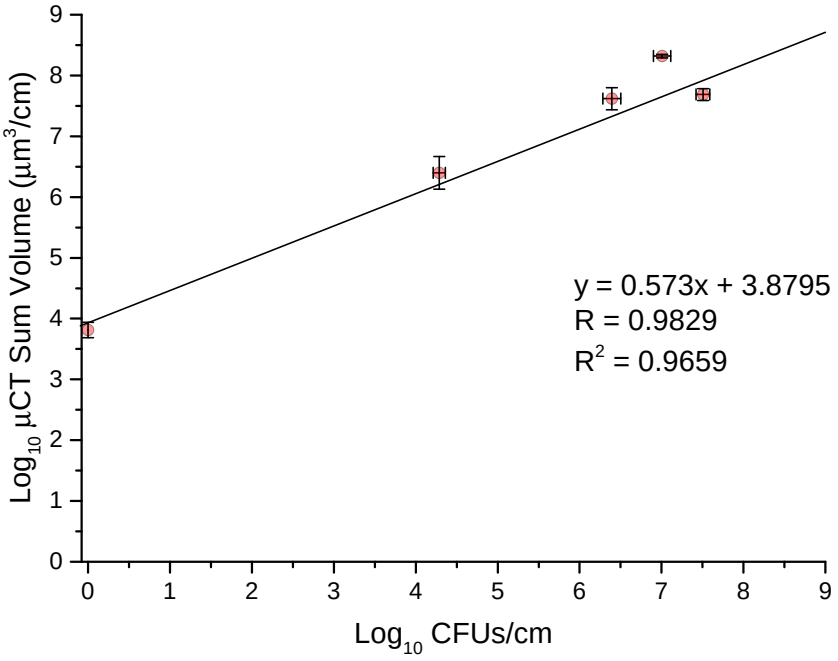

Figure 7.15: Correlation plot comparing biofilm detection using culture and x-ray μCT . The plot showed that there was a strong, statistically significant correlation between the two detection methods , X and Y error bars $= 1SD$ $n = 3$ (Pearson Correlation Coefficient R = 0.9828, R^2 = 0.9659 and P = 0.003)

7.5.2.1 Sample heterogeneity

Although the sum volume was similar for the different repeats some samples had a few large aggregates (Figs. 7.16 (A), (C)). For example, looking at Figure 7.17, the sum volumes (open circles) and largest aggregates (top of the whisker) made up over half of the sum volume of 2 hours A (57.57%, $2.995\times10^5\mu m^3$ vs $1.45\times10^5\mu m^3 + 2.77^4\mu m^3$) 72 hours B (63.44%, $1.68\times10^7\mu m^7$ vs $1.07\times10^7\mu m^7$), 120 hours A (83.7%, $4.71\times10^7\mu m^3$ vs $3.94\times10^7\mu m^3$), 120 hours B (77.34%, $4.71\times10^7\mu m^3$ vs $3.64\times10^7\mu m^3$) and 120 hours C (74.28%, $4.35\times10^7\mu m^3$ vs $3.24\times10^7\mu m^3$; Figs. 7.16 (B) and (D)).

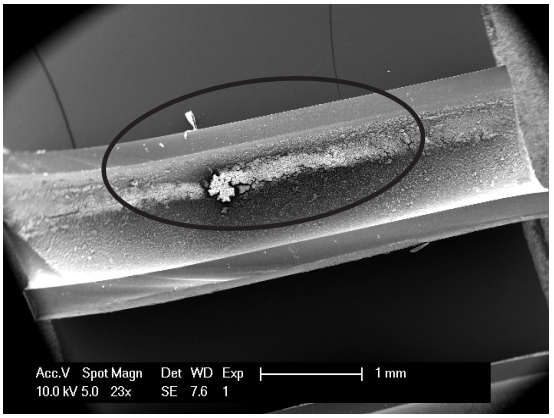

(A) SEM of 120 hours A

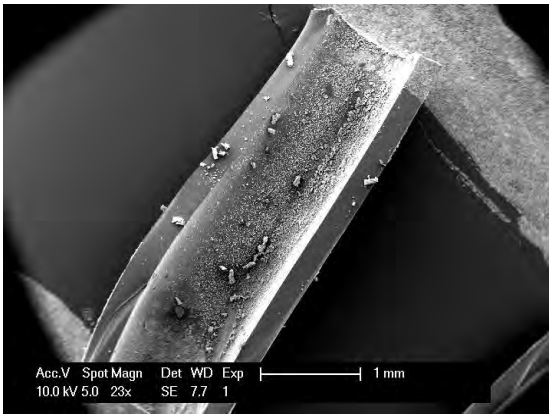

(B) SEM of 120 hourss B

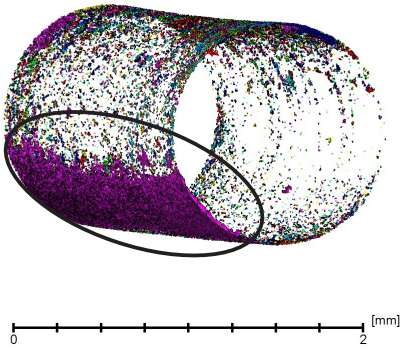

(C) μCT of 120 hours A

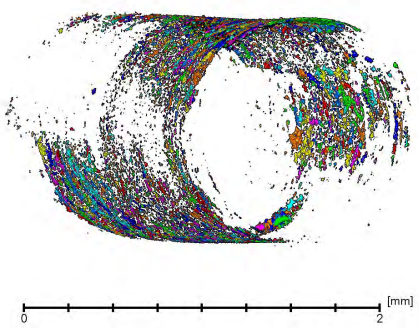

(D) μCT of 120 hours B

Figure 7.16: Scanning electron micrographs and x-ray μCT tomographs showing varying biofilm distribution and aggregate size on the same age biofilm samples. (A) and (C) showed a larger continuous biofilm aggregate circled in black. Whereas (B) and (D), showed smaller biofilm aggregates throughout the CVC.

When the two-sample t-test at 95% CI was applied to the sum volumes of the repeats (Fig. 7.17) there was a statistically difference when the Log_{10} sum volumes of 0 and 2 hours were compared ($P = 0.024$), 2 and 12 hours ($P = 0.017$) and 72 and 120 hours ($P = 0.037$, Fig. 7.17). In contrast, there was no significant difference between 12 and 72 hours ($P = 0.636$). Consequently, suggesting that x-ray μCT was able to detect the differences between the biofilm volumes at each time point.

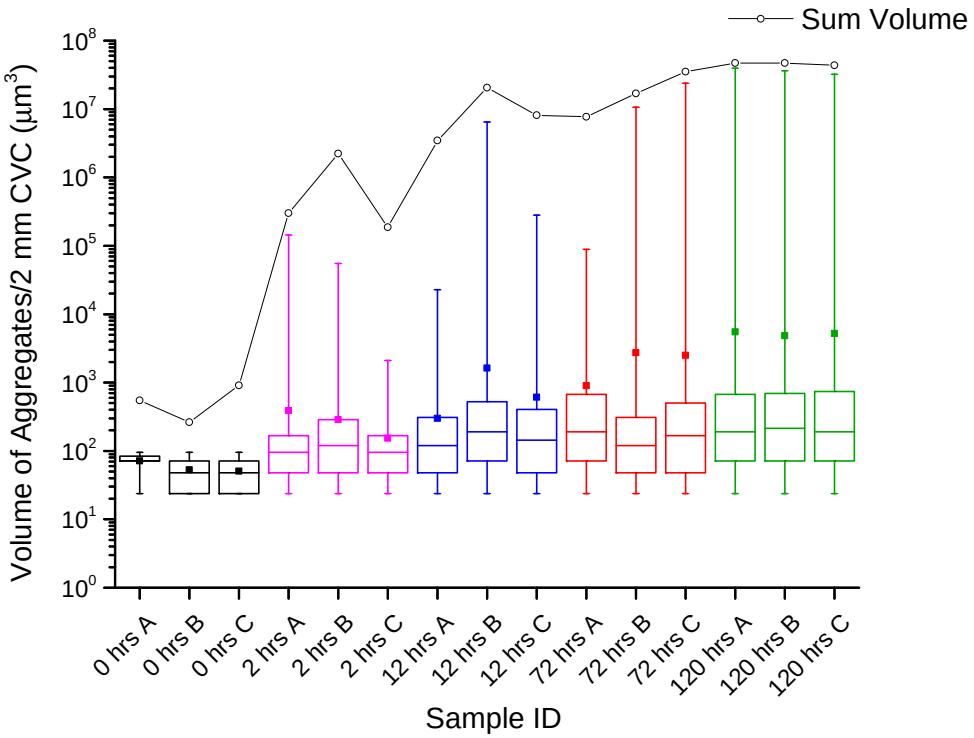

Figure 7.17: Volume distribution plot of biofilm aggregates at different time intervals. Each colour represents a time point with a solid square representing the mean volume, whiskers of box-plot representing minimum and maximum aggregate volume and open circle the sum volume. μCT was able to detect biofilms as early as 2 hours and showed increasing biofilm sum volume with time. Although sum volume was similar for the different repeats some samples had between 1 and 3 large aggregates (i.e. 2 hours A, 12 hours B, 72 hours B and 120 hours A, B and C) alongside smaller aggregates whereas the other samples had many smaller aggregates. When the sum volumes of 0 and 2 hours were compared using the t-test ($P = 0.024$), 2 and 12 hours ($P = 0.017$) and 72 and 120 hours ($P = 0.037$, Fig. 7.17)

When the percentage volume occlusion was compared for 0 and 2 hours, 2 and 12 hours, 12 and 72 hours none were statistically different ($P = 0.305$, $P = 0.159$, $P = 0.956$ respectively). Whereas when the percentage volume occlusion for 0 and 120 hours, 2 and 120 hours, 12 and 120 hours; and 72 and 120 hours there were statistically significant differences (P between 0.006 and 0.015).

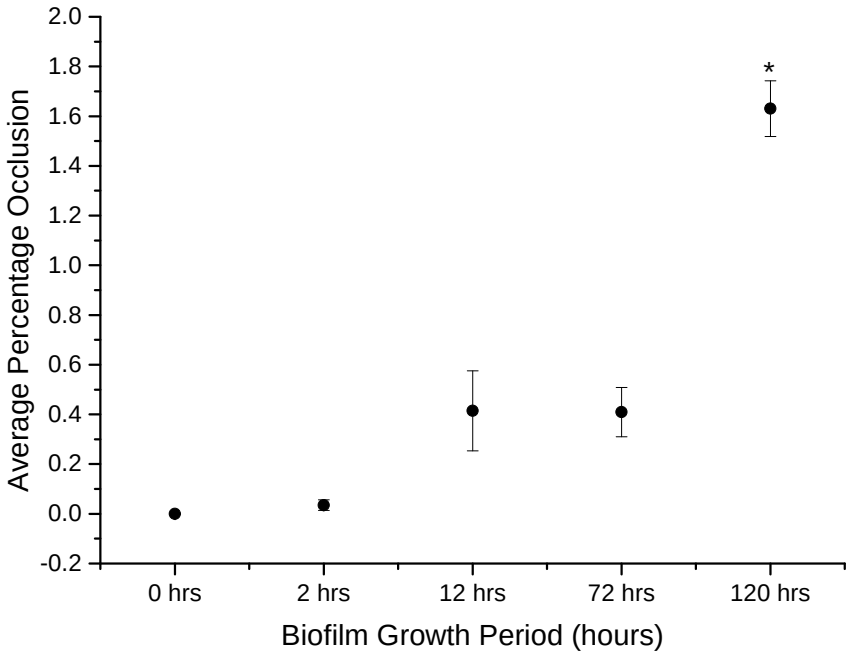

Figure 7.18: Percentage volume occlusion of the CVC at time intervals. The CVC sections were occluded most at 120 hours of growth at 1.63%. There were statistically significant differences when the t-test was applied between 0 and 120 hours *, 2 and 120 hours, 12 and 120 hours; and 72 and 120 (P between 0.006 and 0.015).

7.5.3 X-ray μCT on clinical samples

Initially, clinical samples were stained with 2% Osmium Tetroxide and 2% Uranyl Acetate for one hour each (first *in vitro* tests used 2% Osmium Tetroxide alone (Fig. 7.19). Although deposit was visible, the contrast between the radiopaque CVC and the deposit was not enough to allow for digital segmentation (Fig.7.20A). Even after digital enhancement using the grey scale histogram of the CT data, of a very small region between the bulk grey values (medium x-ray absorption values were from the CVC material) and the grey values for the radiopaque column (high x-ray absorption values) shown in yellow and white, accurate thresholding was not able to separate the CVC and the deposit (Fig.7.20B). The low threshold accuracy was because the grey values for the deposit was too similar to the grey values of the (medium x-ray absorption) CVC material.

Improving the staining methods allowed for digital segmentation of the deposit from the CVC material (Figs.7.21 and 7.22). Increased contrast between the biofilm and CVC material enabled quantification of the deposits in three dimensions (Fig. 7.29 and Fig. 7.23).

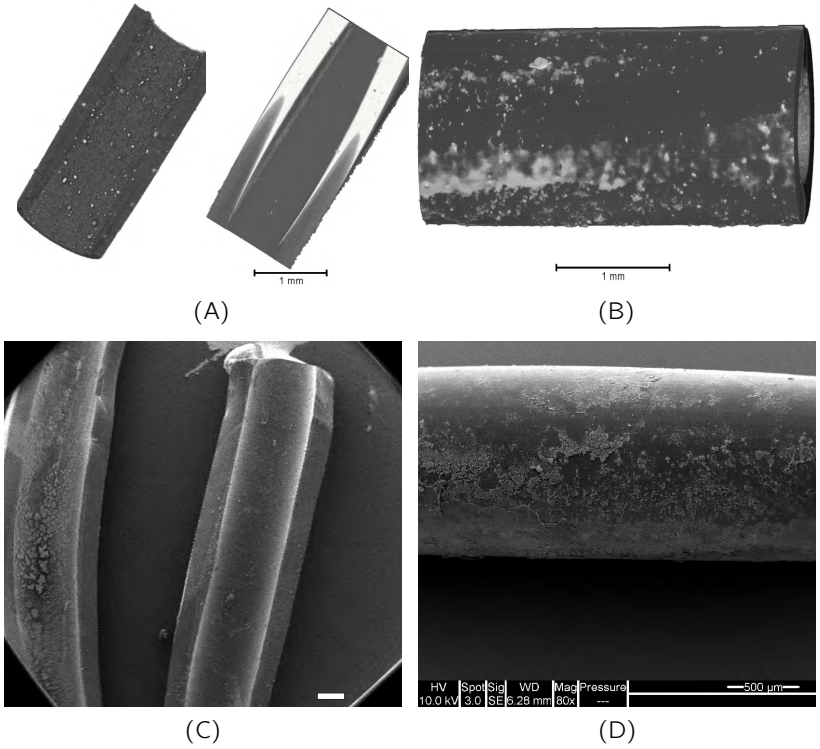

(A) (B)

(C) (D)

Figure 7.19: μCT scanned and SEM micrographs of 12 hour *S. epidermidis* static CVC-biofilm model. (A), CT scanned image and (C), SEM micrograph of Bard clearview CVC on the inside; with the clear half on the left and the blue half on the right. (B), CT scanned and, (D), SEM micrograph outer view of bard clearview PICCs. (A) to (B) scale bars= 1mm, (D) scale bar= 500 μm.

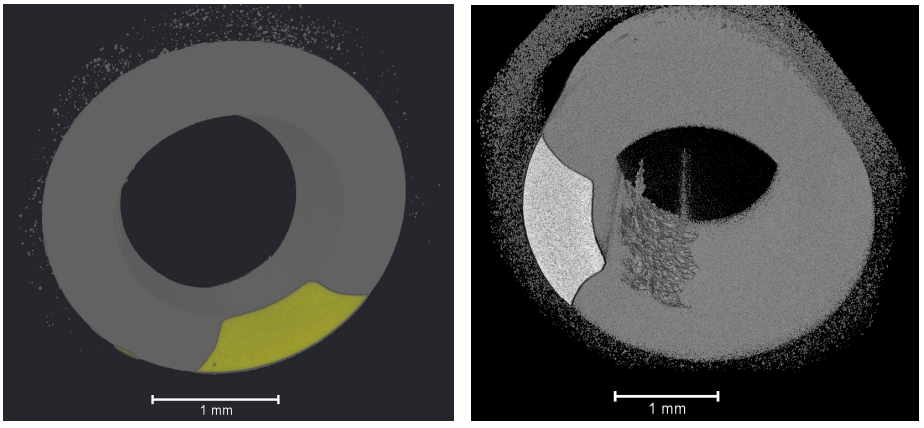

(A) (B)

Figure 7.20: Subcutaneous section from C13 tomograph stained with Osmium Tetroxide and Uranyl Acetate for one hour. (A) showed the most radiopaque part of the Bard port CVC (in yellow) and no deposit was visible. In contrast, (B), the same data, after significant processing showing deposit close to the radiopaque column embedded within the CVC wall.

C5 and C7 samples were scanned with μCT of which both showed evidence of possible biofilms (Fig. 7.21 and Fig. 7.22). When the data from C 5 and C7 was quantified (Fig. 7.21 and Fig. 7.22) the volume distribution appeared similar (Fig. 7.23) as was corroborated with the SEM micrographs (Fig. 7.21(C) and Fig. 7.22(C)). Both samples had one large aggregate (C 5, $4.55\times10^7\mu m^3$; C 7, $4.37\times10^7\mu m^3$), alongside many smaller clusters.

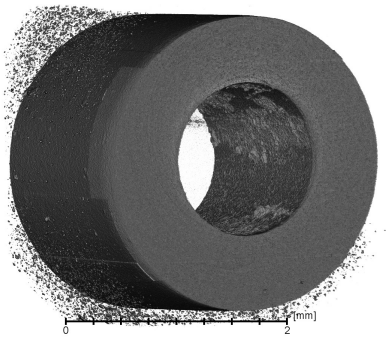

(A) C5 μCT

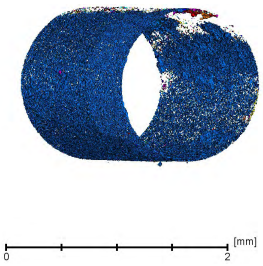

(B) C 5 μCT

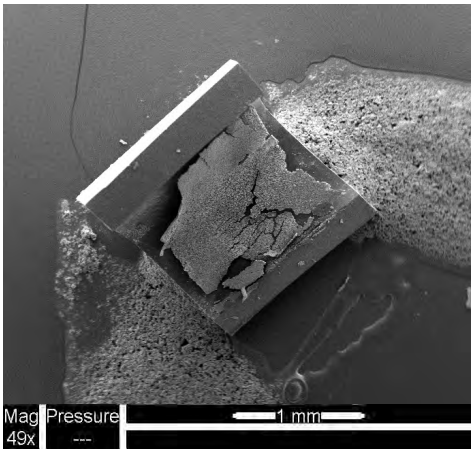

(C) C5 SEM

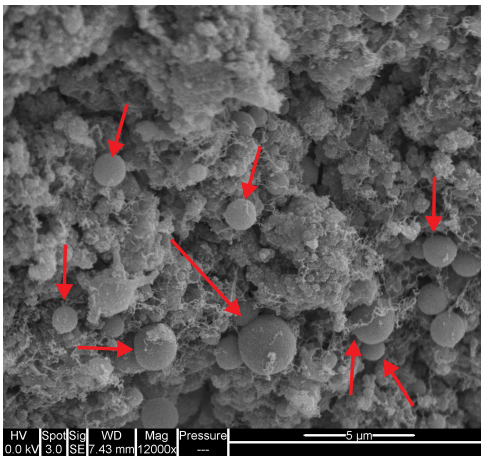

(D) C5 SEM

Figure 7.21: μCT tomographs and corroborating SEM micrographs of C5. (A), the unsegmented section of CVC from C5 showing the aggregates attached to the CVC surface. (B), the MATLAB segmented and Avizo Fire analysed bio-aggregate. (C), a low magnification micrograph showing one half of C 5. (D), higher magnification of C5 highlighting a mixed species biofilm (red arrows).

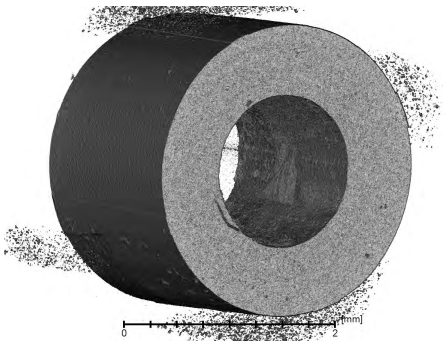

(A) C7 μCT

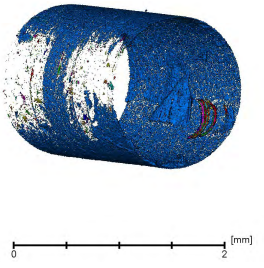

(B) C7 μCT

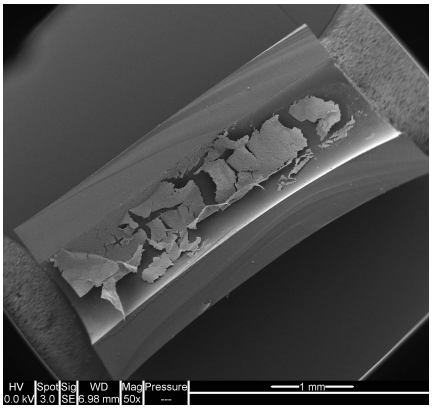

(C) C7 SEM

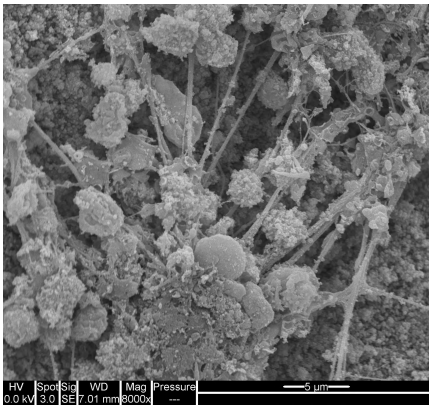

(D) C7 SEM

Figure 7.22: μCT tomographs and corroborating SEM micrographs of C7. (A), the unsegmented section of CVC from C7 showing the aggregates attached to the CVC surface. (B), the MATLAB segmented and Avizo Fire analysed bio-aggregate. (C), a low magnification micrograph showing one half of C7. (D), higher magnification of C7.

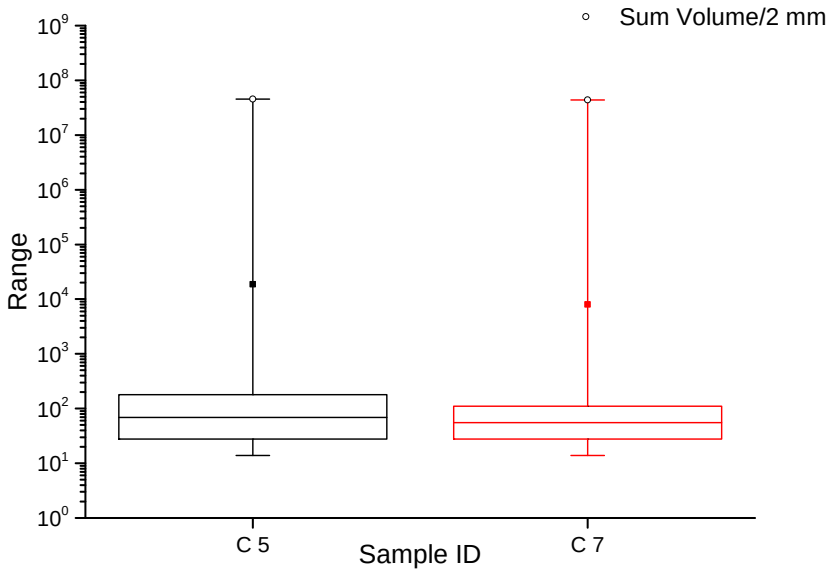

Figure 7.23: Plot showing biofilm volume distribution of C5 and C7. With black representing C5 and red C7. The solid squares represent the mean volume, the whiskers of the box-plot the minimum and maximum aggregate volumes and open circle the sum volume. Each sample had one large aggregate with many smaller clusters (open grey circles).

7.5.3.1 Comparing culture, CLSM, SEM and μCT

When the methods were directly compared using C8 CVC sections the similarities as well as limitations from the methods are highlighted. Both the x-ray CT scanned (Fig.7.24A) tomograph and the scanning electron micrograph (Fig.7.24C) showed similar amounts of deposit on the same sample. A confocal micrograph from a neighbouring section illustrated the limited depth of focus possible with CLSM (Fig.7.24B). Focal depth, material autofluorescence and blurred images due to imprecise sectioning as a result of material deformation all lead to data that could not be quantified (Fig.7.24B). However, the higher magnification scanning electron micrograph clearly showed that the deposits contained a mixed species biofilm (Fig.7.24D).

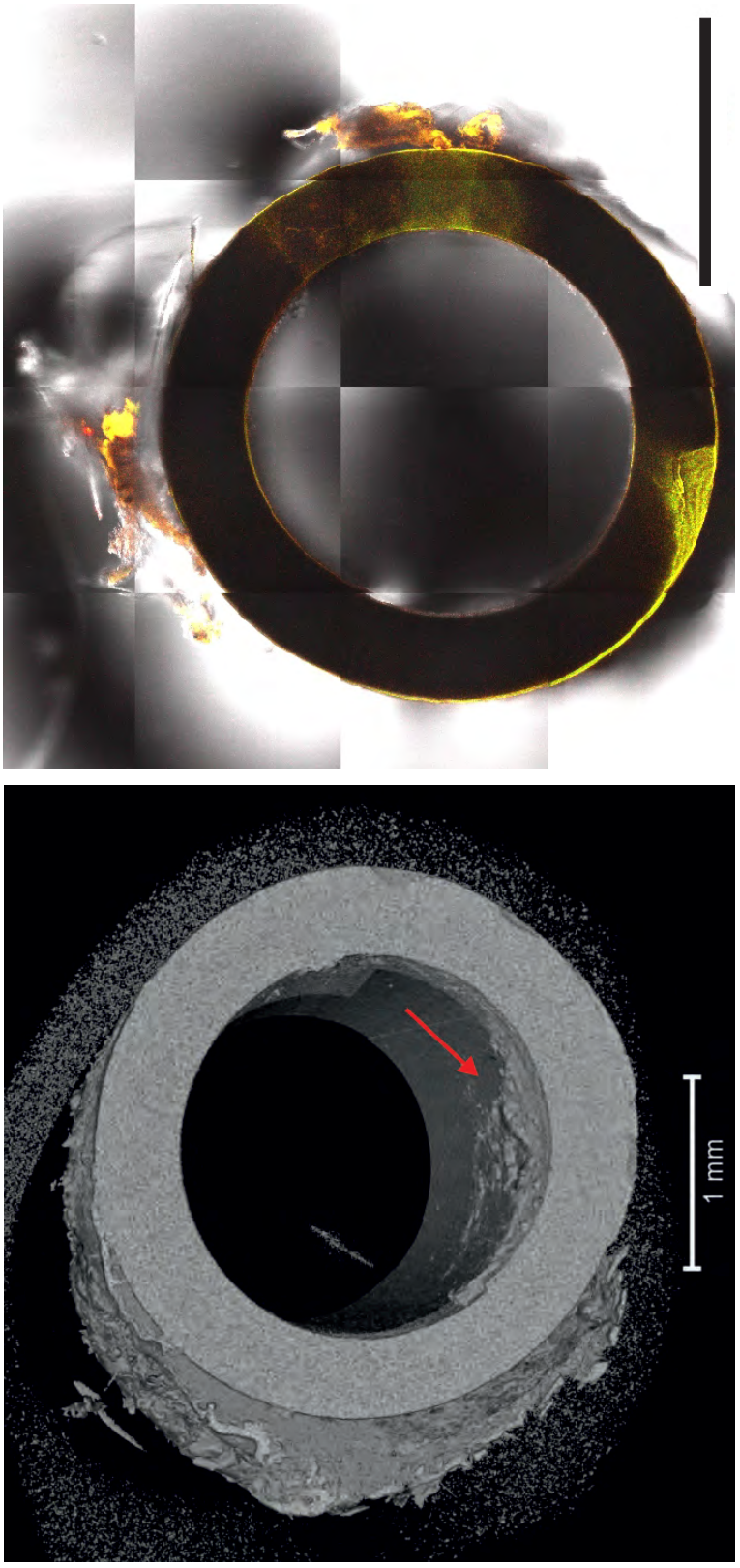

Figure 7.24: (i)

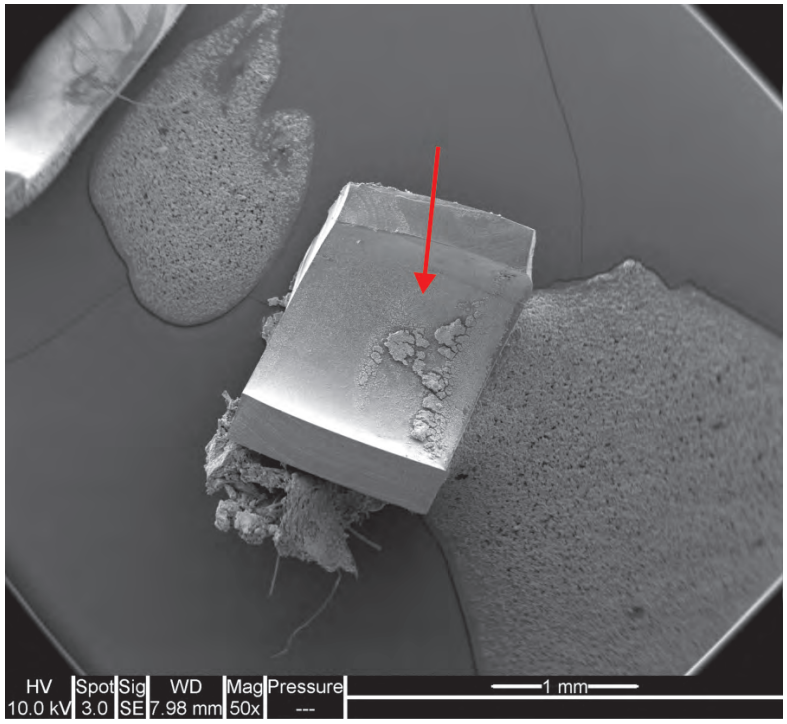

(C) C8 low magnification SEM

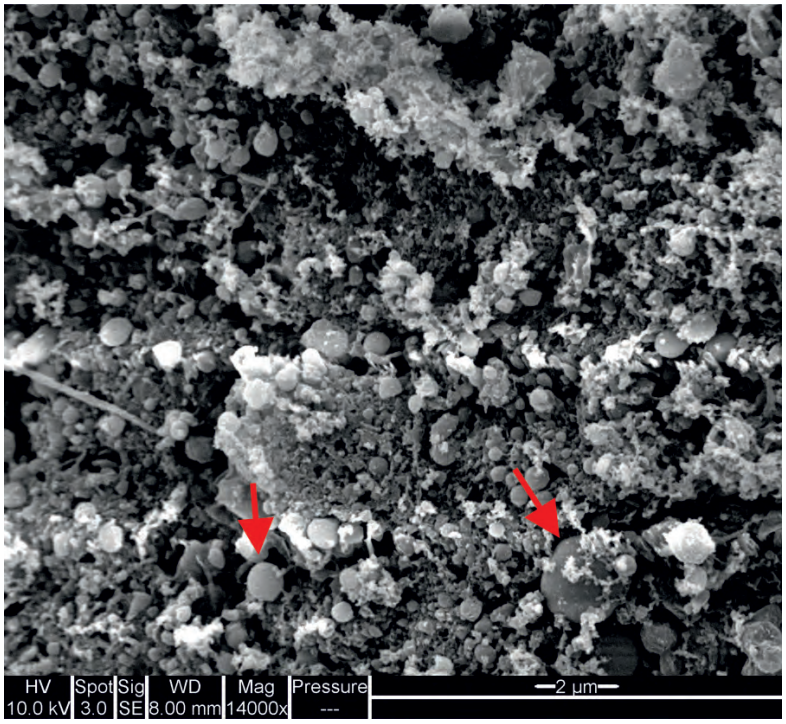

(D) C8 high magnification SEM

Figure 7.24: (ii) μCT, CLSM and SEM micrographs of sections from the subcutaneous region of the CVC removed from C8. (B) was a small section from the same region as (A), fixed an stained with SYPRO Tangerine and SYTO 9 followed by imaging using a $\times$20 oil immersion objective and scanning across the CVC section and reconstructing the images to show the whole lumen. (C) was a low magnification scanning electron micrograph that had previously been x-ray CT scanned prior to preparation for SEM. The micrograph showed that the same deposit could be observed (red arrow) (scale bar=1 mm) in both imaging methods. (D) higher magnification micrograph of the deposit indicating that there was a mixed-species biofilm within the deposit (scale bar=2 μm).

7.6 Discussion

To the knowledge of the author, using x-ray μCT to directly image and analyse biofilms within *in vitro* and clinical CVCs is the first time the method has been applied for such purposes. The current chapter showed that x-ray μCT was able to detect biofilms afer 2 hours of growth and detect difference amounts of biofilms volume at different growth points. In addition, biomass was detected in two clinical samples, albeit the difficulty in distinguishing biofilm from other deposits.

The literature showed that x-ray μCT had been used to study biofilms within model porous media (Davit et al., 2011; Iltis et al., 2011). However, both the existing μCT work on biofilms and small animals highlighted that a contrast agent was required (Metscher, 2009; Davit et al., 2011; Iltis et al., 2011). A MATLAB script based on the geometry and grey scale values allowed for semi-automated segmentation. Once the development of the image segmentation and analysis script was successful the ability of x-ray μCT to detect biofilms within CVCs were tested (Section 7.6.2). X-ray μCT sensitivity for biofilm detection was characterised to be able to detect biofilms after as little as 2 hours of growth and was shown to be positively correlated to enhanced culture by sonication. Lastly the method was applied to detect biofilms within clinical CVCs (Section 7.6.3). X-ray μCT was able to detect biofilms within clinical CVC samples.

7.6.1 Image segmentation and analysis

Before the contrast was improved manual segmentation by the experimenter was the only method to subtract the CVC and fluid accurately to leave the biofilm for analysis. This method however was extremely time consuming because contrast was so poor that global thresholding was not possible. Figure 7.10 showed just how inaccurate manual segmentation was.

In order to ensure accurate semi-automated segmentation the CVC roughness had to be determined to ensure that the roughness of the CVC would not affect the diameter determinations. The roughness of the CVC material was determined by using optical profilometry. The CVC material was fairly smooth and had an average roughness of 206.41 *nm*. Due to the roughness and often shape deformation of the CVC caused a small amount of the material to be present in the mask created by the MATLAB script. Thus we applied a 2 pixel median filter (pixel resolution of x-ray μCT data was between 2.1 and 2.6 μm) in order to remove any CVC material noise in the mask. A median filter is often used in image processing as the filter is better at preserving detail and edges. Due to the smooth CVC surface if the CVCs did not experience any shape deformation and did not suffer from any manufacturing defaults in shape the median filter would not have been necessary.

The semi-automated MATLAB segmentation script was however more accurate compared to the manual method. The one major drawback was that due to the CVC material, often if the tube was slightly deformed or very heavy biofilms were located on the outer surface of the CVC the automated script required some manual intervention (hence this method is semi-automated). The reason why the outer biofilms were not included in the final segmented biofilm was because it was assumed that that handling CVC samples with forceps would compromise the biofilm on the outside surface of the catheter. In addition, during *in vitro* growth of biofilms the CVC was stationary on the bottom of the petri dish therefore the amounts of biofilm varied depending on the orientation of the CVC. The diameter of the CVC was not such a big issue during segmentation as this could be adjusted.

Similar to Iltis et al. (2011) analysis on the data was performed using Avizo Fire. In contrast, Davit et al. (2011) did not analyse their data and merely used the μCT scans for qualitative purposes. The data reported in this thesis had higher resolution compared to Iltis et al. (2011); Davit et al. (2011). The pixel resolution of the data presented was between 2.1 and 2.6 μm, whereas Iltis et al. (2011) had pixel resolution of 4.5 and 11.8 μm even though they used synchrotron sources. Davit et al. (2011) also used a benchtop CT system similar to the equipment used in this study, although they had a much lower pixel resolution of 12 μm. Often however, the resolution is limited by the equipment and sample size.

7.6.2 X-ray μCT biofilm sensitivity

X-ray μCT was able to detect biofilms after as little as 2 hours of biofilm growth (Figs. 7.11, 7.12C and 7.12D). However x-ray μCT picked up signal from the uninoculated control (0 hours of growth, Fig. 7.13). The reason for this may have been due to the way in which the samples were processed or stacked in the sample holder. Non specific staining was suspected but during EDS analysis, in the biofilm negative stained controls there was often unidentified debris that was not of metal origin (Fig 7.25). The debris was composed of the same constituents as glass and may have been dust.

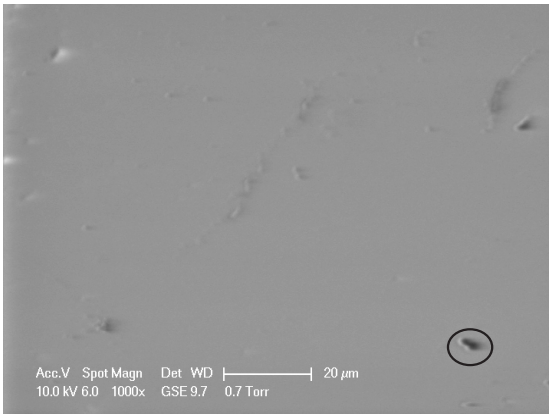

(A) 10 *nm* Gold and silver nitrate control

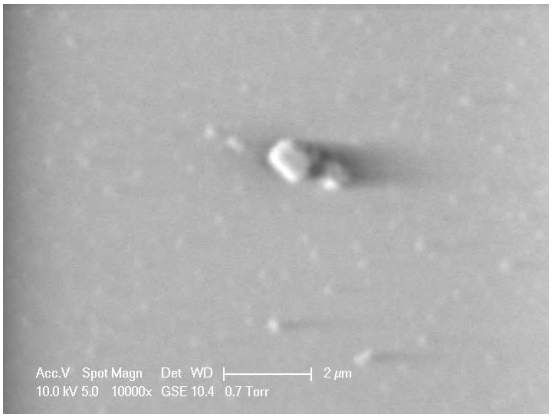

(B) High magnification

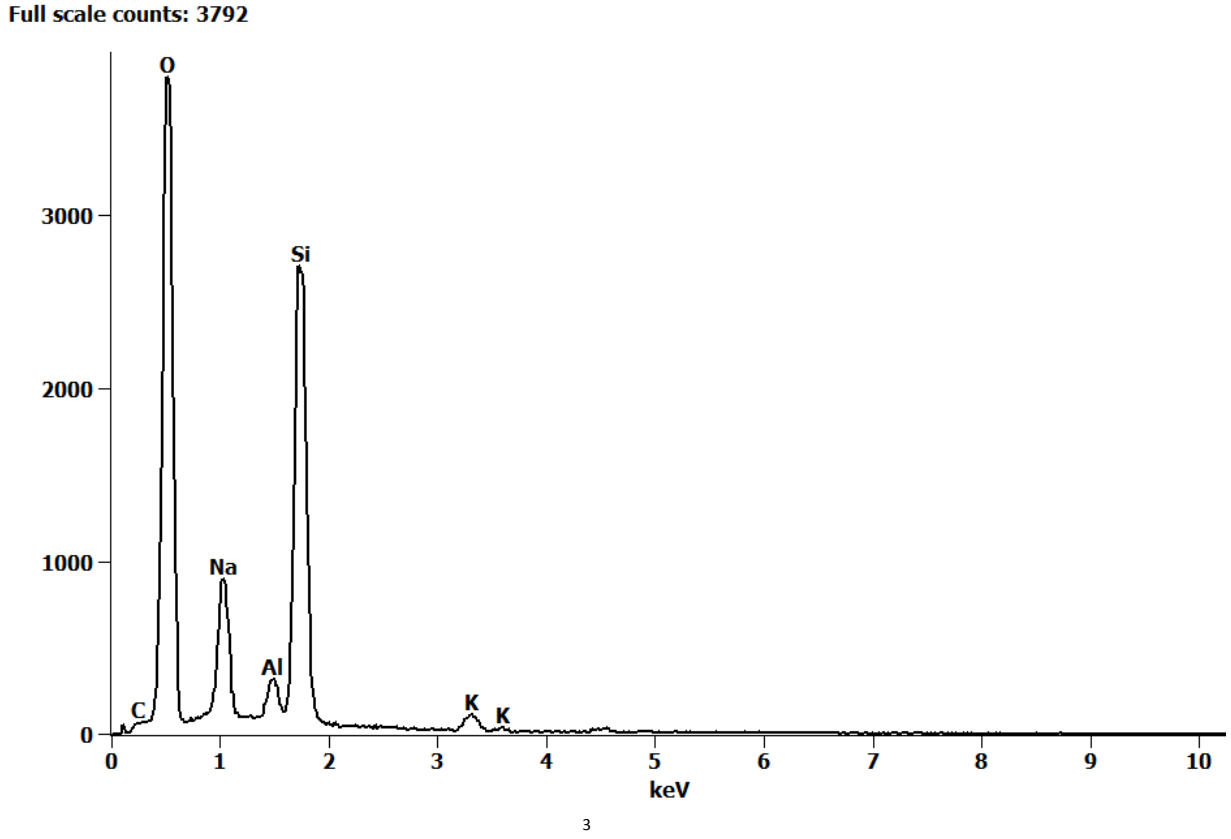

3

(C) 10*nm* Gold and silver nitrate control spectrum

Figure 7.25: EDS analysis and micrographs of gold and silver nitrate biofilm negative control. (A) showed unidentified debris on a biofilm negative glass slide stained with gold and silver nitrate. (B), a higher magnification micrograph of (A). (C), the spectrum from EDS analysis of (A) which gave no evidence of metal in the sample.

In order to reduce costs and increase the number of samples scanned by x-ray μCT CVC samples were stacked on top of each other in a carbon fibre tube. Every effort was made to ensure that the carbon fibre tube was cleared from debris before the samples were inserted prior to imaging. Often during CLSM and SEM processing biofilm destruction occurred due to sample sectioning and critical point drying. Biofilm destruction may have also occurred during μCT scanned samples (although probably less due to no sectioning). The samples for μCT were not critically point dried (required for SEM) but the samples were ethanol dehydrated. In addition, samples were handled with forceps to allow insertion into the carbon fibre tube. Because the samples were so small, deformation from handling and placing the samples in the tube may have loosened and dislodged biofilms from the biofilm positive samples which may have ended up in the control samples. The debris however, were unlikely to stick to the CVC surface during critical point drying because the chamber is flushed with ethanol 3 times before CO_2; before the samples were stubbed and coated for SEM. So the signal picked up by x-ray μCT was unlikely to be the same as the unidentified debris seen in the scanning electron micrographs.

If the bacterial cells accounts for 15% of the biofilm volume (Donlan and Costerton, 2002) and for example the sum volume of biofilm after 120 hours of growth is 4.2×10^7 in 2 mm of CVC, therefore 3.57×10^7 would be EPS and 6.29×10^6 would be bacterial cells. Enhanced culture by sonication determined that there were 2.09×10^6 bacterial cells per 2 mm of CVC. If 1 *S. epidermidis* bacterium (1 μm diameter, 0.5 μm radius) has a volume of 0.524 μm^3 than 2.09×10^6 cells would be 1.09×10^6 μm^3 of bacterial cells per 2 mm of CVC. Therefore, in theory, X-ray μCT detected 17.4% more bacterial cells compared to culture. Whether this was because culture did not remove all of the biofilm from the CVCs, whether μCT sum volume included artefacts or whether it is due to the sum volume of individual cells are smaller than the total volume of a biofilm is now known. It should be noted however, that the volume of individual bacterial cells added together would be much less than bacterial cells packed together and then the volume calculated (Fig 7.26).

Consequently, at each time point we would expect x-ray μCT to detect more biofilm compared to the number of CFUs as determined by culture because the stain is not bacterial specific. Thus, x-ray μCT would have detected, not only live bacteria such as culture; but the signal would have included dead bacteria and EPS. However, the sum volume and CFUs were not significantly differently at all time points apart from 120 hours. At 120 hours (Fig. 7.13), x-ray μCT detected significantly more biofilm volume than 72 hours, whereas culture suggested that the number of live bacteria had started to decrease. The number of live bacteria decreasing would have suggested that the biofilm population had reached maximum at 72 hours. At each time point μCT detected more volume compared to culture because EPS increases even though the number of live bacteria goes down (Lorenz and Wackernagelo, 1994). Even though the data from x-ray μCT was significantly different from culture at 120 hours, when the $\log_{10}(CFU/cm)$ was plotted against the sum volume

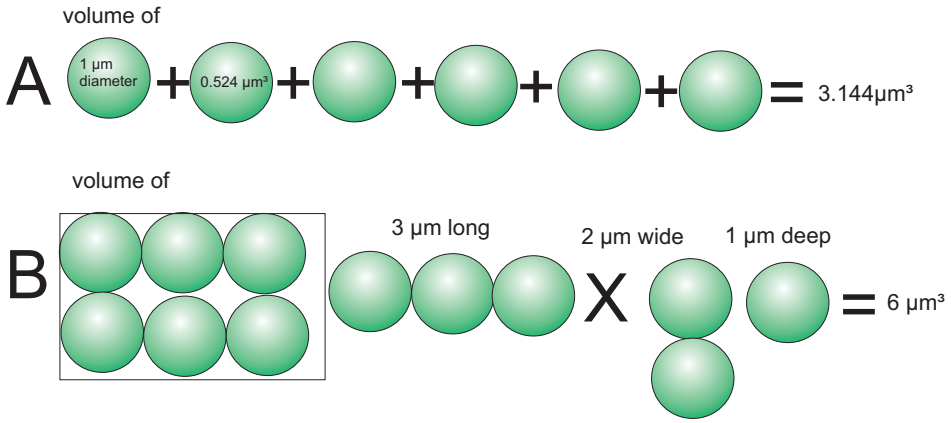

Figure 7.26: Volume of biofilm versus the volume of a few single cells added together. (A), is the method of adding the volume of 6 planktonic cells together and (B) is the volume of a biofilm consisting of 6 bacterial sells.

$\log_{10}$ ($\mu m^3/cm$) the data had a strong positive correlation. Therefore, we can suggest that x-ray μCT could be used to detect biofilms within CVCs.

An interesting variation within the repeats at each time point which was picked up by x-ray μCT was that for some samples there was one big patch of biofilm with many small aggregates and in others the sample contained many small biofilms. Whether this variation was due to sample handling or processing; or whether it was a natural occurrence is unknown and would be interesting to test.

7.6.3 X-ray μCT on clinical samples

Scanning clinical samples with x-ray μCT showed that biofilms could be detected within clinical samples as verified by scanning electron microscopy. The biggest drawback however of x-ray μCT currently was that the technique could not differentiate between blood, other products within the CVC or biofilm. Therefore, at the moment μCT cannot be used as a clinical diagnostic method without further development of bacteria or biofilm specific contrast agents.

Examining clinical specimens using x-ray μCT raised new challenges due to the use of different radiopaque enhancement methods by the various CVC manufacturers. Placement of radiopaque clusters varied between CVC brands as well as between different CVCs manufactured by the same company (Fig.7.27). Cook and Vygon polyurethane CVCs were uniformly visible by x-rays (Fig.7.27A) but also contained clusters of more dense substances scattered throughout the material (Fig.7.28B). In contrast, Bard clearview silicone PICCs and tunnelled CVCs were also uniformly visible by x-rays but contained columns of radiopaque substances (Fig.7.28A). The variability of radiopaque substances

added a degree of difficulty to the image analysis and removal from the image and initially had to be performed manually for some samples (Fig.7.29B). The Avizo Fire software package contained a segmentation editor which enabled the user to select individual objects based on the intensity and/or size but also colour if analysis had already been applied to the ' material 'which could be removed or included in the analysed data (Fig.7.29, (C) and (D)).

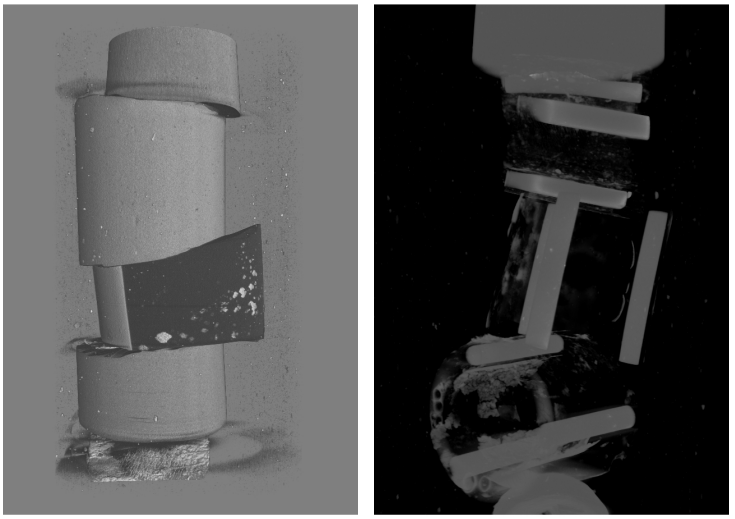

(A) (B)

Figure 7.27: Reconstructed tomographs of clinical CVC sections staked on top of each other showing variable x-ray attenuation coefficients. (A) shows the variability of attenuation coefficients between different CVCs due to containing different radiopaque substances within the material. The darker part of the Bard piece of CVC (2nd from the bottom) contains very low amounts of radiopaque substances. (B) on the other hand, the Bard pieces of CVC contain 3 columns of radiopaque material, see Fig. 7.28.

For both C5 and C7 (subcutaneous) CVC sections had varying results using culture, CLSM and SEM and x-ray μCT . For culture C5 was negative, but for CLSM and SEM C5 was positive. For C7, culture and SEM was positive but CLSM was negative. C8 had the same result using culture, CLSM, SEM and μCT (Fig.7.24). Culture by sonication and agar plating resulted in 400 CFUs per cm of the subcutaneous section (Table 3.6). CLSM, SEM also revealed evidence of biofilms in adjacent sections (Table 4.2 and Table 5.3). Although x-ray μCT cannot distinguish between biofilms and blood within CVCs, development of a biofilm specific stain would enable biofilm specific detection.

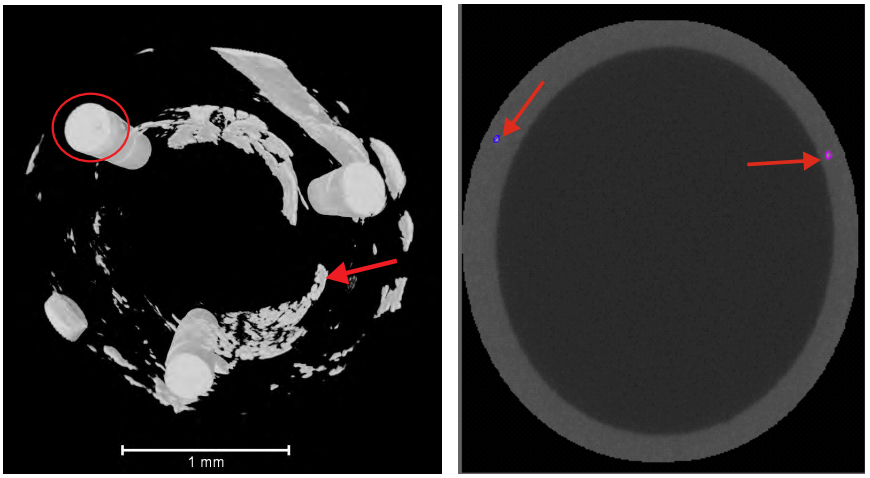

(A) (B)

Figure 7.28: Segmentation editor from P32 and micro-computed tomograph from P29 subcutaneous CVC section showing the radiopaque 'substances. (A) showing radiopaque columns circled in red and the biofilm containing deposit indicated by a red arrow and (B) segmentation editor image highlighting radiopaque clusters in purple and blue (red arrows) within the CVC wall.

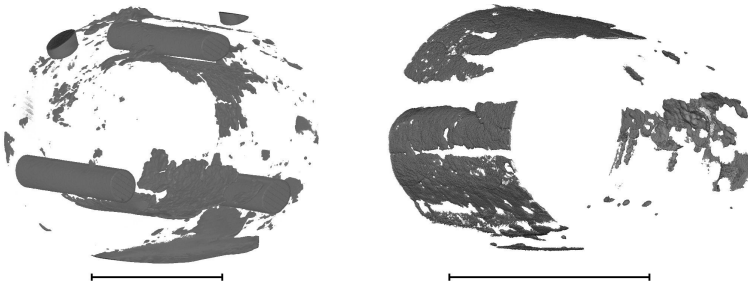

(A) P29 sub CVC and deposit (B) P29 luminal deposit

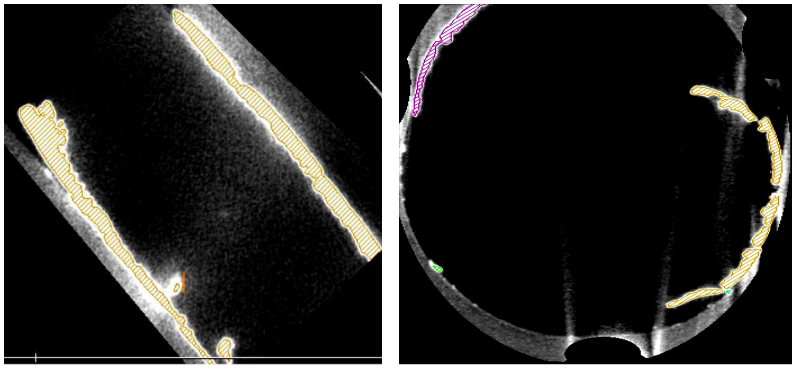

(C) longitudinal segmentation editor view (D) transverse segmentation editor view

Figure 7.29: The process to analyse a μ-CT scanned CVC section using Avizo Fire software. (A) showing a fouled Bard clearview CVC with suspected barium sulphate cylinders along the entire length of CVC and deposit. (B) showing the deposit in the lumen only (CVC digitally subtracted) (scale bars=1 mm). (C) longitudinal and (D) transverse views during segmentation editing showing the deposit selected.

Chapter 8

Conclusions and prospects

The work discussed in this thesis showed that an alternate method using x-ray μCT could potentially be used to detect biofilms within indwelling CVCs without the need for removal. Currently however, the stains explored were not biofilm specific and thus would need more experimentation. The paragraphs below discussed each different method explored for CVC-biofilm detection which lead to the development of using x-ray μCT .

The aim of this thesis was focused around biofilm detection methods within CVCs. There were 4 specific objectives. The first objective was to map where biofilms formed within clinical CVCs using culture, confocal laser scanning and scanning electron microscopy. Culture by sonication and solid agar plating showed that for the adult samples bacteria were not located in any specific region of the CVC. In contrast, for paediatric oncology samples, culture positive sections were mostly located at the subcutaneous sections. There was no significant difference between sections using CLSM and SEM. However, SEM indicated that there was significantly more biofouling of the paediatric oncology subcutaneous sections compared to the adults. More than likely the difference in fouling was probably due to the different CVC types used. For the paediatric oncology CVCs, most often the samples were tunnelled or implanted whereas the adult samples were mostly PICCs.

The second objective was to determine whether biofilms were culturable from clinical samples. Doing so revealed that all three biofilm detection methods were fallible. Culture missed biofilms as was shown by SEM and CLSM. If any sections were positive by culture when the same section was investigated with SEM evidence of biofilms were found for all apart from one section (Table A.1, P3 subcutaneous section). In contrast, SEM found evidence of biofilms on many sections which culture did not. Thus showing that at least for colonised CVCs that culture was not a reliable method. SEM revealed more samples positive (irrespective of the location) for both adult and paediatric samples (Figs. A.1 and A.2). The literature had also established that culture missed biofilms (Raad et al., 1993). CLSM however, did have evidence of biofilms on 2 sections which SEM did not (C2 and

C8 tip sections). SEM showed that most biofilms formed at the tip for adult samples and the subcutaneous sections for the paediatric samples.

The third objective was to develop a protocol for heavy metal stains which would be used to provide contrast for x-ray micro computed tomography. Energy dispersive x-ray analysis (EDS) was able to differentiate between elements using x-ray detection and exploiting the distinct ionisation energies from each element. EDS determined that 10 *nm* gold and silver nitrate was the best suited contrast stains.

The fourth and final objective was to develop x-ray micro computed tomography to detect biofilms within CVCs non-destructively. X-ray μCT was able to detect biofilms at 2 hours after inoculation and showed to be correlated to enhanced culture by sonication. X-ray μCT was also able to detect biofilms in patient samples.

Even with the limitations of detecting biofilms using CLSM, for the adult samples, CLSM and SEM had a higher concordance than CLSM and culture; and SEM and culture. An interesting theory for the lack of culture positive samples for the adult CVCs may be that the biofilms were in a viable but non culturable state (Zandri et al., 2012; Raad et al., 1993). If PCR could have been performed the method would have been able to establish if there were any false culture negative samples. However, PCR is also highly susceptible to contamination.

For the paediatric oncology samples culture and SEM; and culture and CLSM had higher concordance compared to CLSM and SEM. The difference was probably because there were more culture positive samples for the paediatric samples. Whether higher culture positive rates for paediatric samples were because of the sample population or because the use of tunnelled lines in paediatric oncology patients were much higher compared to adult samples were unknown. But bacteria within deeper layers of the skin have been suggested as a potential source of CRIs (Costerton et al., 2004). The bacteria within deeper layers of the skin may not be reached by topical antimicrobial preparations before catheter or device insertion and may be a source of infection. Bacteria present within deeper layers of the skin could also explain why Broekhuizen et al. (2008) found bacteria in peri-catheter tissue. The catheter type used may also influence the source of the bacterial infection. Consequently, because most of the paediatric CVCs were tunnelled or implanted under the skin may be the reason for more culture positive samples. What was known was that due to the autofluorescence from CVC material when using CLSM and the presence of blood and proteins attached to the CVC surface made positive biofilm identification more difficult and may have resulted in false negatives. In addition, sectioning required for CLSM and SEM resulted in biomaterial loss which could have accounted for the false negatives.

The culturability of biofilms however, remains to be questioned. Parsek and Singh (2003) listed 4 criteria to define infections caused by biofilms one of which is the direct examination of the biofilm on surfaces. Direct microscopy imaging may be the only way to confirm a

biofilm related infection (Hall-Stoodley et al., 2006; Hall-Stoodley and Stoodley, 2009). However, microscopy is time consuming, requires specialised training and equipment. Therefore x-ray μCT would eliminate the need for microscopes to detect biofilms.

In order to use μCT to detect biofilms in CVCs a contrast agent is required. Nano metals have been used for x-ray μCT in animals but the rate of clearance, specificity and toxicity of some metals have limited their application (Lui et al., 2012). EDS was used to determine the best stain candidates to improve contrast during x-ray μCT . EDS however detects x-rays produced by the elements within the stained biofilm samples so it was an indirect method. The contrast stains would however have been more likely to absorb x-rays if the material and x-rays were at a similar energy level. Thus it was hypothesised that the stain which produced the best signal by EDS would be more likely to absorb and attenuate the x-rays best. Testing each stain combination using x-ray μCT would have been a more direct approach.

Although the x-ray μCT work reported in this thesis required the removal of the catheter for biofilm detection, the ultimate goal would be *in situ* biofilm detection. If a non-toxic biofilm specific contrast stain could be developed as a CVC lock followed by a CT scan. A biofilm infection could be confirmed or ruled out if a catheter related bloodstream infection was suspected without CVC removal. Assuming that a catheter-biofilm related bloodstream infection was ruled out by μCT , central access in the most vulnerable patients could be protected.

The least toxic metal for such purposes would probably be gold which is why our work investigated the potential of this metal. The only current way however, to ensure biofilm specificity would be to use antibodies attached to a gold particle. Gold labelled lectins (such as concanavalin A, ConA and wheat germ agglutinin, WGA) were considered (Neu et al., 2001). Lectins however, also bind to blood group glycoproteins and platelets (Clarke and Denborough, 1971). All blood cells contain N-acetylglucosamine to which WGA and glucose which ConA binds to (Monsigny et al., 1980; Clarke and Denborough, 1971).

In conclusion, μCT showed good promise as a research tool for biofilms associated medical device infections but will need some development for clinical application. One issue is toxicity, although it could be used in a lock situation where systemic concerns may be less. Further work needs to be done using conventional contrast agents. In addition, the issue with biofilm and or blood clot specificity will require development of bacterial biofilm antibody or other biofilm-specific targets.

Appendix A

Comparing biofilm detection methods

A.1 Method comparison for adult samples

Comparing the methods used to detect biofilms within the adult CVC samples illustrated that SEM examination found evidence of biofilms in a higher percentage of tip and subcutaneous sections when compared to culture and CLSM (Fig.A.1). To map where the biofilms from the adult patients came from there was a significant difference for biofilm positive tips in adult samples between culture and SEM (Mann-Whitney, CI at 95%, $P = 0.01$) but not between culture and CLSM ($P = 0.155$) or CLSM and SEM ($P = 0.919$). For subcutaneous biofilm positive sections there was no significant difference between culture and CLSM ($P = 0.909$) or CLSM and SEM ($P = 0.550$); and culture and SEM ($P = 0.343$).

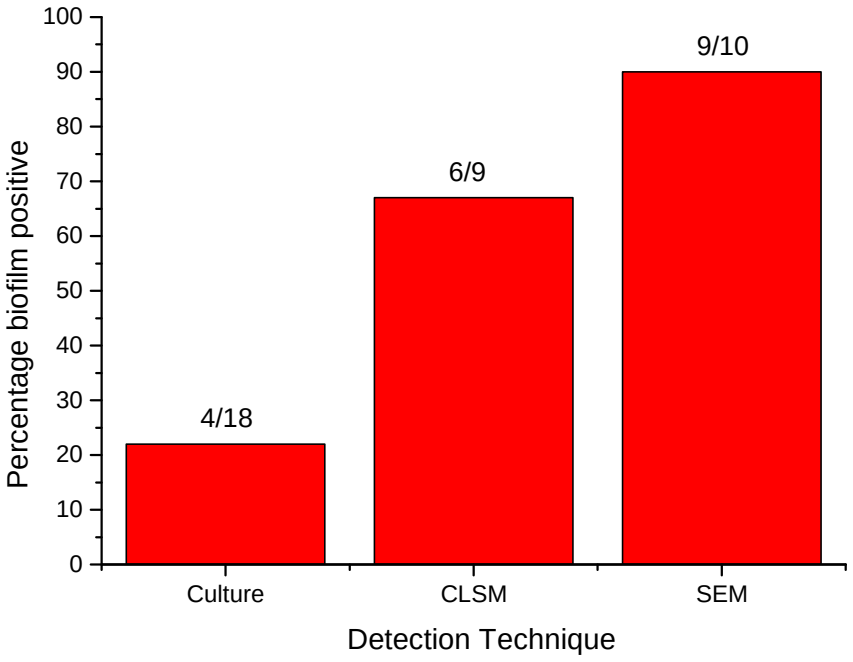

Figure A.1: Plot comparing methods used for detecting biofilms in adult CVC samples. The plot showed that SEM detected the most biofilms followed by CLSM and culture.

Of the 23 cultured adult CVC samples, 11 was also examined using CLSM and 10 using SEM (Table A.1). There was positive agreement between culture and CLSM for 3 adult sections, these were however sections that were taken as positive due to HPA blood cultures (thus not included in agreement rate). There was negative agreement for 7 sections and no agreement for 11 sections. Thus, there was an agreement rate of 39% between culture and CLSM. There was negative agreement for adult sections between culture and SEM for 8 sections, positive agreement for 5 sections and 17 disagreements. Therefore between culture and SEM there was an agreement rate of 43.3%. There was positive agreement for 5 sections between CLSM and SEM, negative agreement for 2 sections and no agreement for 4 sections. Thus there was an agreement between CLSM and SEM of 63.6%. Thus best agreement between the three methods for adult samples was SEM and CLSM followed by culture and SEM and; last culture and CLDSM. But note, only eleven samples were compared for CLSM and SEM whereas there were twenty-two for culture and CLSM and thirty for culture and SEM.

When each patient was looked at individually, for culture and SEM the methods were in agreement for 2 patients (P1 and P7), 2 out of 3 sections were in agreement for 2 patients (P5 and P6) and only 2 patient sections were in agreement for 1 out of 3 sections (P2 and P4, total of 10 patients). For 3 patients culture and SEM were the complete opposite (P3, P18 and P21). Interesting to note was that culture found 8 out of 9 of

these sections negative (only the subcutaneous section of P3 was positive) whereas SEM was the opposite. When these sections were analysed with CLSM (P18 and P21), 4 out of 5 of the sections had the same outcome as SEM (only 1 section had the same result as culture). Only 2 patients (P5 and P9) had the same result for tip and subcutaneous sections using culture and CLSM. For 3 patients (P4, P21 and P26) culture and CLSM results matched for only 1 section (all subcutaneous sections). For 3 of the patients (P18, P32 and P36) the results were opposite, of which 2 of the patients all the sections were culture negative (P18 and P36) whereas these sections were positive for biofilms using CLSM.

Table A.1: Combined method results for adult patients for biofilm detection comparing culture, CLSM and SEM

Patient	CFU/cm/mL			CLSM			SEM		
	Tip	Mid	Sub	Tip	Mid	Sub	Tip	Mid	Sub
1	✓	✓	✓	–	–	–	✓	✓	✓
2	×	×	×	–	–	–	✓	✓	×
3	×	×	✓	–	–	–	✓	✓	×
4	×	×	×	✓	–	×	✓	×	✓
5	×	×	×	×	–	×	✓	×	×
6	✓	×	✓	–	–	–	✓	✓	✓
7	×	×	×	–	–	–	×	×	×
9	×	×	×	×	–	×	✓	✓	×
18	×	×	×	✓	–	✓	✓	✓	✓
21	×	×	×	✓	✓	×	✓	✓	✓
26	×	×	×	✓	–	×	–	–	–
28	×	×	×	–	–	–	–	–	–
29	HPA	HPA	HPA	×	✓	✓	–	–	–
30	HPA	HPA	HPA	×	–	✓	–	–	–
31	×	×	×	✓	–	–	–	–	–
32	✓	×	✓	×	–	×	–	–	–
33	×	×	×	–	–	–	–	–	–
34	×	×	×	–	–	–	–	–	–
35	×	×	×	–	–	–	–	–	–
36	×	×	×	✓	–	✓	–	–	–
Percentage	16.7%	5.6%	22.2%	54.5%	100%	40%	90%	70%	50%

✓ denoted positive, × negative, – no sample and HPA culture results from HPA blood sample

A.2 Method comparison for paediatric camples

Comparing the methods used to detect biofilms within the paediatric oncology CVC samples also found that SEM detected the most biofilms (Fig. A.2). When looking at the sections from each sample to map where the biofilms were most commonly located there was a statistically significant difference for the percentage of positive tips from paediatric samples between culture and SEM (Mann-Whitney, CI at 95%, $P = 0.028$) but not for subcutaneous sections (Mann-Whitney, CI at 95%, $P = 0.480$, Table A.2). There was no significant difference between SEM and CLSM for positive tip sections from paediatric CVCs (Mann-Whitney, CI at 95%, $P = 0.359$) and for subcutaneous sections (Mann-Whitney, CI at 95%, P =1, $P = 0.167$).

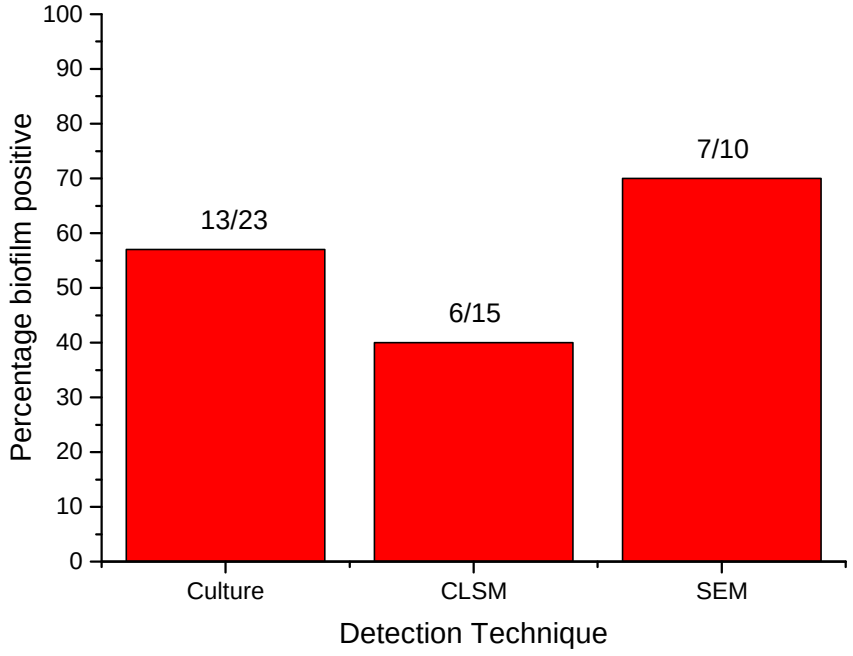

Figure A.2: Plot comparing methods used for detecting biofilms in paediatric CVC samples. The plot showed that SEM detected the most biofilms followed by culture and CLSM.

Of all the sections examined with the different methods there was positive agreement for culture and CLSM for 4 paediatric sections, negative agreement for 10 sections and no agreement for 12 sections (Table A.2). Thus leading to an agreement rate of 53%. There was positive agreement for 5 sections between culture and SEM, negative agreement for 10 sections and no agreement for 8 sections. Therefore an agreement rate of 65%. There was agreement for 5 sections between CLSM and SEM, and disagreement for 7 sections. Thus an agreement rate og 42% between CLSM and SEM.

When each paediatric sample was looked at individually, for culture and SEM the methods were in agreement for all sections for 5 patients (C1, C2, C7, C8 and C9). In contrast CLSM differed for the C2 and C8 tip sections and both C7 sections. For 2 patients, results using culture and SEM was opposite; C4 culture had positive tip culture and negative subcutaneous culture whereas SEM the tip and subcutaneous sections were positive. For C5 the tip and subcutaneous sections were culture negative but evidence of biofilms were found for tip and subcutaneous sections using SEM. Again, CLSM also had evidence of biofilm for the C5 subcutaneous section. For CLSM and culture, 4 patients (C3, C11, C13 and C14) had results that were in agreement for all sections. For CLSM and SEM on the other hand there were opposite outcomes for C6 and C7.

Table A.2: Combined method results for paediatric oncology patients for biofilm detection comparing culture, CLSM and SEM.

Child	CFU/cm/mL			CLSM			SEM		
	Tip	Mid	Sub	Tip	Mid	Sub	Tip	Midd	Sub
1	×	×	×	–	–	–	×	×	×
2	×	×	×	✓	–	×	×	×	×
3	×	×	✓	×	×	✓	✓	–	–
4	✓	×	×	×	–	–	✓	–	✓
5	×	–	×	–	–	✓	✓	–	✓
6	–	×	✓	–	×	×	–	✓	✓
7	✓	–	✓	×	–	×	✓	–	✓
8	×	×	✓	✓	×	✓	×	×	✓
9	×	×	×	–	–	–	×	–	×
10	×	×	✓	–	–	–	✓	✓	✓
11	×	–	×	×	–	×	–	–	–
12	×	–	✓	×	–	×	–	–	–
13	×	–	✓	×	–	✓	–	–	–
14	×	–	×	×	–	×	–	–	–
15	×	✓	✓	–	×	×	–	–	–
16	×	–	✓	–	–	×	–	–	–
17	×	×	✓	–	–	×	–	–	–
19	×	–	×	–	–	–	–	–	–
20	×	–	×	–	–	–	–	–	–
21	×	×	✓	–	–	–	–	–	–
22	×	×	✓	–	–	✓	–	–	–
23	×	–	×	–	–	–	–	–	–
24	×	×	×	–	–	–	–	–	–
	8.7%	8.3%	52.2%	22%	0%	35.7%	44.4%	40%	66.7%

✓ denoted positive, × negative and – no sample

Appendix B

Optical profilometry

Optical profilometry was performed with an Alicona Infinite focus optical profilometer to determine the surface roughness of silicone (Bard clearview) and polyurethane (Semprus control and Semprus sustain coated) PICCs. These samples were placed under the optical profilometer in dry conditions with no biofilm. The surface roughness measurements were done to determine what effect it may have on biofilm attachment and therefore the performance of the PICCs.

Surface roughness scans were performed to determine whether polyurethane and silicone catheters surface roughness could influence biofilm formation. It was only possible to scan the blue side of the bard clearview PICC due to limitations of the instrument which required certain levels of reflectivity. The silicone, Bard Clearview had an average roughness of 55 nm (fig.B.1B) whereas the polyurethane (Semprus uncoated control) had a surface roughness of 80 nm. The profile analysis of the uncoated and coated Semprus PICCs showed that the coated PICC was slightly smoother than the control with an average roughness of 80 and 83 nm respectively (fig.B.1). There was no difference between the mean peak to valley height but the coating reduced the maximum valley height from 430 to 447 nm.

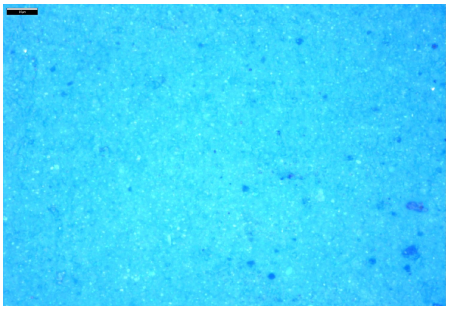

(A) Silicone top down view Bard

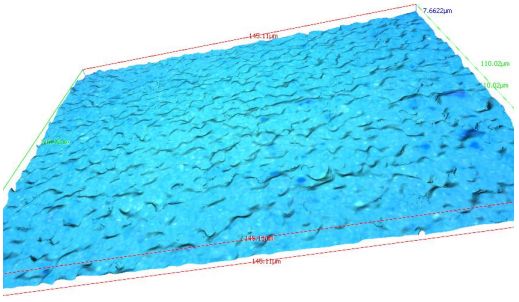

(B) Silicone 3-dimensional view

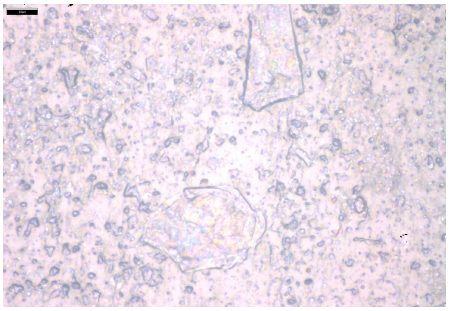

(C) Polyurethane top down view

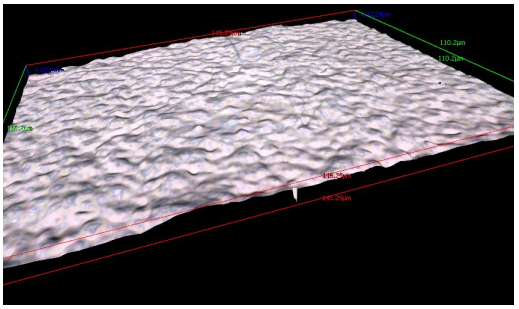

(D) Polyurethance 3-dimensional view

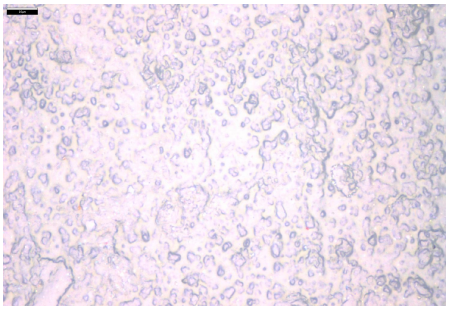

(E) Polyurethance Semprus sustain coated top down view

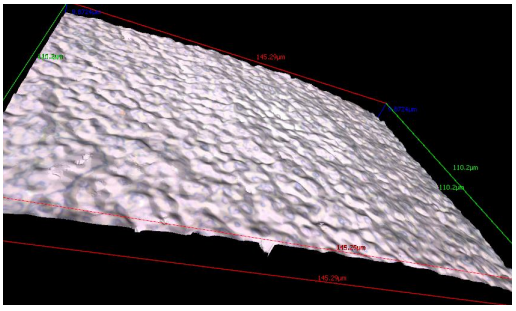

(F) Polyurethance Semprus sustain coated 3-dimensional view

Figure B.1: Surface optical profilometry analysis of silicone and polyurethane PICCs to determine surface roughness. B.1A and B.1B views of silicone (Bard clearview) PICC surface scans, B.1C,B.1D showing surface scans of polyurethane PICCs;and B.1E and B.1F Semprus sustain coated PICC scans (scale bars=10μm).

Appendix C

Micro computed tomography

C.1 Applying the contrast stains

Initially samples for x-ray μCT were stained with Osmium Tetroxide and or Uranyl Acetate. Although the stains did improve contrast, due the toxicity other stains were investigated to move the research toward the possibility of *in vivo* staining (Section 6.1.2).

Aueous Osmium Tetroxide at 4%(w/v) concentration and 2%(w/v) Uranyl Acetate was prepared by adding 2 g to 100 m*l* of 50% ethanol. Uranyl Acetate solution was left in the fridge overnight at 4^{o}C. Initially the samples were immersed in the stains and incubated at room temperature for 1 hour each.

X-ray μCT was able to detect *S. epidermidis* biofilms in the lumen and outer surface of a CVC grown for 24 hours in static conditions, stained with Osmium Tetroxide for 1 hour (Fig.7.19A and (B)). The presence of *S. epidermidis* biofilms were confirmed by examining the same sections using scanning electron microscopy (Fig.7.19, (C) and (D)). Staining biofilms with Osmium Tetroxide enabled biofilm visualisation, but staining for one hour did not produce high enough contrast between the CVC, buffer and the biofilm. Therefore, the type of stain and staining protocol had to be improved to produce enough contrast in order to be able to separate the phases digitally.

C.2 X-ray μCT segmentation pre MATLAB script

Before image or data analysis, the raw XTEC file produced by the HMC x-ray μCT scans were loaded into CT Pro software (Nikon Metrology, US). The centre of rotation was determined (automatically or manually). The centred sample data was reconstructed using CT agent (set to 32 bits of float).

The reconstructed data set was made smaller. The smaller data-set was achieved by importing the reconstructed data into VG Studio Max and digitally cutting out as much of the sample holder and CVC material as possible. A circular module in VG Studio Max was used. The smaller data sets were exported as raw datasets.

C.2.1 Digital volume sectioning and thresholding

VG studio max software (Volume Graphs, US) was used to digitally remove the sample holder and so resulted in a smaller data set. The CVC volume was imported into Avizo Fire 7.0 or 7.1 software (Visualization Sciences Group, France) and the rendered volume produced a 3-dimensional volume and a histogram with corresponding grey values (Fig.C.1A). Handles were added to the histogram to manipulate the volume. Grey values were used to digitally segment unwanted contents such as ethanol(Fig.C.1D).

The 'handle'(vertical line in Fig.C.1F) was moved to change the threshold such as to exclude the CVC material in the volume. The minimum grey value for which the CVC was not visible was used as a first-try threshold value (Fig.C.1E). Using the lowest grey value at which the CVC was no longer visible resulted in a fairly accurate threshold with a small degree of 'noise'. The noise was clumps of radiopaque substances which all CVCs contained to varying degrees.

C.2.2 Digital noise removal and quantification

After a threshold was applied, the noise within the dataset was removed (Fig.C.1E). The biofilm which was left after removing the noise was then quantified which produced a colour coded tomograph volume (Fig.C.1H) . Each colour represented a discrete biofilm cluster and a spreadsheet was produced with the corresponding volume and surface area data of each cluster.

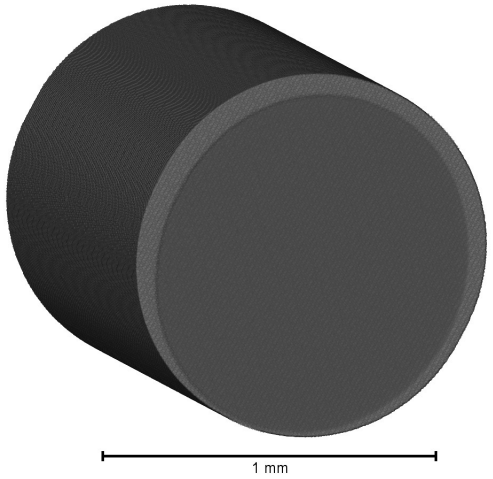

(A) All grey values visible

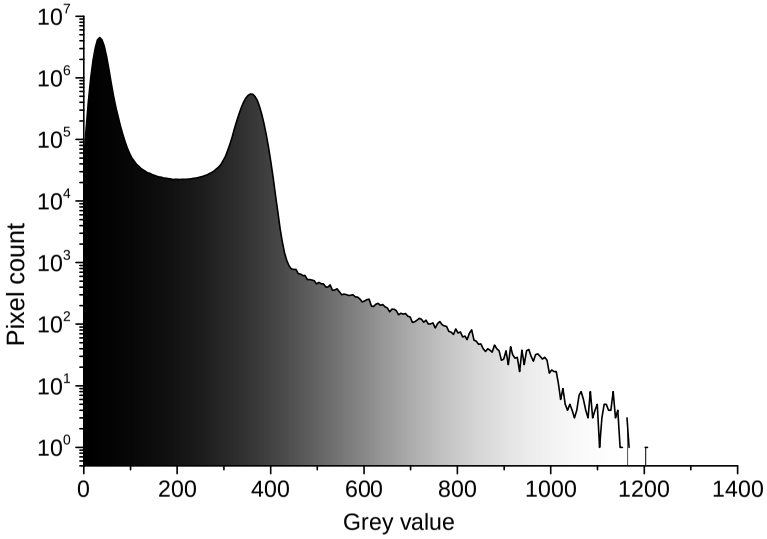

(B) All grey values visible

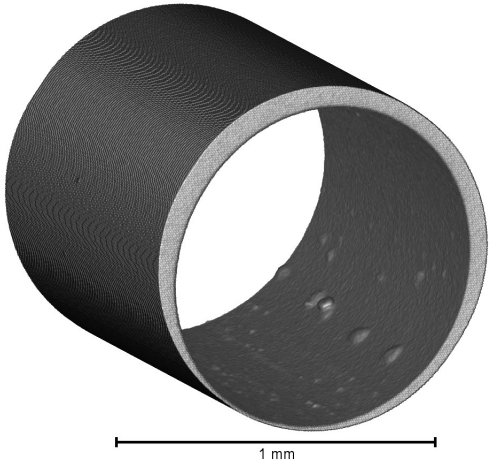

(C) Ethanol not visible

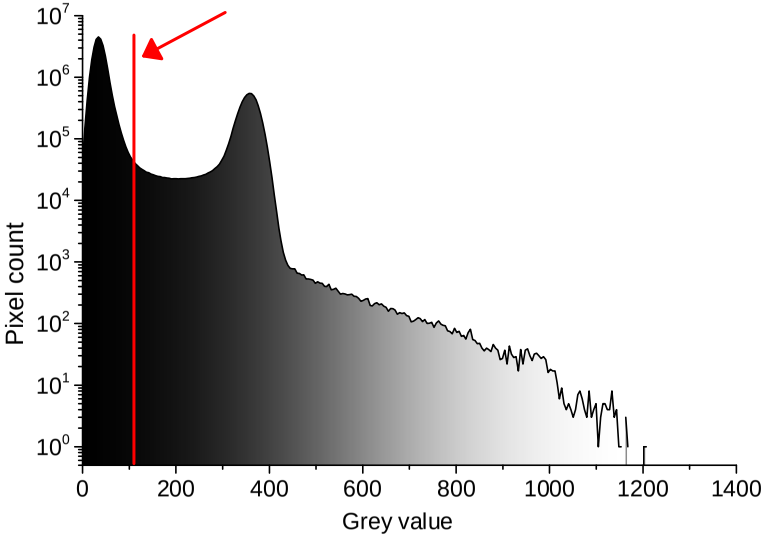

(D) Ethanol not visible

Figure C.1

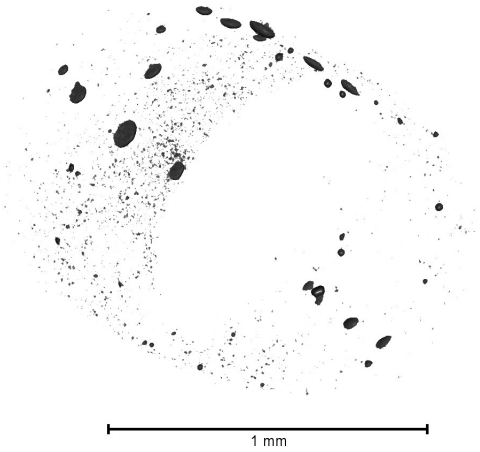

(E) Biofilm visible

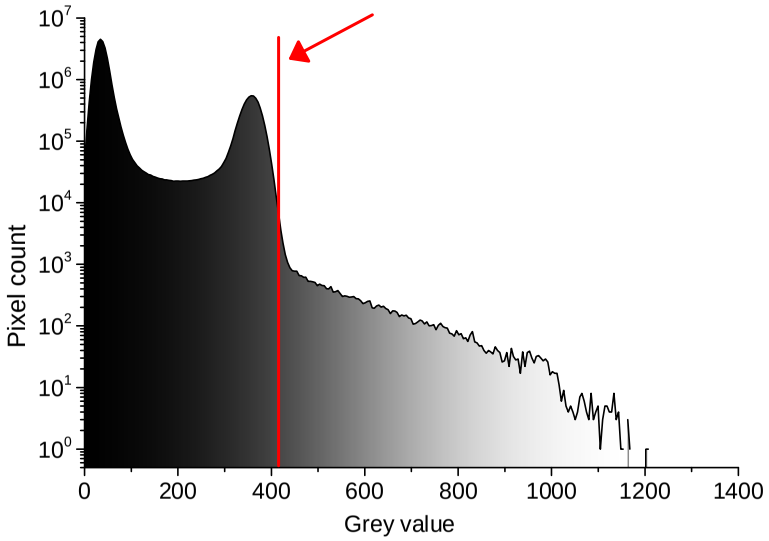

(F) Biofilm visible

(G) Analysis

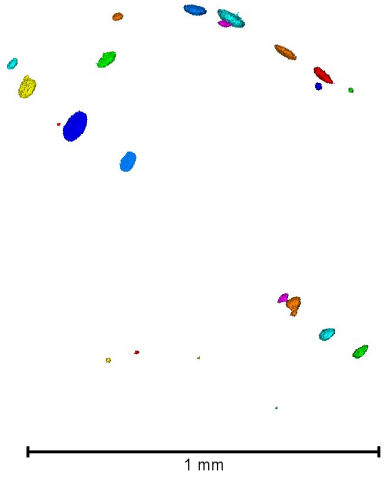

(H) Analysis after segmentation editor

Figure C.1: CT analysis using Avizo fire. (A) showed the inner lumen with a small amount of CVC with no grey scale adjustments, (B) the corresponding grey scale. (C), the CVC and deposits clearly visible after adding a 'handle'(indicated by red arrow) to the histogram to remove the first peak that represented ethanol from the volume, (D). (E) the grey value for the deposit (varied for each sample scale, indicated by the red arrow). (G), the volume after quantification. The software excluded the grey values outside of the upper (CVC) and lower (ethanol) threshold values. Scattered pieces of radiopaque clusters were embedded within the CVC material and fell within the threshold limits. The clusters were removed by the segmentation editor (see figure 3.6). Quantification tools were applied (H) to produce the final tomograph and accompanying data. Each colour represented a discrete cluster.

C.3 MATLAB script for x-ray μCT segmentation

```
clear all
num_images =992;

for k = 0:(num_images-1)
   IMG_NUM = k;
   if k<=9
   IMG_NUM = ['000' int2str(IMG_NUM)];
   end
   if ((k>9) && (k<100))
   IMG_NUM = ['00' int2str(IMG_NUM)];
   end
   if ((k>99) && (k<1000))
   IMG_NUM = ['0' int2str(IMG_NUM)];
   end
   if ((k>999) && (k<10000))
   IMG_NUM = [" int2str(IMG_NUM)];
   end


I_bin = ['Binary1/Mask of Data1_' IMG_NUM '.tif'];
I_bin = imread(I_bin);

I = ['Data1/01 TIFF RECON COR2.2_2_' IMG_NUM '.tif'];
I = imread(I);

%Get size of data
[height,width] = size(I_bin);

K=zeros(height,width);
J=zeros(height,width);

%Convert binary image to 0 1 binary image
for i=1:width,

   for j=1:height,
     if I_bin(j,i) == 255
        K(j,i) = 0;
     end
     if I_bin(j,i) == 0
        K(j,i) = 1;
     end

   end

end

[B,L] = bwboundaries(K,4);

%Determine largest and second largest blob position in B
[nrows, ncols] = cellfun(@size, B);
for i=1:size(nrows),
   nrows(i,2)=i;
```

Figure C.2

```
end

nrows2 = sortrows(nrows,1);
nrows3=flipud(nrows2);

%Find centre of circle
outer = B{nrows3(1,2)};
%center1 = mean(outer);
center = mean(outer);
%center2 = mean(inner);
%centre = (center1 + center2)/2;
inner = B{nrows3(2,2)};


%Calculate radius from centre point to inner - create a circle mask with
%position center and radius average
for i=1:size(inner),
 radius(i,1)= sqrt( (inner(i,1)- center(1,1))^2 + (inner(i,2)- center(1,2))^2);
end


s = std(radius);
%Mean radius plus 3 times standard deviation
mean_radius = 221+s; % change value by measuring diameter in pixels divided by 2.


% Create circle mask based on centre of circle and radius
cx=center(1,2);
cy=center(1,1);
r=mean_radius;
[x,y]=meshgrid(-(cx-1):(width-cx),-(cy-1):(height-cy));
c_mask=((x.^2+y.^2)<=r^2);

%Convert c_mask to 8-bit
c_mask = uint8(c_mask);
K = uint8(K);

%hold on
%imagesc(c_mask)
%imagesc(K)

% Multiply original mask (K) by cirlce mask (c_mask) to leave features mask
feature_mask=zeros(height,width);
feature_mask = uint8(feature_mask);

for i=1:width,

   for j=1:height,
      feature_mask(j,i) = K(j,i) * c_mask(j,i);
   end
end
```

Figure C.2

```
feature=zeros(height,width);
feature= uint8(feature);

% if matlabpool('size') == 0 % checking to see if my pool is already open
%     matlabpool open 2
% end

feature = I.*feature_mask;
% find all values in feature above 150

[index_col,index_row] = find(feature >= 160 & feature <=255);
for i=1:size(index_row),
   feature(index_col(i,1), index_row(i,1)) = 0;
end


write = ['Process2/processed_' IMG_NUM '.tif'];
imwrite(feature, write);
IMG_NUM

clear all
end
```

Figure C.2

C.4 μCT of CVC-flow biofilm model samples

The CVC-flow biofilm model grew heterogeneous amounts of biofilm throughout the catheter (Fig. C.6 and Fig. C.3) The model biofilm system, as already mentioned in Section 5.3.2, the sample at the 'tip' CVC section had the most biofilm formation compared to the middle and tip section (Fig. C.6A).

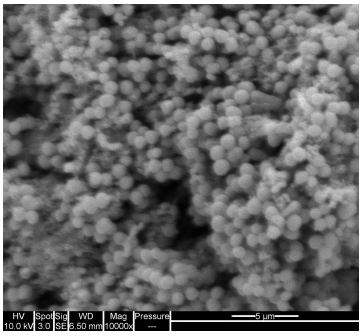

Figure C.3: Representative high magnification electron micrograph of a biofilm from the CVC-flow biofilm model sample. The micrograph show cocci which would indicate that the biofilm contained *S. epidermidis* which was present in the inoculum

The difference between the tip and transcutaneous volume distribution was statistically significant (Mann-Whitney Test, CI at 95%, P = 0.0001) but not between the tip and middle section (P = 0.742, Fig. C.4). The percentage volume occlusion (Fig. C.5)

illustrated just how much more biofilm formed at the tip section compared to the middle and transcutaneous sections.

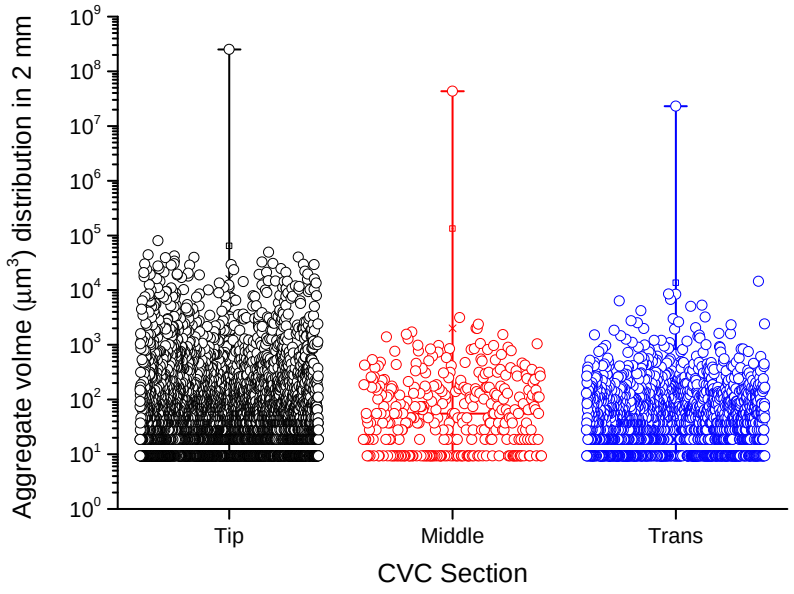

Figure C.4: Plot comparing the biofilm volume distribution of the x-ray μCT scanned CVC-flow model samples. The tip section (in black) shows the most biofilm compared to the middle (red) and transcutaneous (blue) sections.

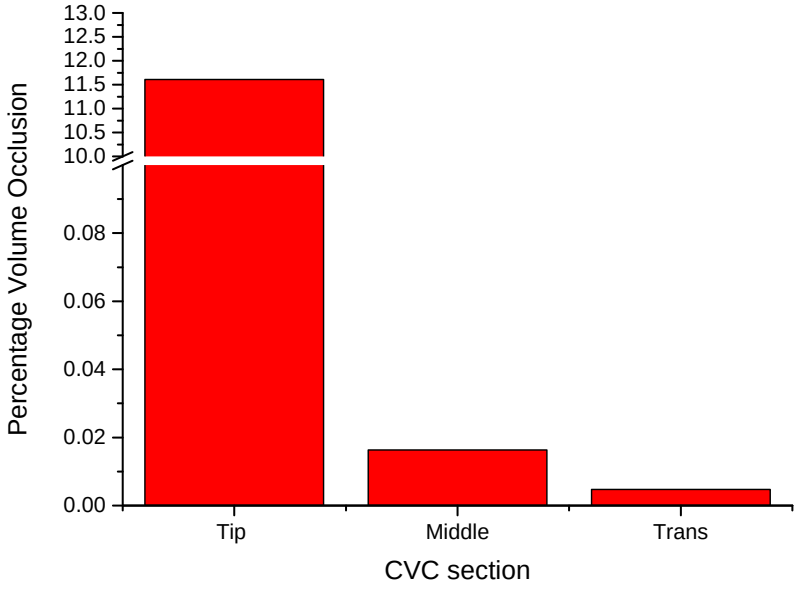

Figure C.5: Bar chart showing percentage occlusion of CVC-flow model biofilms scanned with x-ray μCT . The tip section was much more occluded at 11.6 % compared to the middle (0.016) % and transcutaneous (0.004 %) sections.

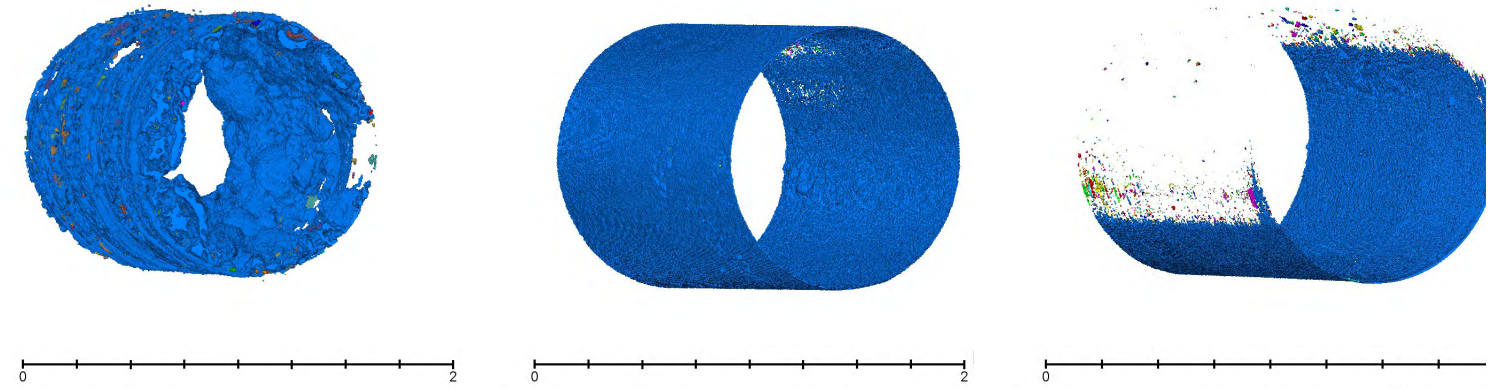

(A) Tip μCT (B) Middle μCT (C) Transcutaneous μCT

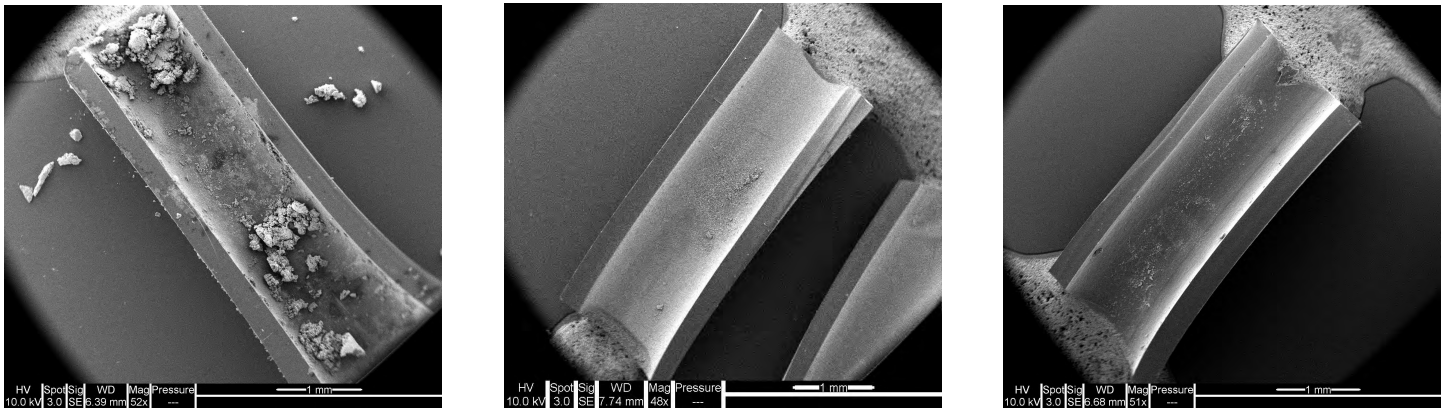

(D) SEM of tip section (E) SEM of middle (F) SEM of trans section

Figure C.6: X-ray μCT tomographs and scanning electron micrographs of CVC-flow biofilm model samples. (A), (B) and (C) were first scanned by x-ray μCT . The tip section had the most biofilm, followed by the middle and transcutaneous section. The same samples were then imaged by scanning electron microscopy (D), (E) and (F).

References

Abdelkefi, A., Torjman, L., Ladeb, S., Othman, T. B., Achour, W., Lakhal, A., Hsairi, M., Kammoun, L., Hassen, A. B. and Abdeladhim, A. B. (2005). Randomized trial of prevention of catheter-related bloodstream infection by continuous infusion of low-dose unfractionated heparin in patients with hematologic and oncologic disease, *Journal of Clinical Oncology* **23**: 7864–7870.

Ajenjo, M. C., Morley, J. C., Russo, A. J., McMullen, K. M., Robinson, C., Williams, R. C. and Warren, D. K. (2011). Peripherally inserted central venous catheter-associated bloodstream infections in hospitalized adult patients, *Infection Control and Hospital Epidemiology* **32**(2): 125–130.

Andes, D., Nett, J., Oschel, P., Albrecht, R., Marchillo, K. and Pitula, A. (2004). Delevopment and characterization of an in vivo central venous catheter /textitCandida albicans biofilm model, *Infection and Immunity* **72**: 6023–6031.

Baena-Monroy, T., Moreno-Maldonado, V., Franco-Martinez, F., Aldape-Barrios, B., Quindos, G. and Sanchez-Vargas, L. (2005). Candida albicans, staphylococcus aureus and streptococcus mutans colonization in patients wearing dental prosthesis., *Medicina Oral* **10**: 27–39.

Bakker, D. P., amd J. van Zanten, H. J. B., de Vries, J., Kliijnstra, J. W. and van der Mei, H. C. (2004). Multiple linear regression analysis of bacterial deposition to polyurethane coatings after conditioning film formation in the marine environment, *Microbiology* **150**: 1779–1784.

Bayaraktar, E., Antolovich, S. D. and Bathias, C. (2008). New development in non-destructive controls of the composite materials and applications in manufacturing engineering, *Journal of Materials Processing Technology* **206**: 30–44.

Becker, L. F. and Pham, C. (1984). Radiopaque catheter.

Bjerkan, G., Witso, E. and Bergh, K. (2009). Sonication is auperior to scraping for retrieval of bacteria in bioiflm on titanium and steel surfaces in vitro., *Acta Orthopaedica* **2**: 245–250.

Boles, B. R. and Horswill, A. R. (2011). Staphylococcal biofilm disassembly, *Trends in Microbiology* **19**: 449–455.

Boles, B. R. and Horswill, R. (2008). agr-mediated dispersal of staphylococcus aureus biofilms, *PLoS Pathogens* **4**: e1000053.

Broekhuizen, C. A. N., Schultz, M. J., van der Wal, A. C., Boszhard, L., de Boer, L., Vandenbroucke-Grauls, C. M. J. E. and Zaat, S. A. J. (2008). Tissue around catheters is a niche for bacteria assocaited with medical device infection, *Critical Care Medicine* **36**(8): 2395–2402.

Burke, J. P. (2003). Infection control- a problem for patient safety, *The New England Journal of Medicine* **348**: 651–656.

Chang, H. T. and Ritman, B. E. (1986). Biofilm loss during sample preparation for scanning electron microscopy, *Water Research* **20**: 1451–1456.

Chittick, P. and Sherertz, R. J. (2010). Recognition and prevention of nosocomial vascular device and related bloodstream infections in the intensive care until, *Critical Care Medicine* **38**: 363–372.

Clarke, A. E. and Denborough, M. A. (1971). The interaction of concanavalin a with blood-group-substance glycoproteins from human secretions, *Biochemical* **121**: 811–816.

Coenye, T. and Nelis, H. J. (2010). *In vitro* and *in vivo* model systems to study microbial biofilm formation, *Journal of Microbiological Methods* **83**: 89–105.

Costerton, B., Cook, G., Shirtiff, M., Stoodley, P. and Pasmore, M. (2004). *) Biofilms, biomaterials, and device-related infections*, Elsevier Academic Press.

Costerton, J. W. and Lewandowski, Z. (1995). Microbial biofilms, *Annual Review of Microbiology* **49**: 711–745.

Costerton, J. W., Stewart, P. S. and Greenberg, E. P. (1999). Bacterial biofilms: A common cause of persistent infections, *Science* **284**: 1318–1322.

Crump, J. A. and Collignon, P. J. (2000). Intravascular catheter-associated infections, *European Journal of Clinical Microbiology and Infectious Diseases* **19**: 1–8.

Cucarella, C., Solano, C., Valle, J., Amorena, B., Lasa, I. and Penadés, J. R. (2001). Bap, a staphylococcus aureus surface protein involved in biofilm formation, *Journal of Bacteriology* **183**: 2888–2896.

Curtis, R. L. (2009). Catheter-related bloodstream infection in the intensive care unit, *The intensive Care Society* **10**: 102–108.

Davis, P. B. (2006). Cystic fibrosis since 1983, *American Journal of Respiratory and Critical Care Medicine* **173**: 475–482.

Davit, Y., Iltis, G., Debenest, G., Veran-Tissoires, S., Wildenschild, D. and Gerino, M. (2011). Imaging biofilm in porous media using x-ray computed tomography, *Journal of Microscopy* **242**: 15–25.

de Beer, D., Stoodley, P., Roe, F. and Lewandowski, Z. (1994). Effects of biofilm structures on oxygen distribution and mass transport, *Biotechnology and Bioengineering* **43**: 1131–1138.

Dobbins, B. M., Kite, P. and Wilcox, M. H. (1999). Diagnosis of central venous catheter related sepsis- a critical look inside, *Journal of Clinical Pathology* **52**: 165–172.

Donlan, R. M. (2001). Biofilms and device-associated infections, *Emerging Infectious Diseases* **7**: 277–281.

Donlan, R. M. (2002). Biofilms: Microbial life on surfaces, *Emerging Infectious Diseases* **8**: 881–890.

Donlan, R. M. (2008). *Bacterial Biofilms*, Springer.

Donlan, R. M. (2011). Biofilm elimination on intravascular catheters: Important considerations for the infectious disease pracitioner, *Healthcare Epidemiology* **52**: 1038–1045.

Donlan, R. M. and Costerton, J. W. (2002). Biofilms: Survival mechanisms of clinically relevant microorganisms, *Clinical Microbiology Reviews* **15**: 167–193.

Drewes, D. A. and Parker, F. T. (1994). Flexible, highly radiopaque plastic material catheter, *US Patent*.

Emori, T. G. and Gaynes, R. P. (1993). An overview of nosocomial infections, including the role of the microbiology laboratory, *Clinical Microbiology Reviews* **6**: 428–442.

Fernandez-Hidalgo, N., Almirante, B., Calleja, R., Ruiz, I., Planes, A. M., Rodriguez, D., Pigrau, C. and Pahissa, A. (2006). Antibiotic-lock therapy for long-term intravascular catheter-related bacteraemia: results of an open, non-comparative study, *Journal of Antimicrobial Chemotherapy* **57**: 1172–1180.

Fey, P. D. (2010). Modality of bacterial growth presents unique targets: how do we treat biofilm-mediated infections?, *Current Opinion in Microbiology* **13**: 610–615.

Flemming, H. and Wingender, J. (2010). The biofilm matrix, *Nature* **8**: 623–633.

Franson, T. R., Sheth, N. K., Rose, H. D. H. and Sohnle, P. G. (1984). Scanning electron microscopy of bacteria adherent to intravascular catheters, *Journal of Clinical Microbiology* **20**: 500–505.

Fux, C. A., Costerton, J. W., Stewart, P. S. and Stoodley, P. (2005). Survival strategies of infectious biofilms, *Trends in Microbiology* **13**(1): 34–40.

Fux, C. A., Stoodley, P., Hall-Stoodley, L. and Costerton, J. W. (2003). Bacterial biofilms: diagnostic and therapeutic challenge, *Expert Review of Anti-Infective Therapy* **1**: 667–683.

Gocmen, J. S., Buyukkocak, U., Azap, A., Pekuz, Y. O. and Caglayan, O. (2012). The effects of four different drugs administered through catheters on slime production in coagulase negative staphylococci, *Journal of Microbiology and Infectious Diseases* **2**: 150–154.

Gottenbos, B., van de Mei H. C. van de Mei, H. C., Klatter, F., Nieuwenhuis, P. and Busscher, H. J. (2002). In vitro and in vivo antimicrobial activity of covalently coupled quaternary ammonium silane coatings on silicone rubber, *Biomaterials* **23**: 1417–1423.

Gotz, F. (2002). Staphylococcus and biofilms, *Molecular Microbiology* **43**: 1367–1378.

Hachem, R., Reitzel, R., Bome, A., Jiang, Y., Tinkey, P., Uthamanthil, R., Chandra, J., Ghannoum, M. and Raad, I. (2009). Novel antiseptic urinary catheters for prevention of urinary tract infections: Correlation of in vivo and in vitro test results, *Antimicrobial Agents and Chemotherapy* **53**: 5145–5149.

Hagle, M. (2007). *Plumer's Principles & Practices of Intravenous Therapy*, Lippincott Williams & Wilkins.

Hall-Stoodley, L., Costerton, J. W. and Stoodley, P. (2004). Bacterial biofilms: From the natural environment to infectious diseases, *Nature Reviews* **2**: 95–108.

Hall-Stoodley, L., Hu, F. and Gieseke, F. (2006). Direct detection of bacterial biofilms on the middle-ear mucosa of children with chronic otitis media, *JAMA* **296**: 202–211.

Hall-Stoodley, L. and Stoodley, P. (2009). Evolving concepts in biofilm infections, *Cellular Microbiology* **11**: 1034–1043.

Hawser, S. P. and Douglas, L. J. (1994). Biofilm formation by candida species on the surface of catheter materials in vitro, *Infection and Immunity* **62**: 915–920.

Health Protection Agency (2006). Healthcare associated infections in acute hospitals, English National Point Prevalence Survey on Healthcare-associated Infections, online.

Herigstad, B., Hamilton, M. and Heersink, J. (2001). How to optimize the drop plate method for enumerating bacteria, *Journal of Microbiological Methods* **44**: 212–129.

Hockenhull, J. C., Dwan, K., Boland, A., Smith, G., Bagust, A. and Dundar, Y. (2008). The clinical effectiveness and cost-effectiveness of central venous catheters treated with anti-infective agents in preventing bloodstream infections: a systematic review and economic evaluation, *Health Technol Assess* **12**: 1–172.

Hsieh, J. (2009). *Computed Tomogarphy Principles, Designs, Artifacts and Recent Advances*, Wiley Inter-Science.

Huang, H., Tian, N., Jin, S., Zhang, Y. and Wang, S. (2014). Syntheses, characterization and nonlinear optical properties of a bismuth subcarbonate bi2o2co3, *Solid Sate Science* **30**: 1–5.

Hubbell, J. H. and Seltzer, S. M. (2014). Tables of x-ray mass attenuation coefficients and mass energy-absorption coefficients from 1 kev to 20 mev for elements z = 1 to 92 and 48 additional substances of dosimetric interest.
URL: *http://www.nist.gov/pml/data/xraycoef/*

Iltis, G., Armstrong, R. T., Jansik, D. P., Wood, B. D. and Wildenschild, D. (2011). Imaging biofilm architecture within porous media using synchrotron-based x-ray computed microtomography, *Water Researches Research* **47**: W02601.

Inan, I., Myers, P. O., Braun, R., Hagen, M. E. and Morel, P. (2008). Pyoderma gangrenosum after totally implanted central venous access device insertion, *World journal of surgical oncology* **6**: 186–191.

Kalender, W. A. (2011). *Computed Tomography: Fundamentals, System Technology, Image Quality, Applications*, Wiley VCH.

Klausen, M., Gjermansen, M., Kreft, J.-U. and Tolker-Nielsen, T. (2006). Dynamics of development and dispersal in sessile microbial communities: examples from pseudomonas aeruginosa and pseudomonas putida model bioślms, *FEMS Microbiology* **261**: 1–11.

Klug, W. S., Cummings, M. R. and Spencer, C. A. (2000). *Concepts of Genetics*, Pearson Education Limited.

Krishnasami, Z., Carlton, D., Bimbo, L., Taylor, M. E., Balkovetz, D. F. and Allon, M. (2002). Management of hemodialysis catheter-related bacteremia with an adjunctive antibiotic lock solution, *Kidney International Journal of Antimicrobial Agents* **61**: 1136–1142.

Kristinsson, K. G., Burnett, I. A. and Spencer, R. C. (1989). Evaluation of three methods for culturing long intravascular catheters, *Journal of Hospital Infection* **14**: 183–191.

Kuminsky, R. E. (2007). Complications of central venous catheterization, *Journal of the American College of Surgeons* **204**: 681–695.

Lackie, P. M. (1996). Immunogold silver staning for light microscopy, *Histochemistry and Cell Biology* **106**: 9–17.

Lackie, P. M., Hennessy, R. J., Hacker, G. W. and Polak, J. M. (1985). Investigation of immonogold-silver staining by electron microscopy, *Histochemistry* **83**: 545–550.

Landis, E. N. and Keane, D. T. (2010). X-ray microtomography, *Materials Characterization* **61**: 1305–1316.

Lawrence, J. R., Swerhone, G. D. W., Leppard, G. G., Araki, T., Zhang, X., West, M. M. and Hitchcock, A. P. (2003). Scanning transmission x-ray, laser scanning, and transmission electron microscopy mapping of the exopolymeric matrix of microbial biofilms, *Applied and Environmental Microbiology* **69**: 5543–5554.

Lewis, K. (2010). Persister cells, *Annual Review of Microbiology* **64**: 357–372.

Lichtman, J. W. and Conchello, J.-A. (2005). Fluorescence microscopy, *Nature Methods* **2**: 910–919.

Lin, M. Y. and Hayden, M. K. (2010). Methicillin-resistant staphylococcus aureus and vancomycin-resistant enterococcus: Recognition and prevention in intensive care units., *Critical Care Medicine* **38**: 335–344.

Lorente, L., Jimenez, A., Iribarren, J. L., Jimenez, J. J., Martin, M. M. and Mora, M. L. (2006). The micro-organism responsible for central venous catheter relatred bloodstream infection depends on catheter site, *Intensive Care Medicine* **32**: 1449–1450.

Lorenz, M. G. and Wackernagelo, W. (1994). Bacterial gene transfer by natural genetic transformation in the environment, *Microbiology and Molecular Biology Reviews* **58**: 563–602.

Lowy, F. D. (1998). Staphylococcus aureus infections, *The New England Journal of Medicine* **339**: 520–532.

Lui, Y., Ai, K. and Lu, L. (2012). Nanoparticulate x-ray computed tomography contrast agents: From design validation to in vivo applications, *Accounts of Chemical Research* **45**: 1817–1827.

Lünsdorf, H., Brümmer, I., Timmis, K. N. and Wagner-Döbler, I. (1997). Metal selectivity of in situ microcolonies in biofilms of the elbe river., *Journal of Bacteriology* **179**: 31–40.

Mack, D. (2007). Microbial interactions in staphylococcus epidermidis biofilms, *Analytical & Bioanalytical Chemistry* **387**: 399–408.

Mah, T. C. and O'Toole, G. A. (2001). Mechanisms of biofilm resistance to antimicrobial agents, *Trends in Microbiology* **9**: 34–39.

Maki, D. G. (1994). *Infections caused by intravascular devices used for infusion therapy: pathogenesis, prevention, and management*, American Society for Microbiology.

Marrie, T. J. and Costerton, J. W. (1984). Scanning and transmission electron microscopy of in situ bacterial colonisation of intravenous and intraarterial catheters, *Journal of Clinical Microbiology* **19**: 687–693.

McGee, D. C. and Gould, M. K. (2003). Preventing complications of central venous catheterization, *The New England Journal of Medicine* **348**: 1123–1133.

Mehall, J. R., Saltzman, D. A., Jackson, R. J. and Smith, S. D. (2002). Fibrin sheath enhances central venous catheter infection, *Critical Care Medicine* **30**: 908–912.

Melter, O. and Radojevic, B. (2010). Small colony variants of *Staphylococcus aureus*-review, *Folia Microbiology* **55**: 548–558.

Mermel, L. A. (2011). What is the predominant source of intravascular catheter infections?, *Clinical Infectious Diseases* **52**: 211–212.

Mermel, L. A., Allon, M., Bouza, E., Craven, D. E., Flynn, P., OŠGrady, N. P., Raad, I. I., Rijnders, B. J. A., Sherertz, R. J. and Warren, D. K. (2009). Clinical practice guidelines for the diagnosis and management of intravascular catheter-related infection: 2009 update by the infectious diseases society of america, *Clinical Infectious Diseases* **49**: 1–45.

Mermel, L. A., Farr, B. M., Sherertz, R. J., Raad, I. I., O'Grady, N., Harris, J. S. and Craven, D. E. (2001). Guidelines for the management of intravascular catheter-related infections, *Clinical Infectious Diseases* **32**: 1249–1272.

Merrer, J., Jonghe, B. D., Golliot, F., Lefrant, J., Raffy, B., Barre, E., Rigaud, J., Casciani, D., Misset, B., Bosquet, C., Outin, H., Brun-Buisson, C. and Nitenberg, G. (2001). Complications of femoral and subclavian venous catheterization in critically ill patients, *JAMA* **286**: 700–707.

Metscher, B. D. (2009). Microct for comparative morphology: simple staining methods allow high-contrast 3d imaging of diverse non-mineralized animal tissues., *BMC Physiology* **9**: 9–11.

Monsigny, M., Roche, A., amd R. Magnet-Dana, C. S. and Delmotte, F. (1980). Sugar-lectin interactions : How does wheat-germ agglutinin bind sialoglycoconjugates ?, *European Journal of Biochemistry* **104**: 147–153.

Morris, N. S., Stickler, D. J. and McLean, R. J. C. (1999). The development of bacterial biofilms on indwelling urethral catheters, *World Journal of Urology* **17**: 345–350.

Muller, M. (2006). *Introduction to Confocal Fluorescence Microscopy*, The International Society for Optical Engineering.

National Audit Office (2000a). Improving patient care by reducing the risk of hospital acquired infection: A progress report.

National Audit Office (2000b). The management and control of hospital acquired infection in acute NHS trusts in england.

National Audit Office (2004). Improving patient care by reducing the risk of hospital acquired infection: A progress report.

Neu, T. R., Manz, B., Volke, F., Dynes, J. J., Hitchcock, A. P. and Lawrence, J. R. (2010). Advanced imaging techniques for assessment of structure, composition and function in biofilm systems, *FEMS Microbiology Ecology* **72**: 1–21.

Neu, T. R., Swerhone, G. D. W. and Lawrence, J. R. (2001). Assessment of lectin-binding analysis for in situ detection of glycoconjugates in biofilm systems, *Microbiology* **147**: 299–313.

Nistico, L., Kreft, R., Gieseke, A., Coticchia, J. M., Burrows, A., Khampang, P., andJ. E. Kerschner, Y. L., Post, J. C., Lonergan, S., Sampath, R., Hu, F. Z., Ehrlich, G. D., Stoodley, P. and Hall-Stoodley, L. (2011). Adenoid reservoir for pathogenic biofilm bacteria, *Journal of Clinical Microbiology* **49**: 1411–1420.

Nunan, N., Ritz, K., Rivers, M., Feeney, D. S. and Young, I. M. (2006). Investigating microbial micro-habitat structure using x-ray computed tomography, *Geoderma* **133**: 398–407.

O'Grady, N. P., Alexander, M., Burns, L. A., Dellinger, P., Garland, J., Heard, S. O., Lipsett, P. A., Masur, H., Mermel, L. A., Pearson, M. L., Raad, I. I., Randolph, A., Rupp, M. E. and Saint, S. (2011). Guidelines for the prevention of intravascular catheter-related infections, 2011, *Centers for Disease Control and Prevention* **52**: 1–83.

Orme, R. M. L., McSwinley, M. M. and Chamberlain-Webber, R. F. O. (2007). Fatal cardiac tamponade as a result of a peripherally inserted central venous catheter: a case report and review of the literature, *British Journal of Anaesthesia* **99**: 384–388.

O'Toole, G., Kaplan, H. B. and Kolter, R. (2000). Biofilm formation as microbial development, *Annual Review of Microbiology* **54**: 49–79.

Otto, M. (2004). Quorum-sensing control in staphylococci Ű a target for antimicrobial drug therapy?, *FEMS Microbiology Letters* **241**: 135–141.

Otto, M. (2009). *Staphylococcus epidermidis*- the 'accidental' pathogen., *Nature* **7**: 555–567.

Paddock, S. W. (1999). Confocal laser scanning microscopy, *Biotechniques* **27**: 992–1004.

Palmer, R. J. and Sternberg, C. (1999). Modern microscopy in biofilm research: confocal microscopy and other approached, *Current Opinion in Biotechnology* **10**: 263–268.

Parsek, M. R. and Singh, P. K. (2003). Bacterial biofilms: An emerging link to disease pathogenesis, *Annual* **57**: 677–701.

Pearson, M. L. (1996). Guidelines for prevention of intravascular-device-relatedinfections, *Infection Control and Hospital Epidemiology* **17**: 438–473.

Pedersen, A. R. and Peiffer, D. A. (2001). Radiopaque catheter tip, *US Patent*.

Periasamy, S., Joo, H., Duong, A. C., Bach, T. L., Tan, V. Y., Chatterjee, S. S., Cheung, G. Y. C. and Otto, M. (2012). How /textitStaphylococcus aureus biofilms develop thier characteristic structure, *Proceedingss of the National Academy of Sciences of the United States of America* **109**: 1281–1286.

Piednoir, E., Thibon, P., Borderan, G., Godde, F., Borgey, F., Coutour, X. L. and Parienti, J. (2011). Long-term clinical and economical benefits associated with the management of a nosocomial outbreak resulting from extended-spectrum beta-lactamase-producing klebsiella pneumoniae, *Critical Care Medicine* **39**: 2672–2677.

Polderman, K. H. and Girbes, A. R. J. (2002). Central venous catheter use: Part 2: infectious complications, *Intensive Care Medicine* **28**: 18–28.

Prassana, S. S. and Doble, M. (2008). Medical biofilms- its formation and prevention using organic molecules, *Journal of the Indian Institute of Science* **88**: 27–35.

Proctor, R. A., von Eiff, C., Kahl, B. C., Becker, K., McNamara, P., Herrmann, M. and Peters, G. (2006). Small colony variants: a pathogenic form of bacteria that facilitates persistent and recurrent infections, *Nature Reviews* **4**: 295–305.

Raad, I. (1998). Intravascular-catheter-related infections, *The Lancet* **351**: 893–351.

Raad, I., Costerton, W., Sabharwal, U., Sacilowski, M. and amd G. P. Bodey, E. A. (1993). Ultrastructural analysis of indwelling vascular catheters: A quantitative relationship between luminal colonization and duration of placement, *The Journal of Infectious Diseases* **168**: 400–407.

Raad, I., Hanna, H. and Maki, D. (2007). Intravascular catheter-related infections: advances in diagnosis, prevention, and management, *The Lancet Infectious Diseases* **7**: 645–657.

Raad, I. I. and Bodey, G. P. (1992). Infectious complications of indwelling vascular catheters, *Clinical Infectious Diseases* **15**: 197–210.

Richards, S. R. and Turner, R. J. (1984). A comparitive study of techniques for the examination of biofilms by scanning electron microscopy, *Water Research* **18**: 767–773.

Ritman, E. L. (2004). Micro-computed tomogarphy–current status and developments, *Annual Review of Biomedical Engineering* **6**: 185–208.

Rockett, P. and Wang, G. (2009). *Biomedical Engineering and Design Handbook Applications*, McGraw-Hill Companies.

Rohde, H., Frankenberger, S., Zahringer, U. and Mack, D. (2010). Structure, function and contribution of polysaccharide intercellular adhesin (pia) to *Staphylococcus epidermidis* biofilm formation and pathogenesis of biomaterial-associated infections, *European Journal of Cell Biology* **89**: 103–111.

Sawyer, R. G. and Leon, C. A. T. (2010). Common complications in the surgical intensive care unit, *Critical Care Medicine* **38**: 483–493.

Schlecht, L., Peters, B., Shirtliff, M. E. and Jabra-Rizk, M. A. (2012). Systemic staphylococcus aureus infection mediated by candida albicans hyphal invasion in a murine model of oral co-infection, *Mycoses* **55**: 14.

Scopsi, L., Larsson, L. I., Bastholm, L. and Nielsen, M. H. (1986). Silver-enhanced colloidal gold probes as markers for scanning electron microscopy, *Histochemistry* **86**: 35–41.

Sherertz, R. J., Heard, S. O. and Raad, I. I. (1997). Diagnosis of tripple-lumen catheter infection: Comparison of roll plate, sonication and flushing methodologies, *Journal of Clinical Microbiology* **35**: 641–646.

Sherertz, R. J., Raad, I., Belani, A., Koo, L. C., Rand, K. H., L.Pickett, D., Straub, S. A. and Fauerback, L. L. (1990). Three-year experience with sonicated vascular catheter cultures in a clinical microbiology laboratory, *Journal of Clinical Microbiology* **28**: 76–82.

Shin, J. H., Kee, S. J., Shin, M. G., Kim, S. H., Shin, D. H., Lee, S. K., Suh, S. P. and Ryang, D. W. (2002). Biofilm production by isolates of candida species recovered from nonneutropenic patients: Comparison of bloodstream isolates with isolates from other sources, *Journal of Clinical Microbiology* **40**: 1244–1248.

Siemens (2014). Simulation of x-ray spectra.
URL: *//w9.siemens.com/cms/oemproducts/Home/X-rayToolbox/spektrum*

Simpkin, D. J. (1999). The aapm/rsna physics tutorial for residents, *Imaging and therapeutic technology* **19**: 155–167.

Sinha, B., Francois, P. P., NuBe, O., Foti, M., Hartford, O. M., Vaudaux, P., Foster, T. J., Lew, D. P., Hermann, M. and Krause, K. (1999). Fibronectin-binding protein acts as *Staphylococcus aureus* invasin via fibronectin bridging to integrin $\alpha 5\beta 1$, *Cellular Microbiology* **1**: 101–117.

Smith, J. A. and Kauffman, C. A. (2010). Recognition and prevention of nosocomail invasive fungal infections in the intensive care unit, *Critical Care Medicine* **38**: 380–387.

Surman, S. B., Walker, J. T., Goddard, D. T., Morton, L. H. G., Keevil, C. W., Weaver, W., Skinner, A., Hanson, K., Caldwell, D. and Kurtz, J. (1996). Comparison of microscope techniques for the examination of biofilms, *Journal of Microbiological Methods* **25**: 57–70.

Surveillance of Central Venous Catheter Related Infection Protocol, National Health Service (2011).

Tessler, M., Dascal, A., Gioseffini, S., Miller, M. and Mendelson, J. (1999). Growth curves of staphylococcus aureus, candida albicans, and moraxella osloensis in propofol and other media, *Canadian Journal of Anesthesia* **88**: 209–212.

Thieme, J., Schneider, G. and Knochel, C. (2003). X-ray tomography of a microhabitat if bacteria and other soil colloids with sub-100 nm resolution, *Micron* **34**: 339–344.

Tubby, S., Wilson, M., Wright, J. A., Zhang, P. and Nair, S. P. (2013). Staphylococcus aureus small colony variants are susceptible to light activated antimicrobial agents, *BMC Microbiology* **13**: 1471–1474.

Turcotte, S., Dube', S. and Beauchamp, G. (2006). Peripherally inserted central venous catheters are not superior to central venous catheters in the acute care pf surgical patients on the ward, *World Journal of Surgery* **30**: 1605–1619.

Vesely, T. M. (2003). Central venous catheter tip position: A continuining controversy, *Journal of Vascular and Interventional Radiology* **14**: 527–534.

von Eiff, C., Heilmann, C., Proctor, R. A., Woltz, C., Peters, G. and Gotz, F. (1997). A site-directed staphylococcus aureus hemb mutant is a small- colony variant which persists intracellularly, *Journal of Bacteriology* **4**: 4706–4712.

Wachowski, I., Jolly, D. T., Hrazdil, J., Galbraith, J. C., Greacen, M. and Clanachan, A. S. (1999). The growth of microorganisms in propofol and mixtures of propofol and lidocaine, *Anesthesia & Analgesia* **88**: 209–212.

Walshe, L. J., Malak, S. F., Eagan, J. and Sepkowitz, K. A. (2002). Complication rates among cancer patients with peripherally inserted central catheters, *Journal of Clinical Oncology* **20**: 3276–3291.

Wargo, M. J. and Hogan, D. A. (2006). Fungal – bacterial interactions: a mixed bag of mingling microbes, *Current Opinion in Microbiology* **9**: 359–364.

Watnick, P. and Kolter, R. (2000). Biofilm, city of microbes, *Journal Of Bacteriology* **182**: 2675–2679.

Weinstein, S. M. (ed.) (2007). *Plumer's Principles & Practices of Intravenous Therapy*, Lippincott Williams & Wilkins.

Wertheim, H. F. L., Melles, D. C., Vos, M. C., van Leeuwen, W., Belhum, A., Verburg, H. A. and Nouwen, J. J. (2005). The role of nasal carriage in *Staphylococcus aureus* infections, *The Lancet Infectious Diseases* **5**: 751–762.

Wildenschild, D. and Sheppard, A. P. (2013). X-ray imaging and analysis techniques for quantifying pore-scale structure and processed in subsurface porous medium systems, *Advances in Water Resources* **51**: 217–246.

Wilson, R. (2008). The use of gold nanoparticles in diagnostics and detection., *Chemical Society Reviews* **37**: 2028–2045.

Woeltje, K. F., Butler, A. M., Goris, A. J., Tutlam, N. T., Doherty, J. A., Westover, M. B., Ferris, V. and Bailey, T. C. (2008). Automoated surveilance for central line-associated bloodstream infection in intensive care units, *Infection control and hospital epidemiology* **29**: 842–846.

World Health Organization (2012). Preventing bloodstream infections from central line venous catheters. [Online; accessed 6th December 2012].
URL: *http://www.who.int/patientsafety/implementation/bsi/en/index.html*

Zaat, S. A. J., Broekhuizen, C. A. N., de Boer, L., Schultz, M. J., Boszhard, L., van der Wal, A. C. and Vandenbroucke-Grauls, C. M. J. E. (2008). Biomaterial-associated infection: breaking out of the biofilm, *European Cells and Materials* **16**: 10.

Zandri, G., Pasquaroli, S., Vignaroli, C., Talevi, S., Manso, E., Donelli, G. and Biasvasco, F. (2012). Detection of viable but non-culturable staphylococci in biofilms from central venous catheters negative on standard microbiological assays, *Clinical Microbiology and Infection* **8**: 259–261.